Journal of Oncology

Promising Drug Targets for Cancer Therapeutics 2022

Lead Guest Editor: Ashok Pandurangan
Guest Editors: Nandakumar Natarajan and Vishnu Priya Veeraraghavan

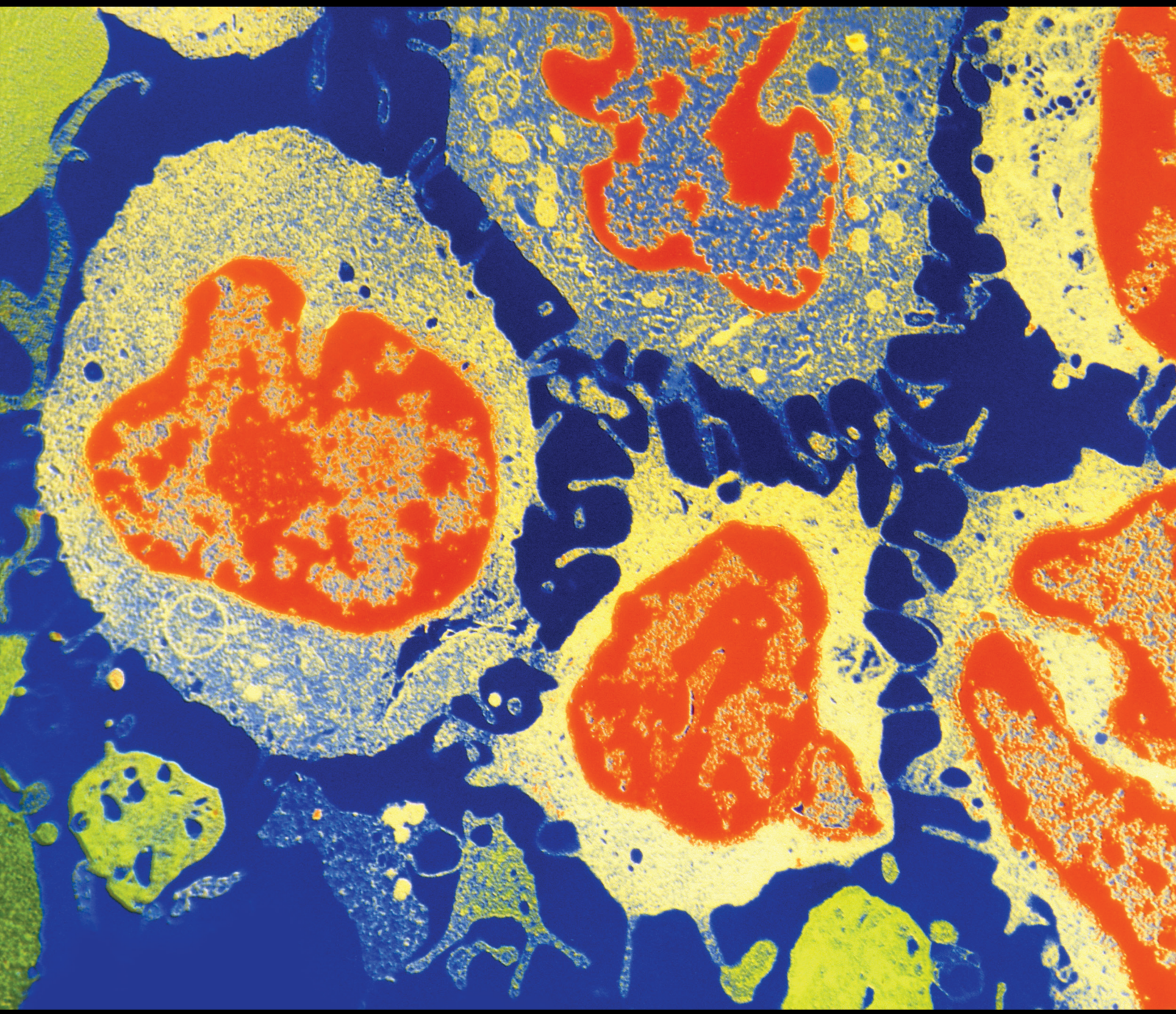

Promising Drug Targets for Cancer Therapeutics 2022

Journal of Oncology

Promising Drug Targets for Cancer Therapeutics 2022

Lead Guest Editor: Ashok Pandurangan
Guest Editors: Nandakumar Natarajan and Vishnu Priya Veeraraghavan

Contents

Hindawi
Journal of Oncology
Volume 2023, Article ID 5486017, 19 pages
https://doi.org/10.1155/2023/5486017

Research Article

Deciphering the Molecular Mechanism of Yifei-Sanjie Pill in Cancer-Related Fatigue

Yingchao Wu,[1] **Shuyao Zhou**,[2] **Dajin Pi**,[1] **Yangyang Dong**,[3] **Wuhong Wang**,[1] **Huan Ye**,[1] **Zhongjia Yi**,[1] **Yiliu Chen**,[1] **Lizhu Lin**,[4] **and Mingzi Ouyang**[1]

[1]*School of Traditional Chinese Medicine, Jinan University, Guangzhou, Guangdong 510632, China*
[2]*College of Forestry and Landscape Architecture, South China Agricultural University, Guangzhou, Guangdong 510642, China*
[3]*Guangdong Metabolic Diseases Research Center of Integrated Chinese and Western Medicine, Guangdong Pharmaceutical University, Guangzhou, Guangdong 510006, China*
[4]*Oncology Center, The First Affiliated Hospital of Guangzhou University of Chinese Medicine, Guangzhou, Guangdong 510405, China*

Correspondence should be addressed to Lizhu Lin; lizhulin26@yahoo.com and Mingzi Ouyang; mingzioy@jnu.edu.cn

Received 13 September 2022; Revised 25 October 2022; Accepted 24 November 2022; Published 13 February 2023

Academic Editor: Nandakumar Natarajan

Background. The incidence of cancer-related fatigue (CRF) is increasing, but its lack of clear pathogenesis makes its prevention and treatment difficult. Therefore, it is of great significance to clarify the pathogenesis of CRF and find effective methods to treat it. *Methods*. The CRF model was established by intraperitoneal injection of LLC cells in ICR mice to explore the pathogenesis of CRF and verify the therapeutic effect of the Yifei-Sanjie pill (YFSJ). The active components of YFSJ were found by LC/MS, the in vitro inflammatory infiltration model of skeletal muscle was constructed by TNF-α and C2C12 myoblasts, and the results of in vivo experiments were verified by this model. *Results.* Behavioral analysis results showed that YFSJ alleviated CRF; histological examination results showed that YFSJ could reverse the tumor microenvironment leading to skeletal muscle injury; ELISA and RNA-seq results showed that the occurrence of CRF and the therapeutic effect of YFSJ were closely related to the tumor inflammatory microenvironment; IHC and WB results showed that the occurrence of CRF and the therapeutic effect of YFSJ were closely related to the Stat3-related signaling pathway and autophagy. *Conclusions.* YFSJ can reduce the level of inflammation in the tumor microenvironment in vivo, inhibit the abnormal activation of the Stat3/HIF-1α/BNIP3 signaling pathway induced by tumor-related inflammation, thereby inhibiting the overactivation of mitophagy in skeletal muscle, and finally alleviate CRF. Quercetin, one of the components of YFSJ, plays an important role in inhibiting the phosphorylation activation of Stat3.

1. Introduction

With the development of society and the improvement of medical level, people's life expectancy is getting longer and longer [1]. Cancer, as a disease closely related to the aging of the body, is accompanied by an increase in life expectancy, and the incidence of cancer is increasingly high [2, 3]. Although the lesions of cancer are mostly confined to one or more places, in the process of their occurrence and development, they have an obvious influence on the whole body. In the process of cancer development, there are a variety of unpleasant symptoms, such as fatigue, weight loss, and pain. The incidence of cancer-related fatigue (CRF) has been reported to be as high as 82% in cancer patients, and tumor burden contributes to varying degrees of fatigue with or without chemotherapy [4]. Unfortunately, the pathogenesis of CRF is not fully understood, and there is no standard treatment.

Previous studies have found that the mechanism of CRF is closely related to tumor-induced overactivation of mitophagy

in skeletal muscle [4]. There are many reasons for excessive mitophagy, such as activation of inflammatory factors, oxidative stress, and energy metabolism disorders [5–7]. Tumor burden will also lead to changes in the body's internal environment, such as changes in the immune microenvironment and energy metabolism level [8, 9]. However, the mechanism by which tumor burden leads to mitophagy and fatigue remains unclear.

The Yifei-Sanjie pill (YFSJ), a traditional Chinese patent medicine, can be used to alleviate CRF in clinical practice [10–12]. The mechanism may be to alleviate CRF by reducing skeletal muscle damage [4, 13]. However, the specific molecular mechanism by which YFSJ attenuates skeletal muscle injury in the tumor microenvironment has not been revealed. Therefore, it is of great significance to clarify the relationship between the occurrence of CRF and mitophagy and to reveal the molecular mechanism of YFSJ in the treatment of CRF. In addition, meta-analysis and network pharmacology predicted that quercetin may play an important role in alleviating CRF, but its specific molecular mechanism has not been revealed [14]. Therefore, we will further study the pathogenesis and treatment of CRF.

In this study, we demonstrated that the tumor inflammatory microenvironment leads to the abnormal activation of the Stat/HIF-1α/BNIP3 signaling pathway in skeletal muscle cells, which induces excessive mitophagy in skeletal muscle and ultimately leads to fatigue. Several miRNAs have previously been reported to regulate these pathways, but the mechanisms are unclear [15]. At the same time, we confirmed that YFSJ could reduce tumor-induced elevated levels of inflammation in vivo, thereby inhibiting excessive mitophagy in skeletal muscle and ultimately alleviating CRF. Meanwhile, we also found that quercetin, a major component in YFSJ, can specifically inhibit the phosphorylation activation of Stat3, thereby inhibiting TNF-α-induced mitophagy, which provides a new paradigm for the modern development and application of traditional drugs.

2. Materials and Methods

2.1. Animal Ethics Statement. Female ICR mice weighing between 20 and 22 g and aged 4 weeks (Charles River Laboratories, Zhejiang, China) were used in this investigation. All experiments were conducted according to the relevant laws and institutional guidelines. Mice were individually housed in independent ventilated cages at 24°C to 26°C under constant humidity with a 12 h light/dark cycle. Based on clinical practice, the mice were divided into 4 groups ($n = 10$), namely, control, CRF, low, and high groups, in a random order. Permission for the experimental scheme from the Laboratory Animal Ethics Committee of Jinan University was granted (Approval No. 20220301-15).

2.2. YFSJ Preparation. YFSJ (Cat. #Z20190015000) was purchased from the First Affiliated Hospital of Guangzhou University of Chinese Medicine (Guangdong, China). Each packet of YFSJ was 8 g, which was equivalent to 16.4 g of herbal medicine. The dosage of the subsequent experiments was the amount of herbal medicine.

2.3. Antibodies. Primary antibodies against Stat3 (Cat. #9139T), Phospho-Stat3 (P-Stat3, Cat. #9145T), HIF-1α (Cat. #36169T), Atg7 (Cat. #8558T), LC3A/B (Cat. #12741S), CD68 (Cat. #97778S), CD206 (Cat. #24595T), GAPDH (Cat. #5174S), rabbit (Cat. #7074P2), or mouse (Cat. #7076P2) and secondary antibodies were purchased from Cell Signaling Technology (Danvers, MA, USA). Primary antibodies against BNIP3 (Cat. #68091-1-Ig), Beclin 1 (Cat. #11306-1-AP), and p62 (Cat. #18420-1-AP), and COX IV (Cat. #66110-1-Ig) were purchased from Proteintech (Wuhan, China).

2.4. Cell Culture. Lewis lung cancer (LLC) cells were acquired from the Guangzhou University of Chinese Medicine (Guangzhou, China). C2C12 myoblasts were purchased from Fuheng BioLogy (Shanghai, China). Dulbecco's modified Eagle's medium, high glucose, L-glutamine, phenol red (DMEM, Cat. #11965092), fetal bovine serum (FBS, Cat. #10270106), penicillin/streptomycin (Cat. #10378016), trypsin-EDTA, and 0.05% phenol red (Cat. #25200072) were purchased by Gibco (NY, USA). All cells were identified by short tandem repeat (STR). Cells were cultured in DMEM supplemented with 10% FBS, 100 U/mL penicillin, and 100 μg/mL streptomycin. Cells are placed in a three gas incubator (Thermo Fisher Scientific, Waltham, MA, USA) containing 5% CO_2, 37°C constant temperature, and damp environment for culture. The medium was changed every 72 hours, and the cells were routinely subcultured when they reached 90% confluence. Logarithmic growth phase LLC and C2C12 cells were used to conduct the experiments. In order to maintain the stability of HIF-1α protein in vitro, C2C12 cells were supplemented with 0.1 μM DMOG (Cat. #D3695, Sigma-Aldrich, Darmstadt, Germany) in an in vitro experiment.

2.5. In Vivo Inflammatory CRF Model. We induced an inflammatory CRF model in mice via intraperitoneal injection of LLC cells following the published protocols [16]. After acclimation for 7 days, mice in groups CRF, Low, and High were intraperitoneally injected with 1×10^7 LLC cells/100 μL each mouse. The experimental protocol is shown in Figure 1(a). Three days after LLC cell inoculation, treatment was initiated, and the dose of YFSJ was referred to in our previous report [4]. The control and CRF groups were given normal saline intragastric administration (0.2 ml/d) for 28 days. Low group was given 2 g/kg/d YFSJ by gavage, 0.2 ml, for 28 days. High group was given 4 g/kg/d YFSJ by gavage, 0.2 ml, for 28 days.

2.6. Behavioral Tests

2.6.1. Forelimb Grip Strength Test (FGST). The muscle strength of mice was measured by FGST according to the published protocol [17]. In short, we first attached a grid to

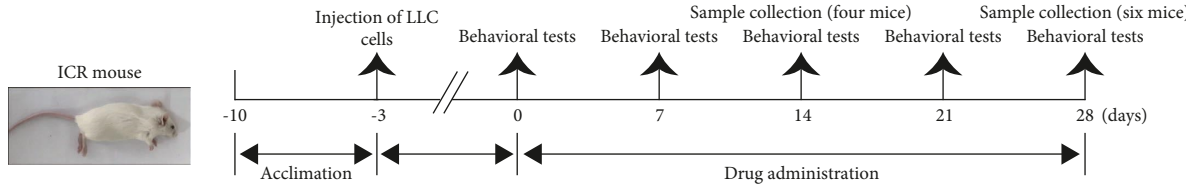

(a)

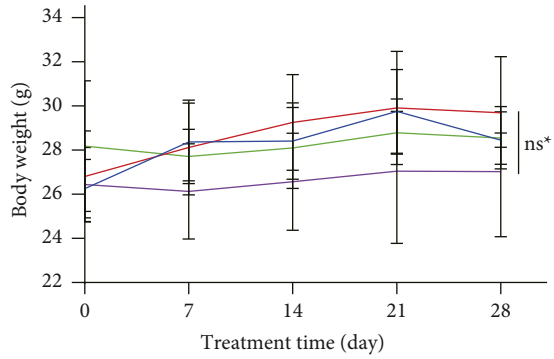

(b)

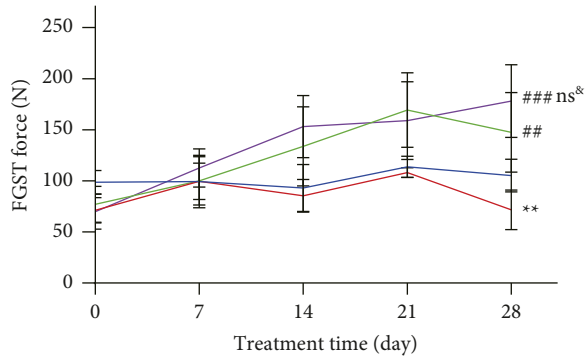

(c)

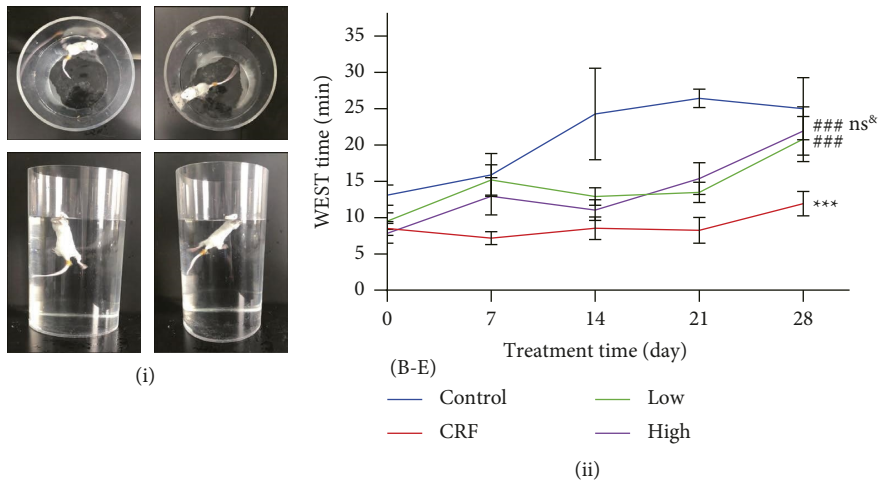

(i)

(ii)

(d)

Figure 1: Continued.

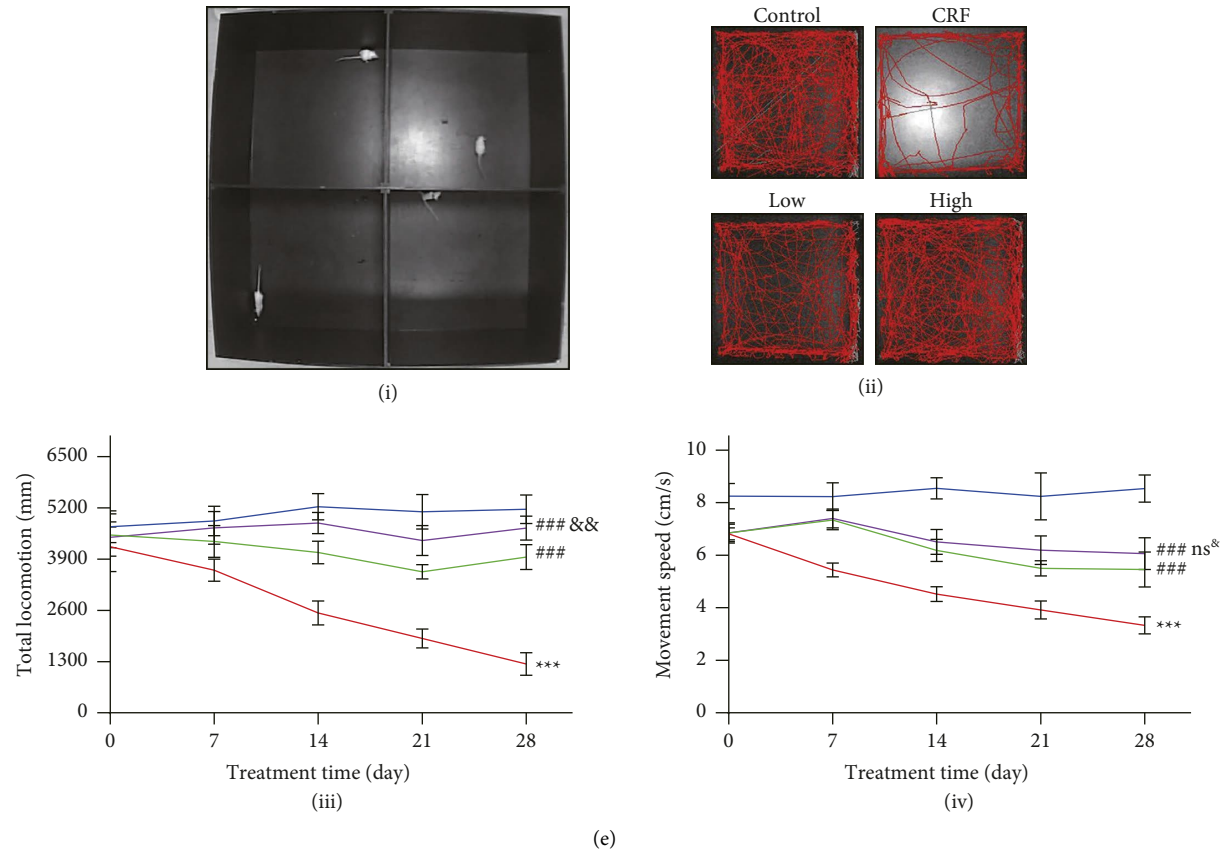

Figure 1: YFSJ attenuates tumor-induced fatigue. (a) The in vivo experimental protocol. (b) Body weight was measured every 7 days. (c) The FGST force. (d) WEST; (i) schematic diagram of WEST; (ii) the WEST time. (e) OFT; (i) schematic diagram of OFT; (ii) the OFT track map; (iii) the OFT movement distance; (iv) the OFT movement speed. The data are presented as means ± SD; $^{ns*}p > 0.05$, $^{**}p < 0.01$, and $^{***}p < 0.001$ compared with the control group; $^{\#\#}p < 0.01$ and $^{\#\#\#}p < 0.001$ compared with the CRF group; $^{ns\&}p > 0.05$ and $^{\&\&}p < 0.01$ compared with the low group; 0, 7, and 14 days, $n = 10$; 21 and 28 day, $n = 6$.

a force transducer, then let the mouse grasp the grid tightly with both forepaws, and then pulled the mouse away from the grid, breaking its grasp. The transducer records the maximum force applied by the mouse on the grid during the pull. Let the mouse pull the grid three times in a row, and take the average of the three pulls.

2.6.2. Weight-Loaded Exhaustive Swimming Test (WEST). The muscle exercise endurance of mice was measured by WEST according to the published protocol [18]. In short, the mice were individually loaded with a lead (7% of body weight) on their tail root and placed in the swimming pool (diameter 30 cm × height 50 cm) filled with 30 cm deep water (maintained at 25 ± 1°C). The exhaustive swimming time was recorded as described in the previous study [19]. Considering that the mice could not fully recover their physical strength before the test in a short time, the test was not repeated for each mouse in a single test.

2.6.3. Open Field Test (OFT). The locomotor willingness and ability of mice were measured by OFT according to the published protocol [20]. In short, the OFT was conducted in an arena made of plexiglass ($100 \times 100 \times 50\ cm^3$). Each mouse was placed in the center of the apparatus and analyzed for 10 min in a quiet room. The total movement distance and movement speed were calculated and analyzed using the EthoVision XT 14 software (Noldus Information Technology Co., Ltd., Beijing, China). In consideration of the adaptation of mice to the experimental environment, the test was not repeated for each mouse in a single test.

2.7. Mouse Euthanasia and Sample Collection. According to the corresponding experimental plan, the mice were anesthetized with pentobarbital (150 mg/kg, i.p.) after all the corresponding behavioral tests were completed (four mice at 14 days and six at 28 days). In order to maintain a sufficient number of mice for behavioral analysis, only 4 mice from each group were sampled at 14 days. The plasma was collected, the mice were euthanized by cervical dislocation, and the lung, liver, spleen, and gastrocnemius muscle tissues were removed for subsequent experiments. The plasma and tissues collected will be pretreated differently depending on the subsequent experiments.

2.8. Histological Analysis

2.8.1. Hematoxylin and Eosin (HE) Staining. HE-stained sections of lung, liver, and kidney were prepared according to previously reported methods [21]. The stained slices were observed and photographed under a light microscope at 100× or 40× magnification (NIKON Eclipse ci, Japan). For quantification of immunostaining intensities, Image *J* software (National Institutes of Health, Bethesda, MD, USA) was used, as stated by Sysel et al. [22]. The inverse mean density was determined, as reported by Vis et al. [23], in 1 randomly chosen field from various sections of 3 mice in each group.

2.8.2. Transmission Electron Microscope (TEM). TEM sections of gastrocnemius muscle were prepared according to previously reported methods [4]. The slices were observed and photographed under an electron microscope (HITACHI HT7700, Japan).

2.8.3. Immunohistochemical (IHC) Staining. IHC-stained sections of gastrocnemius muscle were prepared according to previously reported methods [21]. Primary antibodies include Beclin 1 (1 : 100), LC3 (1 : 500), p62 (1 : 1000), CD68 (1 : 300), and CD206 (1 : 400). Images were captured under a light microscope (Leica, Germany).

2.9. Enzyme-Linked Immunosorbent Assay (ELISA). Mouse IL-6 ELISA kit (Cat. #EK206/3-48) and mouse TNF-α ELISA kit (Cat. #EK282/4-48) were purchased from Multisciences (Zhejiang, China). The serum IL-6 and TNF-α contents of mice were measured according to the instructions of the kit.

2.10. RNA-Seq. The mouse gastrocnemius muscle RNA-seq assay was performed as previously reported [21]. The differential expression analysis and differential gene enrichment analysis (Gene Ontology, GO, and Kyoto Encyclopedia of Genes and Genomes, KEGG), and visualized, were performed on the Novo Magic (URL: https://magic.novogene.com) of Beijing Novogene Biotechnology Co., LTD.; $n = 3$. Datasets for RNA-seq can be obtained from the Sequence Read Archive at the NCBI (URL: https://www.ncbi.nlm.nih.gov/sra/PRJNA874361).

2.11. Western Blotting (WB). WB analysis of gastrocnemius muscles was performed as previously reported [21]. If mitochondrial protein isolation is required, it is done using the mitochondrial protein extraction kit (BB-3171, Best Bio, Shanghai, China). Primary antibodies include Stat3 (1 : 1000), P-Stat3 (1 : 1000), HIF-1α (1 : 1000), BNIP3 (1 : 5000), Beclin 1 (1 : 1000), Atg7 (1 : 1000), LC3A/B (1 : 1000), p62 (1 : 1000), GAPDH (1 : 2500), and COX IV (1 : 2000). After the primary antibody protocol was completed, the corresponding secondary antibody (1 : 5000) was added according to the protocol. The density values of the bands were captured and documented through a gel image analysis system (ChemiDox™, Bio-Rad, USA) and normalized to GAPDH or COX IV; $n = 3$.

2.12. Q-Orbitrap High Resolution Liquid/Mass Spectrometry (LC/MS). As previously reported [4], we identified the components contained in YFSJ by LC/MS. This part was completed by Wuhan Servicebio Company (Hubei, China).

2.13. Access to Active Ingredients and Molecular Docking. LC/MS results were used in conjunction with previously reported methods [24] to obtain the active components in YFSJ. Using the TCM Network Pharmacology Analysis System (TCMNPAS, URL: https://54.223.75.62:3838/), quercetin was used as ligands and Stat3 as receptors for molecular docking, and their binding sites and binding affinity were analyzed. Protein docking pocket parameters were obtained from ligands, and the lower the value of "affinity" (the greater the absolute value), the stronger the binding force. Finally, all the docking results were analyzed by "RMSD," and an RMSD value less than 2 was considered reliable.

2.14. MTT Colorimetric Assay. Cell viability was measured by the MTT colorimetric assay according to the published protocol [21]. Thiazolyl blue tetrazolium bromide (MTT, Cat. #V13154) was supplied by Gibco (NY, USA). If the experimental process needs to be treated with the autophagy inhibitor 3-MA (Cat. #M9281, Sigma-Aldrich, Darmstadt, Germany), the use method is pretreatment for 4 hours. All other factors were treated for 48 hours. IL-6, Mouse (Cat. #CZ52157-EA) and TNF-α, Mouse (Cat. #CZ52347-EA) were purchased from Shanghai Yingxin Laboratory Equipment Co., Ltd. (Shanghai, China). Quercetin (Cat. #S25567) was purchased from Shanghai Yuanye Bio-Technology Co., Ltd. (Shanghai, China). $n = 6$.

2.15. MDC Staining Assay. Cell autophagy was measured by the MDC staining assay according to the manufacturer's instructions. Autophagy staining assay kit with MDC (Cat. #C3018S) was supplied by Beyotime Biotechnology (Shanghai, China). The fluorescence intensities were measured at an emission wavelength of 512 nm and an excitation wavelength of 335 nm using a fluorescence microplate reader (BioTek, Vermont, USA). The data are expressed as the percentage of the fluorescence intensity relative to that of the control group, $n = 6$.

2.16. Statistical Analysis. The experimental data were analyzed using Student–Newman–Keuls (*S-N-K*) in ANOVA with SPSS version 13.0 software (SPSS Inc., IL, USA) and GraphPad Prism 9 (GraphPad Software, LLC, California, USA) to graph the data. The results are presented as the mean values ± standard deviation (SD). A p value <0.05 was considered statistically significant.

3. Results

3.1. YFSJ Improves the Exercise Ability of CRF Mice. The in vivo experiment protocol is shown in Figure 1(a). In order to explore the dynamic changes of biochemical indexes in vivo during tumor development, mice were sampled at two time points in this experiment. At the end of the experiment, there was no significant difference in body weight between the groups (Figure 1(b)). The results of FGST, reflecting exercise intensity; WEST, reflecting exercise endurance; and OFT, reflecting exercise willingness and ability, showed that all aspects of the exercise level indexes in the CRF group were significantly lower than those in the control group (Figures 1(c)–1(e)). At the beginning or after the beginning of the treatment, each fatigue index of mice gradually showed the fatigue state of mice. After the YFSJ treatment, all the indexes reflecting exercise were significantly improved. However, there was no significant difference in the effect of low-dose YFSJ and high-dose YFSJ, and only the total locomotion distance of the high group was higher than that of the low group in the OFT. These behavioral exercise indicators are important indicators to evaluate fatigue in various aspects. Therefore, our data show that the CRF model is successfully constructed, and YFSJ can effectively alleviate CRF.

3.2. YFSJ Reversed Cancer-Induced Mitochondrial Damage in Skeletal Muscle and Inflammation Levels. In order to explore the causes of CRF and the therapeutic effects of YFSJ, we analyzed the samples taken from mice, and the photos of mice before sampling are shown in Figure 2(a). HE staining showed tumor lesions in the lungs and liver of mice after intraperitoneal injection of LLC cells. In addition, LLC cell injection resulted in spleen enlargement and structural disorders (such as germinal center structural changes). High-dose YFSJ treatment could reverse spleen enlargement, but YFSJ has no obvious effect on the reversal of spleen substructural changes (Figure 2(b)). TEM showed that the structure of skeletal muscle fibers was disordered, the sarcoplasmic reticulum was dilated, and the number of mitophagosomes increased significantly in the CRF group. In the CRF group, muscle fiber arrangement was more disordered and structure was more loose at 28 days compared with 14 days. After YFSJ treatment, the number of mitophagosomes in skeletal muscle was significantly reduced, and the morphology of muscle fibers was significantly improved (Figure 2(c)). ELISA results showed that the serum levels of proinflammatory factors, such as IL-6 and TNF-α, were significantly increased in the CRF group, and the level of TNF-α in the CRF group was significantly higher at 28 days than at 14 days. YFSJ could significantly reverse the increase in proinflammatory factor level caused by the tumor, and the reverse effect was more obvious in the high group than in the low group (Figures 2(d) and 2(e)). Based on these results, we suggested that the occurrence of CRF and the therapeutic effect of YFSJ are highly correlated with the tumor inflammatory microenvironment and skeletal muscle mitophagy.

3.3. The Cause of CRF and the Mechanism by Which YFSJ Alleviates CRF Are Closely Related to Inflammation, Mitophagy, and Stat/HIF-1 Signaling Pathway. To explore the potential mechanism of YFSJ in alleviating CRF, RNA-seq was performed to identify the differentially expressed transcripts (DETs) in skeletal muscle tissues among different groups. As shown in Figures 3(a) (i) and 3(a) (ii) (left panels), the CRF group significantly upregulated the expression of 461 transcripts and downregulated the expression of 612 transcripts in skeletal muscle tissues of mice, compared to the control group, while YFSJ treatment significantly upregulated the expression of 776 transcripts and downregulated the expression of 1074 transcripts, compared with the CRF group (Figures 3(b) (i) and 3(b) (ii), right panel).

GO enrichment analysis based on the DETs between control, CRF, and high groups revealed multiple predicted potential functions. As shown in Figure 3(a) (iii), biological process (BP) analysis showed that DETs were mainly associated with intracellular signal transduction, programmed cell death, and cellular immunity. Cellular component (CC) analysis indicated that DETs were mainly involved in the structure of mitochondria. In the molecular function (MF) category, DETs were significantly enriched in signaling receptor binding, cytokine and hydrolase activity, and so on. As shown in Figure 3(b) (iii), BP analysis showed that DETs were associated with intracellular signal transduction, programmed cell death, proteolysis, and immune response. As to CC, DETs were significantly enriched in the mitochondrial membrane part. The MF analysis for these DETs includes lyase and cytokine activity, antioxidant activity, and signal transducer activity.

KEGG pathway analysis based on the DETs between the control and CRF groups revealed multiple enriched signaling pathways, including phagosome, mitophagy, oxidative phosphorylation, TNF signaling pathway, JAK-STAT signaling pathway, and HIF-1 signaling pathway (Figure 3(a) (iv)). Moreover, KEGG pathway analysis based on the DETs between the CRF and YFSJ groups demonstrated multiple enriched signaling pathways, including lysosome, mitophagy, oxidative phosphorylation, TNF signaling pathway, cytokine-cytokine receptor interaction, JAK-STAT signaling pathway, and HIF-1 signaling pathway (Figure 3(b) (iv)). The integrative analysis between the two comparisons (control vs. CRF and CRF vs. high) demonstrated that multiple signaling pathways were enriched in both comparisons. Notably, we find that both cytokine-cytokine receptor interaction, oxidative phosphorylation, and phagosome were significantly enriched in both comparisons, which encouraged us to further explore the regulatory effects of YFSJ on inflammatory cytokines, mitophagy, and activation of the Stat/HIF-1/mitochondria signaling pathway in skeletal muscle tissues of CRF mice.

3.4. In Vivo, YFSJ Alleviates CRF by Inhibiting Mitophagy Induced by the Stat3/HIF-1α/BNIP3 Signaling Pathway Overactivation in Skeletal Muscle. Further verification of YFSJ treatment on autophagy and inflammatory infiltration

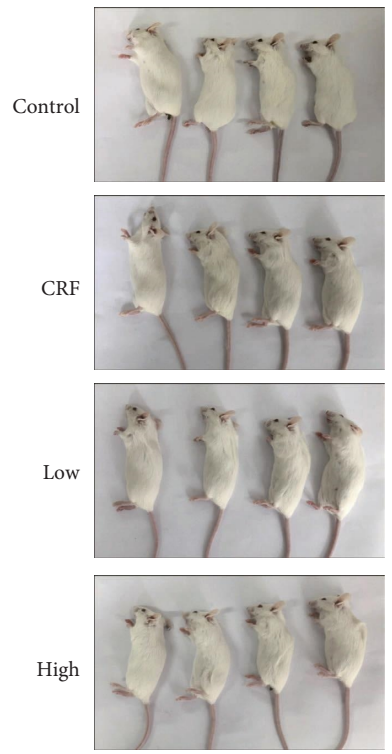

(a)

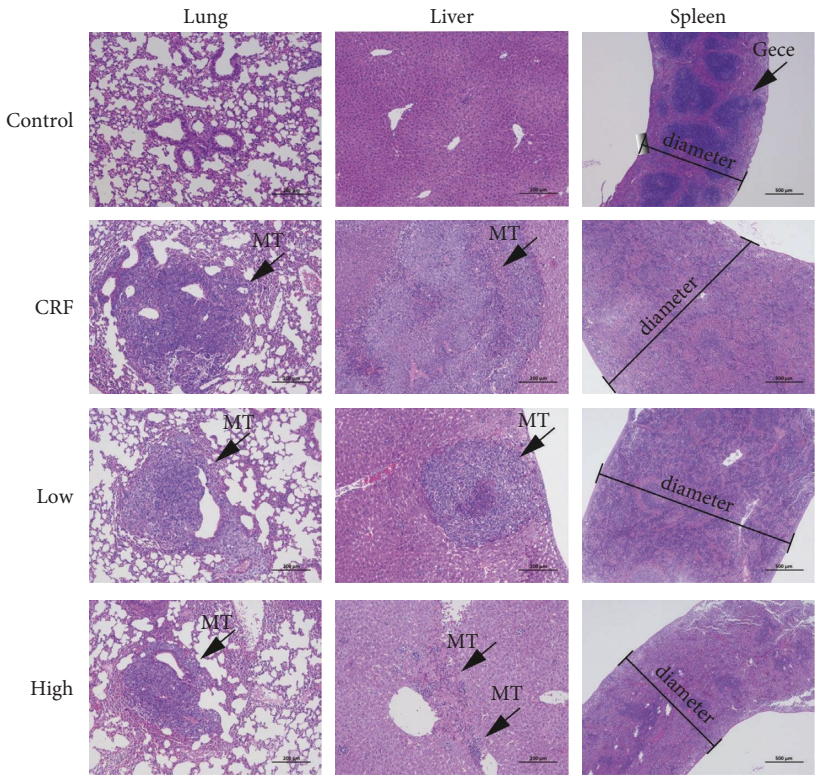

(b)

Figure 2: Continued.

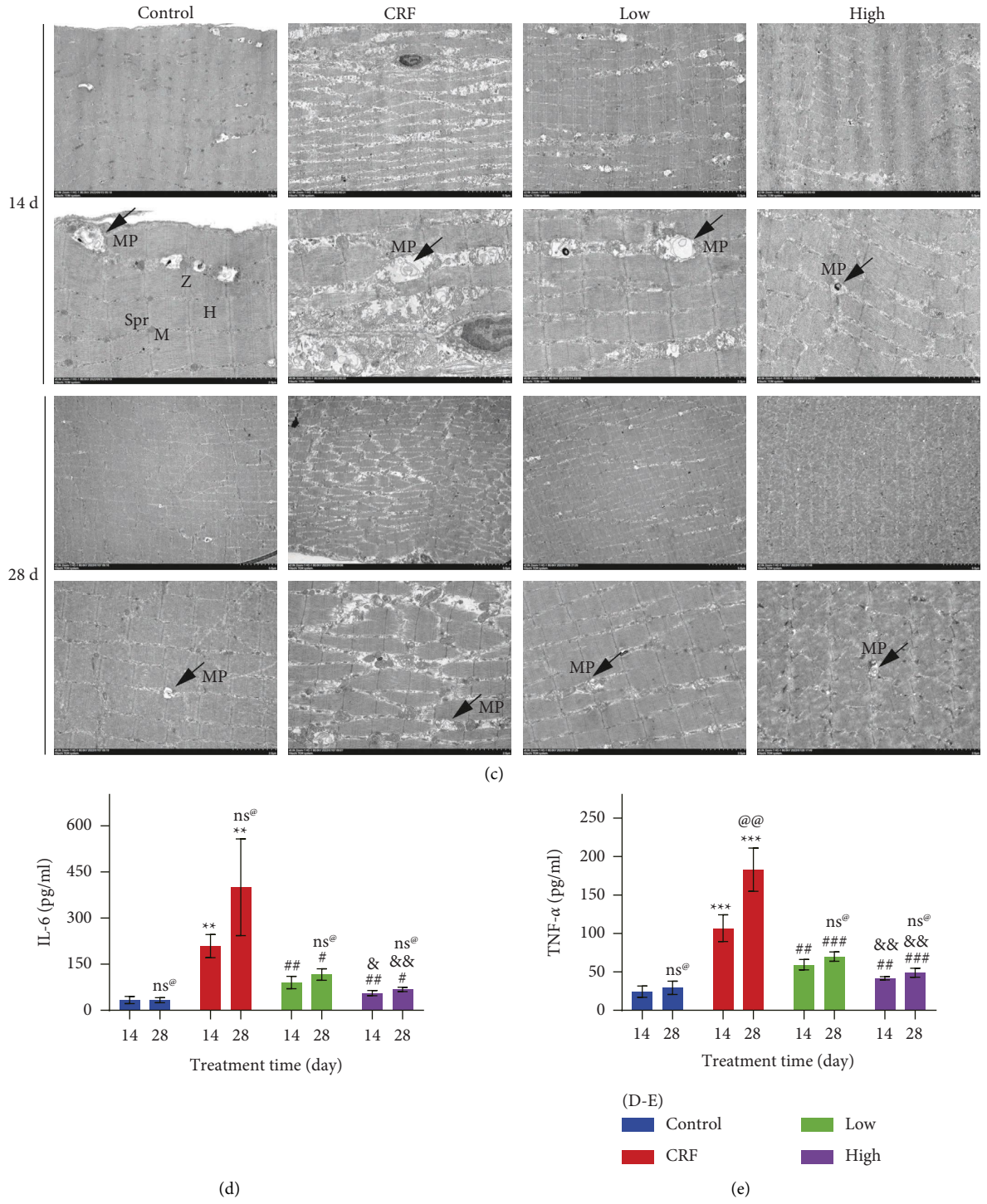

Figure 2: YFSJ reversed cancer-induced mitochondrial damage in skeletal muscle and inflammation levels. (a) Pictures of 28 day mice before sample collection. (b) Representative HE staining slice images of lung, liver, and spleen from 28 day mice; lung and liver, scale bars = 200 μm; spleen, scale bars = 500 μm; MT means metastasis; gece means germinal center. (c) Representative TEM slices images of skeletal muscle; scale bars = 5 μm or 2 μm; MP means mitophagosome; Spr means sarcoplasmic reticulum; *M* means mitochondrion; *Z* means *Z* disk; *H* means *H* band. (d) and (e) IL-6 and TNF-α concentrations in mice serum; data were presented as mean ± SD; $^{**}p < 0.01$ and $^{***}p < 0.001$ compared with the control group; $^{\#}p < 0.05$, $^{\#\#}p < 0.01$, $^{\#\#\#}p < 0.001$ compared with the CRF group; $^{\&}p < 0.05$ and $^{\&\&}p < 0.01$ compared with the low group; $^{ns@}p > 0.05$ and $^{@@}p < 0.01$ compared with the 14 day group; $n = 4$.

of skeletal muscle tissues by performing IHC staining revealed an increase in the percentage of positively stained Beclin 1, LC3, CD68, and CD206 cells and a decrease in the percentage of positively stained p62 cells in the skeletal muscle tissues of CRF mice, while YFSJ treatment significantly reversed the percentage of positively stained cells

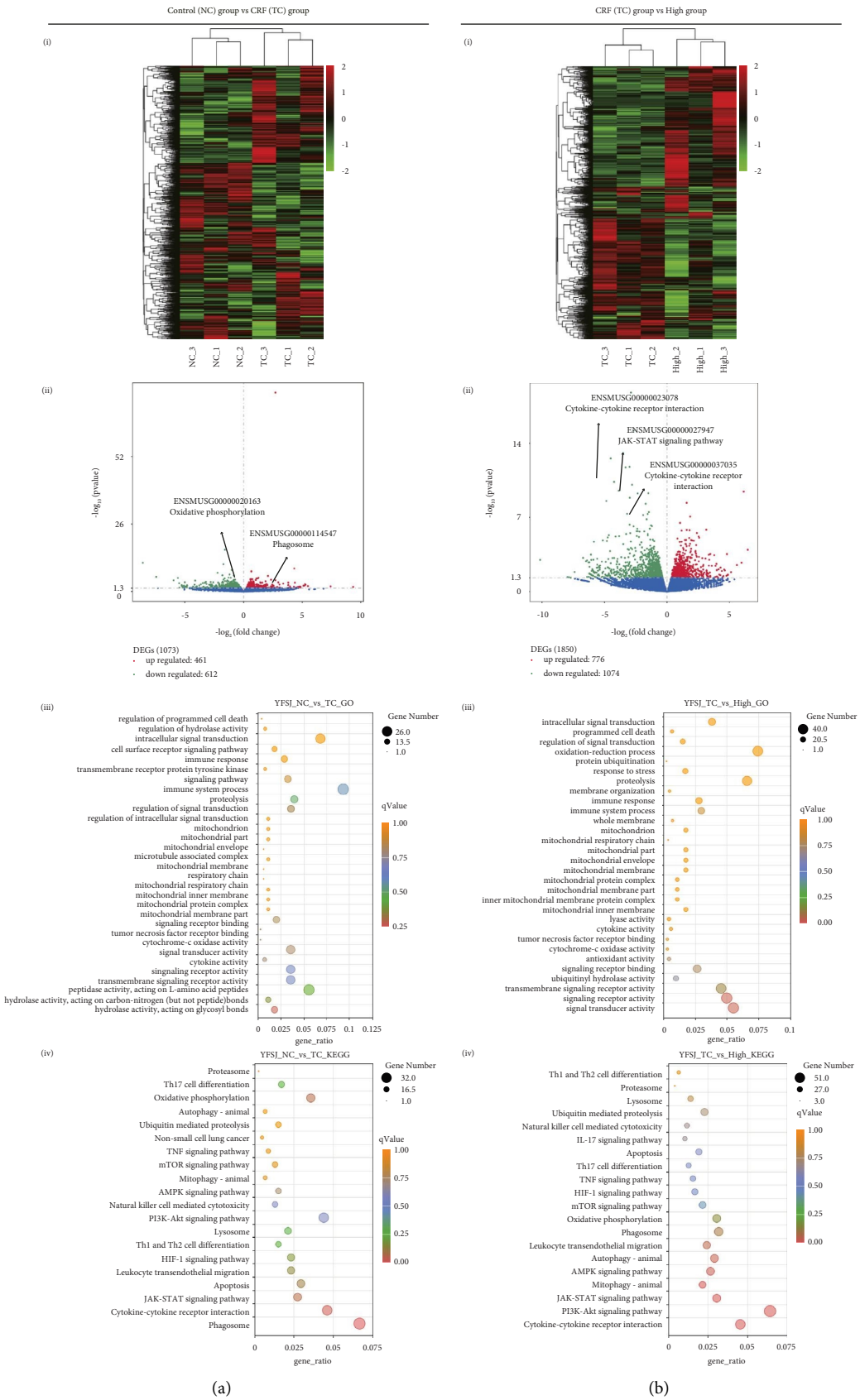

FIGURE 3: YFSJ treatment on gene expression profiling of skeletal muscle tissues in CRF mice. RNA-seq was performed to determine the DETs in skeletal muscle tissues from each group. (a) Comparison of control group with CRF group. (b) Comparison of CRF group with high group. (i) Hierarchical clustering plots and (ii) volcano plots were used to compare gene expression profiles ($|\text{fold change}| \geq 2$, $p < 0.05$). (iii) GO enrichment analysis was performed based on the DETs from both comparisons, from top to bottom are BP, CC, and MF, respectively. (iv) KEGG enrichment analysis was performed to identify the enriched signaling pathway in both comparisons $n = 3$.

(Figure 4(a)). To further confirm the increased level of autophagy in skeletal muscle mitochondria in the CRF group and the effective reversal of excessive mitophagy by YFSJ, total protein and mitochondrial protein were extracted from skeletal muscle tissues for analysis. WB analysis of total protein of skeletal muscle tissue indicated that P-Stat3 and HIF-1α protein expression levels were increased in the CRF group, and YFSJ treatment significantly reversed these changes, and the reversal effect in the high group was more obvious than that in the low group. Moreover, WB analysis of mitochondrial proteins in skeletal muscle tissue indicated that HIF-1α, BNIP3, Beclin 1, Atg7, and LC3B protein expression levels were increased, while p62 protein expression levels were decreased in the CRF group. Similarly, YFSJ treatment reversed these changes in the CRF group, and the effect was more pronounced in the high group than in the low group (except for p62) (Figures 4(b)–4(d)). Therefore, these results indicated that YFSJ can attenuate tumor-induced inflammatory infiltration and overactivation of mitophagy in skeletal muscle tissue.

3.5. Quercetin Is an Active Component of YFSJ Acting on the Stat3-Related Signaling Pathway. The LC/MS results of YFSJ are shown in Figure 5(a). By comparing the LC/MS results with the database, we obtained quercetin, one of the active components of YFSJ (Figure 5(b)). We used TCMNPAS to perform molecular docking between quercetin and Stat3 protein and verified the docking results, which were visualized using software PMV-1.5.7 (DeLano Scientific LLC). The 3D structures of quercetin and Stat3 protein and its phosphorylation sites are shown in Figures 5(c) and 5(d). Molecular docking results show that the binding site of quercetin to Stat3 is highly coincident with the phosphorylation site of Stat3, and the "absolute value of affinity" is relatively large, indicating that the binding of the two is relatively stable. We conducted RMSD verification on the predicted molecular docking modes of quercetin and Stat3, and the results showed that the RMSD values of all the predicted docking modes are less than 2. This suggests that the binding of quercetin to the phosphorylation site of Stat3 is feasible at the level of molecular interaction. In summary, we predict that quercetin, an active component in YFSJ, can effectively and specifically inhibit Stat3 phosphorylation, thereby inhibiting the overactivation of the Stat3/HIF-1α/BNIP3 signaling pathway caused by abnormal phosphorylation of Stat3, and ultimately inhibiting excessive mitophagy.

3.6. Quercetin Can Reverse TNF-α-Induced Mitophagy in C2C12 Myoblasts. In order to determine which inflammatory factors activate mitophagy and whether quercetin can inhibit mitophagic cell death in skeletal muscle induced by inflammatory factors, we used C2C12 myoblasts to establish an in vitro skeletal muscle model. MTT colorimetric results showed that TNF-α inhibited the viability of C2C12 myoblasts much more than IL-6 (Figures 6(a) and 6(b)). Therefore, TNF-α was selected for subsequent in vitro experiments. Although both YFSJ and quercetin alone had effects on the viability of C2C12 myoblasts, their effects were minor (Figures 6(c) and 6(d)). Our results showed that YFSJ, quercetin, and 3-MA could reverse the inhibitory effect of TNF-α on C2C12 myoblasts to a large extent (Figure 6(e)). 3-MA was used here as a positive control for the inhibition of autophagy. MDC autophagy staining showed that TNF-α could significantly induce autophagy in C2C12 myoblasts, which could be reversed by YFSJ, quercetin, and 3-MA (Figure 6(f)). The results of MDC autophagy staining would be even more significant if considering the decrease in cell number caused by TNF-α inhibition of C2C12 myoblast proliferation.

To further confirm that TNF-α can induce mitophagy in C2C12 myoblasts, thereby inhibiting the proliferation of C2C12 myoblasts. We used WB to analyze the total protein and mitochondrial protein of C2C12 myoblasts treated with each factor. WB results showed that the expressions of P-Stat3 and HIF-1α in total proteins increased significantly after TNF-α treatment, which was reversed by YFSJ and quercetin treatment, but not by 3-MA treatment. Moreover, TNF-α treatment increased the protein expression of HIF-1α, BNIP3, Beclin1, Atg7, and LC3B and decreased the protein content of p62 in mitochondria. YFSJ and quercetin treatment significantly reversed these changes, and 3-MA also reversed these changes (except HIF-1α and BNIP3) (Figures 6(g)–6(i)). These evidence suggest that TNF-α can effectively induce mitophagy in C2C12 myoblasts, thereby inhibiting the proliferation of C2C12 myoblasts, while YFSJ and quercetin can restore the viability of C2C12 myoblasts by reversing TNF-α induced mitophagy.

4. Discussion

CRF is an uncomfortable symptom associated with the occurrence and development of cancer, which seriously affects the quality of life of cancer patients [25]. Because the mechanism of CRF is not completely clear, it brings difficulties in the clinical prevention and treatment of the disease. So far, there is no accepted treatment method for CRF. Ethnomedicine, represented by traditional Chinese medicine (TCM), is considered a potential treatment for CRF because TCM has many prescriptions for fatigue [26, 27]. According to our study, we demonstrated that Chinese medicine YFSJ can effectively alleviate CRF. Meanwhile, the pathogenesis of CRF, the effect target, and the underlying molecular mechanism of YFSJ were revealed.

In the process of tumor growth, the body will produce a lot of proinflammatory factors [28], making the body of cancer patients always in a state of high inflammation level [29]. This result was consistent with our studies. Our in vivo results demonstrated that the growth of tumor cells leads to an increase in the level of proinflammatory cytokines in serum, which in turn increases the level of inflammatory infiltration of muscle cells. YFSJ treatment can effectively reduce the level of proinflammatory factors in serum, thereby reducing the degree of inflammatory infiltration of muscle cells. At the same time, the size of the spleen can also reflect the level of inflammation in vivo to a certain extent [30]. We also found that the spleen of mice was significantly

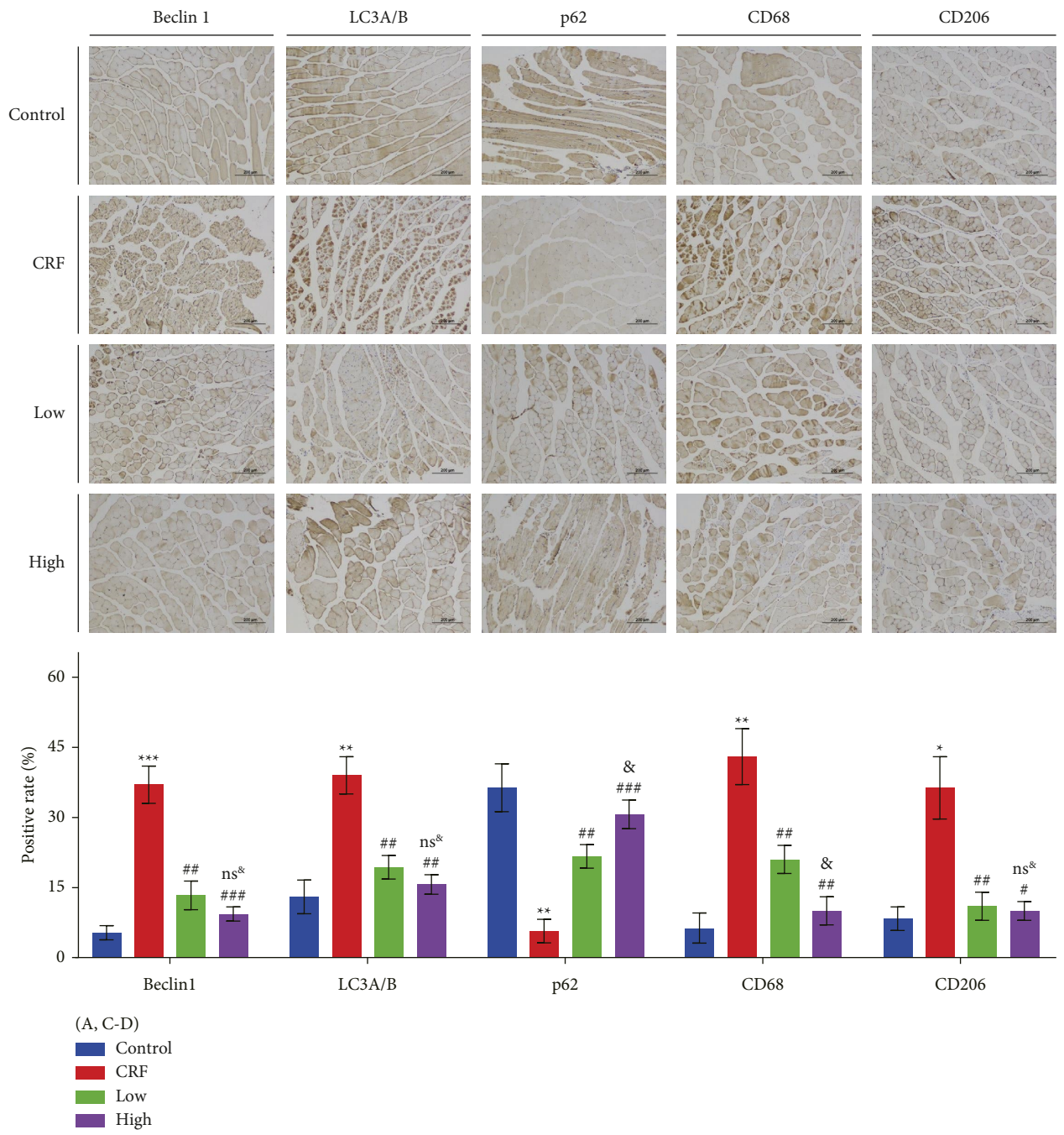

(a)

Figure 4: Continued.

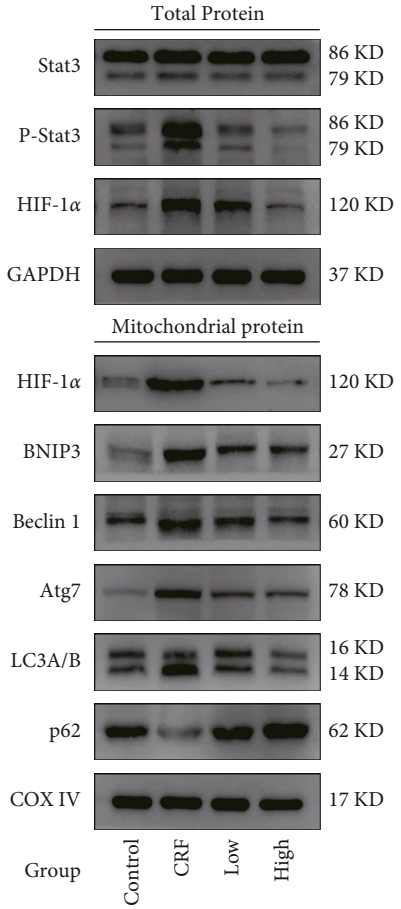

(b)

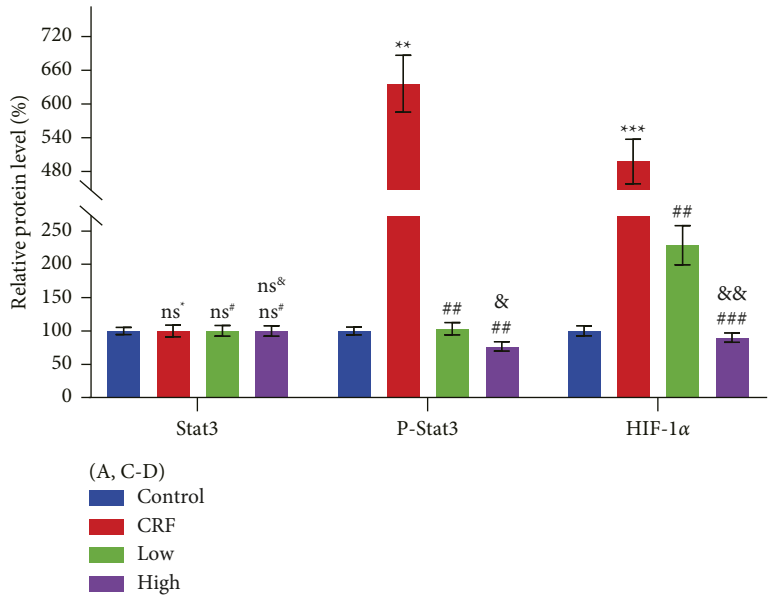

(c)

Figure 4: Continued.

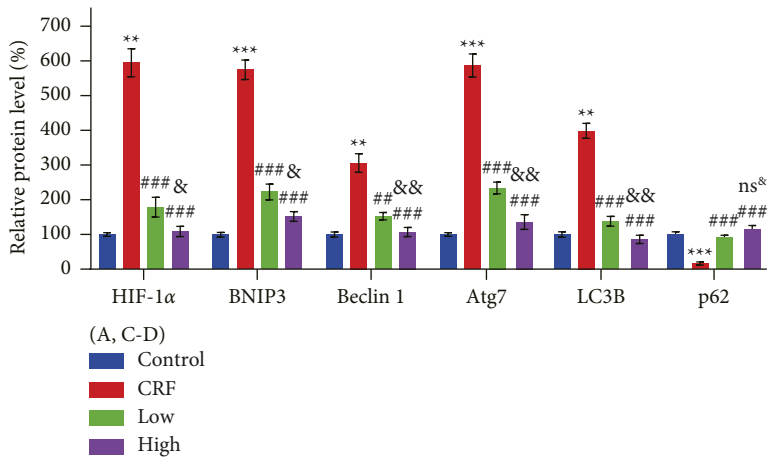

(d)

Figure 4: YFSJ alleviates CRF by inhibiting mitophagy induced by the Stat3/HIF-1α/BNIP3 signaling pathway overactivation in skeletal muscle. (a) The IHC staining and their relative expression levels were performed to observe proteins associated with autophagy and inflammation in skeletal muscle tissues of mice from each group. (b) WB analysis was performed to determine the protein expression of the Stat3/HIF-1α/BNIP3 signaling pathway and mitophagy-related proteins and (c, d) their relative expression levels. GAPDH or COX IV was used as the internal control. Data were presented as mean ± SD; $^{ns*}p > 0.05$, $^{*}p < 0.05$, $^{**} < 0.01$, and $^{***}p < 0.001$ compared to the control group; $^{ns\#}p > 0.05$, $^{\#}p < 0.05$, $^{\#\#}p < 0.01$, and $^{\#\#\#}p < 0.001$ compared to the CRF group; $^{ns\&}p > 0.05$, $^{\&}p < 0.05$, and $^{\&\&}p < 0.01$ compared to the low group; $n = 3$.

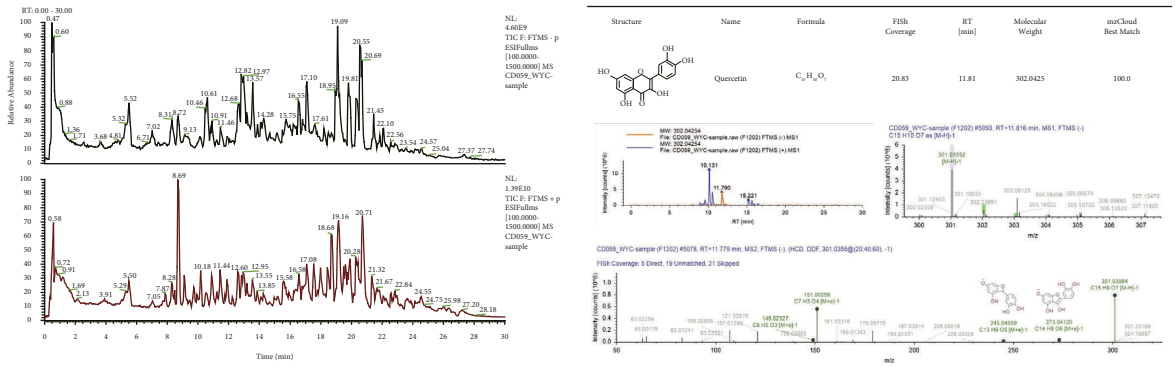

(a) (b)

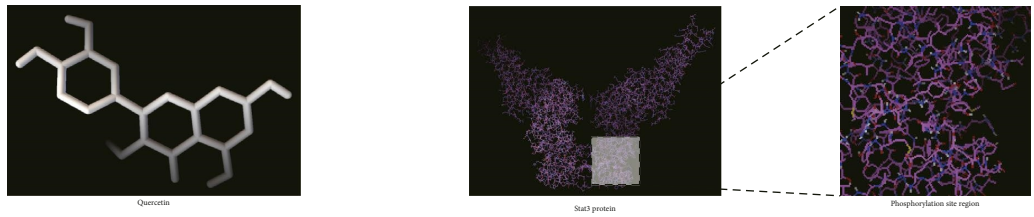

(c) (d)

Figure 5: Continued.

Molecular docking results of Quercetin and Stat3

Mode	Docking	Affinity	RMSD
(1)	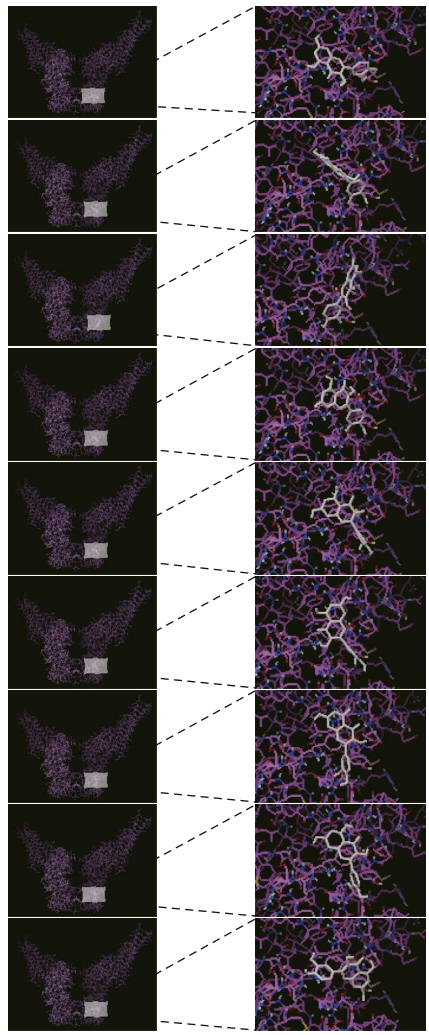	-4.8	1.454
(2)		-4.7	1.145
(3)		-4.3	0.721
(4)		-4.1	0.565
(5)		-4	0.815
(6)		-4	1.376
(7)		-4	0.84
(8)		-4	0.709
(9)		-4	1.513

(e)

Figure 5: Quercetin is an active component of YFSJ acting on the Stat3-related signaling pathway. (a) Total ion current profiles for identification of natural products in samples (black is the total ion current diagram in negative ion mode and red is the total ion current diagram in positive ion mode). (b) The information of the compound (quercetin) obtained by matching the LC/MS map with the database. (c) The 3D structure of quercetin. (d) The 3D structure and phosphorylation site of Stat3 protein. (e) Molecular docking mode prediction of quercetin and Stat3 and its "affinity" and "RMSD."

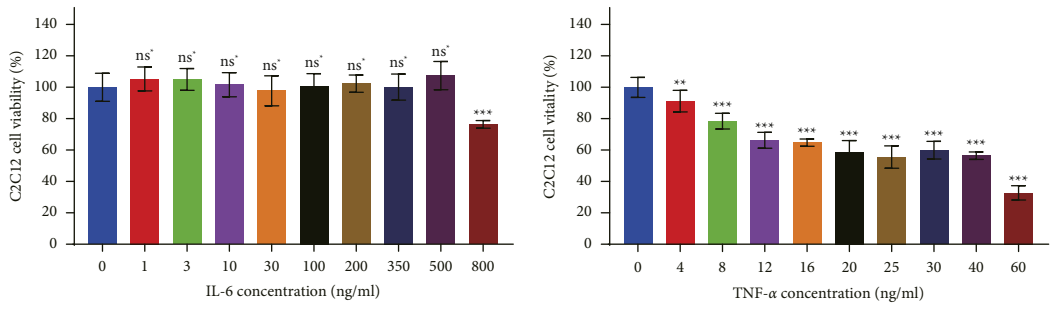

(a) (b)

Figure 6: Continued.

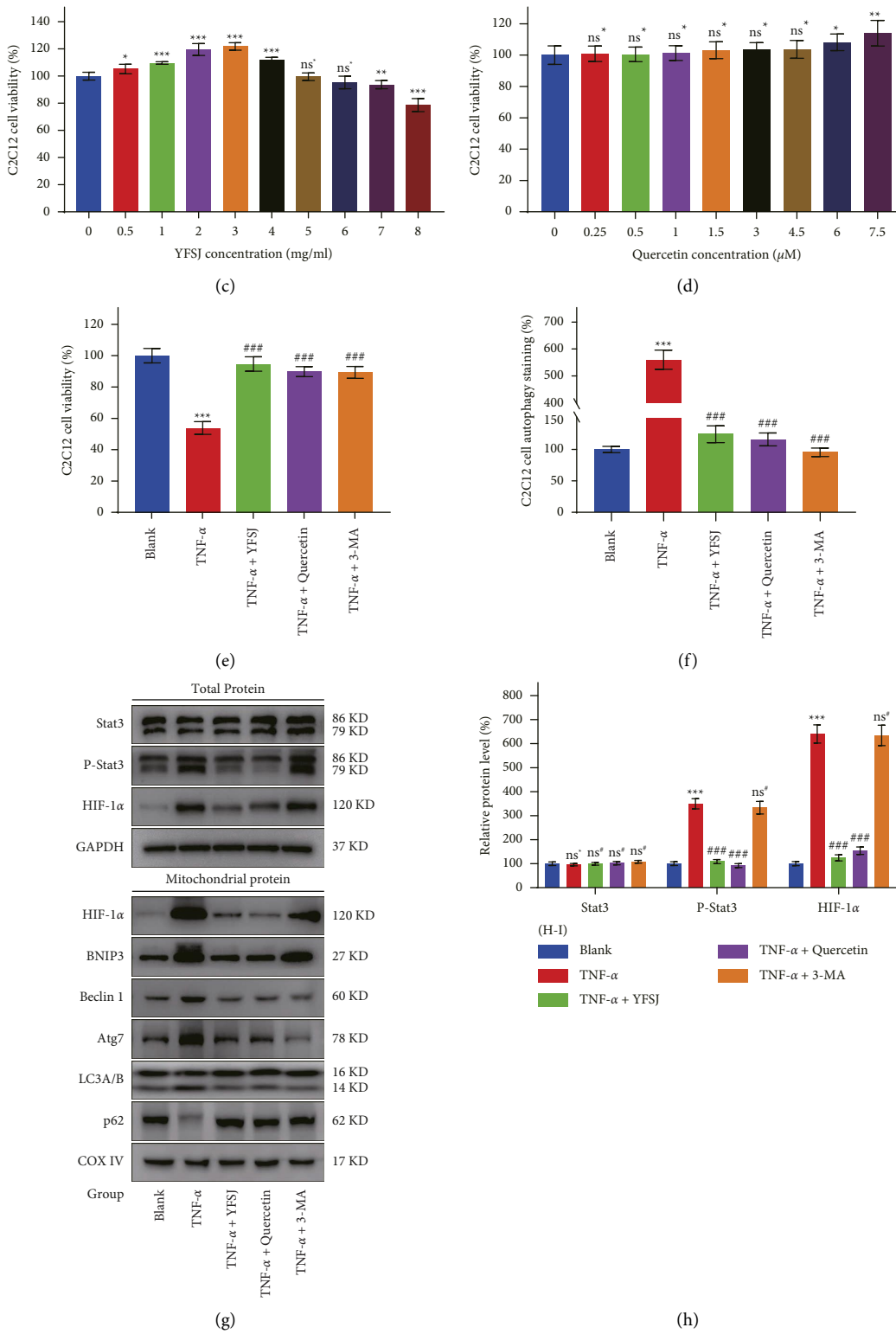

Figure 6: Continued.

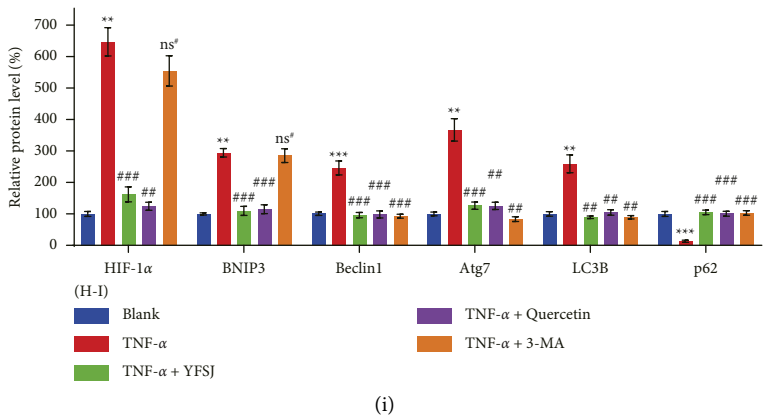

(i)

Figure 6: Quercetin can reverse TNF-α-induced mitophagy in C2C12 myoblasts. (a–d) Effect of IL-6, TNF-α, YFSJ, and quercetin on the viability of C2C12 myoblasts, respectively, $n = 3$. (e) Reverse effect of YFSJ (2 mg/ml), quercetin (1.5 μM), and 3-MA (pretreatment with 2 mM for 4 h) on TNF-α (20 ng/ml)-induced decline viability and (f) increase autophagy in C2C12 myoblast, $n = 3$. (g) WB analysis was performed to determine the protein expression of the Stat3/HIF-1α/BNIP3 signaling pathway and mitophagy related proteins, and (h, i) their relative expression levels. GAPDH or COX IV was used as the internal control. Data were presented as mean ± SD; $^{ns*}p > 0.05$, $^{**}p < 0.01$, and $^{***}p < 0.001$ compared with the blank group; $^{ns\#}p > 0.05$, $^{\#\#}p < 0.01$, and $^{\#\#\#}p < 0.001$ compared with the TNF-α group; $n = 3$.

enlarged after tumor cell inoculation and decreased after high-dose YFSJ treatment compared with the CRF group.

Mitochondria are important places for energy production in the body. The low mitochondrial function will lead to a lack of enough energy in the body, resulting in decreased exercise ability and a sense of fatigue [31]. We observed that the number of mitophagosomes was positively correlated with the degree of fatigue in mice. Our data confirmed that after the injection of tumor cells, all aspects of the motor indexes of mice showed varying degrees of decline, which directly indicated that the growth of tumor cells would cause fatigue in the host body. Fortunately, after YFSJ treatment, all exercise indexes reflecting fatigue degree were improved to a great extent, which indicated that YFSJ could effectively alleviate CRF.

High levels of inflammation in the body lead to mitophagy in skeletal muscle [32]. Our previous studies also confirmed that the occurrence of CRF is closely related to the damage of skeletal muscle [4]. Studies have shown that the tumor inflammatory microenvironment can continuously activate STAT3-related signaling pathways [33]. Therefore, we linked inflammation, Stat3 molecular-related signaling pathways, and mitophagy with the occurrence of CRF and the therapeutic effect of YFSJ. Activation by Stat3 phosphorylation promotes HIF-1α expression in the cytoplasm [34], and the HIF-1α in the cytoplasm binds to the mitochondrial membrane [35], further promoting the expression of BNIP3 in the mitochondria [36]. The BH3 domain of BNIP3 competes with Beclin 1 to bind Bcl-2 or Bcl-xL, resulting in the formation of complexes between Beclin 1 and Class III PI3K, which activates mitophagy. At the mature stage of the autophagosome, BNIP3 can recruit the autophagy-related protein LC3 to the mitochondria. It promotes the formation of autophagosomes and actively participates in the clearance of damaged mitochondria [37]. Atg7 is a key component involved in autophagosome formation [38], and p62 is a marker of autophagic lysosomes. When autophagy occurs, lysosomes are degraded, and the expression of p62 will decrease [39]. Our data confirm that the tumor inflammatory microenvironment in vivo abnormally activates the Stat3/HIF-1α/BNIP3 signaling pathway in skeletal muscle, leading to excessive mitophagy, which disrupts the body's energy balance and ultimately leads to fatigue.

To further validate the in vivo results and simplify the experimental model, we treated C2C12 myoblasts with TNF-α to mimic the inflammatory infiltration of skeletal muscle in vitro. Consistent with our in vivo results, TNF-α significantly induced mitophagy and inhibited cell viability in C2C12 myoblasts. YFSJ and quercetin, the active component of YFSJ, significantly reversed TNF-α-induced mitophagy and cell viability inhibition in C2C12 myoblasts. 3-MA is an inhibitor of PI3K. It is widely used as an inhibitor of autophagy by inhibiting class III PI3K [40]. Therefore, it is able to prevent BNIP3 from further activating Beclin1, ultimately inhibiting the occurrence of autophagy. Data showed that 3-MA reversed TNF-α-induced autophagy in C2C12 myoblasts. These evidence further confirmed that TNF-α plays an important role in activating mitophagy, leading to CRF, and quercetin plays an important role in YFSJ treatment of CRF.

In summary, YFSJ acts as a traditional Chinese medicine compound, which may alleviate CRF through the action of multiple targets (Figure 7). Firstly, it reduces the level of proinflammatory factors in the body, thereby reducing the degree of inflammatory infiltration of skeletal muscle cells. Secondly, it inhibits the overphosphorylation of Stat3 protein (quercetin, an active ingredient in YFSJ, may be at work here), thereby inhibiting the overactivation of the Stat3/HIF-1α/BNIP3 signaling pathway. Finally, it inhibits excessive mitophagy and alleviates CRF under the action of multiple targets. Our results not only confirm that YFSJ is an effective

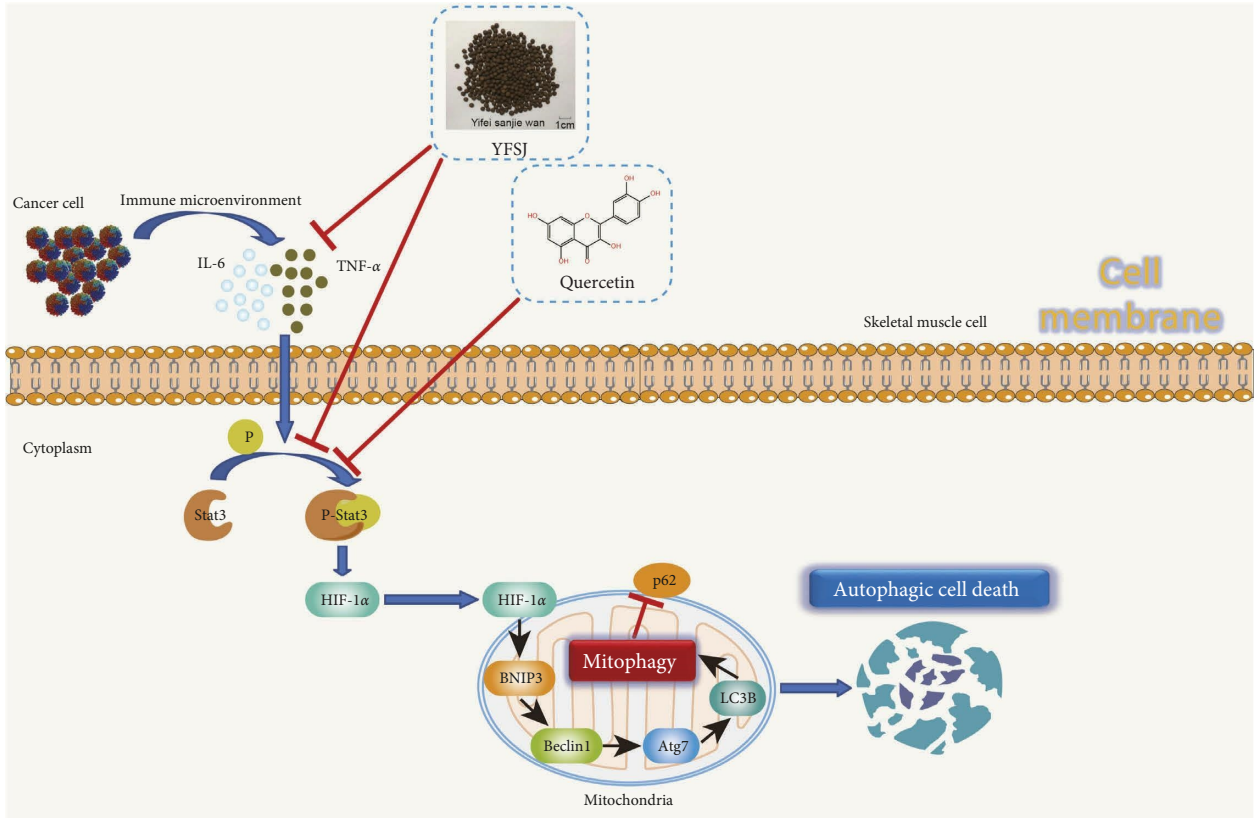

Figure 7: Schematic illustration of the potential underlying mechanism responsible for YFSJ and its component quercetin alleviating CRF.

regimen for the treatment of CRF but also reveal the pathogenesis of the disease and, at the same time, provide new clues for the development of drugs with natural compounds from ethnomedicine.

5. Conclusions

YFSJ and its component quercetin can inhibit the overactivation of skeletal muscle mitophagy mediated by the abnormal activation of the Stat3/HIF-1α/BNIP3 signaling pathway induced by the tumor inflammatory microenvironment, thereby alleviating CRF.

Abbreviations

YFSJ: Yifei-Sanjie pill
CRF: Cancer-related fatigue
HE: Hematoxylin and eosin
TEM: Transmission electron microscope
ELISA: Enzyme-linked immunosorbent assay
IHC: Immunohistochemical
WB: Western blotting
LC/MS: High resolution liquid/mass spectrometry.

Data Availability

All data of this study are available from the first author Yingchao Wu and the corresponding author Mingzi Ouyang if needed. Datasets for RNA-seq can be obtained from the Sequence Read Archive at the NCBI (URL: https://www.ncbi.nlm.nih.gov/sra/PRJNA874361).

Disclosure

Yingchao Wu and Shuyao Zhou are co-first authors. Lizhu Lin and Mingzi Ouyang are co-corresponding authors.

Conflicts of Interest

The authors declare that there are no conflicts of interest regarding the publication of this paper.

Authors' Contributions

Yingchao Wu and Shuayao Zhou performed the experiments and wrote the manuscript; Dajin Pi, Zhongjia Yi, and Yiliu Chen conducted the experiments and analyzed the data; Yangyang Dong, Wuhong Wang, and Huan Ye participated in the revision of the manuscript; Lizhu Lin provided the YFSJ pills and LLC cells used in the study; and Mingzi Ouyang designed the study and provided the initial idea. All authors read and approved the final manuscript. Yingchao Wu and Shuyao Zhou contributed equally to this work.

Acknowledgments

This study was supported by the National Natural Science Foundation of China (grant nos. 81873155 and 81403340).

References

[1] E. M. Crimmins, "Lifespan and Healthspan: Past, Present, and Promise," *GERONTOLOGIST*, vol. 55, no. 6, pp. 901–911, 2015.

[2] X. Cen, D. Wang, W. Sun et al., "The trends of mortality and years of life lost of cancers in urban and rural areas in China, 1990-2017," *Cancer Medicine*, vol. 9, no. 4, pp. 1562–1571, 2020.

[3] L. Lan, Y. Cai, T. Zhang, R. Wu, M. Xue, and Q. Meng, "Influencing factors of inpatient expenditure pattern for cancer in China, 2015," *Chinese Journal of Cancer Research*, vol. 29, no. 1, pp. 11–17, 2017.

[4] Y. Wu, D. Pi, Y. Chen, Q. Zuo, L. Lin, and M. Ouyang, "Yifei sanjie pills alleviate chemotherapy-related fatigue by reducing skeletal muscle injury and inhibiting tumor growth in lung cancer mice," *Evidence-based Complementary and Alternative Medicine*, vol. 2022, Article ID 2357616, 19 pages, 2022.

[5] P. Fan, X. H. Xie, C. H. Chen et al., "Molecular regulation mechanisms and interactions between reactive oxygen species and mitophagy," *DNA and Cell Biology*, vol. 38, no. 1, pp. 10–22, 2019.

[6] I. Gkikas, K. Palikaras, and N. Tavernarakis, "The role of mitophagy in innate immunity," *Frontiers in Immunology*, vol. 9, p. 1283, 2018.

[7] Y. Wang, N. Liu, and B. Lu, "Mechanisms and roles of mitophagy in neurodegenerative diseases," *CNS Neuroscience and Therapeutics*, vol. 25, no. 7, pp. 859–875, 2019.

[8] T. Zhu, J. Han, L. Yang et al., "Immune microenvironment in osteosarcoma: components, therapeutic strategies and clinical applications," *Frontiers in Immunology*, vol. 13, Article ID 907550, 2022.

[9] D. E. Friesen, V. E. Baracos, and J. A. Tuszynski, "Modeling the energetic cost of cancer as a result of altered energy metabolism: implications for cachexia," *Theoretical Biology and Medical Modelling*, vol. 12, no. 1, p. 17, 2015.

[10] L. Wenjiao, O. Mingzi, L. Lizhu, and Z. Jingxu, "Effects of yiqi chutan decoction on chemotherapy-related fatigue of patients with non-small cell lung cancer," *Guiding Journal of Traditional Chinese Medicine and Pharmacy*, vol. 21, no. 10, pp. 31–34, 2015.

[11] G. Jieshan, O. Mingzi, X. Zhiwei, L. Lizhu, and Z. Kexue, "Effects of yiqi chutan decoction on chemotherapy-related fatigue," *Liaoning Journal of Traditional Chinese Medicine*, vol. 496, no. 6, pp. 1211–1213, 2016.

[12] Y. Wu, Y. Chen, D. Pi, and M. Ouyang, "Review and prospect: prevention and treatment of lung related malignant tumors by tonifying qi and resolving phlegm method," *World Scientific Research Journal*, vol. 7, no. 12, pp. 229–235, 2021.

[13] Y. Wu, D. Pi, Y. Chen, and M. Ouyang, "Research progress on pathogenesis and treatment of cancer-related fatigue," *Frontiers in Science and Engineering*, vol. 1, no. 6, pp. 158–166, 2021.

[14] Z. Wang, Z. Wu, Q. Xiang et al., "Effects of botanical drugs in the treatment of cancer-related fatigue in patients with gastric cancer: a meta-analysis and prediction of potential pharmacological mechanisms," *Frontiers in Pharmacology*, vol. 13, Article ID 979504, 2022.

[15] P. K. Raghav and Z. Mann, "Cancer stem cells targets and combined therapies to prevent cancer recurrence," *Life Sciences*, vol. 277, Article ID 119465, 2021.

[16] Y. Heike, M. Takahashi, T. Ohira et al., "Genetic immunotherapy by intrapleural, intraperitoneal and subcutaneous injection of IL-2gene-modified Lewis lung carcinoma cells," *International Journal of Cancer*, vol. 73, no. 6, pp. 844–849, 1997.

[17] A. Aartsma-Rus and M. van Putten, "Assessing functional performance in the mdx mouse model," *Journal of Visualized Experiments*, vol. 85, Article ID 51303, 2014.

[18] P. He, L. Chen, X. Qin, G. Du, and Z. Li, "Astragali Radix-CodonopsisRadix-Jujubae Fructus water extracts ameliorate exercise-induced fatigue in mice via modulating gut microbiota and its metabolites," *Journal of the Science of Food and Agriculture*, vol. 102, no. 12, pp. 5141–5152, 2022.

[19] L. Zhong, L. Zhao, F. Yang, W. Yang, Y. Sun, and Q. Hu, "Evaluation of anti-fatigue property of the extruded product of cereal grains mixed with Cordyceps militaris on mice," *Journal of the International Society of Sports Nutrition*, vol. 14, no. 1, p. 15, 2017.

[20] X. L. Wang, S. T. Feng, Y. T. Wang et al., "Mangiferin, a natural glucoxilxanthone, inhibits mitochondrial dynamin-related protein 1 and relieves aberrant mitophagic proteins in mice model of Parkinson's disease," *Phytomedicine*, vol. 104, Article ID 154281, 2022.

[21] Y. Wu, D. Pi, Y. Chen, Q. Zuo, S. Zhou, and M. Ouyang, "Ginsenoside Rh4 inhibits colorectal cancer cell proliferation by inducing ferroptosis via autophagy activation," *Evidence-based Complementary and Alternative Medicine*, vol. 2022, pp. 1–19, 2022.

[22] A. M. Sysel, V. E. Valli, R. B. Nagle, and J. A. Bauer, "Immunohistochemical quantification of the vitamin B12 transport protein (TCII), cell surface receptor (TCII-R) and Ki-67 in human tumor xenografts," *Anticancer Research*, vol. 33, no. 10, pp. 4203–4212, 2013.

[23] A. N. Vis, R. Kranse, A. L. Nigg, and T. H. van der Kwast, "Quantitative analysis of the decay of immunoreactivity in stored prostate needle biopsy sections," *American Journal of Clinical Pathology*, vol. 113, no. 3, pp. 369–373, 2000.

[24] S. Liu, Q. Li, F. Liu et al., "Uncovering the mechanism of curcuma in the treatment of ulcerative colitis based on network pharmacology, molecular docking Technology, and experiment verification," *Evidence-based Complementary and Alternative Medicine*, vol. 2021, Article ID 6629761, 14 pages, 2021.

[25] J. Wang and Y. Cai, "Study on cancer-related fatigue, quality of life and immunity function in advanced non-small cell lung cancer patients," *Chinese Journal of Nosocomiology*, vol. 21, no. 24, pp. 5217–5219, 2011.

[26] Y. Ling, "Traditional Chinese medicine in the treatment of symptoms in patients with advanced cancer," *Annals of Palliative Medicine*, vol. 2, no. 3, pp. 141–152, 2013.

[27] S. Wang, S. Long, and W. Wu, "Application of traditional Chinese medicines as personalized therapy in human cancers," *The American Journal of Chinese Medicine*, vol. 46, no. 05, pp. 953–970, 2018.

[28] N. Inácio Pinto, J. Carnier, L. M. Oyama et al., "Cancer as a proinflammatory environment: metastasis and cachexia," *Mediators of Inflammation*, vol. 2015, Article ID 791060, 2015.

[29] F. De Vita, M. Orditura, A. Auriemma, S. Infusino, and G. Catalano, "Serum concentrations of proinflammatory cytokines in advanced non small cell lung cancer patients," *Journal of Experimental & Clinical Cancer Research*, vol. 17, no. 4, pp. 413–417, 1998.

[30] N. C. Araujo and J. H. R. Suassuna, "The spleen size in patients undergoing hemodialysis," *Brazilian Journal of Nephrology*, vol. 43, no. 1, pp. 61–67, 2021.

[31] K. Filler, D. Lyon, J. Bennett et al., "Association of mitochondrial dysfunction and fatigue: a review of the literature," *BBA Clinical*, vol. 1, pp. 12–23, 2014.

[32] J. M. Yuk, P. Silwal, and E. K. Jo, "Inflammasome and mitophagy connection in Health and disease," *International Journal of Molecular Sciences*, vol. 21, no. 13, p. 4714, 2020.

[33] C. Ren, T. An, X. Zhao, Y. Liu, and Y. Luo, "Effects of angelica sinensis polysaccharide on BMSCs proliferation and STAT3 signaling pathway in inflammatory microenvironment," *China Journal of Traditional Chinese Medicine and Pharmacy*, vol. 35, no. 10, pp. 5274–5278, 2020.

[34] J. E. Jung, H. S. Kim, C. S. Lee et al., "STAT3 inhibits the degradation of HIF-1α by pVHL-mediated ubiquitination," *Experimental & Molecular Medicine*, vol. 40, no. 5, pp. 479–485, 2008.

[35] W. N. Xu, H. L. Zheng, R. Z. Yang et al., "Mitochondrial NDUFA4L2 attenuates the apoptosis of nucleus pulposus cells induced by oxidative stress via the inhibition of mitophagy," *Experimental & Molecular Medicine*, vol. 51, no. 11, pp. 1–16, 2019.

[36] W. L. Xu, S. H. Wang, W. B. Sun et al., "Insufficient radiofrequency ablation-induced autophagy contributes to the rapid progression of residual hepatocellular carcinoma through the HIF-1α/BNIP3 signaling pathway," *BMB Reports*, vol. 52, no. 4, pp. 277–282, 2019.

[37] A. H. Chourasia and K. F. Macleod, "Tumor suppressor functions of BNIP3 and mitophagy," *Autophagy*, vol. 11, no. 10, pp. 1937-1938, 2015.

[38] H. Cawthon, R. Chakraborty, J. R. Roberts, and S. K. Backues, "Control of autophagosome size and number by Atg7," *Biochemical and Biophysical Research Communications*, vol. 503, no. 2, pp. 651–656, 2018.

[39] I. Tanida and S. Waguri, "Measurement of autophagy in cells and tissues," *Methods in Molecular Biology*, vol. 648, pp. 193–214, 2010.

[40] X. Wang, G. Zhou, C. Liu et al., "Acanthopanax versus 3-methyladenine ameliorates sodium taurocholate-induced severe acute pancreatitis by inhibiting the autophagic pathway in rats," *Mediators of Inflammation*, vol. 2016, Article ID 8369704, 2016.

Hindawi
Journal of Oncology
Volume 2023, Article ID 5135445, 10 pages
https://doi.org/10.1155/2023/5135445

Research Article

Multiple Myeloma Side Population Cells Promote Dexamethasone Resistance of Main Population Cells through Exosome Metastasis of LncRNA SNHG16

Xi Yang, Zenghua Lin, Haiyan Liu, Xinfeng Wang, and Hong Liu

Department of Hematology, Affiliated Hospital of NanTong University, Nantong 226000, China

Correspondence should be addressed to Hong Liu; hongliu_xy@sina.com

Received 25 August 2022; Revised 10 October 2022; Accepted 24 November 2022; Published 9 February 2023

Academic Editor: Ashok Pandurangan

Background. The emergence of dexamethasone (Dex) resistance limits its efficacy. Side population (SP) cells in MM have strong tumorigenicity. Nevertheless, the detailed effect by which SP cells regulate Dex resistance in MP cells has not been completely verified and needs to be further investigated. *Methods*. SP and MP cells were sorted from RPMI-8226. mRNA expression and cell viability were analyzed using quantitative real-time PCR (qRT-PCR) and MTS assays, respectively. The presence of exosomal lncRNA SNHG16 was verified by transmission electron microscopy, differential ultracentrifugation, and qRT-PCR. Protein expression levels were measured using western blotting. Gain or loss function analyses were performed to demonstrate the role of SNHG16 in the Dex resistance of MP cells. *Results*. Dex resistance of SP cells was remarkably stronger than that of MP cells. Compared with MP cells, the survival rate and Dex resistance of MP cells cotreated with SP cell-derived exosomes were increased. SNHG16 expression was significantly enhanced in SP cell-derived exosomes compared to MP cell-derived exosomes. SNHG16 expression was remarkably increased in MP cells transfected with OE-SNHG16 vectors, and Dex resistance of MP cells was enhanced. When SNHG16 was silenced in SP cells, the SNHG16 expression was downregulated in both SP cells and SP cell-derived exosomes. SNHG16 expression and Dex resistance were both remarkably downregulated in MP cells treated with SP-si-SNHG16-exosomes compared to MP cells treated with SP-si-NC-exosomes. *Conclusion*. MM SP cells promote Dex resistance in MP cells through exosome metastasis of SNHG16.

1. Introduction

Multiple myeloma (MM) is one of the most common hematological malignancies in adults worldwide [1]. Despite considerable progress being made in treatment strategies for MM, the 5-year survival rate of MM patients is less than 40%, which is mainly attributed to drug resistance and recurrence [2]. Therefore, there is an urgent need to investigate the potential drug resistance and relapse mechanisms underlying MM.

Cancer stem cells (CSCs) are a small group of tumor cells with self-renewal ability that can drive the formation and growth of tumors and may be the root source of tumor production, metastasis, recurrence, and drug resistance [3]. Side population (SP) cells, which have similar characteristics to those of CSC, have the ability to differentiate into MP cells and exhibit strong tumorigenicity [4, 5]. SP cells are also resistant to dexamethasone (Dex), a conventional chemotherapeutic agent used to treat MM [6]. However, it is vital to understand the role of SP cells in the Dex resistance of MM cells.

Exosomes are membrane-derived vesicles derived from endosomal multivesicular vesicles with a size range of 30–150 nm [7]. Studies have found that exosomes contain various bioactive molecules such as nucleic acids, proteins, and lipids, which can be transferred from donor cells to recipient cells to realize intracellular information transmission [8, 9]. Abnormal expression of long noncoding RNAs (lncRNAs) is markedly related to the Dex resistance of MM [10]. Recent studies have shown that lncRNAs such as NEAT1, CRNDE, and HOTAIR are key regulators of Dex resistance in MM [11–13]. However, whether SP cells

promote Dex resistance in MP cells via exosomal lncRNAs remains unknown.

Our previous studies have found that the lncRNA SNHG16 plays a crucial role in MM proliferation [14]. In the current study, SP and MP cells were sorted from the MM RPMI-8226 cells, and the effects of SNHG16 on SP cells and MP cells on Dex resistance were investigated. Subsequently, exosomes were isolated from SP and MP cells, SNHG16 expression in exosomes was measured, coculture of exosomes and MP cells were performed, and the effects of SNHG16 on MP cell Dex resistance were investigated.

2. Materials and Methods

2.1. Cell Culture and Transfection. Human MM cells RPMI-8226 (Cell Bank of the Chinese Academy of Sciences, Shanghai, China) were cultured in RPMI-1640 (Gibco, Carlsbad, CA, USA) supplemented with 10% fetal bovine serum at 37°C in a humidified atmosphere of 5% CO_2. Overexpression of SNHG16 (OE-SNHG16) and negative control (OE-NC) vectors, siRNAs to SNHG16 (si-SNHG16), and si-NC were purchased from GeneChem (Shanghai, China). All transfections were carried out using Lipofectamine 2000 (Invitrogen, Waltham, MA, USA) in accordance with the manufacturer's instructions.

2.2. SP and MP Cell Separation. SP and MP cells were sorted from the MM RPMI-8226 cells using Hoechst 33342-labeledfluorescence-activated cell sorting, as previously described [15].

2.3. Cell Viability Assays. Cell proliferation was evaluated using the CellTiter 96® AQueous One Solution Cell Proliferation Assay (MTS assay; Promega, Madison, WI, USA) according to the manufacturer's instructions. The cells were added to 96-well plates at concentrations of 0, 2, 5, 10, 20, 50, 100, and 200 μM Dex (Sigma Aldrich) and/or incubated with 40 μg exosome/well for 48 h. MTS reagent was added to the wells and incubated for 2 h. The optical density at 490 nm was measured using a microplate reader (Bio-Rad, Hercules, CA, USA). The half-maximal inhibitory concentration (IC50) and the survival rate were calculated.

2.4. Quantitative Real-Time PCR (qRT-PCR). TRIzol reagent (Invitrogen) was used to extract total RNA from the cells or exosomes. The PrimeScript™ II 1st Strand cDNA Synthesis Kit (TaKaRa Bio, Dalian, China) was used to reverse transcribe the first-strand cDNA to total RNA. PCR was performed using an ABI 7500 RT-PCR system (Applied Biosystems, Foster City, CA, USA) with a SYBR® Premix Ex Taq™ Kit (TaKaRa). PCR primers were obtained from GenePharma (Shanghai, China) with the following sequences: SNHG16 forward, 5′-CCTCTAGTAGCCACG GTGTG-3′, and reverse 5′-GGCT GTGCTGATCCCATCT G-3′; aldehyde dehydrogenase 1 (ALDH1) forward, 5′-TCA CAGGATCAACAGAGGTTGG-3′, and reverse 5′-GCCCTGGTGGTAGAA TACCC-3′; sex-determining region Y (SRY)-box2 (Sox2) forward, 5′-TACAGCATG ATGCAGGACCA-3′, and reverse 5′-CTCGGACTTGAC CACCGAAC-3′; 18S rRNA forward, 5′-CCTGGATACCGC AGCTAGGA-3′, and reverse 5′-GCGGCGCAATACG AATGCCCC-3′; 18S rRNA served as endogenous controls for SNHG16 expression. The fold-change in the expression was computed using the $2^{-\Delta\Delta CT}$ method [16].

2.5. Exosome Isolation, Transmission Electron Microscopy, and Nanoparticle Tracking Analysis. ExoQuick-TC precipitation solution (System Biosciences, Mountain View, CA, UAS) was used to isolate exosomes from the culture medium according to the manufacturer's instructions. A BCA kit (Beyotime, Shanghai, China) was used to measure the concentration of exosomes. To ensure the isolation of exosomes, the protein expression of TSG101 and CD63 was assessed by western blotting. Transmission electron microscopy (TEM; Tokyo, Japan) was used to identify the size and shape of the exosomes. The particle size of the exosomes was determined using nanoparticle tracking analysis (NTA; Zetaview, Particle Metrix Inc., Bavaria, Germany).

2.6. Western Blotting. First, total protein samples from the cells or exosomes were extracted and separated by sodium dodecyl sulfate polyacrylamide gel electrophoresis. After blocking, the membrane was incubated overnight at 4°C with diluted primary antibodies: anti-P-glycoprotein (P-gp) (ab261736, 1/1000), antimultidrug resistance-associated protein 1 (MRP1) (ab260038, 1/1000), anti-hsp70 (ab2787, 1/1000), anti-CD63 (ab134045, 1/1000), and GAPDH (ab181602, 1/10000). After incubation with the primary antibody, the PVDF membranes were rinsed and incubated with horseradish peroxidase (HRP)-labeled secondary antibody (ab205718, 1/2000) for 2 h at 25°C and then washed. Finally, the proteins were quantified using enhanced chemiluminescence (Keygentec, Nanjing, China) and a ChemiDoc™ XRS system (Bio-Rad).

2.7. Statistical Analysis. Data analyses were performed using SPSS 19.0 (IBM Inc., Chicago, IL, USA). All data are expressed as the mean ± standard deviation (SD), according to the data of three independent replicates. Differences between two groups were assessed using the *t*-test, while differences between more than two groups were assessed using one-way analysis of variance. Statistical significance was set at $P < 0.05$.

3. Results

3.1. SP Cells Had Remarkable Dex Resistance. To investigate the relationship between SP and MP cells in MM, SP, and MP cells were isolated from MM (Figure 1(a)). To further prove that the isolated cells were SP and MP cells, qRT-PCR was used to assess ALDH1 and Sox2 expression. ALDH1 and Sox2 mRNA expression levels were remarkably upregulated in SP cells compared with those in MP cells (Figure 1(b)), suggesting that SP and MP cells were resoundingly sorted

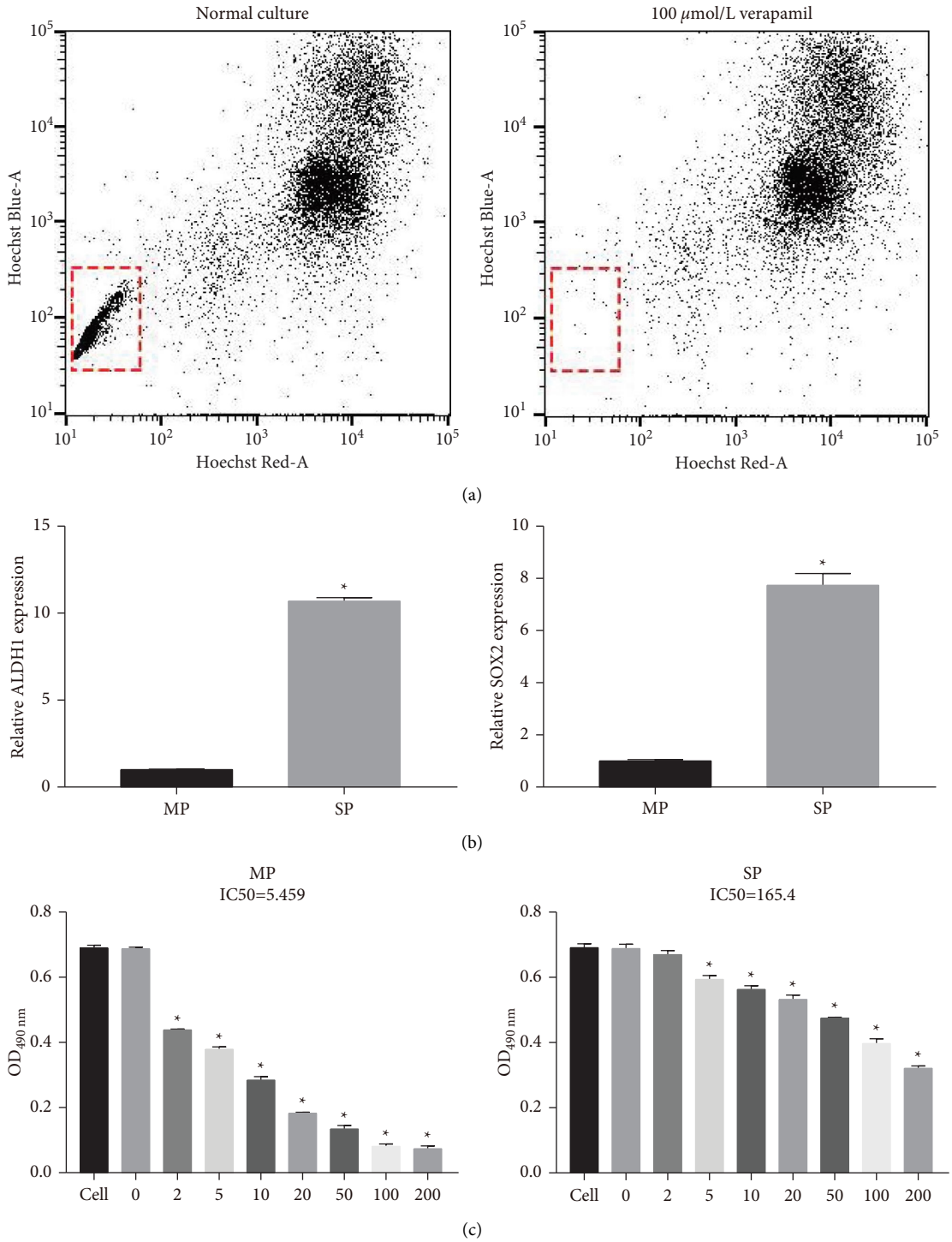

Figure 1: Isolation of SP and MP cells in MM cells and their Dex resistance. (a) SP cells and MP cells were isolated in RPMI-8226 cells using the Hoechst 33342 fluorescence staining method with fluorescence-activated cell sorting. (b) mRNA expression of ALDH1 and sox2 (SP markers) in SP cells and MP cells were assessed by qRT-PCR. (c) The cell viability to Dex of SP and MP cells was measured by MTS assay ($^*P < 0.05$).

from MM cells. To distinguish between the Dex resistance of SP and MP cells, cell viability was measured using MTS assays. The IC50 of SP cells (165.4) was remarkably higher than that of MP cells (5.454) (Figure 1(c)).

3.2. Isolation and Characterization of SP or MP Cell-Derived Exosomes. To investigate the relationship between exosomes and SP or MP cells, the exosomes in SP and MP cells were isolated, and the identification results of TEM and NTA

experiments revealed that exosomes derived from SP and MP cells had a typical dish-shapeddouble-layer membrane structure, with a diameter of 50–150 nm, suggesting that the exosomes were successfully extracted (Figures 2(a) and 2(b)). Western blotting results showed that the exosome markers HSP70 and CD63 were highly expressed in the extracted exosome samples (Figure 2(c)).

3.3. SP Cell-Derived Exosomes Increased Dex Resistance in MP Cells. To investigate the effect of SP cells on the Dex resistance of MP cells, MP cells were treated with 5 μM Dex and then incubated with 40 μg SP cell-derived exosomes. Compared with MP cells (blank group), the survival rate of MP cells cotreated with Dex + SP cell-derived exosomes (SP-exosome group) increased (Figure 3(a)). The Dex IC50 concentration (118.4) of SP-exosome group cells was remarkably higher than that (5.452) of the blank group cells (Figures 3(b) and 3(c)). The protein expression of the drug resistance markers P-gp and MRP1 was assessed by western blotting. P-gp and MRP1 protein expression levels were remarkably increased in SP-exosome group cells compared to those in the blank group cells (Figure 3(d)). These results suggested that MP cells acquire Dex resistance by absorbing SP cell-derived exosomes.

3.4. SP Cell-Derived Exosomes Could Transfer SNHG16. SNHG16 expression in SP- and MP-derived exosomes was measured by qRT-PCR. SNHG16 expression was remarkably upregulated in SP cell-derived exosomes compared to that in MP cell-derived exosomes (Figure 4(a)). Then, SNHG16 expression in MP cells and MP cells incubated with SP cell-derived exosomes was measured. The results showed that SNHG16 expression was remarkably upregulated in MP cells incubated with SP cell-derived exosomes compared to that in MP cells (Figure 4(b)). These results suggested that SP cell-derived exosomes can transmit the expression of SNHG16 into MP cells.

3.5. Overexpression of SNHG16 Promoted MP Cell Dex Resistance. To determine the effect of SNHG16 on Dex resistance in MP cells, SNHG16 was overexpressed in MP cells by transfection with OE-SNHG16 vectors. SNHG16 expression levels in MP cells and MP cells transfected with OE-NC and OE-SNHG16 vectors were measured by qRT-PCR. The results showed that SNHG16 expression was remarkably upregulated in MP cells transfected with OE-SNHG16 vectors compared to that in MP cells and MP cells transfected with OE-NC vectors (Figure 5(a)). The cell viability to Dex assay showed that the Dex IC50 concentration of MP cells transfected with OE-SNHG16 vectors (120.0) was remarkably higher than that of MP cells (5.268) and MP cells transfected with OE-NC vectors (5.433) (Figures 5(b)–5(d)). The western blot results showed that P-gp and MRP1 protein expression levels were remarkably upregulated in MP cells transfected with OE-SNHG16 vectors compared to those in MP cells and MP cells transfected with OE-NC vectors (Figure 5(e)).

3.6. Silencing SNHG16 in SP Cells Hardly Affected MP Cell Dex Resistance. To demonstrate whether MP cells conferred Dex resistance via incorporation into SNHG16 in SP cell-derived exosomes, the expression of SNHG16 in SP cells was knocked down by transfection with si-SNHG16 (Figure 6(a)). Consistently, the expression of SNHG16 in SP cell-derived exosomes was also knocked down (Figure 6(b)). MP cells were then cocultured with SP-si-SNHG16-exosomes, and SNHG16 expression was remarkably downregulated in MP cells treated with SP-si-SNHG16-exosomes compared with that in MP cells treated with SP-si-NC-exosomes and SP-blank-exosomes (Figure 6(c)). Moreover, the IC50 concentration of Dex in MP cells treated with SP-si-SNHG16-exosomes (20.77) was remarkably lower than that in SP cells treated with SP-si-NC-exosomes (119.8) and SP-blank-exosomes (120.0) (Figures 6(d)–6(f)). The western blot results showed that P-gp and MRP1 protein expression levels were remarkably downregulated in MP cells treated with SP-si-SNHG16-exosomes compared to those in SP cells treated with SP-si-NC-exosomes and SP-blank-exosomes (Figure 6(g)). These results suggest that MP cells could acquire drug resistance by absorbing SNHG16 in SP cell-derived exosomes.

4. Discussion

MM is still considered incurable and seriously threatens the health of people. Dex is the most conventional chemotherapeutic drug used for the treatment of MM, and its innate or achieved drug resistance is widely associated with a poor prognosis in MM [17]. The mechanisms of Dex resistance in MM have been studied previously [18]. However, the mechanism by which they acquire resistance remains unclear. In this study, we successfully isolated SP and MP cells from MM cells. In addition, we found that SP cells were more resistant to Dex than to MP cells. This is consistent with previous studies [19]. Exosomes mediate intercellular communication by transferring information from donors to target cells [20]. Tumor cells and tumor-associated stromal cells can release and receive exosomes and are widely involved in MM progression [21]. In this study, exosomes were successfully isolated from SP and MP cells. Moreover, the survival rate and Dex resistance of MP cells cotreated with Dex + SP cell-derived exosomes were enhanced, suggesting that MP cells could acquire Dex resistance by absorbing SP cell-derived exosomes.

Recently, increasing evidence has demonstrated that exosomes serve as a medium for information exchange between different cell types through the transmission of constituents [22]. The effects of exosomal lncRNAs on drug resistance have also been previously demonstrated. Exosomal H19 promotes Dex resistance in breast cancer, and exosomal SNHG7 promotes docetaxel resistance in lung adenocarcinoma [23, 24]. However, the functions of exosomal lncRNAs in MM remain unclear. To elucidate the functional mechanism and resistance to Dex in MM, we focused on lncRNAs, which have been demonstrated to play a vital role in cancer chemoresistance [25]. SNHG16 has oncogenic effects [26]. In our previous study, SNHG16 was

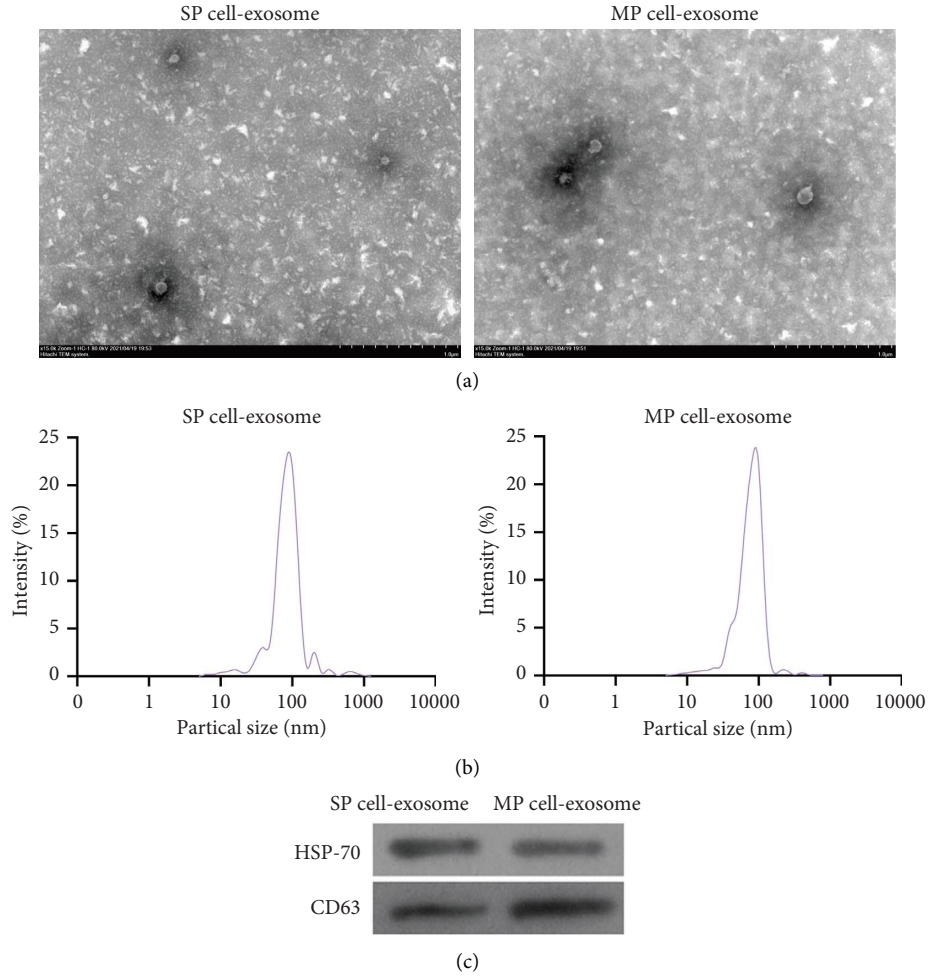

Figure 2: Characterization of SP or MP cell-derived exosomes. (a) Transmission electron microscopy (TEM) was applied to identify exosome size and shape. (b) Nanoparticle tracking analysis (NTA) was applied to identify exosome size. (c) The protein expression of TSG101 and CD63 was assessed using western blot.

upregulated in MM and promoted MM cell proliferation by sponging miR-342-3p [14]. Here, SNHG16 expression was remarkably enhanced in SP cell-derived exosomes compared to MP cell-derived exosomes. In addition, SNHG16 was transferred from SP cells to MP cells, which was first found in exosomes. Some studies have shown that SNHG16 contributes to chemotherapy resistance in cancer. For example, knockdown of SNHG16 inhibited cell function and sorafenib resistance in Hep3B and HepG2 cell lines [27], and SNHG16 silencing weakened cisplatin resistance in neuroblastoma cells [28]. The detailed mechanisms of SNHG16 in MM have not yet been elucidated. Here, overexpression of SNHG16 remarkably enhanced Dex resistance in MP cells. However, when si-SNHG16 downregulated the expression of SNHG16 in SP cell-derived exosomes, SNHG16 expression and Dex resistance were not remarkably enhanced in MP cells treated with SP-si-SNHG16-exosomes. These findings indicate that silencing of SNHG16 in SP cell-derived exosomes prevented MP cells from acquiring SNHG16 and thus failed to enhance Dex resistance.

This study has three main limitations. First, the regulatory mechanism of exosomal SNHG16 in MP remains unclear, the mechanism by which SNHG16 in SP cells is secreted into exosomes also remains unclear, and lastly the role of exosome-derived SNHG16 must be confirmed by *in vivo* experiments.

Taken together, the present findings suggest that MM SP cells promote Dex resistance in MP cells through exosome metastasis of SNHG16 (Figure 7). The functional role of lncRNAs in SP cell-derived exosomes will help discover new and more efficient strategies to reverse drug resistance.

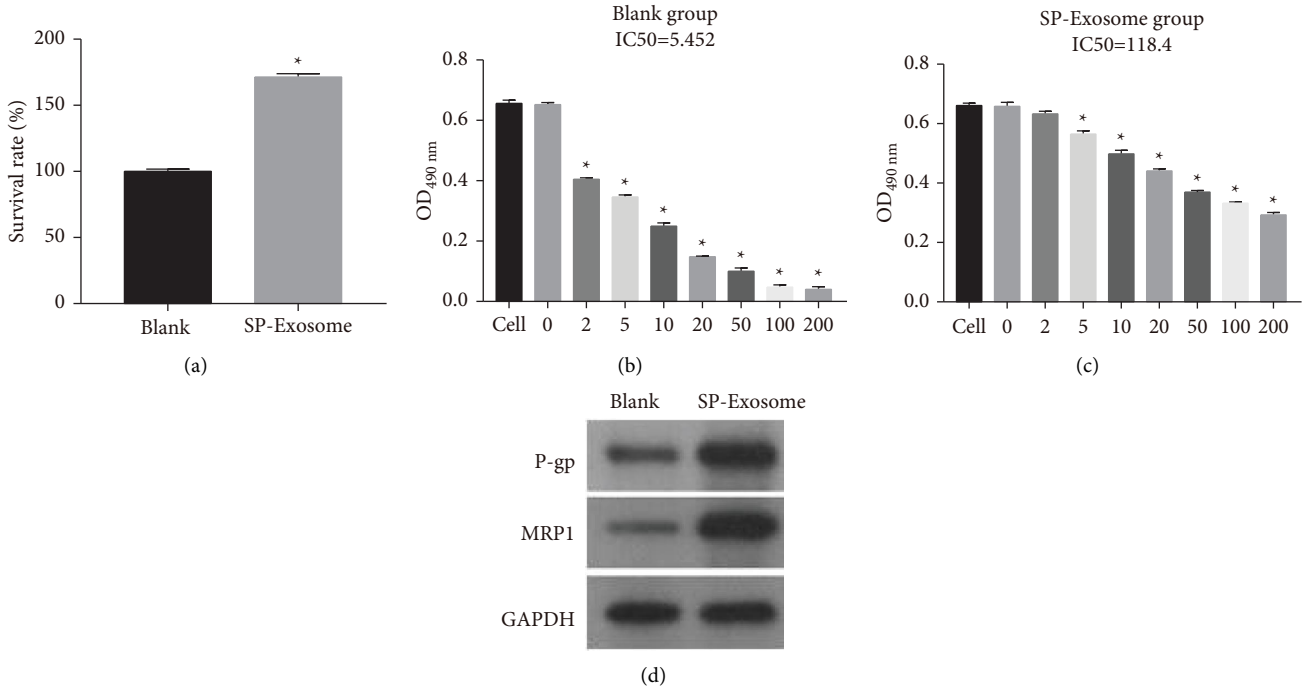

Figure 3: SP cell-derived exosomes induced Dex resistance in MP cells. (a) The cell proliferation of MP cells and MP cell cotreatment with Dex + SP cell-derived exosomes were assessed by MTS assay. (b and c) The cell viability to Dex of MP cells and MP cell cotreatment with Dex + SP cell-derived exosomes was measured by MTS assay. (d) The protein expression of P-gp and MRP1 in MP cells and MP cell cotreatment with Dex + SP cell-derived exosomes were detected by western blot. ($^*P < 0.05$).

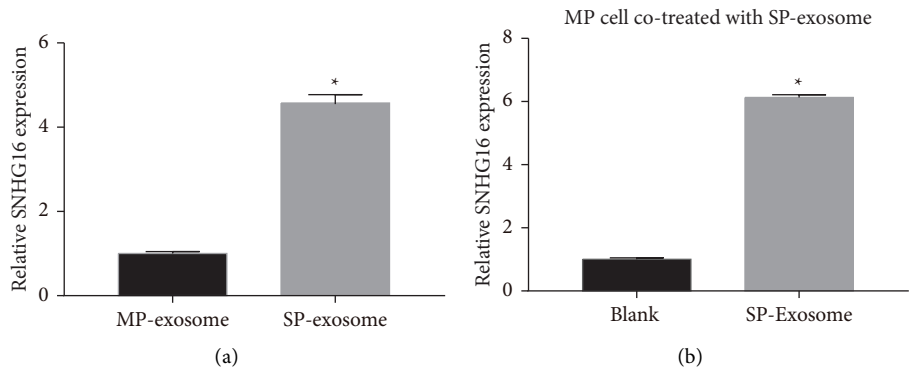

Figure 4: SP cell-derived exosomes could transmit the expression of SNHG16. (a) The SNHG16 expression levels in SP and MP cell-derived exosomes were measured by qRT-PCR. (b) The SNHG16 expression levels in MP cells (blank group) and MP cells incubated with SP cell-derived exosomes (SP-exosome group) were measured by qRT-PCR ($^*P < 0.05$).

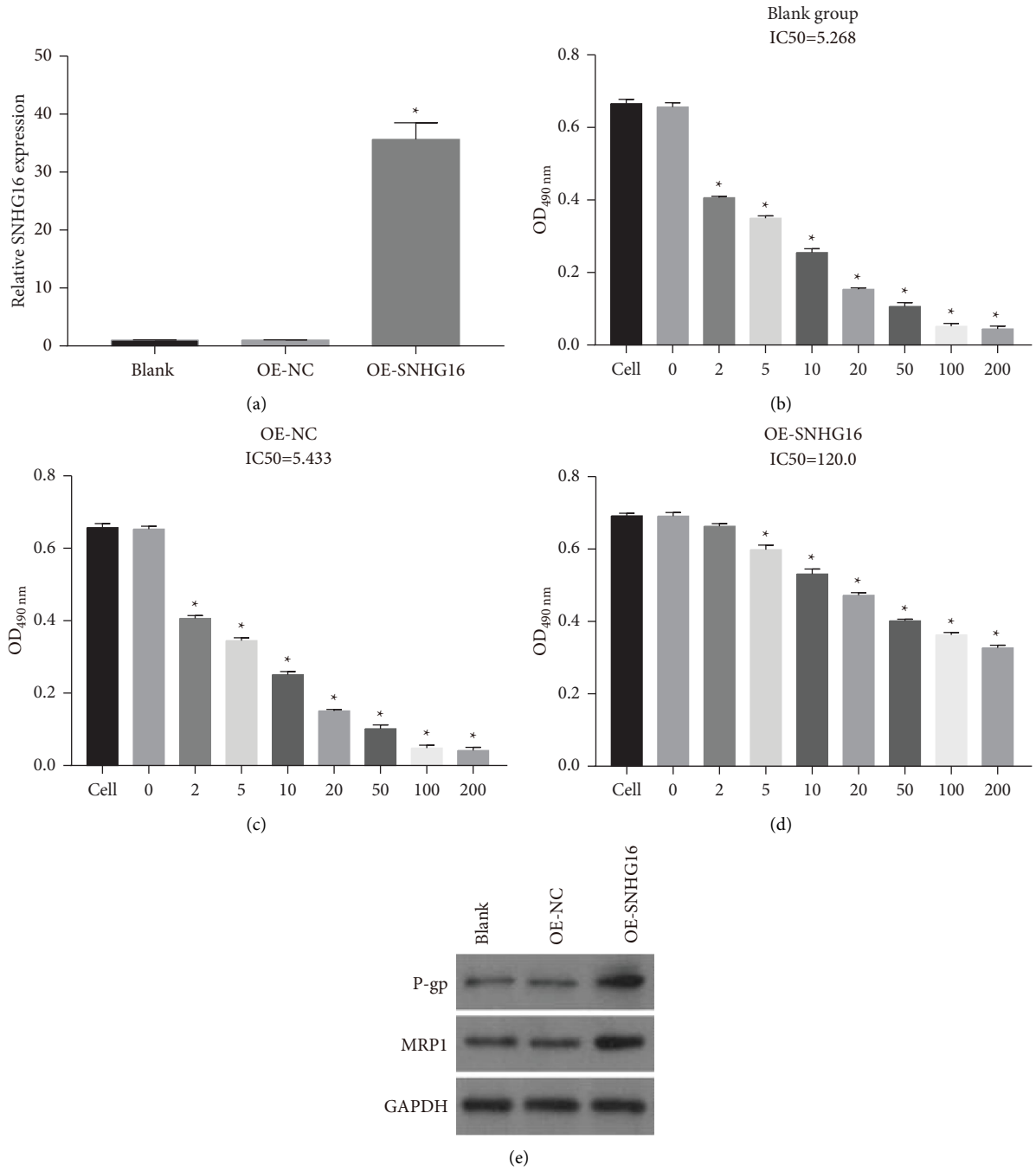

Figure 5: Overexpression of SNHG16 promoted MP cell Dex resistance. (a) SNHG16 expression levels in MP cells, MP cells transfected with OE-NC, and OE-SNHG16 vectors were measured by qRT-PCR. (b)–(d) The cell viability to Dex of MP cells, MP cells transfected with OE-NC, or OE-SNHG16 vectors was measured by MTS assay. (e) The P-gp and MRP1 protein expression levels in MP cells, MP cells transfected with OE-NC, or OE-SNHG16 vectors were measured by western blot ($^*P < 0.05$).

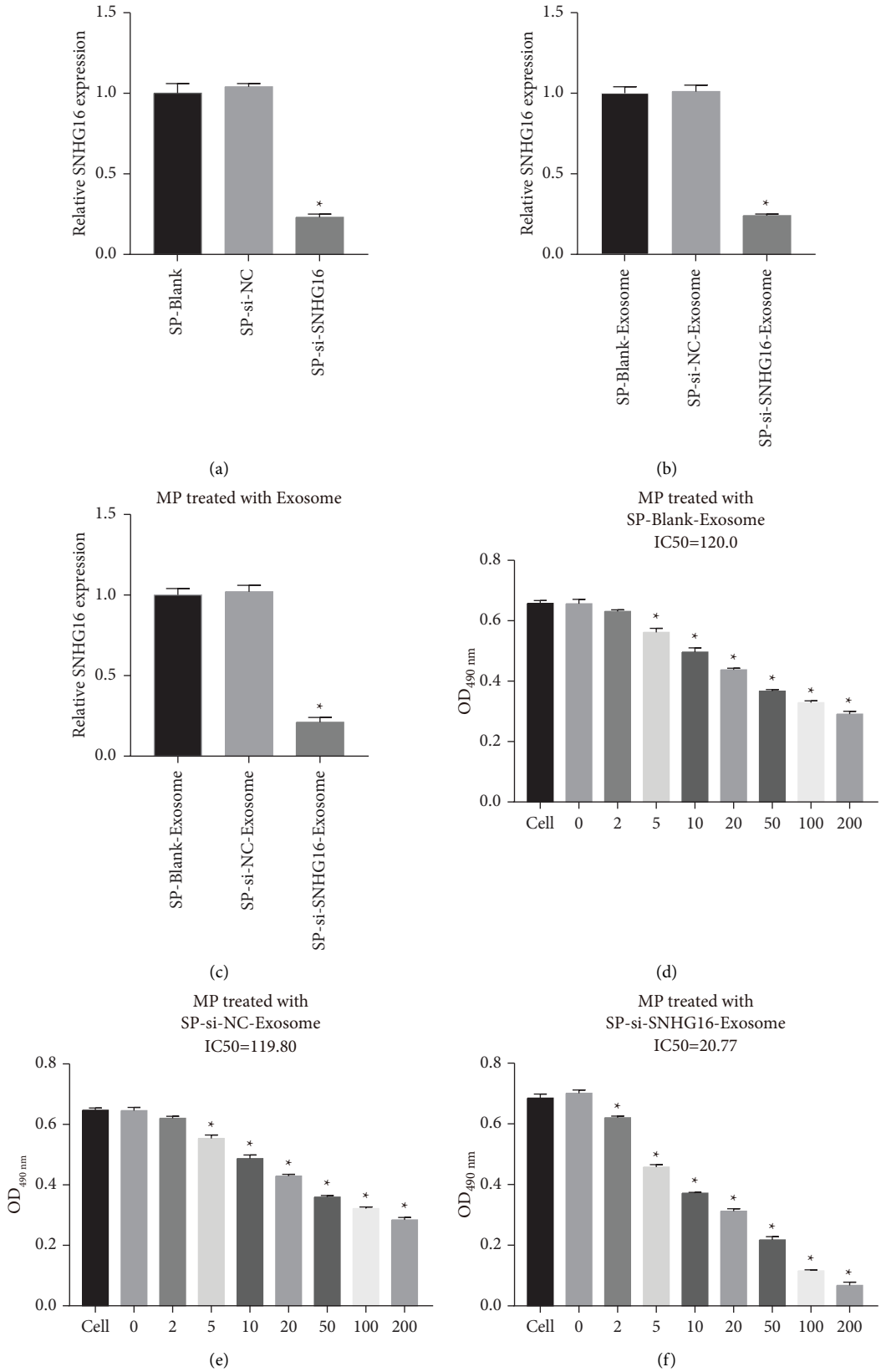

Figure 6: Continued.

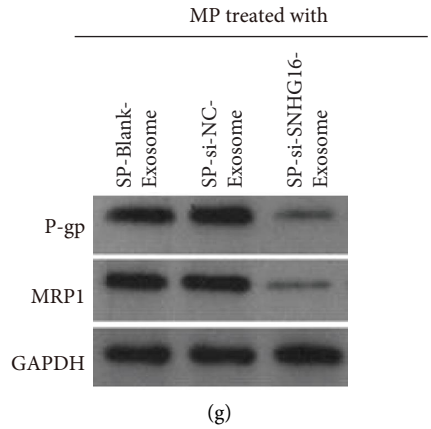

Figure 6: Silencing SNHG16 in SP cells hardly affected MP cell Dex resistance. (a) SNHG16 expression levels in SP cells, SP cells transfected with si-NC, and si-SNHG16 were measured by qRT-PCR. (b) The SNHG16 expression levels in SP cell exosomes, SP cells transfected with si-NC, and si-SNHG16 exosomes were measured by qRT-PCR. (c) SNHG16 expression levels in MP cells treated with exosomes. (d)–(f) The cell viability to Dex of MP cells treated with SP-blank-exosomes, SP-si-NC-exosomes, and SP-si-SNHG16-exosomes was measured by MTS assay. (g) The P-gp and MRP1 protein expression levels in MP cells treated with SP-blank-exosomes, SP-si-NC-exosomes, and SP-si-SNHG16-exosomes were measured by western blot ($^{*}P < 0.05$).

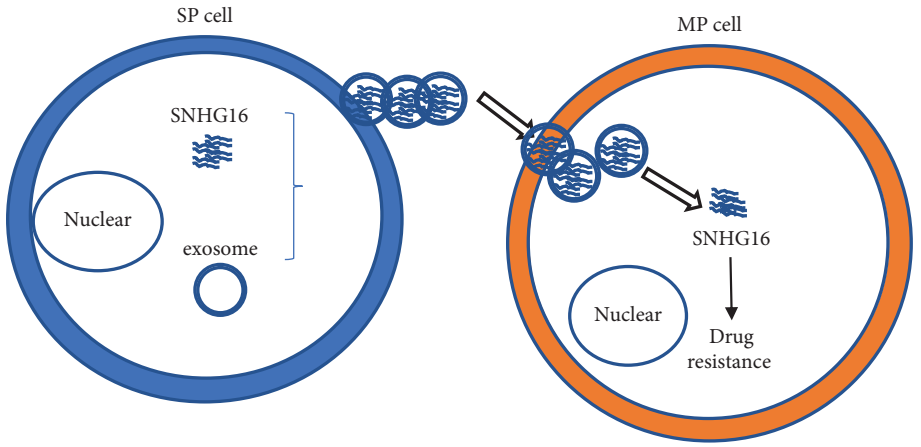

Figure 7: MM SP cells promote Dex resistance of MP cells through exosome metastasis of SNHG16.

Data Availability

The data used to support the findings of this study are included within the article.

Conflicts of Interest

The authors declare that they have no conflicts of interest.

Acknowledgments

The present study was supported by the Social Development Science and Technology Program of Nantong City (Grant no. JC2020050).

References

[1] A. J. Cowan, D. J. Green, M. Kwok et al., "Diagnosis and management of multiple myeloma: a review," *JAMA*, vol. 327, no. 5, pp. 464–477, 2023.

[2] H. Ludwig, S. Novis Durie, A. Meckl, A. Hinke, and B. Durie, "Multiple myeloma incidence and mortality around the globe; interrelations between health access and quality, economic resources, and patient empowerment," *The Oncologist*, vol. 25, no. 9, pp. e1406–e1413, 2020.

[3] R. L. Bighetti-Trevisan, L. O. Sousa, R. M. Castilho, and L. O. Almeida, "Cancer stem cells: powerful targets to improve current anticancer therapeutics," *Stem Cells International*, vol. 2019, pp. 1–15, 2019.

[4] W. Guo, H. Wang, P. Chen et al., "Identification and characterization of multiple myeloma stem cell-like cells," *Cancers*, vol. 13, no. 14, p. 3523, 2021.

[5] J. Wen, W. Tao, I. Kuiatse et al., "Dynamic balance of multiple myeloma clonogenic side population cell percentages controlled by environmental conditions," *International Journal of Cancer*, vol. 136, no. 5, pp. 991–1002, 2015.

[6] W. Yan, J. Du, Y. Du et al., "Fenretinide targets the side population in myeloma cell line NCI-H929 and potentiates the efficacy of antimyeloma with bortezomib and dexamethasone regimen," *Leukemia Research*, vol. 51, pp. 32–40, 2016.

[7] G. N. Alzhrani, S. T. Alanazi, S. Y. Alsharif et al., "Exosomes: isolation, characterization, and biomedical applications," *Cell Biology International*, vol. 45, no. 9, pp. 1807–1831, 2021.

[8] R. Kalluri and V. S. LeBleu, "The biology, function, and biomedical applications of exosomes," *Science*, vol. 367, no. 6478, Article ID eaau6977, 2020.

[9] D. Yu, Y. Li, M. Wang et al., "Exosomes as a new Frontier of cancer liquid biopsy," *Molecular Cancer*, vol. 21, no. 1, p. 56, 2022.

[10] Z. Liu, M. Han, N. Meng, J. Luo, and R. Fu, "lncRNA MSTRG.29039.1 promotes proliferation by sponging hsa-miR-12119 via JAK2/STAT3 pathway in multiple myeloma," *Oxidative Medicine and Cellular Longevity*, vol. 2021, pp. 1–18, Article ID 9969449, 2021.

[11] Y. Wu and H. Wang, "LncRNA NEAT1 promotes dexamethasone resistance in multiple myeloma by targeting miR-193a/MCL1 pathway," *Journal of Biochemical and Molecular Toxicology*, vol. 32, no. 1, Article ID e22008, 2018.

[12] R. Guan, W. Wang, B. Fu, Y. Pang, Y. Lou, and H. Li, "Increased lncRNA HOTAIR expression promotes the chemoresistance of multiple myeloma to dexamethasone by regulating cell viability and apoptosis by mediating the JAK2/STAT3 signaling pathway," *Molecular Medicine Reports*, vol. 20, no. 4, pp. 3917–3923, 2019.

[13] A. David, S. Zocchi, A. Talbot et al., "The long non-coding RNA CRNDE regulates growth of multiple myeloma cells via an effect on IL6 signalling," *Leukemia*, vol. 35, no. 6, pp. 1710–1721, 2021.

[14] X. Yang, H. Huang, X. Wang, H. Liu, H. Liu, and Z. Lin, "Knockdown of lncRNA SNHG16 suppresses multiple myeloma cell proliferation by sponging miR-342-3p," *Cancer Cell International*, vol. 20, no. 1, p. 38, 2020.

[15] W. He, Y. Fu, Y. Zheng, X. Wang, B. Liu, and J. Zeng, "Diallyl thiosulfinate enhanced the anti-cancer activity of dexamethasone in the side population cells of multiple myeloma by promoting miR-127-3p and deactivating the PI3K/AKT signaling pathway," *BMC Cancer*, vol. 21, no. 1, p. 125, 2021.

[16] K. J. Livak and T. D. Schmittgen, "Analysis of relative gene expression data using real-time quantitative PCR and the $2-\Delta\Delta CT$ method," *Methods*, vol. 25, no. 4, pp. 402–408, 2001.

[17] S. K. Kumar, N. S. Callander, M. Alsina et al., "Multiple myeloma, version 3.2017, NCCN clinical practice guidelines in oncology," *Journal of the National Comprehensive Cancer Network*, vol. 15, no. 2, pp. 230–269, 2017.

[18] L. Du, W. Liu, G. Aldana-Masangkay et al., "SUMOylation inhibition enhances dexamethasone sensitivity in multiple myeloma," *Journal of Experimental & Clinical Cancer Research*, vol. 41, no. 1, p. 8, 2022.

[19] J. Du, S. Liu, J. He et al., "MicroRNA-451 regulates stemness of side population cells via PI3K/Akt/mTOR signaling pathway in multiple myeloma," *Oncotarget*, vol. 6, no. 17, pp. 14993–15007, 2015.

[20] Y. Huang, M. Kanada, J. Ye et al., "Exosome-mediated remodeling of the tumor microenvironment: from local to distant intercellular communication," *Cancer Letters*, vol. 543, Article ID 215796, 2022.

[21] Z. Wan, X. Gao, Y. Dong et al., "Exosome-mediatedcell-cell communication in tumor progression," *Am J Cancer Res*, vol. 8, no. 9, pp. 1661–1673, 2018.

[22] J. Cheng, X. Wang, X. Yuan, G. Liu, and Q. Chu, "Emerging roles of exosome-derived biomarkers in cancer theranostics: messages from novel protein targets," *Am J Cancer Res*, vol. 12, no. 5, pp. 2226–2248, 2022.

[23] X. Wang, X. Pei, G. Guo et al., "Exosome-mediated transfer of long noncoding RNA H19 induces doxorubicin resistance in breast cancer," *Journal of Cellular Physiology*, vol. 235, no. 10, pp. 6896–6904, 2020.

[24] K. Zhang, J. Chen, C. Li et al., "Exosome-mediated transfer of SNHG7 enhances docetaxel resistance in lung adenocarcinoma," *Cancer Letters*, vol. 526, pp. 142–154, 2022.

[25] Y. Zhou, W. Sun, Z. Qin et al., "LncRNA regulation: new frontiers in epigenetic solutions to drug chemoresistance," *Biochemical Pharmacology*, vol. 189, Article ID 114228, 2021.

[26] C. Y. Gong, R. Tang, W. Nan, K. S. Zhou, and H. H. Zhang, "Role of SNHG16 in human cancer," *Clinica Chimica Acta*, vol. 503, pp. 175–180, 2020.

[27] Z. Guo, J. Zhang, L. Fan et al., "Long noncoding RNA (lncRNA) small nucleolar RNA host gene 16 (SNHG16) predicts poor prognosis and sorafenib resistance in hepatocellular carcinoma," *Medical Science Monitor*, vol. 25, pp. 2079–2086, 2019.

[28] Z. Xu, Y. Sun, D. Wang, H. Sun, and X. Liu, "SNHG16 promotes tumorigenesis and cisplatin resistance by regulating miR-338-3p/PLK4 pathway in neuroblastoma cells," *Cancer Cell International*, vol. 20, no. 1, p. 236, 2020.

Hindawi
Journal of Oncology
Volume 2023, Article ID 2541391, 8 pages
https://doi.org/10.1155/2023/2541391

Research Article

FOXO1-Induced miR-502-3p Suppresses Colorectal Cancer Cell Growth through Targeting CDK6

Hongwei Fan,[1] Shuqiao Zhao,[1] Rong Ai,[1] Xuemin Niu,[1] Junxia Zhang,[1] and Lin Liu[2]

[1]*Department of Gastroenterology, Shijiazhuang People's Hospital, Shijiazhuang 050011, Hebei, China*
[2]*Department of Pathology, Shijiazhuang People's Hospital, Shijiazhuang 050011, Hebei, China*

Correspondence should be addressed to Lin Liu; doctorliulin@163.com

Received 1 September 2022; Revised 12 October 2022; Accepted 12 October 2022; Published 29 January 2023

Academic Editor: Ashok Pandurangan

Colorectal cancer (CRC) is the most common tumor of the digestive system and the third most common tumor worldwide. To date, the prognosis of CRC patients remains poor. It is urgent to identify new therapeutic targets for CRC. As a tumor suppresser, microRNA (miRNA) miR-502-5p is downregulated in CRC tissues. Nevertheless, the role of miR-502-3p in CRC is largely unclear. Besides, the transcript factor forkhead box protein O1 (FOXO1) could suppress the CRC cell growth. However, the effect of FOXO1 on miR-502-3p in CRC remains unknown. By contrast, cyclin-dependent kinases 6 (CDK6) promotes the CRC cell growth. Yet the regulatory effect of miR-502-3p on CDK6 in CRC has not been reported. Thus, the primary aim of this study was to investigate whether FOXO1 enhanced miR-502-3p expression to suppress the CRC cell growth by targeting CDK6. Here, RNA level and protein level were detected by quantitative reverse transcription-PCR (qRT-PCR) and western blot (WB), respectively. Besides, the cell growth was detected by Cell Counting Kit 8 (CCK8) assay. Moreover, the regulatory effect of FOXO1 on miR-502-3p or miR-502-3p on CDK6 was determined using dual-luciferase reporter gene (DLR) assay. Results revealed that miR-502-3p and FOXO1 were downregulated in CRC cells. Besides, miR-502-3p suppressed the CRC cell growth. Moreover, FOXO1 could increase the miR-502-3p level through facilitating *MIR502* transcription in CRC cells. In addition, miR-502-3p could suppress the CRC cell growth by targeting CDK6. These findings indicated that FOXO1 induced miR-502-3p expression to suppress the CRC cell growth through targeting CDK6, which might provide new therapeutic targets for CRC.

1. Introduction

CRC is the most common tumor of the digestive system and the third most common tumor worldwide [1–3]. In China, 55.5 thousand new CRC cases are reported and 28.6 thousand CRC patients die annually [4–6]. More noteworthy is that the incidence rate of CRC is still growing rapidly [4, 7]. What is worse is that the prognosis of CRC patients remains poor due to postoperative recurrence and metastasis, and the 5-year survival of stage IV patients with CRC is only 10% [8, 9]. Thus, it is urgent to seek new therapeutic targets for CRC to improve the prognosis of patients with CRC.

Numerous studies have revealed that miRNAs play critical roles in CRC. For instance, miR-17-5p facilitates tumorigenesis and metastasis of CRC through suppressing B-cell linker [10]. By contrast, miR-31 reduces serine/threonine kinase 40 (STK40) expression to improve radiosensitivity of CRC cells [11]. A previous study has indicated that miR-502-3p is downregulated in CRC tissues [12]. Besides, several studies have shown that miR-502-3p exerts an anticarcinogenic effect on gallbladder cancer, gastric cancer, and invasive pituitary adenoma. For example, long noncoding RNA (lncRNA) highly expressed in GBC (HGBC) promotes gallbladder cancer progression via sponging miR-502-3p [13]. Moreover, circular RNA ribosomal protein L15 (circ-RPL15) facilitates gastric cancer progression through inhibiting miR-502-3p [14]. In addition, lncRNA LINC00473 stimulates pituitary adenoma cell proliferation served as a competing endogenous RNA (ceRNA) of miR-502-3p [15]. However, the effect of miR-502-3p on CRC is largely unknown.

As a known transcription factor, FOXO1 is downregulated in CRC cells and prohibits the CRC cell growth [16–18]. Besides, FOXO1 could regulate miRNA expression. For example, FOXO1 enhances *MIR148A* transcription to increase miR-148a expression in hepatocytes [19]. Moreover, unacetylated FOXO1 translocates to the nucleus and promotes *MIR449A* transcription to elevate the miR-449a level [20]. Nevertheless, the regulatory effect of FOXO1 on miR-502-3p in CRC remains unclear.

CDK6 is a recognized cell cycle kinase facilitating cancer cell proliferation to promote cancer progression [21]. Besides, CDK6 is upregulated in CRC cells [22]. Moreover, CDK6 promotes CRC progression. A recent study has revealed that miR-500a-3p suppresses CRC progression through inhibiting aerobic glycolysis by targeting CDK6 [22]. By contrast, lncRNA CASC21 enhances the CRC cell growth by inducing CDK6 expression [23]. Yet the role of miR-502-3p in CDK6 expression in CRC has not been reported.

Therefore, the primary aim of the current study was to investigate whether FOXO1 enhanced miR-502-3p expression to suppress the CRC cell growth by targeting CDK6.

2. Methods and Materials

2.1. Cell Culture. Normal colonic mucosa cell line FHC cells and CRC cell line HT29 cells were obtained from the Cell Bank at the Chinese Academy of Sciences (Shanghai, China). Then, FHC and HT29 cells were cultured with Dulbecco's modified eagle's medium (DMEM) and 10% fetal bovine serum (FBS) (Gibco BRL, Grand Island, NY, USA) in a humidified incubator supplemented with 95% O_2 and 5% CO_2 at 37°C.

2.2. Cell Transfection. In this study, miRNA mimic, inhibitor, and vectors were transfected into HT29 cells using Lipofectamine 2000 (Invitrogen, Carlsbad, Calif, USA). Then, HT29 cells were collected and used for subsequent experiments at 48 hours post-transfection.

2.3. QRT-PCR. First, total RNA from HT29 cells were isolated using Trizol (Invitrogen). For mRNA detection, 1 μg RNA was reverse transcribed by PrimeScript RT reagent Kit (Takara, Dalian, Liaoning, China). For miRNA detection, TaqMan miRNA assays (Applied Biosystems, Forest City, CA, USA) was utilized to reverse transcript 1 μg RNA. Then qRT-qPCR analysis was carried out by the ABI 7500 fast real-time PCR system (Applied Biosystems) using SYBR Premix Ex Taq II ((Tli RNaseH Plus)) (Takara). Subsequently, the amount of target RNA was normalized to that of internal control (18 s or U6) and then the data were given by $2^{-\triangle\triangle Ct}$ relative to that of the control group. The primers used for qRT-PCR were listed as follows: miR-502-3p: forward: 5′-ACACTCCAGCTGGGAATGCACCTGGGC AAGGA-3′, reverse: 5′-CTCAACTGGTGTCGTGGA-3′; U6 forward: 5′-CTCGCTTCGGCAGCACA-3′, reverse: 5′-AACGCTTCACGAATTTGCGT-3′; FOXO1 forward: 5′-GGCAGCCAGGCATCTCATAA-3′, reverse: 5′-TTG GGTCAGGCGGTTCATAC-3′; 18 s forward: 5′-CCTGGA TACCGCAGCTAGGA-3′, reverse: 5′-GCGGCGCAATAC GAATGCCCC-3′.

2.4. CCK8 Assay. First, 1×10^4 HT29 cells were collected in a well of the 96-well plate. Then, 10 μL CCK8 solution (#C0038, Beyotime Biotechnology, Shanghai, China) was added into each well at a 1/10 dilution to incubate HT29 cells for 2 hours at 37°C. Next, Multiscan MK3 (Thermo Fisher Scientific, Waltham, MA, USA) was used to read the absorbance at 450 nm. Finally, the rate of HT29 cell proliferation was calculated based on the mean of optical density (OD) at 450 nm.

2.5. WB. First, total proteins were extracted from HT29 cells by RIPA lysis buffer (#P0013D, Beyotime Biotechnology). Then, 30 μg protein was separated by SDS-polyacrylamide gel electrophoresis followed by the transfer onto a PVDF membrane (Millipore, Bedford, MA, USA). Next, 5% nonfat milk was used to block the membrane at room temperature (RT) for 1 hour and subsequently incubated with primary antibodies at 4°C overnight. Subsequently, Tris-buffered saline (TBS) supplemented with 0.1% Tween20 was utilized to wash the membrane three times followed by the incubation with second antibody at RT for 1.5 hour. Finally, the signals of target proteins were determined by the enhanced chemiluminescent (ECL) detection. The primary antibodies used for WB included FOXO1 antibody (1 : 1000, #ab52857, Abcam, Cambridge, UK), CDK6 antibody (1 : 1000, #ab179450, Abcam), and GAPDH antibody (1 : 15000, #KC-5G5, Aksomicks, Shanghai, China).

2.6. Bioinformatics Analysis. HumanTFDB database (https://bioinfo.life.hust.edu.cn/HumanTFDB#!/) was used to analysis potential FOXO1 binding sites on the promoter of *MIR502*. Besides, to mine targets of miR-502-3p, crosslinking-immunoprecipitation and high-throughput sequencing data of ENCORI database (https://starbase.sysu.edu.cn/index.php) were utilized.

2.7. Expression Vector Construction. To construct FOXO1 expression vector, the open reading frame (ORF) of *FOXO1* was cloned into the pcDNA 3.1 vector obtained from TaKaRa.

2.8. DLR Assay. The promoter of *MIR502*, wildtype (WT) CDK6 mRNA 3′UTR or mutant (MUT) CDK6 mRNA 3′UTR containing mutated miR-502-3p binding site was cloned into the luciferase reporter gene vector pGL3-basic. After cotransfection with pGL3-basic vectors and FOXO1 expression vector, with mimic NC or miR-502-3p mimic, respectively, luciferase activity of HT29 cells was detected by the Dual Luciferase Reporter Assay System (Promega, Madison, WI, USA).

2.9. Statistical Analysis. Data in the present study were present as mean ± standard deviation (SD). Besides, statistical differences were analyzed utilizing SPSS 20 software (SPSS Inc., Chicago, IL, USA). Briefly, the comparation between two groups was identified by the unpaired Student's *t*-test, while one way ANOVA was used for statistics among multiple groups. $P < 0.05$ was considered statistically significant.

3. Results

3.1. MiR-502-3p Is Downregulated in CRC Cell Line. First, the miR-502-3p level in HT29 cells was identified. Results of qRT-PCR showed that the level of miR-502-3p was reduced in HT29 cells compared to that in FHC cells (Figure 1), suggesting that miR-502-3p was downregulated in the CRC cell line. These results were consistent with those found in CRC tissues.

3.2. MiR-502-3p Suppresses CRC Cell Growth. Next, the effect of miR-502-3p on CRC cells was determined, and miR-502-3p mimic was used to overexpress miR-502-3p in HT29 cells. Results of CCK8 assay revealed that miR-502-3p overexpression dramatically decreased the HT29 cell growth rate compared to that of control HT29 cells (Figure 2). Besides, mimic NC had no effect on the HT29 cell growth rate (Figure 2). Abovementioned data suggested that miR-502-3p suppressed the CRC cell growth.

3.3. FOXO1 Elevates miR-502-3p Level through Facilitating MIR502 Transcription in CRC Cells. The pri-miR-502 is a transcript from *MIR502*. Moreover, potential FOXO1 binding site was found on the promoter of *MIR502* by bioinformatics analysis (Figure 3(a)). Consistent with the miR-502-3p level, the protein level of FOXO1 was also reduced in HT29 cells compared to that in FHC cells (Figure 3(b)). These results suggested that FOXO1 might regulate the miR-502-3p level in HT29 cells.

Next, results of qRT-PCR confirmed that FOXO1 overexpression by transfection of FOXO1 expression vector upregulated the miR-502-3p level in HT29 cells (Figure 3(c)). Besides, results of DLR assay indicated that the luciferase activity of HT29 cells transfected with pGL3-basic vectors containing the promoter of *MIR502* was increased by transfection of FOXO1 expression vector, while the blank expression vector had no effect on the luciferase activity of HT29 cells (Figure 3(d)). Thus, these data suggested that FOXO1 could elevate the miR-502-3p level through facilitating *MIR502* transcription in CRC cells.

3.4. MiR-502-3p Targets CDK6 in CRC Cells. Bioinformatics analysis showed that CDK6 should be the target of miR-502-3p (Figure 4(a)). Next, results of WB confirmed that miR-502-3p overexpression dramatically reduced the CDK6 protein level in HT29 cells (Figure 4(b)). Besides, mimic NC had no effect on the CDK6 protein level in HT29 cells (Figure 4(b)).

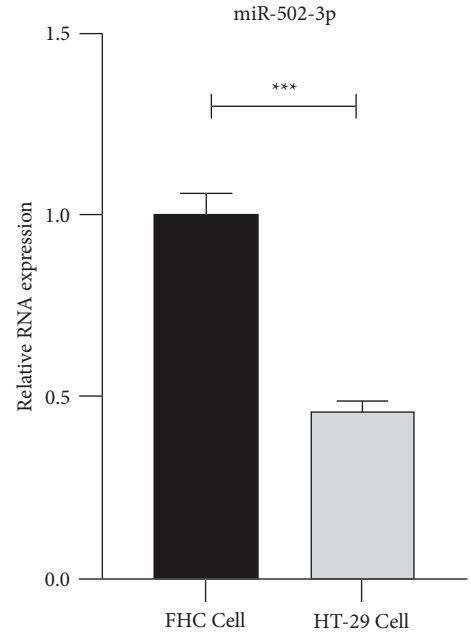

Figure 1: MiR-502-3p is downregulated in CRC cell line. The level of miR-502-3p in FHC cells and HT29 cells detected by qRT-PCR. $N = 3$. $^{***}P < 0.001$.

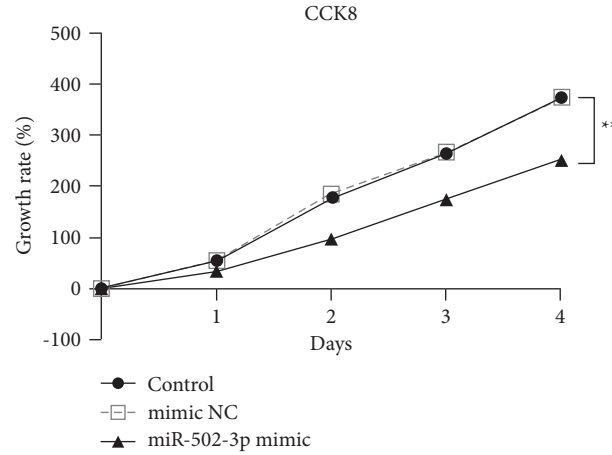

Figure 2: MiR-502-3p suppresses CRC cell growth. The growth rate of HT29 cells treated with or without miR-502-3p mimic detected by CCK8 assay. $N = 3$. NC: negative control. $^{**}P < 0.01$.

To further identify the regulatory effect of miR-502-3p on CDK6, DLR assay was performed. Results showed that the luciferase activity of HT29 cells transfected with pGL3-basic vector containing the WT CDK6 mRNA 3′ UTR was reduced by miR-502-3p mimic whereas elevated by miR-502-3p inhibitor (Figure 4(c)). However, the luciferase activity of HT29 cells transfected with pGL3-basic vector containing the MUT CDK6 mRNA 3′ UTR with mutated miR-502-3p binding site was not regulated by miR-502-3p mimic or inhibitor (Figure 4(c)). Moreover, the luciferase activity of HT29 cells transfected with pGL3-basic vector was not affected by mimic NC and inhibitor NC (Figure 4(c)). As

TF binding site Prediction Result

TF	Source	Sequence	Start	Stop	Strand	Score	P-value	Q-value	Matched Sequence
FOXO1	database	mir502_pro	769	778	-	11.8947	3.07e-05	0.122	AATAAACACG

(a)

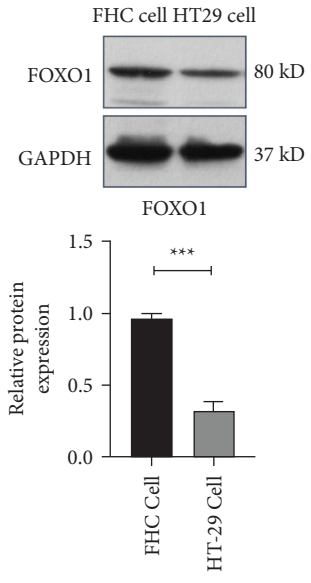

(b)

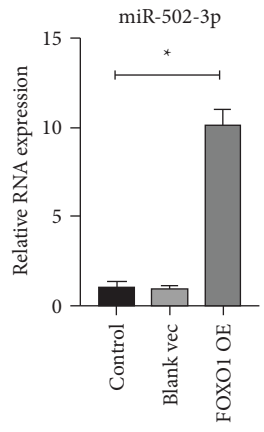

(c)

Figure 3: Continued.

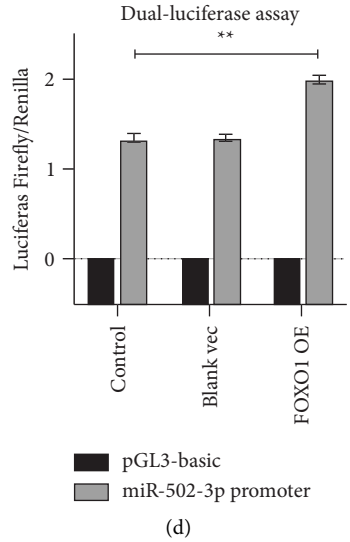

Figure 3: FOXO1 elevates miR-502-3p level through facilitating *MIR502* transcription in CRC cells. (a) Potential FOXO1 binding site on *MIR502* promoter analyzed using HumanTFDB database. (b) The protein level of FOXO1 in FHC cells and HT29 cells detected by WB. (c) The level of miR-502-3p in HT29 cells transfected with or without FOXO1 expression vector identified by qRT-PCR. (d) Luciferase activity of HT29 cells co-transfected with reporter gene vectors containing the promoter of *MIR502* and FOXO1 expression vector. Vec: expression vector; OE: overexpression. $N = 3$. $^{*}P < 0.05$, $^{**}P < 0.01$, $^{***}P < 0.001$.

CDK6 could promote the CRC cell growth [23], these results together suggested that miR-502-3p should suppress the CRC cell growth through targeting CDK6.

4. Discussion

This study revealed the mechanism of miR-502-3p regulating the CRC cell growth. First, miR-502-3p was downregulated in CRC cells and suppressed the CRC cell growth. Second, FOXO1 could elevate the miR-502-3p level through facilitating *MIR502* transcription in CRC cells. Third, miR-502-3p should suppress the CRC cell growth by targeting CDK6.

Numerous studies have demonstrated the anticarcinogenic effect of miR-502-3p. For instance, lncRNA-HGBC facilitates gallbladder cancer progression through sponging miR-502-3p [13]. Besides, circ-RPL15 promotes gastric cancer progression by suppressing miR-502-3p [14]. Similarly, circDLST activates NRAS/MEK1/ERK1/2 pathway to aggravate gastric cancer progression via sponging miR-502-3p [24]. Moreover, lncRNA LINC00473 enhances pituitary adenoma cell proliferation serving as a ceRNA of miR-502-3p [15]. However, the role of miR-502-3p in CRC has not been explored. Therefore, this study for the first time revealed the anticarcinogenic effect of miR-502-3p in CRC, which is consistent with the role of miR-502-3p in other cancers.

The current study had indicated that the FOXO1 protein level was downregulated in CRC cells. Nevertheless, the mechanism regulating the FOXO1 protein level in CRC remains unclear. Several studies have revealed that FOXO1 protein expression is reduced by miRNAs in CRC. For example, miR-544 facilitates CRC progression through decreasing FOXO1 protein expression [25]. Besides, miR-135b decreases sensitiveness of oxaliplatin by reducing the FOXO1 protein level in CRC cells [17]. Moreover, miR-183-5p stimulates angiogenesis through suppressing FOXO1 protein expression in CRC [26]. In addition, miR-96 promotes CRC cell proliferation via downregulating the FOXO1 protein level [27]. Thus, the FOXO1 protein level might be reduced by miRNAs in CRC cells.

CDK6 could be regulated by miRNAs in various cancers. A previous study has revealed that miR-204 suppresses nonsmall cell lung cancer (NSCLC) progression through downregulating the CDK6 level [28]. Similarly, a recent study has indicated that miR-370-3p restrains the progression of ovarian cancer by reducing CDK6 expression [29]. Moreover, miR-576 represses CDK6 expression to promote bladder cancer cell proliferation [30]. In addition, miR-186 decreases the CDK6 level to inhibit the prostate cancer cell growth [31]. In CRC, both miR-539-5p and miR-500a-3p depress CRC progression via targeting CDK6 [22, 23]. Nevertheless, the effect of miR-502-3p on CDK6 is largely unknown. Therefore, this study for the first time revealed the inhibitory role of miR-502-3p in CDK6 during CRC progression.

However, there are still some limitations in the current study. For example, the association between FOXO1 and *MIR502* promoter should be further identified by chromatin immunoprecipitation (ChIP), while the interaction of miR-502-3p and CDK6 mRNA should be further determined using miRNA pulldown. In addition, the effect of miR-502-3p on the CRC cell growth should be confirmed by *in vivo* study performed in nude mice.

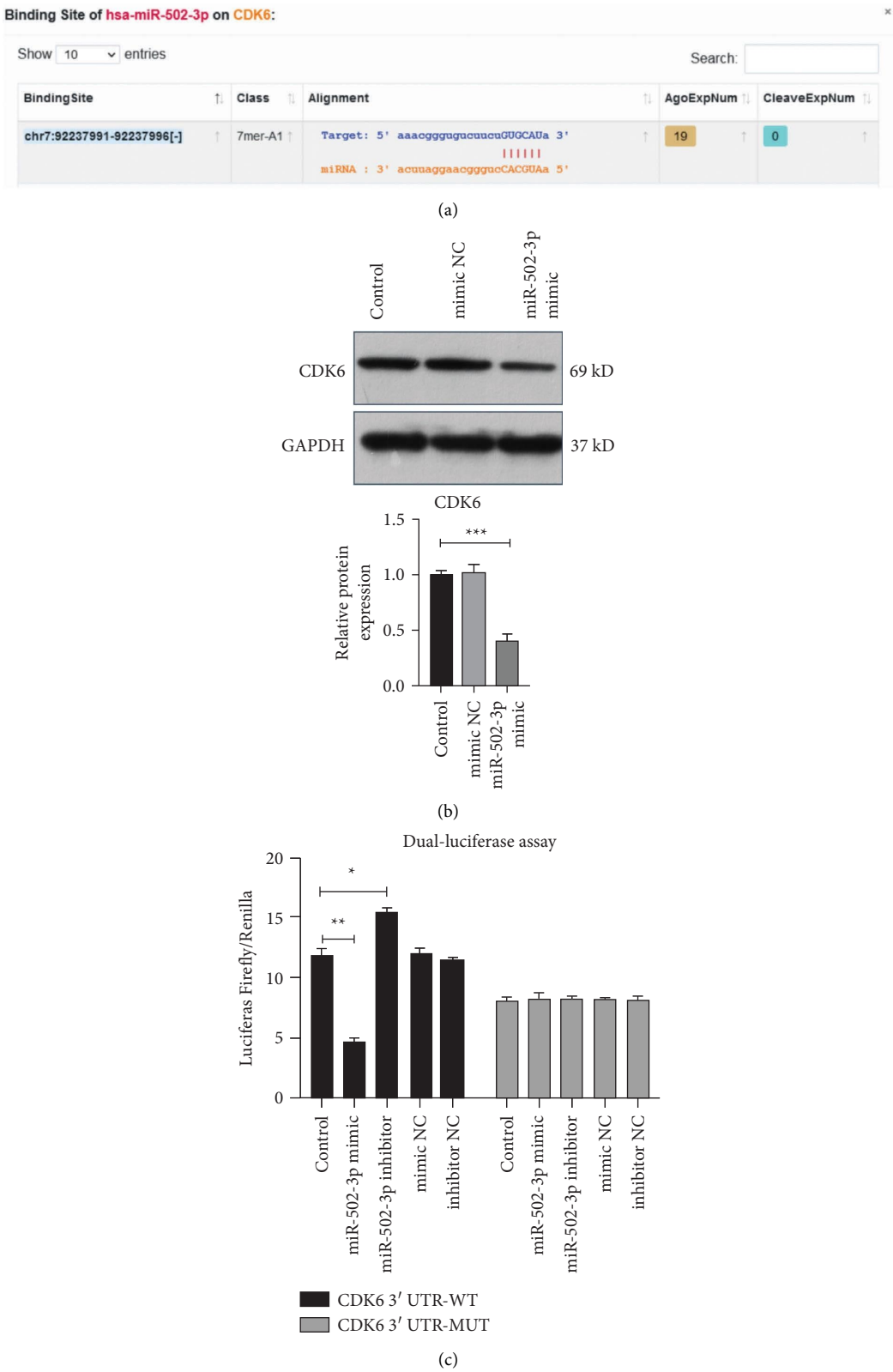

Figure 4: MiR-502-3p targets CDK6 in CRC cells. (a) miR-502-3p binding site on CDK6 mRNA 3′ UTR analyzed using ENCORI database. (b) The protein level of CDK6 in HT29 cells treated with or without miR-502-3p mimic detected by WB. (c) Luciferase activity of HT29 cells co-transfected with reporter gene vectors containing the binding site of miR-502-3p on CDK6 mRNA 3′ UTR and miR-502-3p mimic or inhibitor. $N = 3$. NC: negative control; WT: wildtype; MUT: mutant. $^{*}P < 0.05$, $^{**}P < 0.01$, $^{***}P < 0.001$.

5. Conclusion

In summary, the current study revealed that downregulated miR-502-3p suppressed the CRC cell growth. Besides, FOXO1 could increase the miR-502-3p level through facilitating *MIR502* transcription in CRC cells. Moreover, miR-502-3p should suppress the CRC cell growth by targeting CDK6. These findings indicated that FOXO1 induced miR-502-3p expression to suppress the CRC cell growth through targeting CDK6, which might provide novel therapeutic targets for CRC.

Data Availability

The data used to support the findings of this study are included within the article.

Conflicts of Interest

The authors declare that they have no conflicts of interest.

Acknowledgments

This work was supported by grants from the Scientific and Technological Research and Development Guidance Plan of Shijiazhuang (No. 191460973).

References

[1] H. The Lancet Gastroenterology, "Colorectal cancer screening: is earlier better?" *The Lancet Gastroenterology & Hepatology*, vol. 3, no. 8, p. 519, 2018.

[2] T. Yue, S. Chen, J. Zhu et al., "The aging-related risk signature in colorectal cancer," *Aging (Albany NY)*, vol. 13, no. 5, pp. 7330–7349, 2021.

[3] E. Dekker, P. J. Tanis, J. L. A. Vleugels, P. M. Kasi, and M. B. Wallace, "Colorectal cancer," *The Lancet*, vol. 394, no. 10207, pp. 1467–1480, 2019.

[4] W. Cao, H. D. Chen, Y. W. Yu, N. Li, and W. Q. Chen, "Changing profiles of cancer burden worldwide and in China: a secondary analysis of the global cancer statistics 2020," *Chinese Medical Journal*, vol. 134, no. 7, pp. 783–791, 2021.

[5] H. Chen, N. Li, J. Ren et al., "Participation and yield of a population-based colorectal cancer screening programme in China," *Gut*, vol. 68, no. 8, pp. 1450–1457, 2019.

[6] J. F. Shi, L. Wang, J. C. Ran et al., "Clinical characteristics, medical service utilization, and expenditure for colorectal cancer in China, 2005 to 2014: overall design and results from a multicenter retrospective epidemiologic survey," *Cancer*, vol. 127, no. 11, pp. 1880–1893, 2021.

[7] R. L. Siegel, K. D. Miller, A. Goding Sauer et al., "Colorectal cancer statistics, 2020," *CA: A Cancer Journal for Clinicians*, vol. 70, no. 3, pp. 145–164, 2020.

[8] J. Kryczka, E. Sochacka, I. Papiewska-Pajak, and J. Boncela, "Implications of ABCC4–mediated cAMP efflux for CRC migration," *Cancers*, vol. 12, no. 12, p. 3547, 2020.

[9] H. Brenner, M. Kloor, and C. P. Pox, "Colorectal cancer," *The Lancet*, vol. 383, no. 9927, pp. 1490–1502, 2014.

[10] J. Xu, Q. Meng, X. Li et al., "Long noncoding RNA MIR17HG promotes colorectal cancer progression via miR-17-5p," *Cancer Research*, vol. 79, no. 19, pp. 4882–4895, 2019.

[11] W. Zhang, Y. Zhu, Y. Zhou, J. Wang, P. Jiang, and L. Xue, "MiRNA-31 increases radiosensitivity through targeting STK40 in colorectal cancer cells," *Asia-Pacific Journal of Clinical Oncology*, vol. 18, no. 3, pp. 267–278, 2022.

[12] A. Fonseca, S. V. Ramalhete, A. Mestre et al., "Identification of colorectal cancer associated biomarkers: an integrated analysis of miRNA expression," *Aging (Albany NY)*, vol. 13, no. 18, pp. 21991–22029, 2021.

[13] Y. P. Hu, Y. P. Jin, X. S. Wu et al., "LncRNA-HGBC stabilized by HuR promotes gallbladder cancer progression by regulating miR-502-3p/SET/AKT axis," *Molecular Cancer*, vol. 18, no. 1, p. 167, 2019.

[14] Y. Li, Y. Gong, J. Ma, and X. Gong, "Overexpressed circRPL15 predicts poor survival and promotes the progression of gastric cancer via regulating miR-502-3p/OLFM4/STAT3 pathway," *Biomedicine & Pharmacotherapy*, vol. 127, Article ID 110219, 2020.

[15] J. Li, Y. Qian, C. Zhang et al., "LncRNA LINC00473 is involved in the progression of invasive pituitary adenoma by upregulating KMT5A via ceRNA-mediated miR-502-3p evasion," *Cell Death & Disease*, vol. 12, no. 6, p. 580, 2021.

[16] Y. C. Chae, J. Y. Kim, J. W. Park et al., "FOXO1 degradation via G9a-mediated methylation promotes cell proliferation in colon cancer," *Nucleic Acids Research*, vol. 47, no. 4, pp. 1692–1705, 2019.

[17] Y. Qin, L. Li, F. Wang et al., "Knockdown of mir-135b sensitizes colorectal cancer cells to oxaliplatin-induced apoptosis through increase of FOXO1," *Cellular Physiology and Biochemistry*, vol. 48, no. 4, pp. 1628–1637, 2018.

[18] Z. Du, T. Yu, M. Sun, Y. Chu, and G. Liu, "The long noncoding RNA TSLC8 inhibits colorectal cancer by stabilizing puma," *Cell Cycle*, vol. 19, no. 23, pp. 3317–3328, 2020.

[19] M. J. Heo, T. H. Kim, J. S. You, D. Blaya, P. Sancho-Bru, and S. G. Kim, "Alcohol dysregulates miR-148a in hepatocytes through FoxO1, facilitating pyroptosis via TXNIP overexpression," *Gut*, vol. 68, no. 4, pp. 708–720, 2019.

[20] S. H. Lan, S. C. Lin, W. C. Wang et al., "Autophagy upregulates miR-449a expression to suppress progression of colorectal cancer," *Frontiers in Oncology*, vol. 11, Article ID 738144, 2021.

[21] S. Nebenfuehr, K. Kollmann, and V. Sexl, "The role of CDK6 in cancer," *International Journal of Cancer*, vol. 147, no. 11, pp. 2988–2995, 2020.

[22] Y. Liu, W. Tang, L. Ren et al., "Activation of miR-500a-3p/CDK6 axis suppresses aerobic glycolysis and colorectal cancer progression," *Journal of Translational Medicine*, vol. 20, no. 1, p. 106, 2022.

[23] T. Gong, Y. Li, L. Feng et al., "CASC21, a FOXP1 induced long non-coding RNA, promotes colorectal cancer growth by regulating CDK6," *Aging (Albany NY)*, vol. 12, no. 12, pp. 12086–12106, 2020.

[24] J. Zhang, L. Hou, R. Liang et al., "CircDLST promotes the tumorigenesis and metastasis of gastric cancer by sponging miR-502-5p and activating the NRAS/MEK1/ERK1/2 signaling," *Molecular Cancer*, vol. 18, no. 1, p. 80, 2019.

[25] G. D. Yao, Y. F. Zhang, P. Chen, and X. B. Ren, "MicroRNA-544 promotes colorectal cancer progression by targeting forkhead box O1," *Oncology Letters*, vol. 15, no. 1, pp. 991–997, 2018.

[26] A. Shang, X. Wang, C. Gu et al., "Exosomal miR-183-5p promotes angiogenesis in colorectal cancer by regulation of FOXO1," *Aging (Albany NY)*, vol. 12, no. 9, pp. 8352–8371, 2020.

[27] F. Gao and W. Wang, "MicroRNA-96 promotes the proliferation of colorectal cancer cells and targets tumor protein p53 inducible nuclear protein 1, forkhead box protein O1

(FOXO1) and FOXO3a," *Molecular Medicine Reports*, vol. 11, no. 2, pp. 1200–1206, 2015.

[28] D. Wu, B. Y. Qin, X. G. Qi, L. L. Hong, H. B. Zhong, and J. Y. Huang, "LncRNA AWPPH accelerates the progression of non-small cell lung cancer by sponging miRNA-204 to upregulate CDK6," *European Review for Medical and Pharmacological Sciences*, vol. 24, no. 8, pp. 4281–4287, 2020.

[29] Y. Wang, M. Ding, X. Yuan et al., "lncRNA SNHG15 promotes ovarian cancer progression through regulated CDK6 via sponging miR-370-3p," *BioMed Research International*, vol. 2021, Article ID 9394563, 9 pages, 2021.

[30] G. Zhou, K. Yan, J. Liu, L. Gao, X. Jiang, and Y. Fan, "FTO promotes tumour proliferation in bladder cancer via the FTO/miR-576/CDK6 axis in an m6A-dependent manner," *Cell Death & Disease*, vol. 7, no. 1, p. 329, 2021.

[31] S. Lu, M. S. Wang, P. J. Chen, Q. Ren, and P. Bai, "MiRNA-186 inhibits prostate cancer cell proliferation and tumor growth by targeting YY1 and CDK6," *Experimental and Therapeutic Medicine*, vol. 13, no. 6, pp. 3309–3314, 2017.

Hindawi
Journal of Oncology
Volume 2022, Article ID 6051512, 11 pages
https://doi.org/10.1155/2022/6051512

Research Article

Effects of Long Noncoding RNA HOXA-AS2 on the Proliferation and Migration of Gallbladder Cancer Cells

Peng Zhang,[1] Luhao Liu,[1] Weiting Zhang,[1] Jiali Fang,[1] Guanghui Li,[1] Lei Zhang,[1] Jiali Li,[1] Xuanying Deng,[1] Junjie Ma,[1] Kun Li,[2] and Zheng Chen[1]

[1]*Organ Transplant Center, The Second Affiliated Hospital of Guangzhou Medical University, Guangzhou 511447, China*
[2]*Department of Hepatobiliary Surgery, The Second People's Hospital of Guiyang, Guiyang 550023, China*

Correspondence should be addressed to Kun Li; 386801779@qq.com and Zheng Chen; docchenzheng@163.com

Peng Zhang and Luhao Liu contributed equally to this work.

Received 4 August 2022; Revised 29 August 2022; Accepted 2 September 2022; Published 17 October 2022

Academic Editor: Ashok Pandurangan

To explore the function and mechanism of lncRNA HOXA-AS2 in cancer-associated fibroblasts (CAFs)-derived exosomes in gallbladder cancer metastasis, and provide new research targets for the treatment of gallbladder cancer. At the same time, in order to clarify the early predictive value of lncRNA HOXA-AS2 for gallbladder cancer metastasis, and to provide a theoretical basis for clinical individualized treatment of gallbladder cancer. *Methods*. In our previous work, we used TCGA database analysis to find that lncRNA HOXA-AS2 was highly expressed in gallbladder cancer tissues compared with normal tissues. In this study, the expression levels of HOXA-AS2 in gallbladder cancer cell lines and control cells were first verified by QPCR and Western blot methods. Then, lentiviral tools were used to construct knockdown vectors (RNAi#1, RNAi#2) and negative control vectors targeting two different sites of HOXA-AS2, and the vectors were transfected into NOZ and OCUG-1 cells, respectively. Real-time PCR was used to detect knockdown efficiency. Then, the effects of silencing HOXA-AS2 on the proliferation, cell viability, cell migration, and invasion ability of gallbladder cancer cells were detected by MTT, plate cloning assay, Transwell migration chamber assay, and Transwell invasion chamber assay. Finally, the interaction between HOXA-AS2 and miR-6867 and the 3′UTR of YAP1 protein was detected by luciferase reporter gene. The results showed that the expression level of HOXA-AS2 in gallbladder cancer cell lines was higher than that in control cells. The expression of HOXA-AS2 in gallbladder carcinoma tissues was significantly higher than that in adjacent tissues ($p < 0.05$). After successful knockout of HOXA-AS2 by lentiviral transfection, the expression of HOXA-AS2 in gallbladder cancer cell lines was significantly decreased. Through cell proliferation and plate clone detection, it was found that silencing HOXA-AS2 inhibited cell proliferation and invasion. Through software prediction and fluorescein reporter gene detection, it was found that HOXA-AS2 has a binding site with miR-6867, and the two are negatively correlated, that is, the expression of miR-6867 is enhanced after the expression of HOXA-AS2 is downregulated. And the 3′UTR of YAP1 protein in the Hippo signaling pathway binds to miR-6867. Therefore, HOXA-AS2 may affect the expression of YAP1 protein by regulating miR-6867, thereby inhibiting the Hippo signaling pathway and promoting the proliferation and metastasis of gallbladder cancer cells. HOXA-AS2 is abnormally expressed in gallbladder cancer cells. HOXA-AS2 may promote the migration and invasion of gallbladder cancer cells by regulating the Hippo signaling pathway through miR-6867. HOXA-AS2 may serve as a potential diagnostic and therapeutic target for gallbladder cancer in clinic.

1. Introduction

Clinically, gallbladder cancer (GBC), as one of the nauseating tumors, has a very high mortality rate despite its low incidence [1], usually found in the biliary system [2, 3]. However, due to the limited potential for curative resection and its resistance to chemotherapeutic agents, gallbladder carcinoma is an aggressive malignancy with high mortality [4]. Finding therapeutic targets for gallbladder cancer is an important process to prolong the survival of patients with

gallbladder cancer. Local invasion and distant metastasis are important biological features of gallbladder cancer. The development of effective molecular targets plays an important role in inhibiting the metastasis of gallbladder cancer. Many previous studies have found that miRNAs are involved in the metastatic process of gallbladder cancer. Bao et al. found that miR-101 inhibits the metastasis of gallbladder cancer [5]. MicroRNA-135a [6] and miR-20 [7] have been shown to be closely related to gallbladder cancer metastasis.

In the field of oncology research, a number of studies in recent years have demonstrated that lncRNAs are involved in the formation and development of tumors [8–10]. lncRNAs in the invasion of gallbladder cancer has so far been unclear. On the basis of previous studies, screening gallbladder cancer cell lines with different metastatic characteristics and searching for differentially expressed genes/lncRNAs by sequencing is a more effective research method. Through this experimental method, Wang et al. successfully demonstrated that CLIC1 promotes the migration and invasion of gallbladder cancer cells [11]. Related studies have shown that lnc-H19 promotes gallbladder cancer metastasis by regulating EMT [12]. lnc-CCAT1 promotes gallbladder cancer metastasis by negatively regulating miR-218-5p [13]. Therefore, it is necessary to screen lncRNAs related to gallbladder cancer metastasis by lncRNA chip. In our previous work, we collected tumor tissues from patients with gallbladder cancer, isolated CAFs-derived exosomes, and used lncRNA microarray chip and TargetScan software to analyze the differential lncRNAs related to metastasis. Finally, an lncRNA with significant differential expression was screened out, namely, lncRNA HOXA-AS2. The lncRNA HOXA-AS2 is an unknown lncRNA, and its biological function and mechanism of action are unclear. Therefore, lncRNA HOXA-AS2-specific siRNAs targeting different targets which were selected for a series of experimental studies to study their effects invasion of gallbladder cancer cells at the cellular level and to explore new targets for molecular targeted therapy of gallbladder cancer.

2. Materials and Methods

2.1. Cells, Tissue Samples, and Clinicopathological Data. Human gallbladder cancer cell lines: GEC, SGC-996, EH-GB, NOZ, GBC-SD, and OCUG-1. Clinical tissue samples from 15 patients with gallbladder cancer who underwent cholecystectomy for gallbladder cancer in the Second Affliated Hospital of Guangzhou Medical University and Zhujiang Hospital of Southern Medical University from May 2019 to March 2021 were collected, including cancer tissues and normal paracancerous tissues of different TNM stages. Collected clinical tissue samples were kept in liquid nitrogen until total RNA extraction.

2.2. Real-Time PCR. For the extraction of total RNA from gallbladder cancer cell lines and clinical gallbladder cancer tissue samples, the specific steps refer to previous studies [14]. The extracted total RNA was synthesized into cDNA using a reverse transcription system kit (Thermo Fisher Scientific) as a reaction template for real-time fluorescence quantitative PCR. The content of lncRNA HOXA-AS2 was detected using a fluorescence quantitative PCR kit (Applied Biosystems, USA). Refer to previous studies for specific steps [15].

2.3. Cell MTT Assay. The NOZ cells and OCUG-1 cells in logarithmic growth phase in which the HOXA-AS2 gene was knocked out were collected and counted. Select an appropriate cell density for passage in a 96-well plate (about 5,000 cells per well), set 3 parallel wells, and take out a well every 48 hours. Add preprepared MTT solution (Aladdin, Shanghai) and DESO solution.

2.4. Cell Clone-Formation Assay. The gallbladder cancer cell lines before and after the knockout of the HOXA-AS2 gene were selected for cell clone formation experiments, including, trypsinizing and counting cells in logarithmic growth phase, and inoculating cells with appropriate density in 6-well plates (each well). Seed about 500-2000 cells, mix well, and set 3 parallel wells. Finally, observe under an inverted microscope, count and take pictures, and make statistics of the results.

2.5. Cell Transwell Migration and Invasion Assay. Select NOZ and OCUG-1 cells successfully transfected with RNAi#1, RNAi#2, and NC (and the cells are in logarithmic growth phase), and use serum-free cell culture medium to culture the cells overnight before the experiment to reduce the effect of serum on the experiment. Cells were then trypsinized, washed 3 times with serum-free medium, counted, and made into suspension. Add the cell suspension to the Transwell chamber and incubate the cells with serum-free medium. PBS solution was used to wash the cells that did not invade the upper layer and were observed, photographed, and counted under a microscope (Zeiss, Germany). Data processing and result analysis are then carried out. The specific steps of related experiments refer to previous studies [16].

2.6. Preparation of Gallbladder Cancer Cell Lines with Reduced HOXA-AS2 Expression Mediated by Lentivirus Infection. Select freshly grown 30% monolayer cells as transfected cells for future use. The transfection groups are as follows: blank group NOZ cells, OCUG-1 cells (without any treatment); negative control NC (transfected with Scramble siRNA); and experimental group: against specific valid sequences of lncRNA HOXA-AS2 targeting two different target sites and GV112 lentiviral integration plasmids (RNAi#1, RNAi#2). Change the cell culture medium to serum-free medium before infection, and add HOXA-AS2 to interfere with lentivirus sh-RNAi#1, sh-RNAi#2, and negative control lentivirus sh-Ctrl according to 10MOI (multiplicity of infection). To infect cells, add a certain amount of polybrene solution to the cell culture medium to improve the efficiency of virus infection. Normal cell passaging was performed after cells were confluent. On the 4th day after infection, the virus infection of cells was checked with an inverted fluorescence microscope, and finally NOZ and OCUG-1 cells with knockdown of HOXA-AS2 were obtained and analyzed by qRT-PCR. Interference efficiency at different sites in HOXA-AS2 was obtained.

2.7. Western Blot. The total protein extraction kit (Teyebio, Shanghai, China) was used to lyse and extract tissue proteins

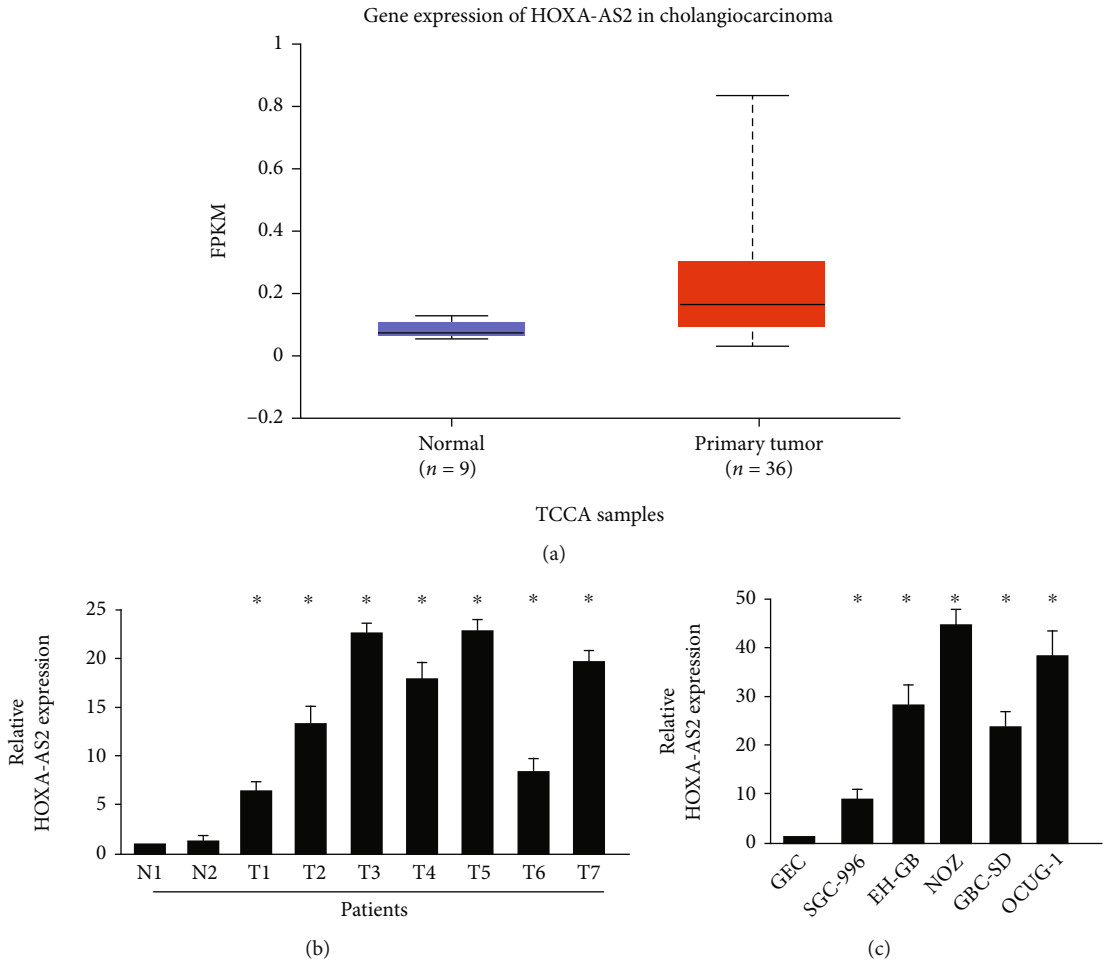

Figure 1: Expression of HOXA-AS2 in clinical tissue samples and cell lines of patients with gallbladder cancer. (a) Shows the high expression of HOXA-AS2 in gallbladder cancer tissues and low expression in normal tissues from the analysis of TCGA database. (b, c) The expression of HOXA-AS2 in clinical tissues and cell line samples of gallbladder cancer, respectively.

and cellular proteins. The specific experimental operation can refer to the previous research [17]. The protein concentration was subsequently determined using the BCA method (Teyebio, Shanghai, China). After the denatured protein was separated by gel running, the resultant was blotted onto a polyvinylidene fluoride membrane. The entire transfer system was placed in an ice-water mixture, and the membrane was transferred for about an hour under the conditions of 100 V, 400 mA. This was followed by overnight incubation with 5% nonfat dry milk in blocking solution. Use the desired antibody as the primary antibody to incubate the blocked PVDF membrane according to the instructions, and add an appropriate amount of secondary antibody and incubate with shaking at room temperature. A development kit (Teyebio, Shanghai, China) visualized the bands. The antibodies used are as follows: CyclinD1, p21, MMP9, snail, YAP1, p-YAP, TAZ, p-TAZ, GAPDH antibodies (1 : 2000, Abcam), and HRP labeled IgG antibody (1 : 10000, Cell Signaling Technology).

2.8. Luciferase Reporter Gene Assay. Wild and mutant HOXA-AS2/YAP1 was cotransfected with miR-6867-5p mimic/NC into HEK-293 T cells. Then luciferase activity was measured on a luciferase reporter system (Promega) using a dual-luciferase reporter gene detection kit (Beyotime, Shanghai, China).

2.9. Statistical Analysis. Statistical software SPSS22.0 was used for data analysis. All data were repeated at least 3 times. The two-tailed student's t-test was used to assess the difference between the two groups, and the level of statistical difference was expressed as p value: *, p value <0.05.

3. Results

3.1. HOXA-AS2 Expression Pattern in Gallbladder Carcinoma. In the TCGA database, the expression of HOXA-AS2 was analyzed in normal tissues and gallbladder cancer tissues, and it was found that HOXA-AS2 was abnormally expressed in gallbladder cancer tissues (Figure 1(a)). Analyze the level of lncRNA HOXA-AS2 in clinical tissue samples of different stages of gallbladder cancer. The expression of HOXA-AS2 in the clinical tissues of different stages of gallbladder cancer was higher than that in the corresponding normal tissues (Figure 1(b)). In addition, we further detected the expression of lncRNA HOXA-AS2 in

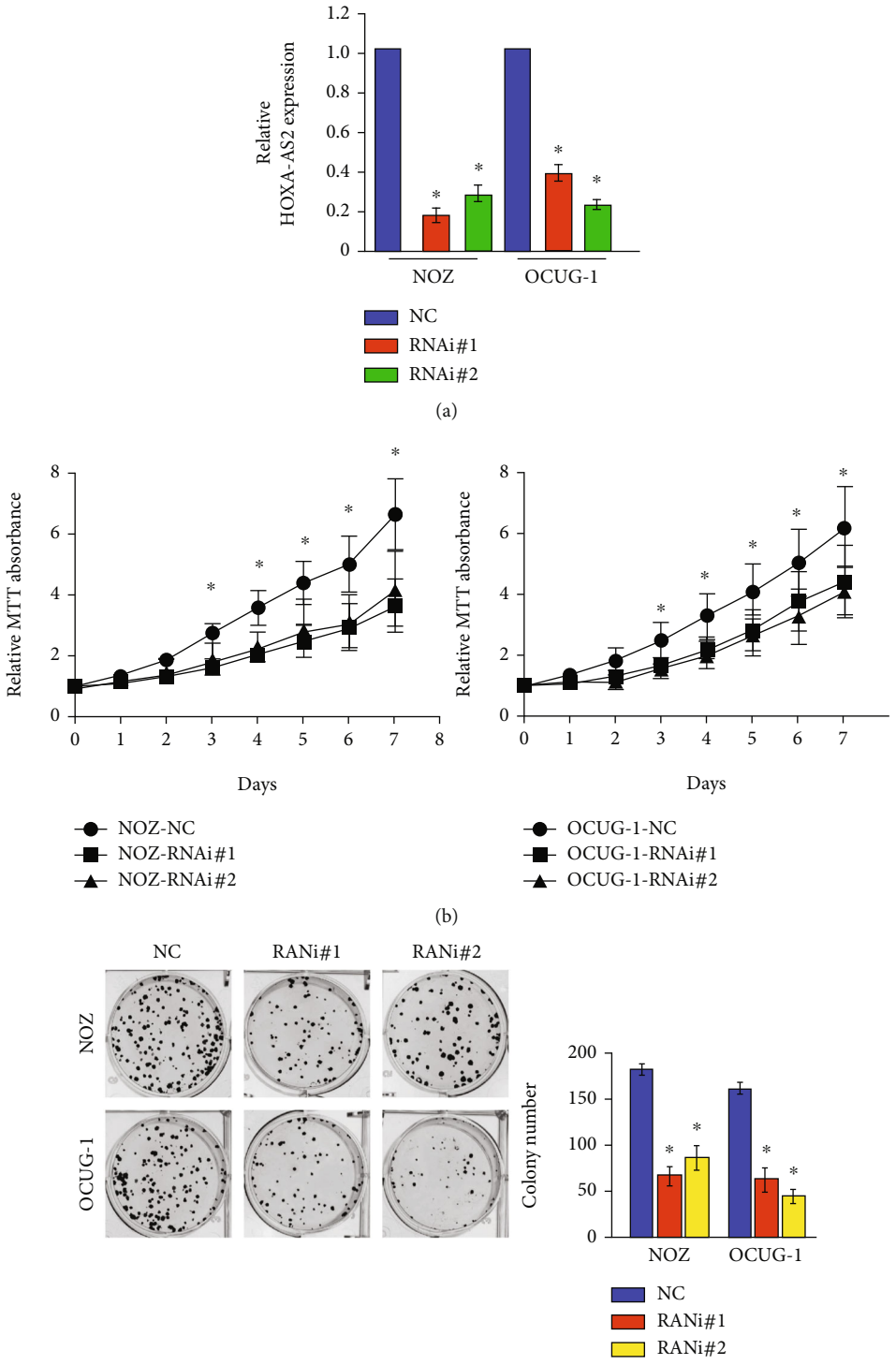

Figure 2: Continued.

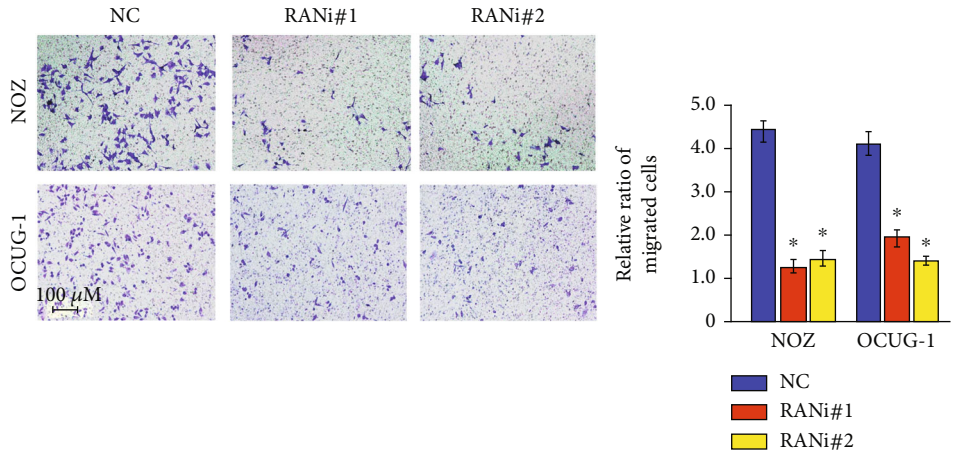

(d)

Figure 2: Effects of HOXA-AS2 knockout on proliferation, migration, and invasion of gallbladder cancer cells. (a) Real-time PCR results show that the expression of HOXA-AS2 in the knockdown group is significantly decreased. (b) MTT detects the change of cell viability after silencing HOXA-AS2 cells. (c) Clone formation detects the silence of HOXA-AS2 cells. Cell proliferation ability after AS2. (d) Transwell migration and invasion assay to detect changes in cell migration and invasion ability after HOXA-AS2 silencing.

hepatoma cells. As shown in Figure 1(c), the level of HOXA-AS2 in normal gallbladder cell GECs was used as a reference. HOXA-AS2 was highly expressed in multiple gallbladder cancer cell lines.

3.2. Effects of Knockdown of HOXA-AS2 on Viability, Proliferation, Migration, and Invasion of Gallbladder Cancer Cells. NOZ and OCUG-1 cells were transfected with specific shRNAs (RNAi#1, RNAi#2) targeting two different sites of lncRNA HOXA-AS2 carried by lentiviral tools, 96 hours after transfection, the expression level of RNAi#2 was only 2.6% of the Lv-shCon (NC) group (Figure 2(a)). The above results suggested that Lv-shHOXA-AS2 specifically knocked down HOXA-AS2 in NOZ and OCUG-1 cells. MTT cell viability assays and cell colony formation experiments were performed. As shown in Figure 2(b), we found that the absorbance at 490 nm of NOZ and OCUG-1 cells infected with sh-HOXA-AS2 lentivirus was significantly lower than that of cells infected with sh-Ctrl lentivirus, indicating that knockdown of SNHG16 inhibited viability of NOZ and OCUG-1 cells. Clonogenic assays showed decreased cell growth in NOZ and OCUG-1 cells knocked down HOXA-AS2 (Figure 2(c)). The results of in vitro proliferation experiments showed that the level of HOXA-AS2 was downregulated in NOZ and OCUG-1 cells and inhibited cell proliferation. In addition, in the Transwell migration and invasion experiments, we found that under the premise of maintaining the same initial cell number, after 48 hours of cell culture, the NOZ and OCUG-1 cells in the HOXA-AS2 expression-decreased group showed reduced migration and invasion cells (Figure 2(d)), suggesting that the mutation of HOXA-AS2 inhibits the migration and invasion of cancer cells in vitro.

3.3. Knockdown of lnc-HOXA-AS2 Reduces the Expression of Transcription Factors Associated with Proliferation and Metastasis in NOZ and OCUG-1 Cells. The expression of key cell cycle-related regulators CyclinD1 and P21 proteins was detected by real-time PCR and Western blot (Figures 3(a) and 3(b)). The expression of CyclinD1 protein was found to be decreased in the RNAi#1 and RNAi#2 groups. The levels of MMP9 and Snail, which affect cell migration and invasion were subsequently detected, and the levels of MMP9 and Snail were significantly reduced after silencing lnc-HOXA-AS2 (Figures 3(a) and 3(b)).

3.4. miR-6867-5p Is a Downstream Target of lncRNA HOXA-AS2. RNA from clinical tissue samples of gallbladder carcinoma was detected using RT-PCR, and the expression of HOXA-AS2 was found to be inversely correlated with MiR-6867-5p (Figure 4(a)). Subsequently, the results were analyzed by TargetScan software, and it was found that HOXA-AS2 and miR-6867 have the same binding site (Figure 4(b)). MiR-6867-5p was significantly increased in NOZ and OCUG-1 cells in RNAi#1 and RNAi#2 group which HOXA-AS2 was knocked down (Figure 4(c)). HOXA-AS2 expression was decreased after overexpression of miR-6867 in NOZ and OCUG-1 cells and increased upon addition of miR-6867 inhibitor (Figure 4(d)). These experimental results indicated that HOXA-AS2 was inversely correlated with the expression of miR-6867-5p in related cell lines. These further support the idea that miR-6867-5p is the target of lncRNA HOXA-AS2.

3.5. lncRNA HOXA-AS2 Affects the Occurrence and Development of Gallbladder Cancer Cells by Regulating miR-6867-5p/YAP1. We performed analysis using TargetScan prediction software and found that YAP1 was a target of miR-6867-5p (Figure 5(a)). Subsequently, by RT-qPCR and Western blot detection, the level of YAP1 was increased in the RNAi#1/RNAi#2 group and miR-6867-5p overexpression group. RNAi#1/RNAi#2 group and miR-6867-5p significantly decreased in the inhibitor group (Figures 5(b) and 5(c)). As lncRNA HOXA-AS2 was not silenced resulting

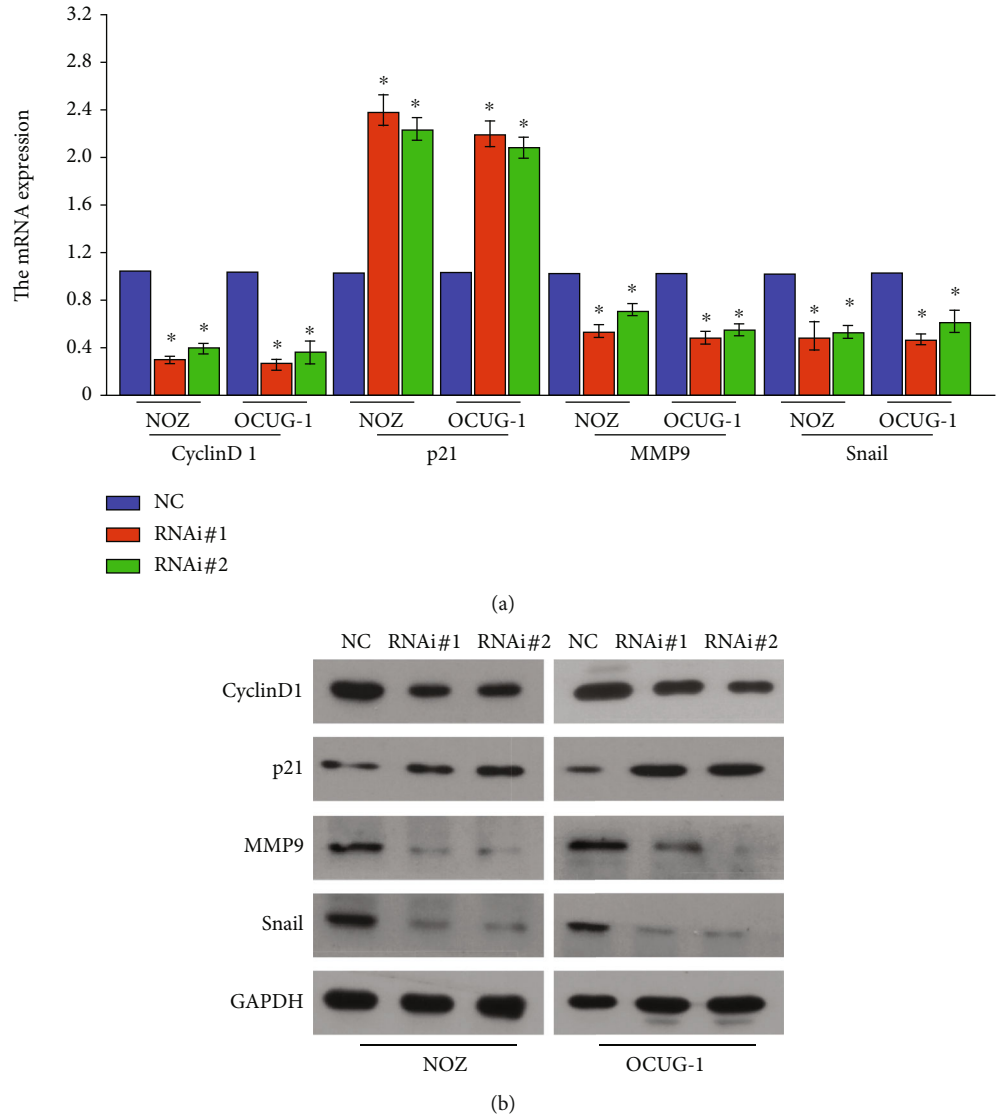

Figure 3: Expression of related regulatory factors affecting the cycle of gallbladder cancer cells after knockout of HOXA-AS2. QPCR of (a) Western blot. (b) Detection of knockdown of HOXA-AS2 after knockdown of HOXA-AS2 significantly decreased the expression of key regulators related to cell proliferation, metastasis, and invasion.

in upregulation of miR-6867-5p, this may further upregulate YAP1 levels. Furthermore, we found that the luciferase activity was significantly reduced in the HOXA-AS2-miR-6867-5p group at two specific sites (Figure 5(d)). All the results demonstrate a consistent axis of regulatory relationship between lncRNA HOXA-AS2-miR-6867-5p–YAP1.

The transcriptional coactivator YAP/TAZ in the Hippo signaling pathway loses its transcriptional activity when phosphorylated, and YAP/TAZ itself is a transcriptional coactivator that cannot bind DNA, so it needs to be combined with other transcription factors such as TEAD1-4, coinitiated the transcription of downstream genes. Therefore, we detected the phosphorylation and activation of YAP and TAZ after HOXA-AS2 knockdown by Western blot. The phosphorylation of YAP was significantly reduced in RNAi#1\RNAi#2 gallbladder cancer cells (Figure 6(a)). At the same time, the results of luciferase activity detection showed that the activities of TEAD1-4 transcription factors that interacted with YAP also decreased correspondingly (Figure 6(b)), indicate that silencing of HOXA-AS2 affects the expression of Hippo signaling pathway-related regulators. In addition, adding an agonist of the Hippo signaling pathway to HOXA-AS2 knockdown gallbladder cancer cells, and through cell cloning and invasion experiments found that the increased expression of Hippo signaling pathway-related regulators inhibited the proliferation and invasion of gallbladder cancer cells (Figures 6(c) and 6(d)).

4. Discussion

Gallbladder cancer is a pathogenic malignancy, affecting 2.5 per 100,000 people [18, 19]. lncRNA HOXA-AS2 has been found to be aberrantly expressed in a variety of human tumor tissues and cells (Supplementary Figure 1). HOXA-

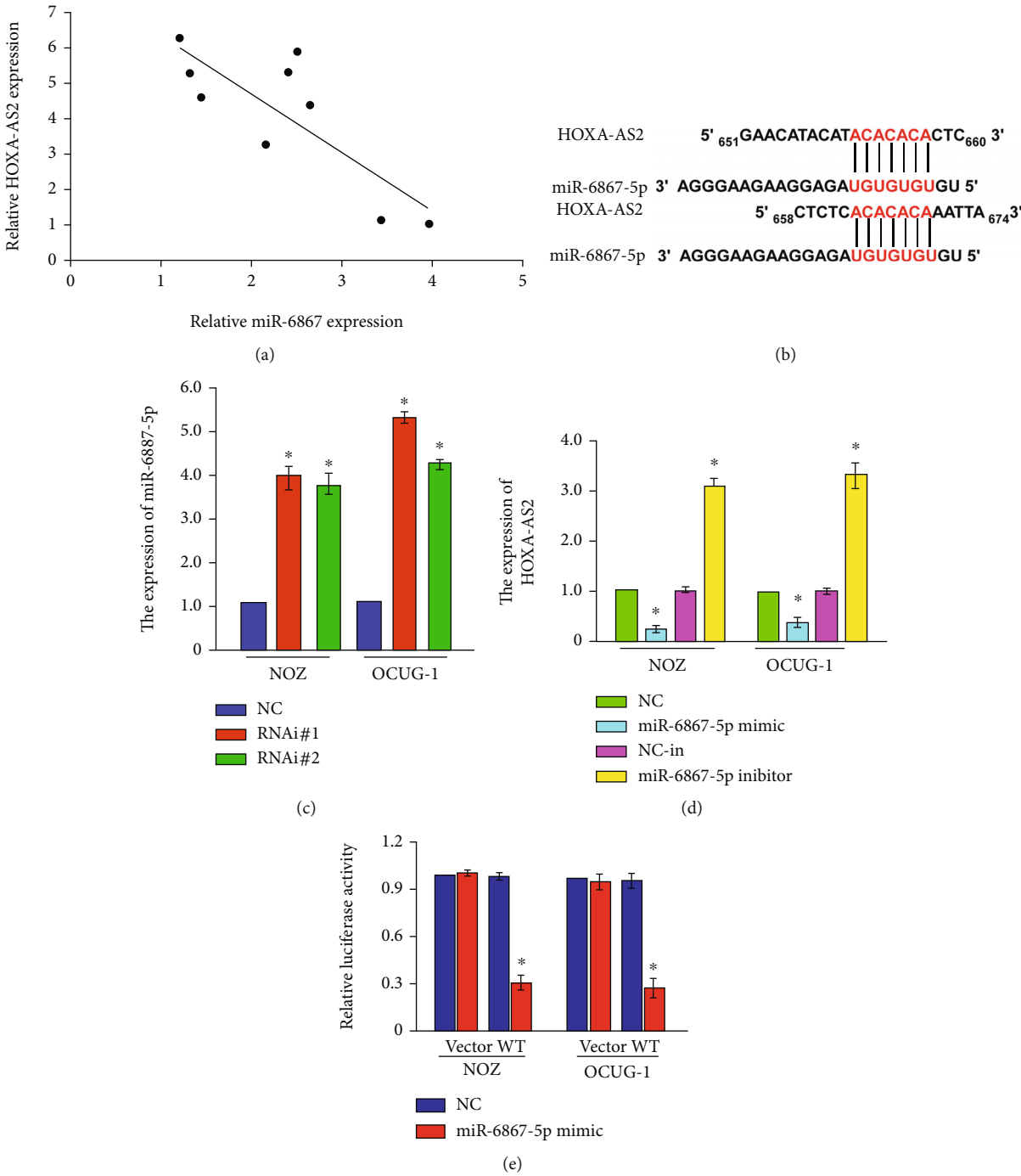

Figure 4: Regulation of miR-6867-5p by HOXA-AS2. (a) RT-qPCR detection of the correlation between HOXA-AS2 and miR-6867-5p expression. (b) Targets can predict the binding site prediction of HOXA-AS2 and miR-6867-5p. (c) RT-qPCR to detect the expression level of miR-6867 after HOXA-AS2 silencing in NOZ and OCUG-1 cells. (d) RT-qPCR is used to detect the overexpression of miR-6867 in NOZ and OCUG-1 cells and the expression of HOXA-AS2 after expression inhibition expression level; luciferase activity to detect the target regulation of HOXA-AS2 and miR-6867.

AS2 was highly expressed in gallbladder tumor tissues and cells. The molecular occurrence and progression of tumors is an extremely complex problem, in which cell cycle disturbance and epithelial-mesenchymal transition are common features of many types of human malignant tumor cells. Cell cycle disorders lead to uncontrolled cell proliferation, which greatly enhances the ability of cells to proliferate, while epithelial-mesenchymal transition makes cells lose contact inhibition and can move around [20, 21]. Epithelial-mesenchymal transition (EMT) also plays a significant role in the migration of gallbladder cancer cells. On the basis of this study, whether EMT is involved in the

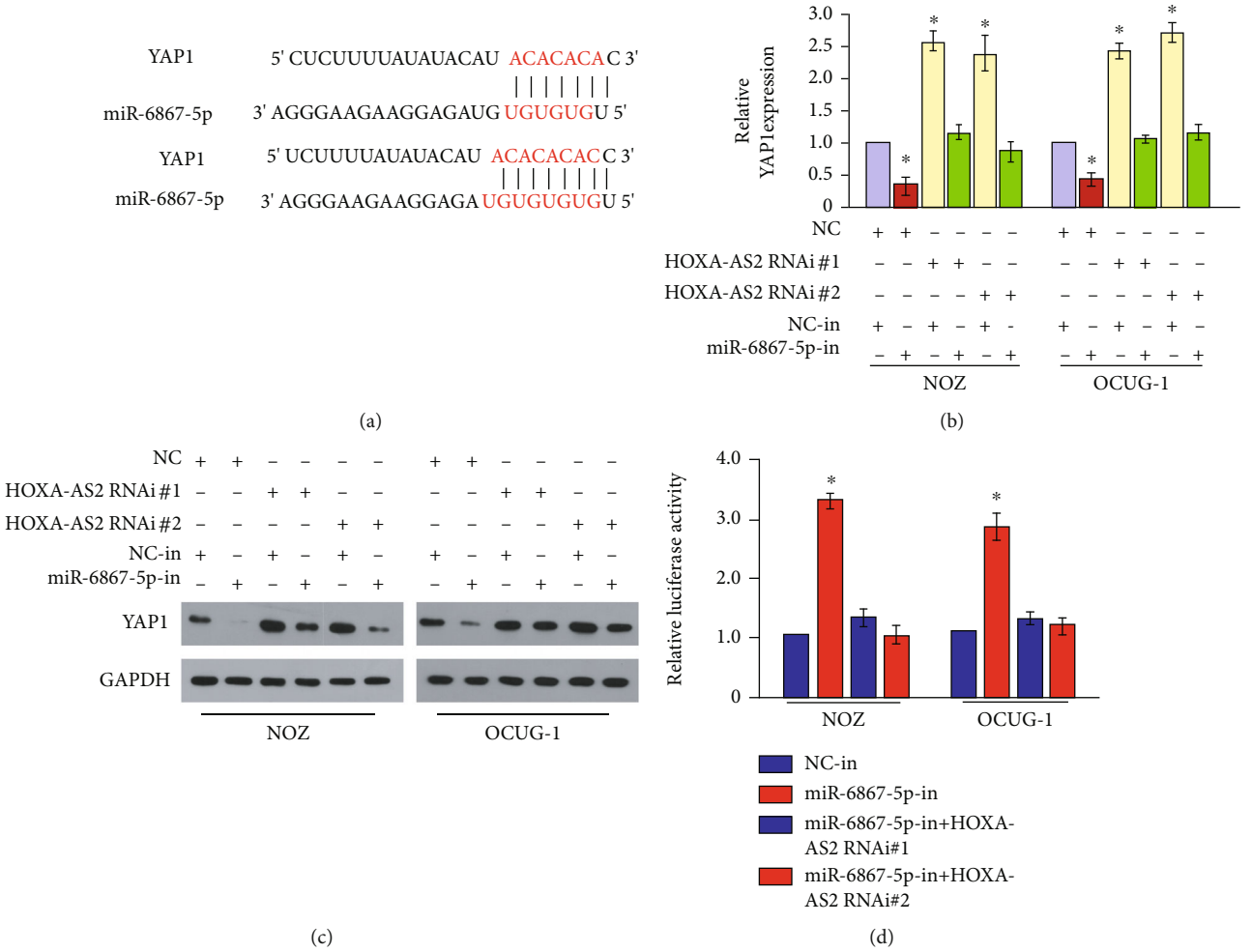

Figure 5: YAP1-related regulatory effects of HOXA-AS2 and miR-6867-5p. (a) Targets can software analyze the prediction of YAP1 3'UTR binding to miR-6867-5p targets. (b) RT-qPCR detects HOXA-AS2 and miR-6867 regulates the expression of YAP. (c) Western blot detection of HOXA-AS2 and miR-6867 regulate the expression of YAP. (d) Luciferase activity detection of HOXA-AS2 and miR-6867 regulation of YAP 3'UTR luciferase activity changes.

regulation of AS2 on the migration of gallbladder cancer cells can be further explored in the future. Our study confirmed that reducing HOXA-AS2 expression attenuated tumor cell proliferation in gallbladder cancer cell lines by the results of MTT assay and clone formation assay. The results of in vitro cell function experiments showed that interfering with the expression of HOXA-AS2 could inhibit the speed of in vitro migration of gallbladder cancer cells and the ability to invade other cells. At the same time, Western blot analysis of the expression of regulatory factors related to cell cycle and metastasis further confirmed that downregulation of HOXA-AS2 inhibited the migration of gallbladder cancer cells, but P21 protein and CyclinD1 protein were related to cell cycle. This may be related to the antiapoptotic effect of P21 protein [22–24]. Therefore, in this study, we explored the effect of HOXA-AS2 on cell cycle by detecting the expression of P21 protein and CyclinD1 protein.

Usually, lncRNAs and microRNAs (miRNAs) work together to regulate each other. We found that miR-6867-5p may be targeted by lncRNA HOXA-AS2 through bioinformatics tools. miR-6867-5p is a newly discovered miRNA with less research in the field of cancer. miR-6867-5p was found to be important in promoting angiogenesis under hypoxic conditions [25]. In this study, the expression of lncRNA HOXA-AS2 and miR-6867-5p strongly proves that lncRNA HOXA-AS2 and miR-6867-5p interact in the development of gallbladder cancer.

According to the prediction of the related software, YAP1 was predicted to be the target of miR-6867-5p, which was also confirmed by the detection of the luciferase reporter gene. The core components of signal transduction, Lats1/2, and Mst1/2, are often downregulated in some tumors due to the hypermethylation of their promoters, thereby promoting the malignant transformation of tumors [26]. Yes-associated proteins (YAPs) typically regulate signal transduction and gene transcription in cells [27, 28]. YAP is generally highly expressed in many tumors, and its nuclear activity is significantly enhanced, thereby inducing tumor progression [29–31]. lncRNA GAS5 interacts with YAP1 phosphorylation and degradation to inhibit rectal cancer progression [32]. However,

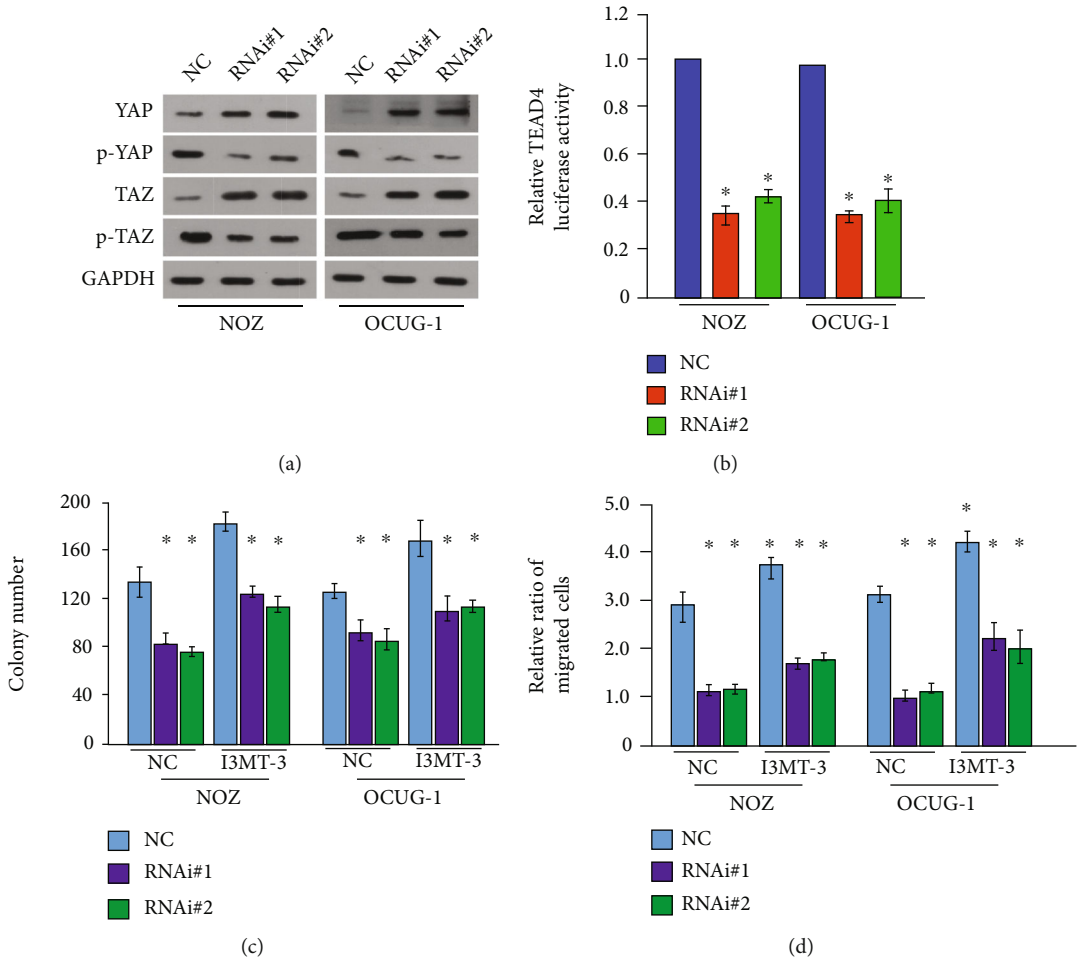

Figure 6: HOXA-AS2 affects the proliferation and invasion of gallbladder cancer cells through the regulation of YAP1 on the Hippo pathway. (a) Western blot detection of YAP and TAZ phosphorylation activation in Hippo signaling pathway after HOXA-AS2 silencing. (b) Luciferase activity detection of TEAD transcription factor activation after HOXA-AS2 downregulation (c). Clonal formation assay to detect Hippo pathway agonist-stimulation cell proliferation ability. (d) Transwell assay to detect cell invasion ability after Hippo pathway agonist stimulation.

how the Hippo-Yap signaling pathway plays its regulatory role in gallbladder cancer remains to be further clarified. The effect of lncRNA HOXA-AS2 on gallbladder cancer cells may affect the downregulation of miR-6867-5p and further affect the role of YAP1. In our study, YAP1 was first investigated in HOXA-AS2-knockdown gallbladder cancer cells. We found that YAP1 was downregulated in miR-6867-5p inhibitor and lncRNA HOXA-AS2 unsilenced groups, and upregulated in HOXA-AS2 knockout cells, indicating a regulatory relationship between lncRNA HOXA-AS2-miR-6867-5p-YAP1. In addition, unphosphorylated YAP is an active form, but YAP itself is a transcriptional coactivator that cannot bind DNA, so it needs to combine with other transcription factors such as TEAD1-4 to jointly initiate the transcription of downstream genes [33, 34]. Studies have shown that the downregulation of lncRNA HOXA-AS2 inhibits the phosphorylation of Yap/TAZ coactivator and its cytoplasmic retention, promotes its nuclear translocation, and promotes its function as a transcriptional coactivator, thereby promoting the expression of TEAD1-4 transcription factors. Activation. luciferase gene activity assay solution proves this. Our study also confirmed that after adding a Hippo pathway agonist, the invasive ability of gallbladder cancer cells with knockout of HOXA-AS2 were still lower. It is further proved that the Hippo signaling pathway-related regulates.

5. Conclusion

In conclusion, HOXA-AS2 may further regulate the occurrence and development of gallbladder cancer by regulating the miR-6867-5p-Yap pathway. HOXA-AS2 has important research significance in the study of potential diagnostic and therapeutic targets for gallbladder cancer. Due to the abnormal expression of HOXA-AS2 in hepatocellular carcinoma and other malignant tumors, the conclusion of this study may also be applicable to other tumor tissues. Subsequent experiments could also use the genes in this study to explore more cancer treatments.

Data Availability

The datasets used and/or analyzed during the current study are available from the corresponding author upon reasonable request.

Ethical Approval

This study has obtained the ethical approval of the Second Affiliated Hospital of Guangzhou Medical University and Zhujiang Hospital of Southern Medical University.

Conflicts of Interest

The authors declare that they have no conflicts of interest.

Acknowledgments

This study was supported by the Natural Science Foundation of Guangdong Province (2018A030313434), the Guangdong Provincial Medical Science Research Foundation (A2018259 and A2022250), the Guangzhou Municipal Science and Technology Project (201904010006), and Guangzhou Key Discipline of Urology.

Supplementary Materials

Supplemental Figure 1: TCGA analysis of HOXA-AS2 expression in different disease samples. *(Supplementary Materials)*

References

[1] H. Hong, C. L. He, S. Y. Zhu et al., "CCR7 mediates the TNF-α-induced lymphatic metastasis of gallbladder cancer through the "ERK1/2 - AP-1" and "JNK - AP-1" pathways," *Journal of Experimental & Clinical Cancer Research*, vol. 35, no. 1, p. 51, 2016.

[2] M. Li, Z. Zhang, X. Li et al., "Whole-exome and targeted gene sequencing of gallbladder carcinoma identifies recurrent mutations in the ErbB pathway," *Nature Genetics*, vol. 46, no. 8, pp. 872–876, 2014.

[3] X. S. Wu, L. B. Shi, M. L. Li et al., "Evaluation of two inflammation-based prognostic scores in patients with resectable gallbladder carcinoma," *Annals of Surgical Oncology*, vol. 21, no. 2, pp. 449–457, 2014.

[4] M. Zhan, X. Zhao, H. Wang et al., "miR-145 sensitizes gallbladder cancer to cisplatin by regulating multidrug resistance associated protein 1," *Tumour Biology*, vol. 37, no. 8, pp. 10553–10562, 2016.

[5] R. F. Bao, Y. J. Shu, Y. P. Hu et al., "miR-101 targeting ZFX suppresses tumor proliferation and metastasis by regulating the MAPK/Erk and Smad pathways in gallbladder carcinoma," *Oncotarget*, vol. 7, no. 16, pp. 22339–22354, 2016.

[6] H. Zhou, W. Guo, Y. Zhao et al., "MicroRNA-135a acts as a putative tumor suppressor by directly targeting very low density lipoprotein receptor in human gallbladder cancer," *Cancer Science*, vol. 105, no. 8, pp. 956–965, 2014.

[7] Y. Chang, C. Liu, J. Yang et al., "miR-20a triggers metastasis of gallbladder carcinoma," *Journal of Hepatology*, vol. 59, no. 3, pp. 518–527, 2013.

[8] R. Bonasio and R. Shiekhattar, "Regulation of transcription by long noncoding RNAs," *Annual Review of Genetics*, vol. 48, no. 1, pp. 433–455, 2014.

[9] I. M. Dykes and C. Emanueli, "Transcriptional and post-transcriptional gene regulation by long non-coding RNA," *Genomics, Proteomics & Bioinformatics*, vol. 15, no. 3, pp. 177–186, 2017.

[10] C. P. Ponting, P. L. Oliver, and W. Reik, "Evolution and functions of long noncoding RNAs," *Cell*, vol. 136, no. 4, pp. 629–641, 2009.

[11] J. W. Wang, S. Y. Peng, J. T. Li et al., "Identification of metastasis-associated proteins involved in gallbladder carcinoma metastasis by proteomic analysis and functional exploration of chloride intracellular channel 1," *Cancer Letters*, vol. 281, no. 1, pp. 71–81, 2009.

[12] S. H. Wang, X. C. Wu, M. D. Zhang, M. Z. Weng, D. Zhou, and Z. W. Quan, "Upregulation of H19 indicates a poor prognosis in gallbladder carcinoma and promotes epithelial-mesenchymal transition," *American Journal of Cancer Research*, vol. 6, no. 1, pp. 15–26, 2016.

[13] M. Z. Ma, B. F. Chu, Y. Zhang et al., "Long non-coding RNA CCAT1 promotes gallbladder cancer development via negative modulation of miRNA-218-5p," *Cell Death & Disease*, vol. 6, no. 1, article e1583, 2015.

[14] S. V. Mullegama, M. O. Alberti, C. Au et al., "Nucleic acid extraction from human biological samples," *Methods in Molecular Biology*, vol. 1897, pp. 359–383, 2019.

[15] K. N. Kasturi and T. Drgon, "Real-time PCR method for detection of salmonella spp. in environmental samples," *Applied and Environmental Microbiology*, vol. 83, no. 14, 2017.

[16] J. Pijuan, C. Barceló, D. F. Moreno et al., "In vitro cell migration, invasion, and adhesion assays: from cell imaging to data analysis," *Frontiers in Cell and Development Biology*, vol. 7, p. 107, 2019.

[17] S. Mikami, T. Kobayashi, and H. Imataka, "Cell-free protein synthesis systems with extracts from cultured human cells," *Methods in Molecular Biology*, vol. 607, pp. 43–52, 2010.

[18] T. O. Goetze, "Gallbladder carcinoma: prognostic factors and therapeutic options," *World Journal of Gastroenterology*, vol. 21, no. 43, pp. 12211–12217, 2015.

[19] A. Sharma, K. L. Sharma, A. Gupta, A. Yadav, and A. Kumar, "Gallbladder cancer epidemiology, pathogenesis and molecular genetics: recent update," *World Journal of Gastroenterology*, vol. 23, no. 22, pp. 3978–3998, 2017.

[20] S. Lamouille, J. Xu, and R. Derynck, "Molecular mechanisms of epithelial-mesenchymal transition," *Nature Reviews. Molecular Cell Biology*, vol. 15, no. 3, pp. 178–196, 2014.

[21] G. K. Schwartz and M. A. Shah, "Targeting the cell cycle: a new approach to cancer therapy," *Journal of Clinical Oncology*, vol. 23, no. 36, pp. 9408–9421, 2005.

[22] A. L. Gartel and S. K. Radhakrishnan, "Lost in transcription: p21 repression, mechanisms, and consequences," *Cancer Research*, vol. 65, no. 10, pp. 3980–3985, 2005.

[23] A. L. Gartel and A. L. Tyner, "The role of the cyclin-dependent kinase inhibitor p21 in apoptosis," *Molecular Cancer Therapeutics*, vol. 1, no. 8, pp. 639–649, 2002.

[24] M. Yeganeh, Y. Gui, R. Kandhi et al., "Suppressor of cytokine signaling 1-dependent regulation of the expression and oncogenic functions of $p21^{CIP1/WAF1}$ in the liver," *Oncogene*, vol. 35, no. 32, pp. 4200–4211, 2016.

[25] G. Yan, H. Zhao, and X. Hong, "lncRNA MACC1-AS1 attenuates microvascular endothelial cell injury and promotes angiogenesis under hypoxic conditions via modulating miR-6867-5p/TWIST1 in human brain microvascular endothelial cells," *Annals of Translational Medicine*, vol. 8, no. 14, p. 876, 2020.

[26] C. Seidel, U. Schagdarsurengin, K. Blümke et al., "Frequent hypermethylation of MST1 and MST2 in soft tissue sarcoma," *Molecular Carcinogenesis*, vol. 46, no. 10, pp. 865–871, 2007.

[27] C. D. K. Nguyen and C. Yi, "YAP/TAZ signaling and resistance to cancer therapy," *Trends in Cancer*, vol. 5, no. 5, pp. 283–296, 2019.

[28] S. Piccolo, S. Dupont, and M. Cordenonsi, "The biology of YAP/TAZ: hippo signaling and beyond," *Physiological Reviews*, vol. 94, no. 4, pp. 1287–1312, 2014.

[29] C. A. Hall, R. Wang, J. Miao et al., "Hippo pathway effector yap is an ovarian cancer oncogene," *Cancer Research*, vol. 70, no. 21, pp. 8517–8525, 2010.

[30] A. A. Steinhardt, M. F. Gayyed, A. P. Klein et al., "Expression of yes-associated protein in common solid tumors," *Human Pathology*, vol. 39, no. 11, pp. 1582–1589, 2008.

[31] B. Zhao, X. Wei, W. Li et al., "Inactivation of YAP oncoprotein by the hippo pathway is involved in cell contact inhibition and tissue growth control," *Genes & Development*, vol. 21, no. 21, pp. 2747–2761, 2007.

[32] W. Ni, S. Yao, Y. Zhou et al., "Long noncoding RNA GAS5 inhibits progression of colorectal cancer by interacting with and triggering YAP phosphorylation and degradation and is negatively regulated by the m6A reader YTHDF3," *Molecular Cancer*, vol. 18, no. 1, p. 143, 2019.

[33] W. M. Mahoney, J.-H. Hong, M. B. Yaffe, and I. K. G. Farrance, "The transcriptional co-activator TAZ interacts differentially with transcriptional enhancer factor-1 (TEF-1) family members," *The Biochemical Journal*, vol. 388, no. 1, pp. 217–225, 2005.

[34] B. Zhao, X. Ye, J. Yu et al., "TEAD mediates YAP-dependent gene induction and growth control," *Genes & Development*, vol. 22, no. 14, pp. 1962–1971, 2008.

Hindawi
Journal of Oncology
Volume 2022, Article ID 3379330, 14 pages
https://doi.org/10.1155/2022/3379330

Research Article

Seven Hub Genes Predict the Prognosis of Hepatocellular Carcinoma and the Corresponding Competitive Endogenous RNA Network

Xueqiong Han,[1] Jianxun Lu,[1] Chun Chen,[2] Yongran Deng,[1] Mingmei Pan,[1] Qigeng Li,[1] Huayun Wu,[1] Zhenlong Li,[1] and Bingqiang Ni[1]

[1]*Department of Oncology, The Fifth Affiliated Hospital of Guangxi Medical University & the First People's Hospital of Nanning, 89 Qixing Road, Nanning, Guangxi 530022, China*
[2]*Department of Cardiology and Endocrinology, The Guangxi Zhuang Autonomous Region Workers' Hospital, Nanning, China*

Correspondence should be addressed to Zhenlong Li; zhenlongli@gxzarwh.org and Bingqiang Ni; nbq181@aliyun.com

Xueqiong Han, Jianxun Lu, and Chun Chen contributed equally to this work.

Received 20 June 2022; Revised 15 August 2022; Accepted 18 August 2022; Published 12 October 2022

Academic Editor: Ashok Pandurangan

Purpose. This study was aimed at identifying hub genes and ceRNA regulatory networks linked to prognosis in hepatocellular carcinoma (HCC) and to identify possible therapeutic targets. *Methods*. Differential expression analyses were performed to detect the differentially expressed genes (DEGs) in the four datasets (GSE76427, GSE6764, GSE62232, and TCGA). The intersected DEmRNAs were identified to explore biological significance by enrichment analysis. We built a competitive endogenous RNA (ceRNA) network of lncRNA-miRNA-mRNA. The mRNAs of the ceRNA network were used to perform Cox and Kaplan-Meier analyses to obtain prognosis-related genes, followed by the selection of genes with an area under the curve >0.8 to generate the random survival forest model and obtain feature genes. Furthermore, the feature genes were subjected to least absolute shrinkage and selection operator (LASSO) and univariate Cox analyses were used to identify the hub genes. Finally, the infiltration status of immune cells in the HCC samples was determined. *Results*. A total of 1923 intersected DEmRNAs were identified in four datasets and involved in cell cycle and carbon metabolism. ceRNA network was created using 10 lncRNAs, 67 miRNAs, and 1,923 mRNAs. LASSO regression model was performed to identify seven hub genes, SOCS2, MYOM2, FTCD, ADAMTSL2, TMEM106C, LARS, and KPNA2. Among them, TMEM106C, LARS, and KPNA2 had a poor prognosis. KPNA2 was considered a key gene base on LASSO and Cox analyses and involved in the ceRNA network. T helper 2 cells and T helper cells showed a higher degree of infiltration in HCC. *Conclusion*. The findings revealed seven hub genes implicated in HCC prognosis and immune infiltration. A corresponding ceRNA network may help reveal their potential regulatory mechanism.

1. Introduction

According to 2018 estimates provided by Bray about the incidence of cancer, liver cancer was responsible for 841,080 new cancer cases globally [1] and the incidence rates are expected to increase remarkably by the year 2030 [2]. Hepatocellular carcinoma (HCC) is the most prevalent form of liver cancer, representing 75-85% of all liver cancer cases [3]. Previous studies confirmed that the main pathogenic factors of HCC are the chronic hepatitis B virus (HBV) or hepatitis C virus (HCV) infection, alcoholic liver disease, and nonalcoholic fatty liver disease [4]. Statistics indicate that 30%-40% of HCC patients are diagnosed in the early stage [5]. Only a few methods for the prognosis and treatment of HCC, these methods have been limited because most HCC patients are diagnosed in advanced stages and

surgically unresectable. Additionally, the methods depend mainly on the tumor stage [6] to reflect the development of tumor cells [7]. Therefore, identifying a sound risk stratification system can effectively treat and improve outcomes.

Competing endogenous RNA (ceRNA), including long noncoding RNA (lncRNA) and circle RNA (circRNA), can combine competitive microRNA (miRNA) and interfere with miRNA binding to messenger RNA (mRNA) to regulate gene expression and play important roles [8]. It has been shown that microRNAs, by virtue of their capacity to interact with many target genes, affect a wide variety of crucial biological processes, including growth, proliferation, and apoptosis of cells [9]. High expression of YKT6 [10] and MTFR2 [11] associated with progression and poor prognosis of HCC. Furthermore, EPHX2 was identified as an independent prognostic biomarker for overall survival of patients with HCC [12]. In summary, ceRNA is a factor that influences the incidence of HCC as well as its progression [13, 14]. The ceRNA was used to understand the interactions of complex genes and identified the potential biomarkers for diagnosing and treating HCC.

In this research, we mainly used the expression patterns of the databases in the Gene Expression Omnibus (GEO) (https://www.ncbi.nlm.nih.gov/geo/) and the Cancer Genome Atlas (TCGA) (https://portal.gdc.cancer.gov/) between HCC and normal samples to perform bioinformatics analysis. The purpose of this study is to construct a potentially competitive endogenous RNA (ceRNA) network to identify the underlying biological mechanisms of HCC. Furthermore, the model classifier and the risk score model were utilized to more precisely identify possible markers associated with prognosis in HCC patients.

2. Material and Methods

2.1. Data Preprocessing. There were a total of 600 HCC and 122 normal samples included within four different datasets (GSE76427, GSE6764, GSE62232, and TCGA datasets). RNA sequencing (RNA-seq) data, microRNA sequencing data, and the corresponding survival data of liver hepatocellular carcinoma (LIHC) patients were obtained from the TCGA database [15]. RNA-seq data and microRNA sequencing data of TCGA contained 369 primary HCC and 50 normal tissues as well as 370 primary HCC and 50 normal tissues, respectively. Corresponding clinicopathological features (age, sex, tumor differentiation degree, TNM stage, survival time, and status) were also obtained from the TCGA database are publicly available. Among these samples, one formalin sample and one relapse sample were excluded. Gene expression data of GSE76427, GSE6764, and GSE62232 were available from the GEO database. GSE76427 comprised 52 adjoining nontumor tissues as normal control and 115 tumor tissues with HCC. HCC patients included in this dataset had a mean age of 63.45 ± 12.63 years, and 93 male and 22 female [16], conducted by GPL10558 platform (Illumina HumanHT-12 V4.0 expression beadchip). GSE6764 was conducted by the GPL570 platform (Affymetrix Human Genome U133 Plus 2.0 Array) and comprised 35 HCC tissues and 10 adjoining nontumor tissues. HCV infection cases observed in 13 samples from cirrhotic tissues and 17 samples from dysplastic nodules were excluded [17]. GSE62232 containing 81 solid HCC and 10 nontumor liver samples was acquired on the basis of the GPL570 platform (Affymetrix Human Genome U133 Plus 2.0 Array). The individuals of HCC included in this dataset had a mean age of 60.6 ± 13.49 years, and 67 male and 14 female [18]. The "varianceStabilizingTransformation" function of the DESeq2 package [19] was utilized for normalizing the expression patterns of RNA sequencing data and microRNA sequencing from the TCGA dataset. Furthermore, expression profiles of GSE6764 and GSE62232 were normalized using the "RMA" function in the Affy package. The expression profile of GSE76427 was used to normalize by the "lumiExpresso" function in the Lumi R package.

2.2. Identification of Differentially Expressed Genes. By employing the limma package in R, differential expression analysis was carried out for gene expression to find the DEGs between HCC tumor tissues and nontumor liver tissues in GSE76427, GSE6764, and GSE62232 [20]. We also utilized the DESeq2 package [19] to identify the DEGs of TCGA. DEGs of all the four datasets (GSE76427, GSE6764, GSE62232, and TCGA) were deemed to have statistical significance if the adjusted P value was <0.05. Subsequently, the intersected DEGs of four datasets were identified using the Venn diagrams to obtain consistent expression, including upregulated and downregulated DEGs.

2.3. Gene Ontology (GO) and Pathway Enrichment Analysis. Cellular components (CCs), Biological processes (BPs), and molecular functions (MFs) of intersected DEGs were used to explore the biological significance by performing a GO analysis. Kyoto Encyclopedia of Genes and Genomes (KEGG) was utilized to explore significantly altered pathways enriched in the gene list. GO and KEGG pathways were executed with the help of the clusterProfile package [21]. Gene enrichment in the GO and KEGG pathway with P value <0.05 were judged as significant.

2.4. Gene Set Enrichment Analysis (GSEA). GSEA is a computational approach that enables gene sets to identify genomes excessively increasing or decreasing between biological phenotypes [22]. GSEA analysis was carried out to ascertain the functions premised on the expressed profiles of TCGA using the GSEA software (Version 4.1.0).

2.5. ceRNA Network Analysis. We examined the regulated miRNAs using up/downregulated lncRNAs in four datasets by Starbase databases (http://starbase.sysu.edu.cn/index.php) while retaining the opposite expression direction of lncRNAs and miRNAs. Among them, we extracted the intersection of the regulated miRNAs of TCGA for the next analysis. Meanwhile, we screened for miRNA-regulated mRNAs on the Targetscan databases (https://www.targetscan.org/vert_72/) while retaining the same expression direction of lncRNAs and mRNAs. Subsequently, we generated the lncRNA-miRNA-mRNA regulatory network

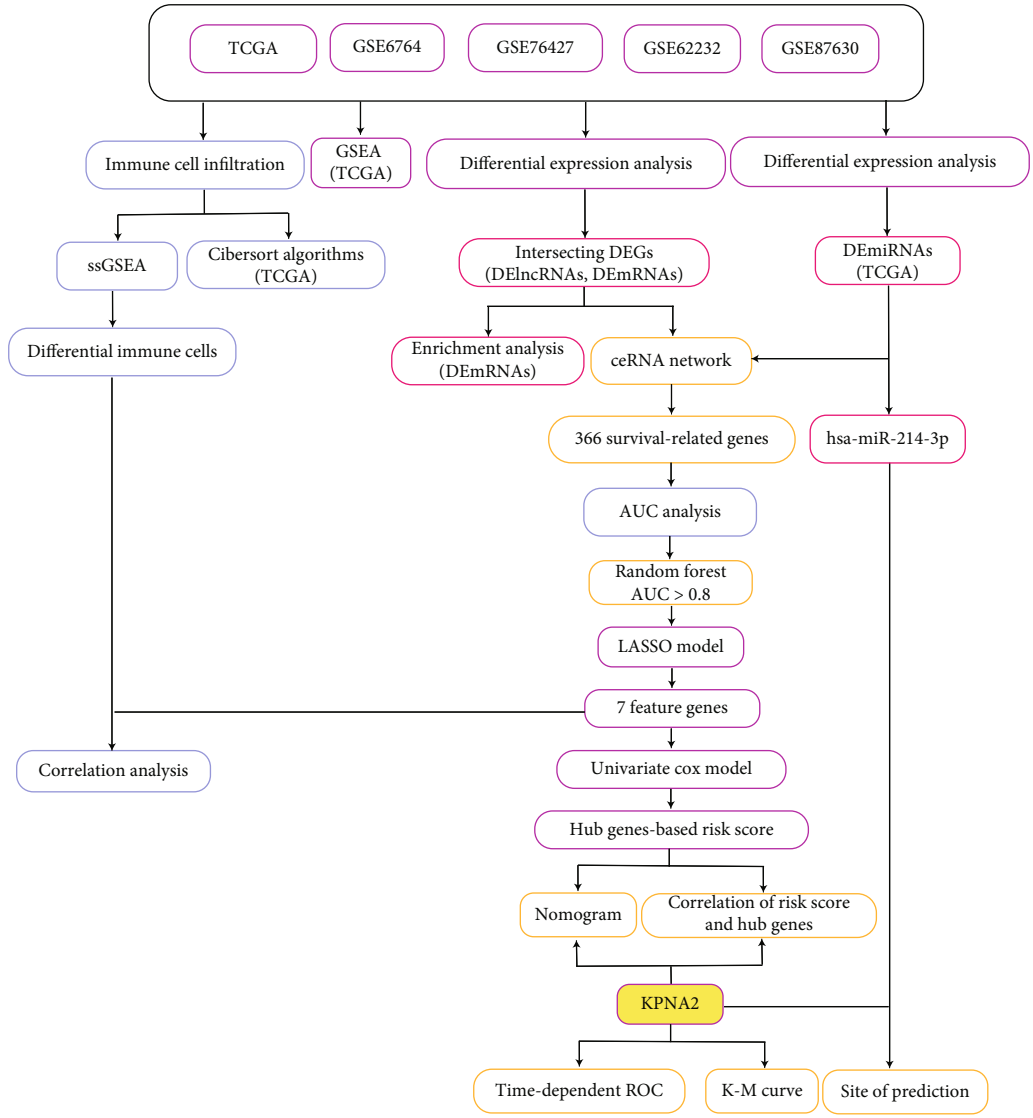

Figure 1: The detailed flow chart for this research AUC, area under the curve; DElncRNA, differentially expressed long noncoding RNA; DEG, differentially expressed genes; DEmRNA, differentially expressed messenger RNA; Gene Set Enrichment Analysis; LASSO, least absolute shrinkage, and selection operator; K-M curve, Kaplan-Meier curve; TCGA, The Cancer Genome Atlas; ssGSEA, single sample Gene Set Enrichment Analysis; ROC, receiver operating characteristic curve.

by downloading the binding sites of mRNA, miRNA, and lncRNA using the Starbase and Targetscan databases.

2.6. Establishment of Random Survival Forest Model and Least Absolute Shrinkage and Selection Operator (LASSO) Regression Model. The mRNAs of the ceRNA regulatory network were used to perform Cox and Kaplan-Meier analyses in TCGA to obtain prognosis-related genes. We selected the prognosis-related genes for the area under the curve (AUC) analysis by pROC package. Next, we used prognosis-related genes with an AUC >0.8 to construct the random survival forest model with the help of the RandomSurvivalForest R package. It was determined that genes with a relative importance >0.4 were the ultimate feature genes by examining the link between the error rate and the number of classification trees. Moreover, the feature genes were used to construct the LASSO model and the hub genes were obtained using "cv.glmnet" function in glmnet R package [23]. Subsequently, a univariate Cox analysis was carried out on the hub genes to determine the prognostic significance utilizing the forestplot R package. The hub genes with a hazard ratio >1 were considered to lead to a poor prognosis.

2.7. Seven Hub Gene-Risk Scores Based on Cox Regression Analysis. After performing a multivariate Cox regression analysis premised on the outcomes of seven hub genes, risk scores were then computed. Following the construction of the risk score model premised on the median risk score, the HCC patients of the TCGA dataset were further classified into high- and low-risk groups, and their overall survival (OS) rates were compared. Furthermore, to determine the impact that hub genes have on the HCC patients' prognoses,

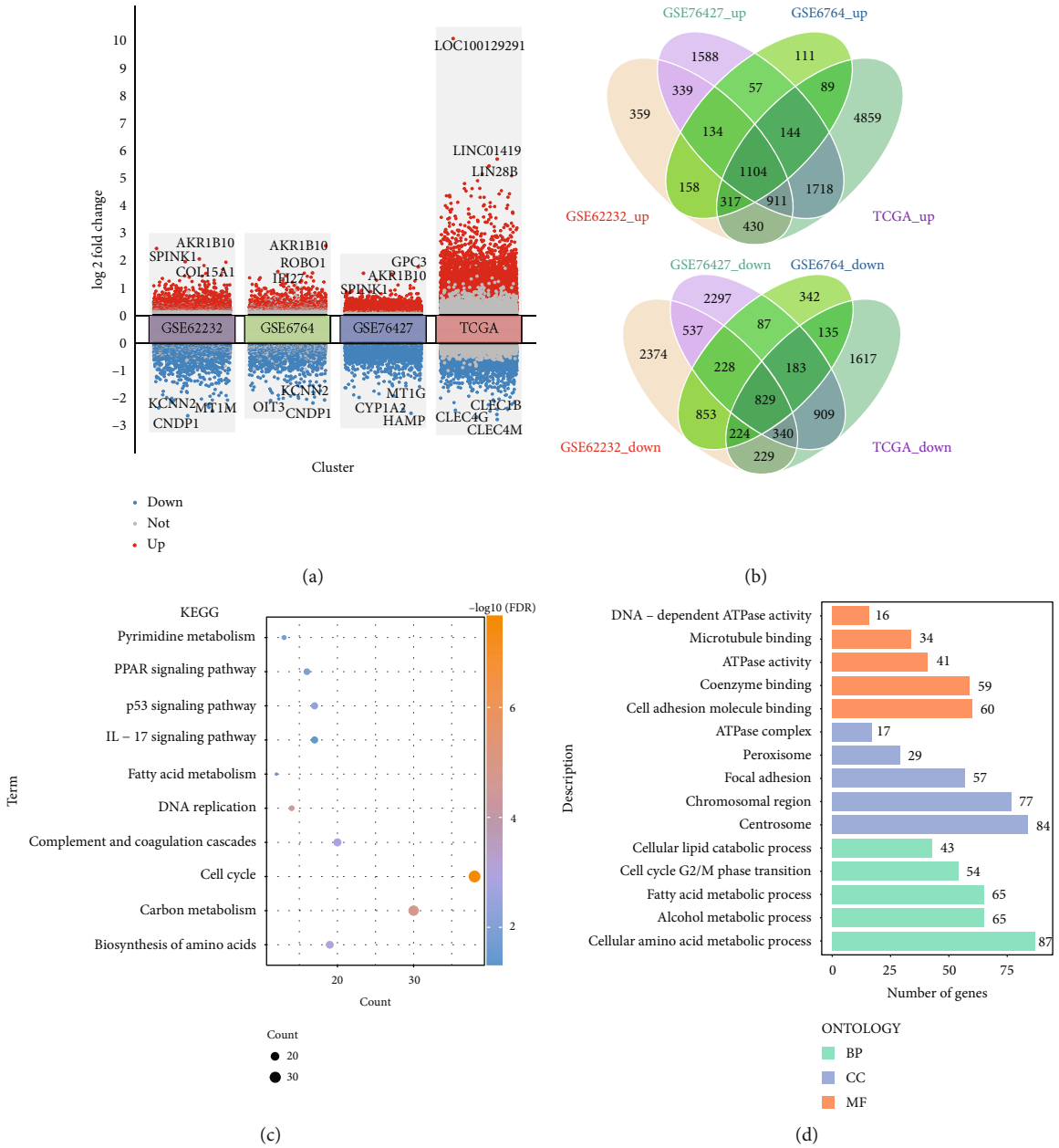

Figure 2: Continued.

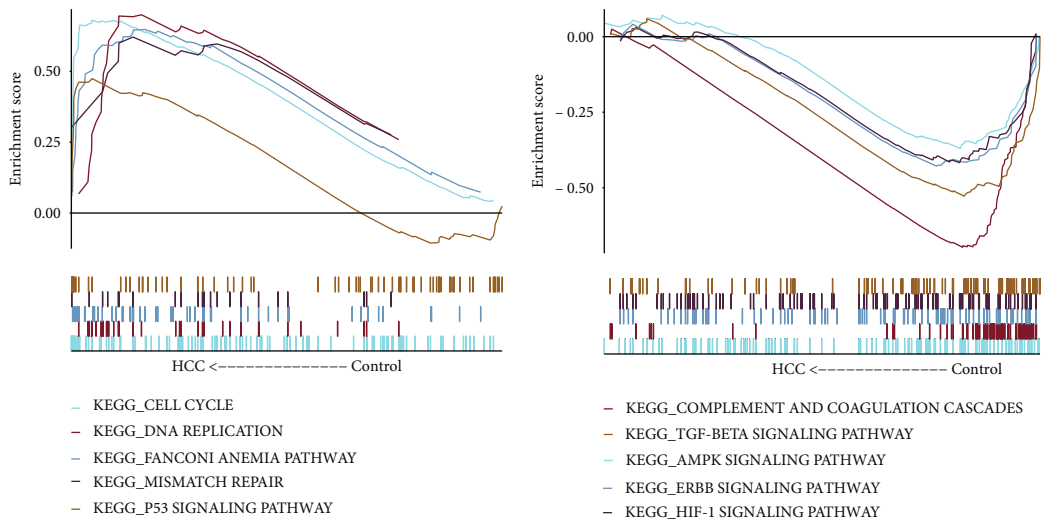

Figure 2: Enrichment analysis of differentially expressed genes (DEGs). (a) DEGs of GSE62232, GSE6764, GSE76427, and TCGA datasets between HCC and controls. Red denotes upmodulated DEGs, whereas blue denotes downmodulated DEGs. (b) DEGs in the same direction across all four datasets are shown by a Venn diagram. (c) Intersected DEGs of four datasets were involved in pathways by enrichment analysis. (d) Intersected DEGs of four datasets were involved in biological process, molecular function, and cellular component. (e, f) Gene set enrichment analysis illustrated the head and tail of five pathways enriched in HCC patients. KEGG, Kyoto Encyclopedia of Genes and Genomes; HCC, hepatocellular carcinoma; CC, cellular component; MF, molecular function; BP, biological process.

a nomogram was developed with the use of the rms package of the R program. With the help of the ggstatsplot package, correlations between hub genes and risk scores were derived.

2.8. Identification of Key Gene. To further illustrate the expression of hub genes between HCC and control samples in the TCGA dataset, we created a heat map and a violin plot. Above all, time-dependent receiver operating characteristic curve (ROC) analysis was conducted using the "survivalROC" R package to evaluate the prediction accuracy of the 1-, 3-, 5- year of the key gene. The Kaplan–Meier survival curve was utilized to make a comparison between the high- and low-risk groups for the survival of the key gene. Furthermore, P adjust value <0.05 was selected as the criterion for determining differentially expressed miRNAs (DEmiRs), after which we plotted the associated ceRNA regulatory network of key genes.

2.9. Immune Infiltration Analysis. Single-sample gene set enrichment analysis (ssGSEA) calculated the degree of immune cell infiltration in the HCC patients of 24 immune cell types using marker gene sets [24]. Using the limma R program, variations in the types of immune cells seen between HCC and control samples were computed Radar and scatter plots show correlation plots of risk score of immune cells and hub gene. Second, we adopted the Pearson correlation to determine the link between the seven hub genes and the immune cell types. Additionally, The CIBERSORT algorithm was utilized to execute an analysis of the infiltration levels of 22 different types of immune cells in HCC samples taken from the TCGA dataset.

2.10. Statistical Analysis. The analyses of the present study were conducted utilizing the Bioinforcloud platform (http://www.bioinforcloud.org.cn).

3. Results

Workflow of the present study (Figure 1).

3.1. Biological Function of DEGs between HCC and Controls. To obtain dysfunctional genes associated with HCC, we identified DEGs between HCC and controls (Figure 2(a)). In total, 9,366 DEGs were identified in GSE62232, 11405 DEGs in GSE76427, 4995 DEGs in GSE7696, and 14,038 DEGs in TCGA. A total of 1,933 intersected DEmRNAs were detected in four datasets, including 10 lncRNA and 1,923 mRNA. Among them, 1,104 were upregulated and 829 downregulated DEGs in HCC and controls (Figure 2(b)). Intersected DEGs were involved in the cell cycle and carbon metabolism (Figure 2(c)). Additionally, intersected DEGs were involved in 1,584 BP, 210 CC, and 213 MF (Figure 2(d)). GSEA showed that genes of the TCGA dataset were positively linked to DNA replication and the cell cycle (Figure 2(e)) and were inversely linked to the ERBB signaling pathway and HIF-1 signaling pathway (Figure 2(f)).

3.2. Identification of Hub Genes Related to Prognosis. The ceRNA regulatory network was constructed using the 366 prognosis-related mRNAs that were obtained from Kaplan-Meier and Cox survival analyses (Table S1). Based on AUC analysis, 366 prognosis-related mRNAs were analyzed to determine their possible involvement in the GSE76427 and TCGA datasets. As depicted in Figure 3(a), 211 genes with

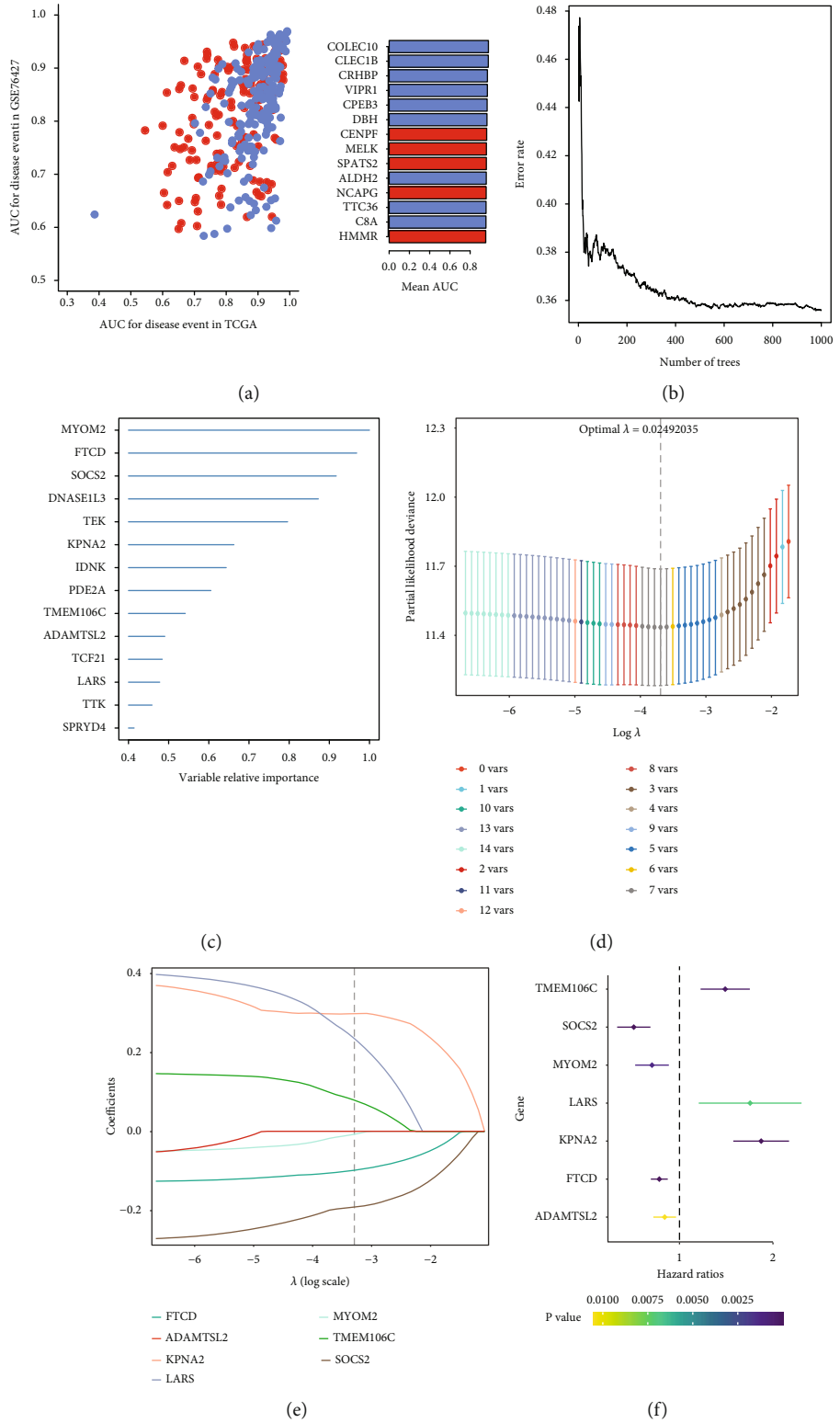

Figure 3: Identification of hub genes by least absolute shrinkage and selection operator (LASSO) and univariate Cox models. (a) The top 14 genes are shown with AUC>0.80 in TCGA and GSE76427. Genes that have been upregulated are shown in red, whereas genes that have been downregulated are shown in blue. (b) The correlation between the number of trees and the error rate. (c) A random forest model was constructed to determine the importance of the 14 genes in an order. (d) LASSO coefficient profiles of the 7 feature genes. (e) 10-fold cross-validation of parameter selection in the LASSO analysis. (f) Univariate analysis of feature genes. The feature genes with hazard ratios >1 are poor prognosis genes, and hazard ratios <1 are protective genes. TCGA, The Cancer Genome Atlas; AUC, area under the curve.

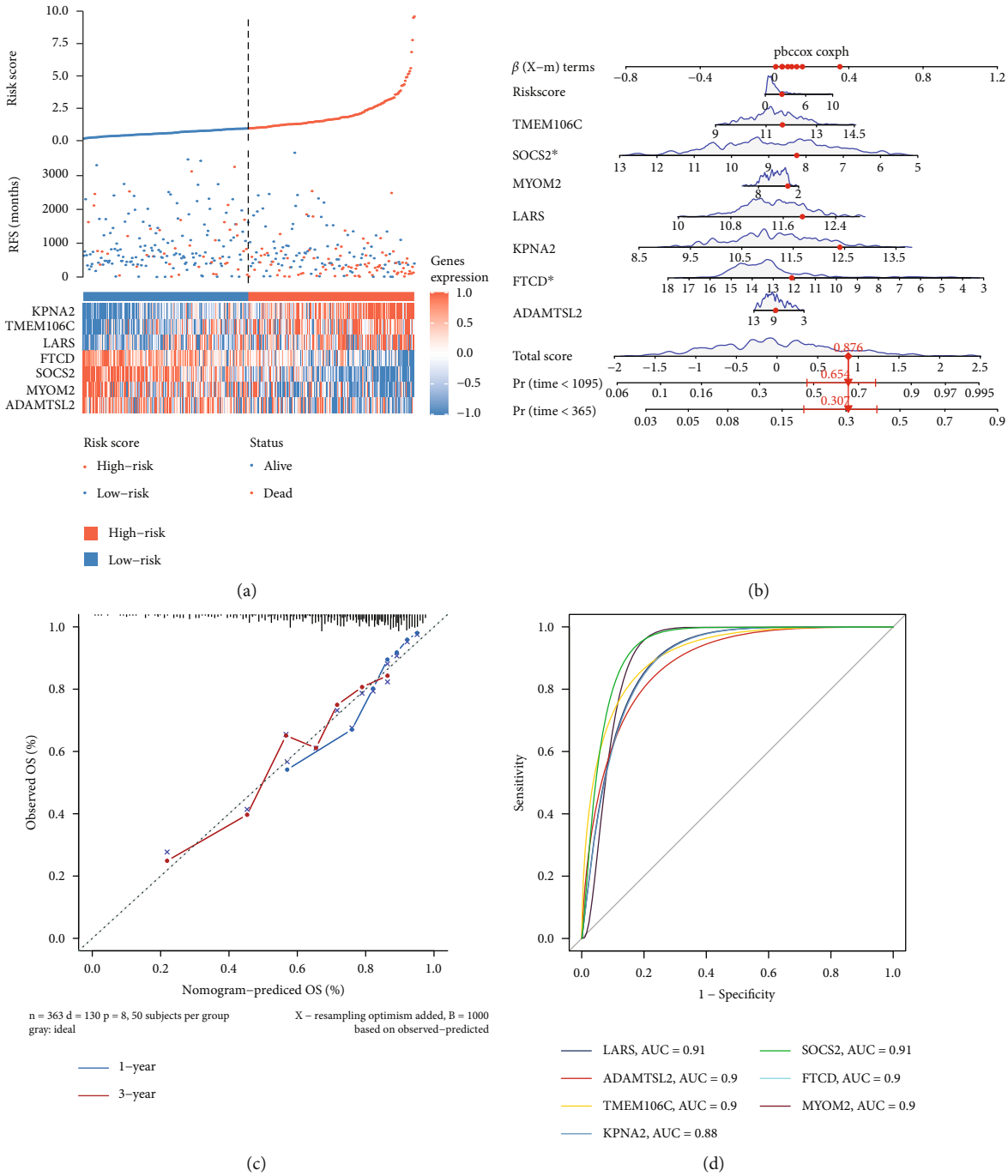

Figure 4: Continued.

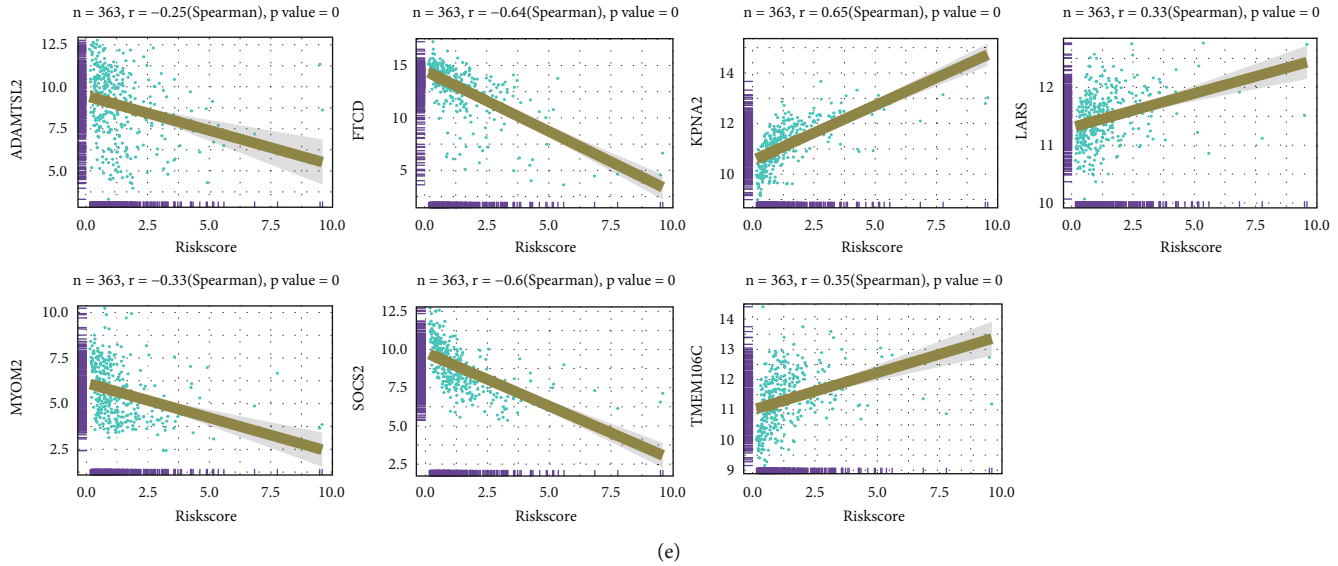

(e)

Figure 4: Seven feature gene-risk scores based on Cox analyses. (a) Expression, risk score, and survival status of seven genes in HCC patients of the TCGA dataset. (b) Nomogram for the prediction of 1- and 3-year overall survival (OS) for HCC patients with seven feature genes. (c) Calibration curves for seven feature genes and 1-, 3-year OS in the validation set (TCGA). (d) AUCs value of seven feature genes. (e) Correlation of risk score and seven hub genes. OS, overall survival; AUC, area under the curve.

an AUC of <0.80 were found in both datasets. Figures 3(b) and 3(c) provide an orderly representation of the association between the error rate for the data, the number of classification trees, and the importance of the 14 genes. LASSO regression model was performed to identify 7 hub genes, SOCS2, MYOM2, FTCD, ADAMTSL2, TMEM106C, LARS, and KPNA2 (Figures 3(e) and 3(f)). In univariate Cox regression analysis, TMEM106C, LARS, and KPNA2 had a poor prognosis (Figure 3(f)).

3.3. Construction of Hub Genes and Calculation of Risk Score in HCC. The distributions of the risk scores, RFS and hub gene expression of the 369 patients in the TCGA dataset are shown in Figure 4(a). The hub genes were incorporated into a nomogram model to predict the HCC patients' prognoses (Figure 4(b)). The calibration curve demonstrated excellent agreement between the observed and predicted OS over 1 and 3 years in the TCGA cohort (Figure 4(c)). The AUC analysis of seven hub genes as illustrated in Figure 4(d) and the relevant findings illustrated that the seven hub genes had a better diagnostic power in the prognostic model. We additionally examined the link between hub genes and risk scores and found that KPNA2, LARS, and TMEM106C had a positive link to risk scores, whereas an inverse correlation was observed between ADAMTSL2, MYOM2, FTCD, SOCS2, and risk scores (Figure 4(e)).

3.4. KPNA2 as a Key Gene in Prognosis for HCC. In four datasets (GSE76427, GSE6764, GSE62232, and TCGA), the results suggested that hub genes of AUCs value, adjusted *P* value, and fold change were depicted in Figure 5(a). A heat map showed the expression level of hub genes, stage, gender, event, and groups in TCGA (Figure 5(b)). In comparison with controls, ADAMTSL2, FTCD, KPNA2, LARS, and TMEM106C were found to be expressed at a high level in HCC (Figure 5(c)). Time-dependent ROC survival analysis was employed to examine the prognosis of KPNA2 and the findings illustrated that the AUCs values over 1, 3, and 5 years were all greater than 0.66 (Figure 5(d)). Moreover, the predicted 1-year survival time for HCC patients indicated that KPNA2 had considerably improved OS (Figure 5(e)). The volcano plot showed a total of 901 DEmiRs, comprising 730 upmodulated miRNAs and 171 downmodulated miRNAs (Figure 5(f)). Ultimately, Figure 5(g) depicts the obtained binding sites within the lncRNA HCP5-KPNA2-miR-214-3p as ceRNA regulatory network. Above all, KPNA2 performs an essential function in the ceRNA regulatory network, making it a key gene in the prognosis and fundamental biological processes involving HCC.

3.5. Estimation of Infiltrating Immune Cells in HCC. T helper (Th) 2 cells, T helper cells, and plasmacytoid dendritic cells (pDCs) all have higher degrees of infiltration between HCC and controls in four datasets (Figure 6(a)). Figure 6(b) depicts the association between the median risk score and the types of immune cells. Among them, CD8 T cells, Th17 cells, and DC exhibited a substantially positive correlation, whereas Th2 cells exhibited a significantly negative correlation (Figure 6(c)). By determining the Pearson correlation between the hub genes and the 24 different types of immune cells, we observed that KPNA2 and Th2 cells had a considerably high association in HCC samples (Figure 6(d)). To further evaluate the proportion of immune cells for TCGA, the findings indicated that HCC samples were extensively infiltrated by Macrophages M2 (Figure 6(e)).

Gene	TCGA AUC	TCGA logFold Change	TCGA p adjust	GSE76427 AUC	GSE76427 logFold Change	GSE76427 p adjust	GSE62232 AUC	GSE62232 logFold Change	GSE62232 p adjust	GSE6764 AUC	GSE6764 logfold change	GSE6764 p adjust
ADAMTSL2	0.8972358	−1.51 (rank: 03)	3.141662e-09	0.8933110	−1.88 (rank: 01)	1.710110e-16	0.8382716	−0.63 (rank: 07)	4.578539e-03	0.7885714	−0.42 (rank: 07)	4.185487e-02
FTCD	0.8968022	−1.39 (rank: 06)	2.860642e-09	0.9132107	−1.54 (rank: 03)	7.726937e-18	0.9641975	−1.59 (rank: 02)	4.777393e-04	0.7600000	−0.98 (rank: 03)	1.485547e-02
KPNA2	0.8829268	1.41 (rank: 05)	1.177452e-28	0.9408027	0.77 (rank: 06)	1.941301e-20	0.9592593	1.46 (rank: 03)	7.176953e-07	0.9600000	1.61 (rank: 01)	3.135729e-05
LARS	0.9142547	0.69 (rank: 07)	3.485848e-25	0.8655518	0.59 (rank: 07)	5.578071e-14	0.9901235	0.82 (rank: 05)	3.199658e-08	0.8800000	0.57 (rank: 06)	1.606274e-03
MYOM2	0.9402710	−2.06 (rank: 02)	4.677377e-16	0.9568562	−1.70 (rank: 02)	1.946919e-32	0.9444444	−0.80 (rank: 06)	1.390891e-06	0.9628571	−0.73 (rank: 05)	8.686889e-07
SOCS2	0.9147425	−2.19 (rank: 01)	4.233325e-25	0.8839465	−1.53 (rank: 04)	3.799142e-18	0.9370370	−1.93 (rank: 01)	1.373581e-07	0.8285714	−1.44 (rank: 02)	6.238659e-03
TMEM106C	0.8986992	1.50 (rank: 04)	4.330979e-31	0.8494147	1.01 (rank: 05)	1.868355e-12	0.9617284	0.86 (rank: 04)	1.179064e-05	0.9514286	0.76 (rank: 04)	1.409836e-04

(a)

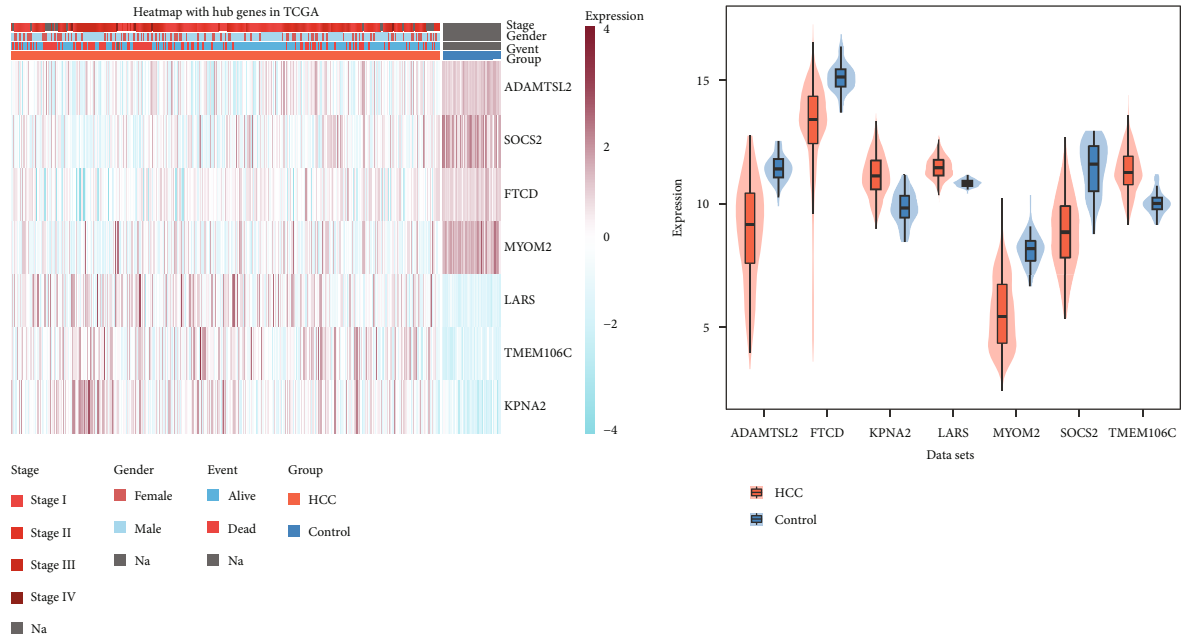

(b)

(c)

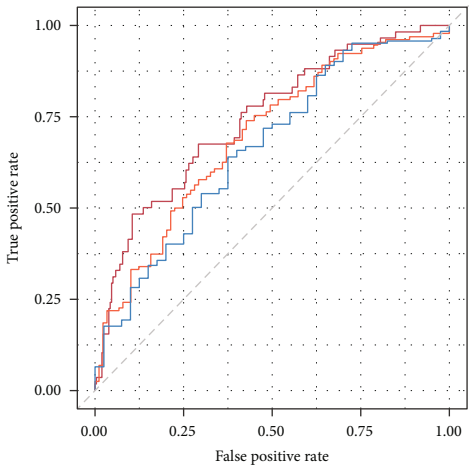

(d)

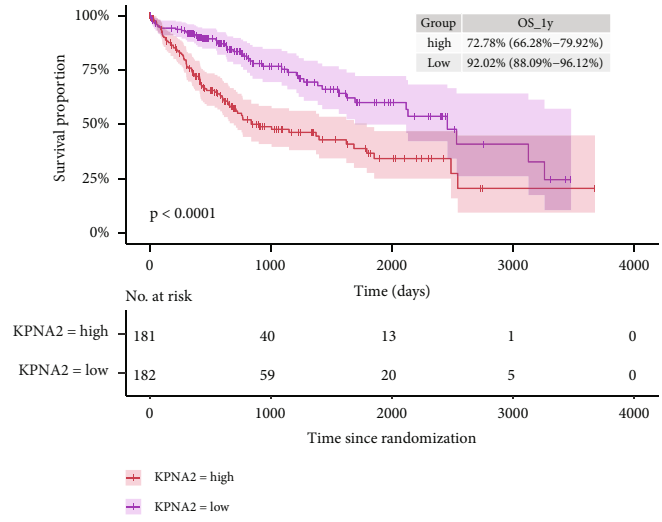

(e)

Figure 5: Continued.

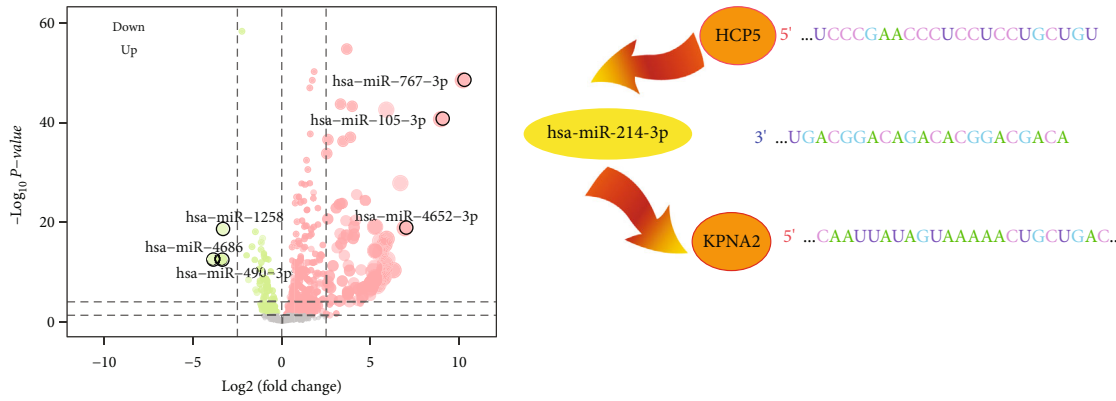

(f) (g)

FIGURE 5: Expression of hub genes and construction of ceRNA regulated network. (a) The log-fold change, AUC, and adjusted *P* value of seven genes in TCGA, GSE76427, GSE62232, and GSE6764. (b) Stage, gender, event, and expressed levels were shown in HCC and control in HCC. (c) Violin plots illustrated the expression of seven hub genes. The thick black bar in the middle indicates the interquartile range, and the black line extending from it represents the 95% confidence interval. (d) Time-dependent receiver operating characteristic curve analysis displayed the AUC values over 1, 3, and 5 years. (e) Estimating the survival time of the KPNA2d by Kaplan-Meier survival curve. (f) Differentially expressed miRNAs were identified between controls and HCC samples in TCGA. Red represents upregulated miRNAs, whereas green represents downregulated miRNAs. (g) Bind sites of HCP5/has-miR-214-3p/KPNA2. Orange indicates upregulated, and yellow indicates down-regulated. HCC, hepatocellular carcinoma; AUC, area under the curve; TCGA, The Cancer Genome Atlas.

4. Discussion

HCC is a malignancy with a high death rate and an unfavorable prognosis, necessitating novel diagnostic and therapeutic markers [25]. In this research, we determined the seven hub genes of HCC prognosis as vital biomarkers, which can be used to improve outcomes of patients with HCC. We constructed a ceRNA regulatory network to explore the biological mechanism, including lncRNA HCP5-hsa-miR-214-3p-KPNA2. Furthermore, we also found a high degree of immune cell infiltration with seven hub genes.

Intersected DEGs of four datasets were involved in the cell cycle and carbon metabolism. Previous research has shown that cell cycle regulation inhibits the proliferative ability of HCC cells [26]. Importantly, GSEA showed that genes of the TCGA dataset were enriched in the cell cycle and carbon metabolism. Studies have shown that tumor cells often regulate the genes of the cell cycle producing damage and inactivation of this pathway may be involved in tumor development [27]. Furthermore, high expression of miR-452-5p performs an integral function in the progression of HCC through carbon metabolism [28].

Seven hub genes (SOCS2, MYOM2, FTCD, ADAMTSL2, TMEM106C, LARS, and KPNA2) involved in the process of the HCC prognosis were identified. SOCS2 was associated with distinct stages that indicated poor survival outcomes for patients with HCC [29]. Previous studies have shown that FTCD is a protective factor in HCC development and prognosis [30]. Overexpression of TMEM106C [31] and KPNA2 [32] predicted an unsatisfactory prognosis in HCC patients. Downregulated MYOM2 was observed in a majority of clinical cases of breast cancer [33], however, the role of MYOM2, ADAMTSL2, and LARS in HCC development and prognosis remains unclear.

In this present research, in the TCGA liver cancer cohorts, a high level of KPNA2 expression accurately predicted the 1-, 3-, and 5-year survival times, with AUCs of 0.742, 0.697, and 0.663, correspondingly. A risk score and nomogram model also indicated that high-expressed KPNA2 led to an unfavorable prognosis. There was also a strong association between the risk score and KPNA2, which suggests that KPNA2 could be a crucial biological marker in determining the prognosis of patients with HCC. Recently, an increasing number of studies have demonstrated that lncRNA and miRNA primarily mediated posttranscriptional regulation, and that dysregulation of this process has been linked to many malignancies [34]. Interestingly, through targeting KPNA2, the lncRNA HCP5 served as a ceRNA, which had the effect of adversely modulating the expression of miR-214-3p. Downmodulation of lncRNA HCP5 in HCC tissues, when contrasted to normal samples, could affect the proliferation, metastatic and invasive, while the relevant mechanism of HCC still needs to be elucidated [35]. miR-214-3p is shown to modulate cell growth, metastasis, and apoptosis in HCC cells, endometrial cancer cells, and retinoblastoma cells by directly targeting certain genes linc00665 [36], ATWIST1 [37], BCB1, and XIAP [38]. In general, this ceRNA regulatory network further helps us understand the regulatory mechanisms of these genes in HCC.

ssGSEA indicated that Th2 cells and plasmacytoid dendritic cells (pDCs) all exhibited a higher degree of infiltration between HCC and controls. An intratumoral infiltration of pDCs is predictive of an unfavorable prognosis among patients who undergo curative resection for HCC; pDCs exist in numerous primary as well as metastatic human neoplasms [39]. Furthermore, the significantly positive correlation between Th2 cells and KPNA2 that Th2 cells were linked to HCC patient survival [40]. Th17 cells, dendritic

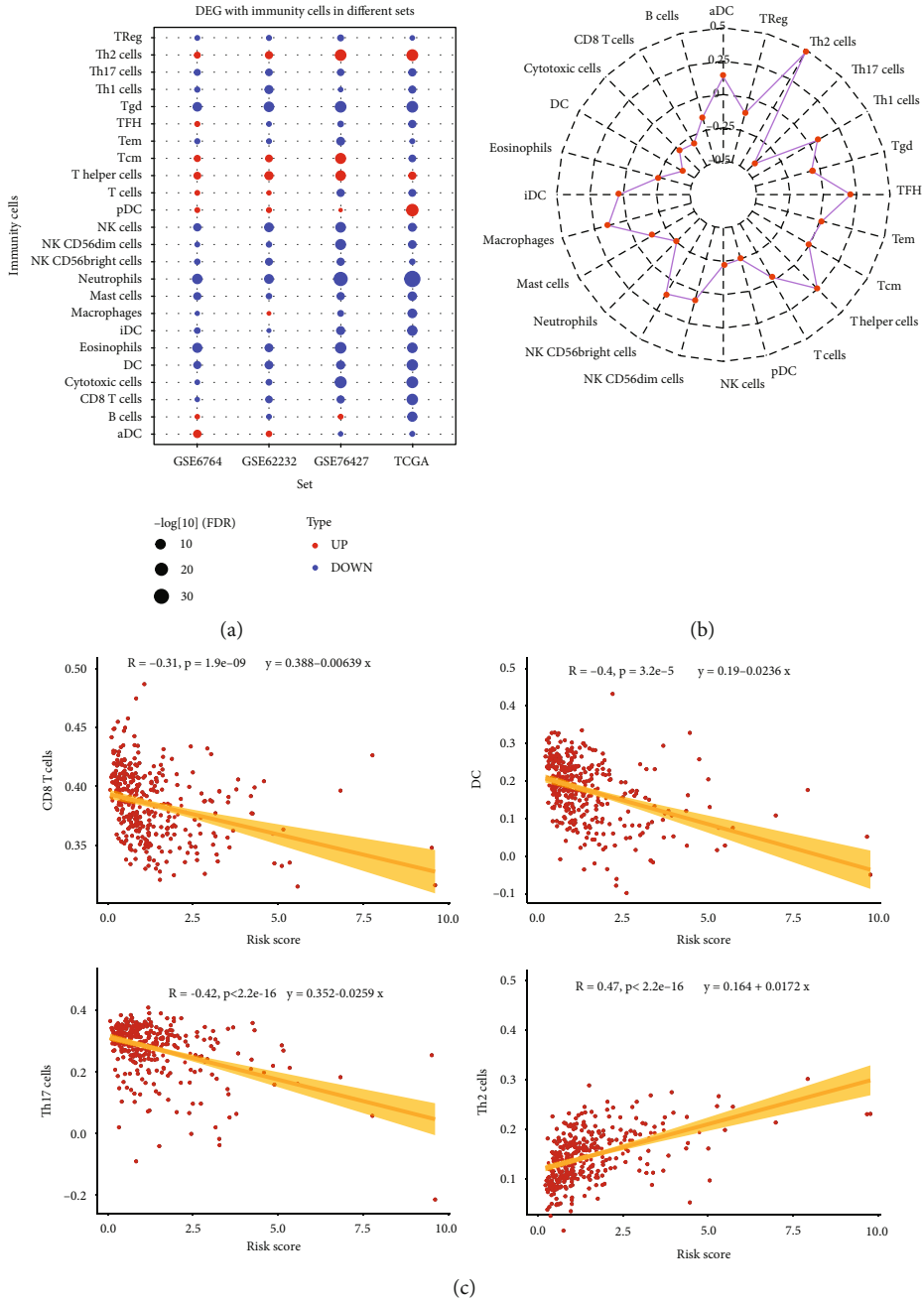

Figure 6: Continued.

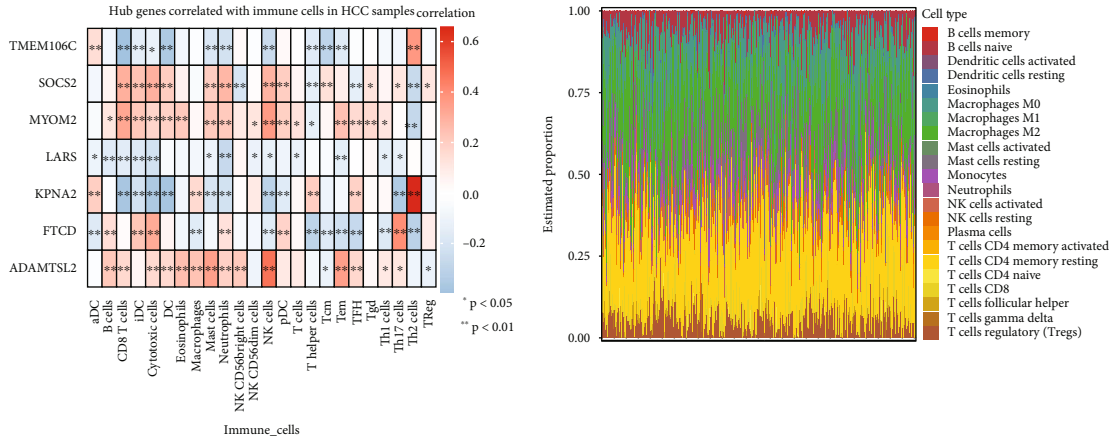

Figure 6: Immune cell infiltration in HCC. (a) Single sample gene set enrichment analysis was used to estimate the infiltration of immune cells. Red indicates high infiltration and blue indicates low infiltration. (b) Radar plot shows the correlation between 24 immune cell types and risk score of seven hub genes. (c) Correlation scatter plots shows the most significant infiltrating cells and risk score. (d) Correlation with seven hub genes and immune cells in HCC samples. (e) Estimated proportions of 22 immune cell types. DEGs, differentially expressed genes; HCC, hepatocellular carcinoma.

cells (DCs), and CD8 T cells were positively linked to the risk score of prognosis. The levels of Th17 cells were substantially elevated in tumors of patients with HCC [41]. DCs and CD8+ T cells have increased infiltration levels and are associated with relapse, compared with primary HCC [42]. The seven hub genes were defined as biomarkers for OS and we constructed a high immune cell infiltration model to predict the HCC patients' prognoses.

Despite the new findings at the level of bioinformatics analysis, understanding of the prognosis and immune-related biomarkers are still limited. Firstly, the markers associated with HCC currently lack sufficient sensitivity and specificity. Secondly, molecular and animal experiments are needed to verify the biomarkers and apply the biomarkers from preclinical studies in clinical practice.

5. Conclusion

SOCS2, MYOM2, FTCD, ADAMTSL2, TMEM106C, LARS, and KPNA2 are vital biomarkers and involved in the process of the HCC prognosis and immune infiltration.

Data Availability

The datasets (GSE76427, GSE6764, GSE62232) supporting the conclusions of this article are available in the Gene Expression Omnibus (http://www.ncbi.nlm.nih.gov/geo) and the Cancer Genome Atlas https://portal.gdc.cancer.gov/) database.

Conflicts of Interest

The authors declare that they have no competing interest.

Authors' Contributions

Xueqiong Han was responsible for manuscript writing, Jianxun Lu was responsible for manuscript writing and proofreading, Yongran Deng was responsible for data collection, Mingmei Pan was responsible for data analysis, Qigeng Li was responsible for data collation, Huayun Wu was responsible for picture typesetting, Zhenlong Li was responsible for the construction of ideas, Bingqiang Ni was responsible for overall proofreading and review. Xueqiong Han, Jianxun Lu and Chun Chen contributed equally to this work and share first authorship.

Acknowledgments

The authors would like to thank Shaowen Mo and Qiong Song for assisting with bioinformatics analysis on the BioInforCloud platform.

Supplementary Materials

Supplementary Table 1 366 prognosis-related mRNA list. *(Supplementary Materials)*

References

[1] F. Bray, J. Ferlay, I. Soerjomataram, R. L. Siegel, L. A. Torre, and A. Jemal, "Global cancer statistics 2018: GLOBOCAN estimates of incidence and mortality worldwide for 36 cancers in 185 countries," *CA: a Cancer Journal for Clinicians*, vol. 68, no. 6, pp. 394–424, 2018.

[2] P. C. Valery, M. Laversanne, P. J. Clark, J. L. Petrick, K. A. McGlynn, and F. Bray, "Projections of primary liver cancer to 2030 in 30 countries worldwide," *Hepatology*, vol. 67, no. 2, pp. 600–611, 2018.

[3] S. Mittal and H. B. El-Serag, "Epidemiology of hepatocellular carcinoma: consider the population," *Journal of Clinical Gastroenterology*, vol. 47, Supplement 1, pp. S2–S6, 2013.

[4] F. Kanwal and A. G. Singal, "Surveillance for hepatocellular carcinoma: current best practice and future direction," *Gastroenterology*, vol. 157, no. 1, pp. 54–64, 2019.

[5] I. C. Lee, H. J. Lei, G. Y. Chau et al., "Predictors of long-term recurrence and survival after resection of HBV-related hepatocellular carcinoma: the role of HBsAg," *American Journal of Cancer Research*, vol. 11, no. 7, pp. 3711–3725, 2021.

[6] C. Liu, L. G. Duan, W. S. Lu et al., "Prognosis evaluation in patients with hepatocellular carcinoma after hepatectomy: comparison of BCLC, TNM and Hangzhou criteria staging systems," *PLoS One*, vol. 9, no. 8, article e103228, 2014.

[7] L. Zhou, J. A. Rui, W. X. Zhou, S. B. Wang, S. G. Chen, and Q. Qu, "Edmondson-Steiner grade: a crucial predictor of recurrence and survival in hepatocellular carcinoma without microvascular invasio," *Pathology, Research and Practice*, vol. 213, no. 7, pp. 824–830, 2017.

[8] L. Salmena, L. Poliseno, Y. Tay, L. Kats, and P. P. Pandolfi, "A *ceRNA* Hypothesis: the rosetta stone of a hidden RNA language?," *Cell*, vol. 146, no. 3, pp. 353–358, 2011.

[9] W. R. Farid, Q. Pan, A. J. van der Meer et al., "Hepatocyte-derived microRNAs as serum biomarkers of hepatic injury and rejection after liver transplantation," *Liver Transplantation*, vol. 18, no. 3, pp. 290–297, 2012.

[10] J. Z. Xu, J. J. Jiang, H. J. Xu, X. D. Sun, Z. C. Liu, and Z. M. Hu, "High expression ofYKT6associated with progression and poor prognosis of hepatocellular carcinoma," *Scandinavian Journal of Gastroenterology*, vol. 56, no. 11, pp. 1349–1354, 2021.

[11] D. Li, Y. Ji, J. Guo, and Q. Guo, "Upregulated expression ofMTFR2as a novel biomarker predicts poor prognosis in hepatocellular carcinoma by bioinformatics analysis," *Future Oncology*, vol. 17, no. 24, pp. 3187–3201, 2021.

[12] K. Zhan, Y. Bai, S. Liao et al., "Identification and validation of EPHX2 as a prognostic biomarker in hepatocellular carcinoma," *Molecular Medicine Reports*, vol. 24, no. 3, 2021.

[13] B. Li, R. Mao, C. Liu, W. Zhang, Y. Tang, and Z. Guo, "LncRNA FAL1 promotes cell proliferation and migration by acting as a CeRNA of miR-1236 in hepatocellular carcinoma cells," *Life Sciences*, vol. 197, pp. 122–129, 2018.

[14] W. Y. Hu, H. Y. Wei, K. M. Li, R. B. Wang, X. Q. Xu, and R. Feng, "LINC00511 as a ceRNA promotes cell malignant behaviors and correlates with prognosis of hepatocellular carcinoma patients by modulating miR-195/EYA1 axis," *Biomedicine & Pharmacotherapy*, vol. 121, article 109642, 2020.

[15] K. Tomczak, P. Czerwinska, and M. Wiznerowicz, "Review The cancer genome atlas (TCGA): an immeasurable source of knowledge," *Contemporary Oncology/Współczesna Onkologia*, vol. 2015, no. 1A, pp. 68–77, 2015.

[16] O. V. Grinchuk, S. P. Yenamandra, R. Iyer et al., "Tumor-adjacent tissue co-expression profile analysis reveals pro-oncogenic ribosomal gene signature for prognosis of resectable hepatocellular carcinoma," *Molecular Oncology*, vol. 12, no. 1, pp. 89–113, 2018.

[17] E. Wurmbach, Y. B. Chen, G. Khitrov et al., "Genome-wide molecular profiles of HCV-induced dysplasia and hepatocellular carcinoma," *Hepatology*, vol. 45, no. 4, pp. 938–947, 2007.

[18] K. Schulze, S. Imbeaud, E. Letouzé et al., "Exome sequencing of hepatocellular carcinomas identifies new mutational signatures and potential therapeutic targets," *Nature Genetics*, vol. 47, no. 5, pp. 505–511, 2015.

[19] M. I. Love, W. Huber, and S. Anders, "Moderated estimation of fold change and dispersion for RNA-seq data with DESeq2," *Genome Biology*, vol. 15, no. 12, p. 550, 2014.

[20] M. E. Ritchie, B. Phipson, D. Wu et al., "Limma powers differential expression analyses for RNA-sequencing and microarray studies," *Nucleic Acids Research*, vol. 43, no. 7, p. e47, 2015.

[21] G. Yu, L. G. Wang, Y. Han, and Q. Y. He, "clusterprofiler: an R package for comparing biological themes among gene clusters," *OMICS*, vol. 16, no. 5, pp. 284–287, 2012.

[22] A. Subramanian, P. Tamayo, V. K. Mootha et al., "Gene set enrichment analysis: a knowledge-based approach for interpreting genome-wide expression profiles," *Proceedings of the National Academy of Sciences of the United States of America*, vol. 102, no. 43, pp. 15545–15550, 2005.

[23] S. Engebretsen and J. Bohlin, "Statistical predictions with glmnet," *Epigenetics*, vol. 11, no. 1, p. 123, 2019.

[24] G. Bindea, B. Mlecnik, M. Tosolini et al., "Spatiotemporal dynamics of intratumoral immune cells reveal the immune landscape in human cancer," *Immunity*, vol. 39, no. 4, pp. 782–795, 2013.

[25] S. Shen, Y. Lin, X. Yuan et al., "Biomarker MicroRNAs for diagnosis, prognosis and treatment of hepatocellular carcinoma: a functional survey and comparison," *Scientific Reports*, vol. 6, no. 1, p. 38311, 2016.

[26] Y. Zhao, C. Zhu, Q. Chang et al., "MiR-424-5p regulates cell cycle and inhibits proliferation of hepatocellular carcinoma cells by targeting E2F7," *PLoS One*, vol. 15, no. 11, article e0242179, 2020.

[27] C. J. Sherr, "Cancer cell cycles," *Science*, vol. 274, no. 5293, pp. 1672–1677, 1996.

[28] M. H. Rong, K. T. Cai, H. P. Lu et al., "Overexpression of MiR-452-5p in hepatocellular carcinoma tissues and its prospective signaling pathways," *International Journal of Clinical and Experimental Pathology*, vol. 12, no. 11, pp. 4041–4056, 2019.

[29] J. Liu, Z. Liu, W. Li, and S. Zhang, "SOCS2 is a potential prognostic marker that suppresses the viability of hepatocellular carcinoma cells," *Oncology Letters*, vol. 21, no. 5, p. 399, 2021.

[30] J. Liu, S. Q. Zhang, J. Chen et al., "Identifying prognostic significance of RCL1 and four-gene signature as novel potential biomarkers in HCC patients," *Journal of Oncology*, vol. 2021, Article ID 5574150, 20 pages, 2021.

[31] X. Luo, G. Han, R. Lu et al., "Transmembrane protein 106C promotes the development of hepatocellular carcinoma," *Journal of Cellular Biochemistry*, vol. 121, no. 11, pp. 4484–4495, 2020.

[32] X. Guo, Z. Wang, J. Zhang et al., "Upregulated KPNA2 promotes hepatocellular carcinoma progression and indicates prognostic significance across human cancer types," *Acta biochimica et Biophysica Sinica*, vol. 51, no. 3, pp. 285–292, 2019.

[33] F. Yamamoto and M. Yamamoto, "Identification of genes that exhibit changes in expression on the 8p chromosomal arm by the systematic multiplex RT-PCR (SM RT-PCR) and DNA microarray hybridization methods," *Gene Expression*, vol. 14, no. 4, pp. 217–227, 2008.

[34] Y. Li, X. Liu, X. Cui et al., "lncRNA PRADX-mediated recruitment of PRC2/DDX5 complex suppresses UBXN1 expression and activates NF-κB activity, promoting tumorigenesis," *Theranostics*, vol. 11, no. 9, pp. 4516–4530, 2021.

[35] Y. Zhou, K. Li, T. Dai et al., "Long non-coding RNA HCP5 functions as a sponge of miR-29b-3p and promotes cell growth and metastasis in hepatocellular carcinoma through upregulating DNMT3A," *Aging (Albany NY)*, vol. 13, no. 12, pp. 16267–16286, 2021.

[36] H. Wan, Y. Tian, J. Zhao, and X. Su, "LINC00665 targets miR-214-3p/MAPK1 Axis to accelerate hepatocellular carcinoma growth and Warburg effect," *Journal of Oncology*, vol. 2021, Article ID 9046798, 14 pages, 2021.

[37] Y. Y. Fang, M. R. Tan, J. Zhou et al., "miR-214-3p inhibits epithelial-to-mesenchymal transition and metastasis of endometrial cancer cells by targeting TWIST1," *Oncotargets and Therapy*, vol. 12, pp. 9449–9458, 2019.

[38] L. Yang, L. Zhang, L. Lu, and Y. Wang, "miR-214-3p regulates multi-drug resistance and apoptosis in retinoblastoma cells by targeting ABCB1 and XIAP," *Oncotargets and Therapy*, vol. 13, pp. 803–811, 2020.

[39] Z. J. Zhou, H. Y. Xin, J. Li, Z. Q. Hu, C. B. Luo, and S. L. Zhou, "Intratumoral plasmacytoid dendritic cells as a poor prognostic factor for hepatocellular carcinoma following curative resection," *Cancer Immunology, Immunotherapy*, vol. 68, no. 8, pp. 1223–1233, 2019.

[40] F. Foerster, M. Hess, A. Gerhold-Ay et al., "The immune contexture of hepatocellular carcinoma predicts clinical outcome," *Scientific Reports*, vol. 8, no. 1, p. 5351, 2018.

[41] J. Yan, X. L. Liu, G. Xiao et al., "Prevalence and clinical relevance of T-helper cells, Th17 and Th1, in hepatitis B virus-related hepatocellular carcinoma," *PLoS One*, vol. 9, no. 5, article e96080, 2014.

[42] Y. Sun, L. Wu, Y. Zhong et al., "Single-cell landscape of the ecosystem in early-relapse hepatocellular carcinoma," *Cell*, vol. 184, no. 2, pp. 404–421.e16, 2021.

Hindawi
Journal of Oncology
Volume 2022, Article ID 3426407, 13 pages
https://doi.org/10.1155/2022/3426407

Review Article

Managing Cancer Drug Resistance from the Perspective of Inflammation

Shuaijun Lu,[1,2] **Yang Li**,[3] **Changling Zhu**,[4] **Weihua Wang**,[1] **and Yuping Zhou**[1,2]

[1]*The Affiliated Hospital of Medical School, Ningbo University, Ningbo 315020, China*
[2]*Institute of Digestive Disease of Ningbo University, Ningbo 315020, China*
[3]*West China School of Basic Medical Sciences and Forensic Medicine, Sichuan University, Chengdu 610064, China*
[4]*Ningbo First Hospital, Ningbo 315010, China*

Correspondence should be addressed to Yuping Zhou; nbuzhouyuping@126.com

Received 5 July 2022; Accepted 17 August 2022; Published 19 September 2022

Academic Editor: Nandakumar Natarajan

The development of multidrug resistance in cancer chemotherapy is a major obstacle to the effective treatment of human malignant tumors. Several epidemiological studies have demonstrated that inflammation is closely related to cancer and plays a key role in the development of both solid and liquid tumors. Therefore, targeting inflammation and the molecules involved in the inflammatory process may be a good strategy for treating drug-resistant tumors. In this review, we discuss the molecular mechanisms underlying inflammation in regulating anticancer drug resistance by modulating drug action and drug-mediated cell death pathways. Inflammation alters the effectiveness of drugs through modulation of the expression of multidrug efflux transporters (e.g., ABCG2, ABCB1, and ABCC1) and drug-metabolizing enzymes (e.g., CYP1A2 and CYP3A4). In addition, inflammation can protect cancer cells from drug-mediated cell death by regulating DNA damage repair, downstream adaptive response (e.g., apoptosis, autophagy, and oncogenic bypass signaling), and tumor microenvironment. Intriguingly, manipulating inflammation may affect drug resistance through various molecular mechanisms validated by *in vitro*/*in vivo* models. In this review, we aim to summarize the underlying molecular mechanisms that inflammation participates in cancer drug resistance and discuss the potential clinical strategies targeting inflammation to overcome drug resistance.

1. Introduction

Current cancer treatments (e.g., surgery, chemotherapy, radiotherapy, targeted therapy, and immune therapy) benefit an increasing number of patients who suffer from cancer [1]. Still, the effectiveness of these strategies is limited by drug resistance, which remains a primary obstacle to the curative treatment of various cancers [2]. Resistance to anticancer drugs can be divided into two categories: intrinsic and acquired drug resistance [3, 4]. Intrinsic resistance indicates that resistance regulators are present in a large number of tumor cells prior to chemotherapy, rendering treatment ineffective. Acquired resistance may develop during treatment as a result of nongenetic changes, which enhance tumor cell survival [5, 6]. The anticancer drug resistance mechanism involves many aspects, such as deregulated drug transport, altered target proteins/receptors, and abnormal regulation of cellular metabolic pathways [7, 8]. Of note, several new cancer treatment strategies have been applied to the clinic in response to the above mechanisms.

Inflammation is an immune response to bodily injury that can fight infection and trauma by removing harmful factors and damaged tissue, thereby repairing the tissue and returning it to normal [9]. In detail, in the early or acute phase of inflammation, pathogen-associated molecular patterns (PAMPs) are recognized by tissue macrophages or mast cells, which in turn activate the secretion of inflammatory cytokines, chemokines, vasoactive amines, and other substances, thereby enhancing the immune response around the blood vessels [10, 11]. Activated inflammatory cells produce anti-inflammatory cytokines as well as pro-

inflammatory cytokines [12, 13]. The former mainly includes IL-4, IL-13, IL-10, and TGF-β, and the latter mainly includes TNF-α, IL-1β, IL-2, IL-6, IL-8, IL-17, and IFN-γ. Pro-inflammatory and anti-inflammatory cytokines interact to form a complex network whose dynamic balance determines the development and outcome of inflammation [14]. Studies have shown that multiple pathways are involved in the initial regulation of the inflammatory response, such as Jak/Stat signaling [15], NF-kB signaling [16], Wnt signaling [17], and Toll-like receptor signaling [18, 19]. Many similarities have been found between inflammatory response and tumor development in regulating signaling pathways and gene expression [20, 21]. For instance, NF-κB is a transcription factor that can be activated by a variety of cytokines and plays a key role in inflammatory processes. In cancer, it is usually kept active and can regulate the cell cycle and apoptosis process by activating genes encoding related proteins, thereby inducing survival and promoting cancer progression [22].

As one of the hallmarks of cancer, multiline evidence indicates that inflammation contributes to tumorigenesis, tumor progression, metastasis, and resistance, yet its specific mechanism in most tumors remains unclear [23]. If the inflammatory response persists for too long, it may turn into chronic inflammation, which has many carcinogenic mechanisms, including inducing gene mutation, promoting angiogenesis, changing gene status, promoting cell proliferation and malignant transformation, etc [24]. It proved that inflammation plays a promoting role in the occurrence and development of tumors [25]. Nevertheless, there are few studies on the effect of inflammation on tumor drug resistance. In the current review, we suspect that inflammation plays a certain role in tumor drug resistance and focus on several aspects underlying inflammation-mediated drug resistance (Figure 1).

2. Inflammation-Mediated Changes in Drug Transport and Metabolism

Abnormal activation of drug efflux is one of the important reasons for tumor chemotherapy resistance. Meanwhile, the metabolic pathways are also major routes of drug resistance due to their drug-clearing and activation functions, particularly for anti-infectives and cancer drugs [26]. Abnormal activation of tumor efflux and excessive drug metabolism will cause the drug concentration in tumor cells to be lower than the killing concentration during tumor chemotherapy, resulting in tumor cell survival [27]. Therefore, exploring the activation level of drug efflux and drug metabolism in the inflammatory state is helpful to deeply understand the molecular mechanism of drug resistance under an inflammatory state. Here we attempt to explore the effects of inflammation on drug transport and metabolism.

2.1. Inflammation and Drug Efflux Transporters. There exist 48 ATP-binding cassette (ABC) transporters that can be subdivided into seven distinct subfamilies A-G [28, 29]. These drug efflux transporters reduce the intracellular drug concentration and inhibit drug efficacy [30]. Sufficient experimental results suggest that ABC transporter family proteins are associated with drug resistance, especially multidrug resistance protein 1 (MDR1; also known as P-glycoprotein and ABCB1), MDR-associated protein 1 (MRP1; also known as ABCC1), and breast cancer resistance protein (BCRP; also known as ABCG2) [31]. Some research has found that inflammation directly or indirectly impacts drug transporters. For example, peripheral inflammatory pain changes paracellular permeability and increases the expression and activity of P-glycoprotein (P-gp) at the blood-brain barrier, leading to arduous drug uptake by the brain [32]. MDR1 expression in immune cells has been studied in recent years. The inflammatory environment can cause upregulation of MDR1 in some cells involved in innate immunity [33]. Furthermore, the expression of BCRP was significantly reduced by IL-1, IL-6, and TNF-α during acute inflammation, and IL-2 can stimulate JAK3 activation, thus phosphorylating tyrosine residues in BCRP promote their drug efflux function [34]. Endotoxin-induced systemic inflammation in rats is correlated with the apparent changes in the placental expression of several drug transporters; with the increased level of pro-inflammatory cytokines IL-6 and TNF-α, the mRNA expression of Abcc3 increased, while the expression of transporters such as Abcb1a and Abcc2 decreased [35]. Researchers found that gene polymorphisms of ABCG2 potentially affect the serum levels of pro-inflammatory markers by drug efflux in some chronic inflammatory arterial diseases, implying an interaction between inflammation and drug transporters [36]. Several endogenous compounds related to inflammation development, such as cAMP and PGs, are also substrates of MRPs, which could provide new targets for the treatment of inflammatory diseases [37]. Together, inflammatory cytokines have different effects on drug transporters. Several cytokines (e.g., IL-6, TNF-α, and IL-1) inhibit drug efflux, while IL-2 increases drug efflux. The dual roles of cytokines indicate that the effect of inflammation on tumor cell drug resistance is the result of a multifactorial interaction, which is affected by the inflammatory microenvironment, the stage of inflammation induction, and the type of inflammation. Systematic studies on tumor resistance will help continue to elucidate the molecular events of inflammation-induced drug efflux and drug metabolism.

2.2. Inflammation and Drug Metabolism. In addition to drug efflux, activation or inactivation of drugs conducted by cytochrome P450 enzymes (CYPs) have been assumed to be important molecular mechanisms underlying cancer drug resistance [38]. The effects of cancer-induced inflammation on the hepatic metabolism of anticancer drugs have been noticed in recent years. Several inflammatory states were associated with decreased expression of some hepatic CYP enzymes such as 1A, 2A, 2C, 2E, and 3A subfamilies operated by pro-inflammatory cytokines at the transcriptional level [39]. Studies have shown that IL-6-mediated pathways, especially the MAPK/ERK and PI3K/AKT signaling pathways, are critical for the downregulation of CYP enzymes

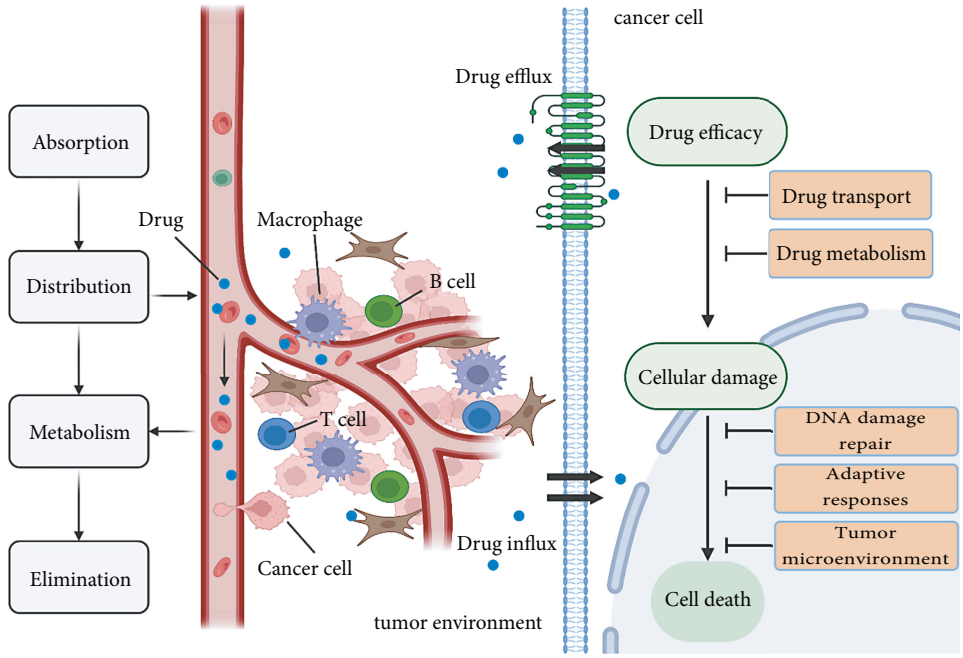

Figure 1: Factors affecting tumor drug resistance. Quantitative and qualitative changes in drug influx and efflux systems affect the distribution of anticancer drugs throughout the body and their accumulation in tumor cells. The drug metabolism of the body determines the efficacy of drugs. DNA damage repair, activation of pro-survival pathway or oncogenic bypass pathway, and changes in the tumor microenvironment are the main influencing factors of drug resistance.

during inflammation [40], whereas IL-6 inhibitor tocilizumab can upregulate the expression of CYP3A4 mRNA [41]. Furthermore, JAK inhibitor has been found to reverse the IL-6-mediated downregulated CYP1A2 and CYP3A4 mRNA levels in HepaRG and PHHS cells, suggesting a prominent role of the JAK/STAT pathway mediated by IL-6 in CYP downregulation [42]. It is noteworthy that CYP enzyme activity is differentially affected by the presence of tumor-associated inflammation. For instance, increased activity of CYP2E1 was associated with raised serum levels of IL-6, IL-8, and TNF-α [43]. Beyond this exception, IL-6 predominantly reduces CYP expression and thus attenuates the biotransformation of some drugs that are metabolized through CYP enzymes. Furthermore, studies found that after the TNF-α treatment for 24 h, the induction of CYP3A4 mRNA downregulation is not the same as protein downregulation. The latter is not obvious, suggesting that post-transcriptional mechanisms are involved in the downregulation of CYP protein levels or enzyme activity by TNF-α [44, 45]. As mentioned above, the same cytokines (e.g., IL-6 and TNF-α) had opposite effects on different P450 enzymes. Since different drug-metabolizing enzymes are selective for specific drugs, the characteristics of inflammation in patients during clinical drug treatment can indicate the activation or inhibition of specific drug enzymes, thereby assessing the risk of clinical drug resistance.

3. DNA Damage Response

The DNA damage response (DDR) is a protective mechanism under physiological conditions involved in DNA repair, checkpoint activation, and transcription regulation [46, 47]. On the other hand, it can help tumor cells survive the distractions of drug treatment [48–50]. Cancer treatment usually consists of some chemotherapy drugs that rely on the induction of DNA damage. Thus, the DNA damage repair capacity of cancer cells significantly influences the efficiency of DNA-damaging medications [51]. Recent studies indicate a positive correlation between IL-17 expression and the DDR in mice after cigarette smoke exposure, and excessive damage responses, in turn, lead to increased DNA mutation rates, which contribute to the genetic instability of cancer [52]. Meanwhile, by measuring DDR markers like activation of ataxia-telangiectasia mutated kinase (ATM), researchers found that inflammation in the gastric cardia mucosa may cause accumulated DNA damage, leading to mutagenesis and chromosomal rearrangements [53]. After treating lipopolysaccharides (LPS), the increased mRNA transcription of some DNA repair enzymes like AP endonuclease and DNA glycosylase excising εA can be detected in rat intestines, which implies stimulation of the repair of oxidative DNA damage. Thus, inflammation may cause an imbalance in genome instability, more generally, to cancer development and drug resistance [54].

The DNA damage incurred during the inflammatory response triggers the activation of DNA repair pathways by stimulating a cascade of pro-inflammatory signals required for cell survival [55, 56]. Many DNA repair pathways are involved in regulating the transcription of molecules important for infection control, which implies a link between DDR and the inflammatory system [57, 58]. However, when DNA repair is not sufficient to deal with increasing DNA damage, the genes in the cells often mutate. Some cell mutations (e.g., BRAF V600E and EGFR T790M) can drive

the development of tumors, causing tumor resistance. Among them, the occurrence of inflammation will accelerate this process [59]. For example, a recent study indicated the synergic effect between bacterial-driven inflammation and a mutant BRAF V600E to promote colon tumorigenesis in an enterotoxigenic *Bacteroides fragilis* (ETBF) murine model [60]. Similarly, the pro-inflammatory STAT3 pathway was found to be an important mechanism for EGFR T790M mutation-mediated drug resistance in NSCLC [61]. Inflammation can promote DNA repair in tumor cells, leading to tumor chemotherapy resistance. Blocking the inflammatory response is expected to act as an adjuvant therapy strategy for tumor-resistant treatment.

4. Downstream Adaptive Responses

In addition to the intake and elimination of drugs, tumor cells can also obtain drug resistance through downstream adaptive responses [62, 63]. Currently, commonly used tumor therapy drugs are chemotherapeutic drugs and targeted therapeutic agents. Chemotherapy drugs ultimately lead to tumor cell apoptosis by injuring biomolecules within cells, while targeted therapies suppress tumor progression by inhibiting key regulators in tumor survival-maintaining mechanisms [64–66]. Tumor cells can escape death through various pathways, and these mechanisms are also important reasons for tumor drug resistance, where inflammation plays an essential role (Figure 2).

4.1. Evade from Apoptosis. Cancer cells can regulate the expression of some apoptosis-related proteins, such as B-cell lymphoma 2 (Bcl-2) and inhibitors of apoptosis proteins (IAPs), thus reducing their sensitivity to anticancer drugs that induce cell apoptosis and surviving the treatment [67, 68]. Bcl-2-related proteins are a large family that maintains the normal life state of cells by regulating apoptosis, which can be influenced by various cytokines associated with inflammation factors. For example, IL-13 has been found to induce Bcl-2 expression in airway epithelial cells [69, 70]. Results showed that the Bcl-2 level was increased after adding IL-6 in lymphoblast cells [71]. In addition, IL-22 activates the expression of the antiapoptotic protein Bcl-2 in renal cortex tissues [72]. Meanwhile, IL-10 has a role in protecting cells from apoptosis through upregulating Bcl-2 expression, especially in breast tumors [73]. It has worth noting that the effect of inflammation on apoptosis is not unilateral. By targeting the overexpressed Bcl-2 protein with the nanoparticle Bcl-2 inhibitor ABT-199, apoptosis of inflammatory cells and the reduction of IL-4 and IL-5 levels were observed [74]. Moreover, given that TNFα is one of the key mediators of cancer-related inflammation, at the same time, cIAP1 and cIAP2 function as key mediators of TNFα-induced the activation of NF-κB and then allow the cell to survive against external interference, which indicates the interaction between inflammation and IAPs [75, 76]. Inflammation often accompanies the whole process of tumor occurrence and development and plays a key role in the process of tumor drug resistance [10]. Targeting tumor inflammation may act as a potential strategy to promote tumor apoptosis.

4.2. Autophagy. Autophagy is an evolutionarily conserved mechanism that disposes of excessive or potentially dangerous cytosolic entities through lysosomal degradation to maintain cellular biosynthesis and viability during stress conditions [77, 78]. Therefore, this process may result in the survival of cancer cells that are undergoing anticancer drug treatment. Inflammatory cytokines, including IFN-γ, TNF-α, IL-17, and the IL-1 family, are closely related to autophagy in tumors [79]. In human melanoma cells, blocking the IL-1 pathway by IL-1α or IL-1β treatment increases autophagy-related components such as LC3-I and LC3-II, indicating an increase of autophagy [80]. The overexpression of IFN-γ upregulated Beclin-1 mRNA expression and protein levels in the stomachs of mice, indicating that IFN-γ induces autophagy in part through upregulation of Beclin-1 [81]. However, inflammatory cytokines also play a role in inhibiting autophagy. For example, IL-6 overexpression was sufficient to block autophagy by supporting Beclin-1/Mcl-1 interaction and promoting arsenic-induced cell transformation in lung carcinoma cell lines [82]. Autophagy may also modulate inflammatory cytokine release and secretion through different mechanisms such as secretion of mediators of inflammation, regulation of inflammasomes, and p62/SQSTM1 proteins [83]. Since autophagy plays a dual role in tumor survival, the regulation of autophagy by inflammation is also context dependent. Further research is critically needed to understand the crosstalk between autophagic processes and inflammation as well as the underlying molecular mechanism.

4.3. Oncogenic Bypass Pathway. Activating the oncogenic bypass signaling pathways (e.g., MAPK, c-MET, or PI3K/AKT signaling) is crucial in tumor drug resistance. Studies have found that inflammation can directly or indirectly affect signal transduction in these pathways [84, 85]. For example, the JNK and p38 MAPK signaling pathways can be activated by pro-inflammatory cytokines such as TNF-α and IL-1β, associated with anticancer drug resistance in colon and liver cancer [86]. Studies have shown that the pro-inflammatory cytokine IL-22 can downregulate Cx43 gene transcription and promote keratinocyte proliferation and migration through the JNK-dependent pathway [87]. IL-17A stimulation leads to upregulation of Plet1 expression, which contributes to tissue regeneration and colonic tumorigenesis via regulating ERK [88]. IL-33 can activate the classical MyD88/IRAK/TRAF6 module, which activates three subfamily pathways of MAPK, including ERK, p38, and JNK [89]. Interestingly, activation of the JNK pathway can promote inflammatory actions such as directly activated NF-κB by promoting IκBα degradation, which indicates a positive feedback regulation of inflammation on the JNK pathway [90]. As for cholangiocarcinoma, inflammatory mediators such as IL-6 and TNF-α activate several pathways such as JAK-STAT, p38 MAPK, and Akt, resulting in increased cell growth and survival and proliferation [91].

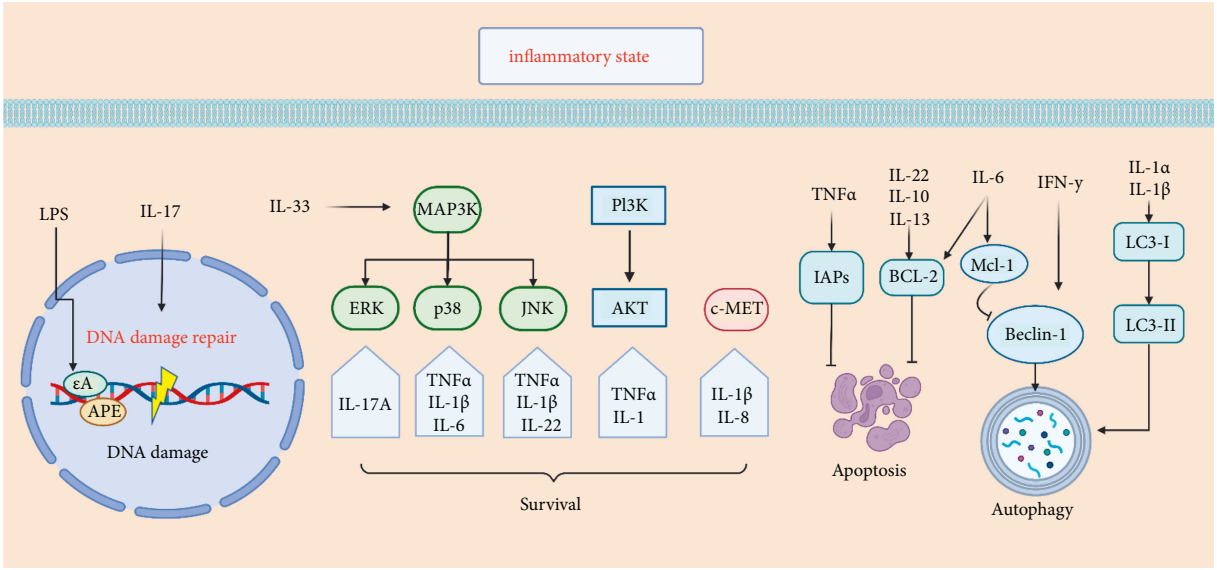

Figure 2: Molecular mechanisms of anticancer drug resistance. Inflammation not only aggravates DNA damage but also affects the expression of DNA repair enzymes, which leads to the instability of tumor genes and further promotes tumor drug resistance. Inflammation can regulate apoptosis and autophagy of tumor cells. For example, IL-6, 10, and 22 may inhibit the apoptosis of tumor cells by promoting the expression of BCL-2. Interferon and IL-1α/β can act on Beclin and LC3, respectively, to promote autophagy, while IL-6 can promote the binding of Mcl-1 and Beclin-1 to inhibit autophagy. Inflammatory mediators activate oncogenic bypass signaling pathways (e.g., MAPK, C-MET, or PI3K/AKT signaling pathways) leading to tumor resistance.

Moreover, the expression of three major inflammatory cytokine genes, IL-1β, IL-8, and CXCL1, was positively correlated with c-MET expression in patients with brain metastases. In addition, the MAPK pathway is the central downstream transducer between c-Met and IL-1β [92].

Furthermore, under the chronic inflammation state, multiple inflammatory factors are associated with the PI3K/Akt pathway, which plays an important role in the initiation and development of downstream inflammatory pathways. For example, studies have shown that NF-κB is triggered by PI3K/Akt by activating protein kinase C, which confirms the link between inflammation and oncogenic pathways [93]. In summary, inflammation promotes the activation of oncogenic bypass pathways in tumor cells, which may lead to targeted drug resistance. Therefore, the level of inflammation in the tumor microenvironment should be considered during clinical treatment, and combination with anti-inflammatory drugs may improve the efficacy.

5. Inflammatory Tumor Microenvironment

5.1. Oxidative Stress. Oxidative stress refers to the imbalance between the generation of free oxygen radicals and their elimination through the antioxidant defense system after being stimulated [94, 95]. As a by-product of normal metabolic processes, reactive oxygen species (ROS) are indispensable for various biological processes in normal and cancer cells [96]. Recent evidence suggests that ROS is closely related to tumor cell proliferation, heterogeneity, dormancy, and stemness, which are considered the critical requirements for tumor progression [97, 98]. However, the effects of excess ROS on tumor cells can be quite different in its anticancer properties, such as inducing apoptosis. Although most current chemotherapeutic agents increase ROS to cytotoxic levels when targeting cancer cells, exposure to ROS inevitably reduces the efficacy of chemotherapy in the long term, resulting in cancer drug resistance [99].

During inflammation, mast cells and white blood cells are recruited to the site of injury, resulting in increased release and accumulation of ROS at the site of injury due to increased oxygen uptake, leading to oxidative stress [100]. ROS promotes cancer growth and progression via different signaling pathways (PI3/Akt/mTOR, MAPK, etc.) when accumulating to a particular concentration [95]. Studies have shown that ROS-mediated drug resistance in cancer cells may be due to the activation of redox-sensitive transcription factors such as NF-κB, Nrf2, c-Jun, and HIF-1α 30471641. Nrf2, a transcription factor involved in cellular homeostasis, is responsible for targeting genes related to cellular defense and plays a crucial role in regulating REDOX homeostasis [101]. Under oxidative stress, the specific cysteine residues of KEAP1 in the KEAP1-CUL3-RBX1 complex are destroyed, thus interfering with the ubiquitination process of Nrf2, which may ultimately lead to cancer drug tolerance [102]. Inhibition of Nrf2 gene expression has been found to reverse the resistance of head and neck tumors to iron death inducers [103].

Studies have found that oxidative stress and inflammation are interdependent and interrelated processes in the inflammatory RA joint, where inflammatory cells release large amounts of ROS, leading to excessive oxidative damage. In addition, many ROS and oxidative stress products enhance the pro-inflammatory response [104].

Exposure of phagocytes to pro-inflammatory cytokines such as TNF, IFN-γ, and/or IL-1β induces the formation of the NOX2 complex, which significantly increases

intracellular ROS levels [105]. What's more, as a pro-inflammatory factor, TNF mainly acts through multiple TNF receptor-mediated signaling pathways, such as NF-KB and MAPKs, to regulate inflammatory responses. It is now clear that ROS/RNS are an integral part of TNF signaling because they are closely involved in numerous feedback loops, which are part of TNFR's downstream signaling pathways. Furthermore, ROS production also creates a positive feedback loop through autocrine TNF-α-mediated inflammatory cytokine/chemokine expression, which contributes to tumor progression [106, 107]. These findings suggest that inflammation may play a role in tumor resistance by stimulating the production of ROS.

5.2. Immune Response. The immune system has a crucial role in cancer development and treatment [108, 109]. Deregulation of the immune response may cause cancer cells to evade immunogenic cancer cell death; however, the underlying molecular mechanisms involved in resistance to immunotherapy need further elucidation [109]. There is increasing evidence that immune response and systemic inflammation play an important role in tumor progression, and there is a complex interaction between them [110]. Researchers have found that tumor regulates the inflammatory environment by secreting soluble growth factors and chemokines so that inflammatory cells inhibit the anticancer T-cell response [111]. In the chronic inflammatory state, pro-inflammatory cytokines recruit immune cells such as M2, N2, and MDSCs, which are associated with suppressing immune surveillance and maintaining depleted T-cell phenotypes [112]. As a major pro-inflammatory cytokine, IL-6 plays an immunosuppressive role by inhibiting IFN-γ production and Th1 differentiation through SOCS1 induction, making CD8+T cells helpless. Studies have shown that upregulation of IL-6 activates STAT3, thereby inhibiting CD8 T-cell infiltration in non-small cell lung cancer and pancreatic cancer [113, 114]. While IL-10 has different effects on most immune cells and can inhibit the activation and effector functions of T cells, monocytes, and macrophages, it can also stimulate CD8+T cells and inhibit tumors to a certain extent [115]. The activation of MAPK signaling leads to increased VEGF and IL-8 expression, which then restrains T-cell recruitment and function [116]. Under the condition of inflammation, the metabolism of the stimulated immune cells may be disturbed, thus causing the abnormal function of the immune system [117]. Neutrophils under inflammatory conditions can affect other immune cells like T cells by producing chemokines and secreting granule contents and then promote immune paralysis of the adaptive immune system [118]. To avoid continuous inflammation, the cytokine IL-27 promotes Treg expression of T-bet and CXCR3 and triggers Tr1 cells. It has also been linked to increased expression of inhibitory receptors by T cells, antagonizing the development of Th2 and Th17 cell subsets. In addition, the observation that IL-27 induces PD-L1 and PD-1 suggests that IL-27 may be an important molecule in controlling cancer-related immune checkpoint mechanisms [119]. In summary, the relationship between tumor-associated inflammation and immune response still needs to be elucidated in many experiments. Furthermore, in-depth knowledge of the molecular mechanism of inflammation-influenced immune response could be beneficial to overcoming immunotherapy failure (Figure 3).

6. Targeting Inflammation to Overcome Drug Resistance

As mentioned in the previous discussion, inflammation can affect tumor development and drug resistance in multiple ways (Table 1). Of note, evidence increasingly suggests that drugs with anti-inflammatory properties have been shown to resist cancer. However, anti-inflammatory drugs are still in the early stages of clinical use in treating cancer due to drug risk. Here we summarize some of the current clinical advances that support the use of anti-inflammatory approaches for treating tumors (Table 2).

Conventional anti-inflammatory drugs like NSAIDs (aspirin) have been identified as a broad-spectrum anticancer agent based on data from epidemiological studies [129–131]. Aspirin can inhibit the nuclear translocation of NF-κB, thereby inhibiting the PI3 kinase/Akt-mediated cell survival pathway and promoting cell apoptosis. In multiple myeloma cells, aspirin inhibited tumor cell proliferation and induced apoptosis by upregulating Bax and downregulating Bcl-2, changing the ratio of Bax/Bcl-2 [132]. Based on this, aspirin has been combined with other drugs in clinical trials treating drug-resistantnon-small cell cancers.

Several studies have shown that corticosteroids have significant anticancer effects both alone or in combination. As a selective COX-2 inhibitor and a nonsteroidal anti-inflammatory drug that inhibits prostaglandin production, celecoxib can induce apoptosis by activating transcriptional regulators of ER stress in hepatoma cells [133]. Dexamethasone can induce cell death in multiple myeloma mediated by miR-125b expression [134]. Other glucocorticoids, such as prednisone, its inhibition of prostate cancer growth may be due to inhibition of tumor-associated angiogenesis by reducing VEGF and IL-8 production [135].

As some infectious diseases that cause chronic inflammation have been linked to the development of cancer, anti-infective agents including antiviral, antibacterial, and antifungal drugs may play a role in cancer treatment [136–138]. Statins, which inhibit HMG-CoA reductase, also have anti-inflammatory properties and may have a beneficial effect on HCC caused by hepatitis [139].

Tumor immunotherapy is very effective in some patients, but resistance to which can also develop due to the immunosuppressive tumor microenvironment. Therefore, anti-inflammatory drugs that target immunosuppressive cells or cytokines may make tumor cells more sensitive to immunotherapy drugs and thus avoid resistance [115]. Studies found that monotherapy with COX-2 inhibitors or prostaglandin 2 (PGE2) receptor antagonists activate IFN-γ-driven transcriptional remodeling and synergy with immune checkpoint inhibitors to enhance effector T-cell accumulation in tumors [140].

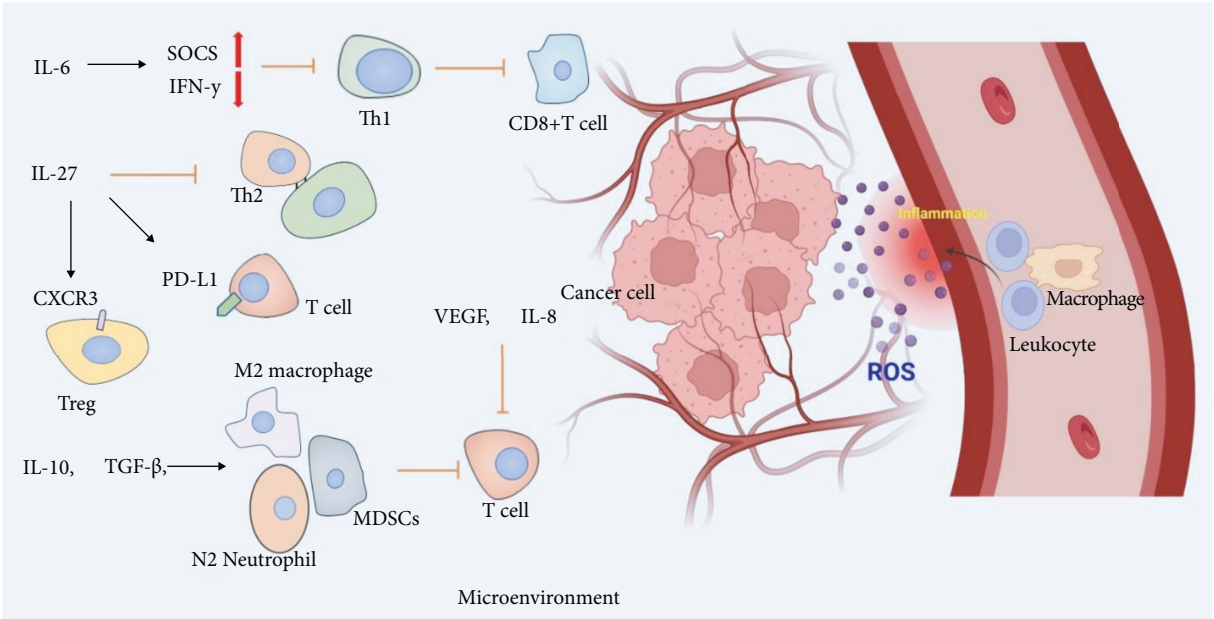

Figure 3: Inflammatory regulation of tumor microenvironment. In the tumor microenvironment, inflammatory factors can specifically activate or inhibit the function of immune cells, thus affecting the survivability of tumor cells. At the same time, the large amount of reactive oxygen species produced in the inflammatory site also plays a role in tumor resistance.

Table 1: Summary of cytokine-mediated effects on drug resistance.

Cytokines	Downstream effector	Resistance mechanism	Role	References	Potential targeted drugs
IL-6	BCRP	Reducing drug efflux	Anti-resistant	[34]	Tocilizumab, sarilumab, clazakizumab, siltuximab [120]
	P-gp	Reducing drug efflux	Anti-resistant	[35]	
	CYP1A2 and CYP3A4	Inhibiting drug metabolism	Pro-resistant	[42]	
	CYP2E1	Promoting drug metabolism	Anti-resistant	[43]	
	Beclin-1/Mcl-1 interaction	Inhibiting autophagy	Anti-resistant	[82]	
	Bcl-2	Inhibiting apoptosis	Pro-resistant	[71]	
	JAK-STAT, p38 MAPK, Akt	Mediating survival signaling pathways	Pro-resistant	[91]	
TNF-α	BCRP	Reducing drug efflux	Anti-resistant	[34]	Adalimumab [121]
	P-gp	Reducing drug efflux	Anti-resistant	[35]	
	CYP2E1	Promoting drug metabolism	Anti-resistant	[43]	
	CYP3A4	Inhibiting drug metabolism	Pro-resistant	[44]	
	Beclin-1, LC3	Increasing autophagy	Pro-resistant	[79]	
	IAPs	Inhibiting apoptosis	Pro-resistant	[75]	
	JAK-STAT, p38 MAPK, Akt	Mediating survival signaling pathways	Pro-resistant	[91]	
IL-1	BCRP	Inhibiting drug efflux	Anti-resistant	[34]	Anakinra, canakinumab [122]
	LC3-I, LC3-II	Increasing autophagy	Pro-resistant	[80]	
	JNK, p38 MAPK, c-MET	Mediating survival signaling pathways	Pro-resistant	[86, 92]	
IL-22	Bcl-2	Inhibiting apoptosis	Pro-resistant	[72]	IL-22BP [123]
	JNK	Mediating survival signaling pathways	Pro-resistant	[87]	
IL-8	CYP2E1	Promoting drug metabolism	Anti-resistant	[43]	Tocilizumab [124]
	c-MET	Mediating survival signaling pathways	Pro-resistant	[92]	
IL-17	DDR	Inhibiting DNA damage	Pro-resistant	[52]	Secukinumab, ixekizumab, brodalumab [125]
	ERK	Mediating survival signaling pathways	Pro-resistant	[88]	

Table 1: Continued.

Cytokines	Downstream effector	Resistance mechanism	Role	References	Potential targeted drugs
IL-2	BCRP	Increasing drug efflux	Pro-resistant	[34]	Ro26-4550 [126]
IFN-γ	Beclin-1	Increasing autophagy	Pro-resistant	[81]	Emapalumab
IL-10	Bcl-2	Inhibiting apoptosis	Pro-resistant	[73]	AS101 [127]
IL-33	JNK, p38 MAPK, ERK	Mediating survival signaling pathways	Pro-resistant	[89]	N.A.
IL-13	Bcl-2	Inhibiting apoptosis	Pro-resistant	[69]	Suplatast tosilate [128]

Table 2: Summary of clinical trials of anti-inflammation drugs treating drug-resistant tumors.

Agent	Tolerated drug	Drug-resistant tumor type	Mechanism	Phase	Clinical trial number
Celecoxib	Platinum	Ovarian cancer/primary peritoneal cavity cancer	Stops the growth	II	NCT00084448
Dexamethasone	Platinum	Ovarian cancer	Stops the growth	II	NCT00003449
Aspirin	Osimertinib	"Non-small cell lung cancer"	Promotes cells apoptosis	I	NCT03532698
Prednisone	Hormone-resistant	Prostate cancer	Stops the growth	III	NCT00110214
Aspirin	EGFR-TKI	NSCLC	Promotes cells apoptosis	I	NCT03543683
Dexamethasone	Most MM drugs	Multiple myeloma	Inhibits tumor metastasis	II	NCT02626481
Dexamethasone	Chemotherapy	Recurrent plasma cell myeloma	Inhibits tumor metastasis	II	NCT03457142

As inflammatory mediators, cytokines and chemokines also mediate the tumor's response to external disturbances, which provides new targets for tumor drug therapy. For example, siltuximab and tocilizumab were used for ovarian cancer treatment as IL-6 antibodies [141]. MABp1 was used for colorectal cancer treatment as an anti-IL-1α antibody [142]. Blockade of inflammatory pathways such as TGFβ signaling by galunisertib, which inhibits the TGFβR1 kinase, has been used to treat many types of cancer [143]. Due to the inflammation network within the tumor microenvironment being complex, inhibiting one molecule can cause a cascade effect, so the safety of the targeted drugs still needs to be tested in more trials.

Finally, some natural anti-inflammatory supplements might also help control cancer and they have the advantage of fewer side effects and greater safety. Berberine, which is a plant-derived alkaloid, may have the potential to improve colorectal adenomas [144]. Likewise, vitamin C has been extensively explored for potential anticancer effects [145].

Vitamin C's anti-inflammatory and antioxidant abilities can be attributed to its ability to regulate the DNA-binding activity of NF-κB and reduce the production of inflammatory factors [146]. Dietary supplementation of vitamin C was found to result in a significant decrease in the mRNA expression of pro-inflammatory cytokines (e.g., IL-1β, IL-6, and IFN-γ) [147]. Cancer cells depend primarily on the gene expression of KRAS or BRAF to survive. Vitamin C gets inside these cancer cells and disrupts the expression of KRAS or BRAF genes. Once vitamin C has an effect, the mutation probability of cancer cells will also be greatly reduced, which reduces the resistance of targeted drugs [148].

The idea of targeting inflammation to treat drug-resistant tumors is innovative, but the molecular mechanisms behind the drugs still need extensive research and clinical trials to ensure the efficacy and safety of treatment regiments.

7. Conclusions

In this review, we summarize the recent studies on inflammation in influencing cancer drug resistance from several aspects including drug transport and metabolism, DNA damage response, downstream adaptive responses, oncogenic bypass signaling, and tumor microenvironment.

The activity of drug transporters and CYP enzymes changes in the inflammatory state [39]. Of note, different inflammatory cytokines have different effects on diverse drug transporters and CYP enzymes. Except for CYP2E1, the expression level of most liver drug enzymes is reduced in the inflammatory state, which inhibits the drug metabolism of tumors. In this regard, the mechanism of drug resistance to tumors remains to be studied. As DNA repair determines the potential of tumor cells to resist DNA-damaging drugs, the distinct roles of inflammatory cytokines in DDR emphasize the necessity to clarify the molecular mechanisms underlying the inflammation-related drug resistance. The role of multiple pro-inflammatory factors including IFN-γ, TNF-α, IL-17, and the IL-1 family in promoting drug resistance through autophagy has been confirmed by detecting the expression of autophagy-related molecules like LC3 and Beclin-1. It has also been suggested that IL-6, IL-22, and IL-10 can influence tumor drug resistance by regulating apoptosis-related proteins like BCL-2 and IAPs. Moreover, it is noteworthy that autophagy and apoptosis can also regulate inflammatory signaling pathways, thus forming a feedback regulatory pathway. We also summarized the regulatory role of some inflammatory factors in activating the oncogenic bypass signaling pathway, especially the cross-connections between NF-κB and three typical pathways including MAPK, c-MET, and PI3K/AKT signaling. In the tumor microenvironment, the production of ROS is closely related to the failure of anticancer drugs. Some targets of the oxidative stress pathway are involved in the conduction of the

inflammatory pathways, and some pro-inflammatory factors such as TNFα, IFN-γ, and IL-1β can promote the production of ROS. Although some studies have found that the function of some immune cells is suppressed under chronic inflammation, the specific mechanism of inflammatory components on cancer immune escape remains to be further elucidated due to the complexity of the immune system. At last, we summarize some anti-inflammatory applications in tumor therapy and propose some hypotheses for targeting inflammation against tumor resistance. Therefore, further studies on the molecular mechanism at multiple levels behind inflammation and cancer are required to overcome cancer drug resistance.

Data Availability

No data were used to support this study.

Conflicts of Interest

The authors declare that the research was conducted in the absence of any commercial or financial relationships that could be construed as potential conflicts of interest.

Authors' Contributions

Shuaijun Lu and Yang Li contributed equally to this article.

Acknowledgments

The authors thank BioRender for helping in creating figures.

References

[1] H. Sung, J. Ferlay, R. L. Siegel et al., "Global cancer statistics 2020: GLOBOCAN estimates of incidence and mortality worldwide for 36 cancers in 185 countries," *CA: A Cancer Journal for Clinicians*, vol. 71, no. 3, pp. 209–249, 2021.

[2] R. A. Ward, S. Fawell, N. Floc'h, V. Flemington, D. McKerrecher, and P. D. Smith, "Challenges and opportunities in cancer drug resistance," *Chem Rev*, vol. 121, no. 6, pp. 3297–3351, 2021.

[3] A. S. Nam, R. Chaligne, and D. A. Landau, "Integrating genetic and non-genetic determinants of cancer evolution by single-cellmulti-omics," *Nat Rev Genet*, vol. 22, no. 1, pp. 3–18, 2021.

[4] R. Brown, E. Curry, L. Magnani, C. S. Wilhelm-Benartzi, and J. Borley, "Poised epigenetic states and acquired drug resistance in cancer," *Nature Reviews. Cancer*, vol. 14, no. 11, pp. 747–753, 2014.

[5] N. Chatterjee and T. G. Bivona, "Polytherapy and targeted cancer drug resistance," *Trends in Cancer*, vol. 5, no. 3, pp. 170–182, 2019.

[6] B. Li, J. Jiang, Y. G. Assaraf, H. Xiao, Z. S. Chen, and C. Huang, "Surmounting cancer drug resistance: new insights from the perspective of N(6)-methyladenosine RNA modification," *Drug Resistance Updates*, vol. 53, Article ID 100720, 2020.

[7] S. Boumahdi and F. J. de Sauvage, "The great escape: tumour cell plasticity in resistance to targeted therapy," *Nature Reviews Drug Discovery*, vol. 19, no. 1, pp. 39–56, 2020.

[8] Y. G. Assaraf, A. Brozovic, A. C. Gonçalves et al., "The multifactorial nature of clinical multidrug resistance in cancer," *Drug Resistance Updates*, vol. 46, Article ID 100645, 2019.

[9] V. A. K. Rathinam and F. K. M. Chan, "Inflammasome, inflammation, and tissue homeostasis," *Trends in Molecular Medicine*, vol. 24, no. 3, pp. 304–318, 2018.

[10] H. Zhao, L. Wu, G. Yan et al., "Inflammation and tumor progression: signaling pathways and targeted intervention," *Signal Transduction and Targeted Therapy*, vol. 6, no. 1, p. 263, 2021.

[11] J. Zindel and P. Kubes, "DAMPs, PAMPs, and LAMPs in immunity and sterile inflammation," *Annual Review of Pathology: Mechanisms of Disease*, vol. 15, no. 1, pp. 493–518, 2020.

[12] C. Dong, "Cytokine regulation and function in T cells," *Annu Rev Immunol*, vol. 39, no. 1, pp. 51–76, 2021.

[13] D. C. Fajgenbaum, C. H. June, and C. H. Cytokine, "Cytokine s," *N Engl J Med*, vol. 383, no. 23, pp. 2255–2273, 2020.

[14] F. Balkwill, "Tumour necrosis factor and cancer," *Nature Reviews. Cancer*, vol. 9, no. 5, pp. 361–371, 2009.

[15] A. V. Villarino, Y. Kanno, and J. J. O'Shea, "Mechanisms and consequences of Jak-STAT signaling in the immune system," *Nat Immunol*, vol. 18, no. 4, pp. 374–384, 2017.

[16] K. Taniguchi and M. N. F.-κB. Karin, "NF-κB, inflammation, immunity and cancer: coming of age," *Nature Reviews. Immunology*, vol. 18, no. 5, pp. 309–324, 2018.

[17] X. Li, Y. Xiang, F. Li, C. Yin, B. Li, and X. Ke, "WNT/β-Catenin signaling pathway regulating T cell-inflammation in the tumor microenvironment," *Front Immunol*, vol. 10, p. 2293, 2019.

[18] Y. T. Yeung, F. Aziz, A. Guerrero-Castilla, and S. Arguelles, "Signaling pathways in inflammation and anti-inflammatory therapies," *Current Pharmaceutical Design*, vol. 24, no. 14, pp. 1449–1484, 2018.

[19] K. A. Fitzgerald and J. C. Kagan, "Toll-like receptors and the control of immunity," *Cell*, vol. 180, no. 6, pp. 1044–1066, 2020.

[20] G. Andrejeva and J. C. Rathmell, "Similarities and distinctions of cancer and immune metabolism in inflammation and tumors," *Cell Metabolism*, vol. 26, no. 1, pp. 49–70, 2017.

[21] D. C. McFarland, D. R. Jutagir, A. H. Miller, W. Breitbart, C. Nelson, and B. Rosenfeld, "Tumor mutation burden and depression in lung cancer: association with inflammation," *Journal of the National Comprehensive Cancer Network*, vol. 18, no. 4, pp. 434–442, 2020.

[22] P. Viatour, M. P. Merville, V. Bours, and A. Chariot, "Phosphorylation of NF-κB and Iκ B proteins: implications in cancer and inflammation," *Trends in Biochemical Sciences*, vol. 30, no. 1, pp. 43–52, 2005.

[23] F. R. Greten and S. I. Grivennikov, "Inflammation and cancer: triggers, mechanisms, and consequences," *Immunity*, vol. 51, no. 1, pp. 27–41, 2019.

[24] R. Khandia and A. Munjal, "Interplay between inflammation and cancer," *Advances in Protein Chemistry and Structural Biology*, vol. 119, pp. 199–245, 2020.

[25] N. Singh, D. Baby, J. P. Rajguru, P. B. Patil, S. S. Thakkannavar, and V. B. Pujari, "Inflammation and cancer," *Ann Afr Med*, vol. 18, no. 3, pp. 121–126, 2019.

[26] J. Kirchmair, A. H. Göller, D. Lang et al., "Predicting drug metabolism: experiment and/or computation?" *Nature Reviews. Drug Discovery*, vol. 14, no. 6, pp. 387–404, 2015.

[27] K. McIntosh, C. Balch, and A. K. Tiwari, "Tackling multidrug resistance mediated by efflux transporters in tumor-

initiating cells," *Expert Opinion on Drug Metabolism & Toxicology*, vol. 12, no. 6, pp. 633–644, 2016.

[28] R. J. Kathawala, P. Gupta, C. R. Ashby Jr., and Z. S. Chen, "The modulation of ABC transporter-mediated multidrug resistance in cancer: a review of the past decade," *Drug Resistance Updates*, vol. 18, pp. 1–17, 2015.

[29] W. Li, H. Zhang, Y. G. Assaraf et al., "Overcoming ABC transporter-mediated multidrug resistance: molecular mechanisms and novel therapeutic drug strategies," *Drug Resistance Updates*, vol. 27, pp. 14–29, 2016.

[30] S. Wilkens, "Structure and mechanism of ABC transporters," *F1000Prime Rep*, vol. 7, p. 14, 2015.

[31] R. W. Robey, K. M. Pluchino, M. D. Hall, A. T. Fojo, S. E. Bates, and M. M. Gottesman, "Revisiting the role of ABC transporters in multidrug-resistant cancer," *Nature Reviews Cancer*, vol. 18, no. 7, pp. 452–464, 2018.

[32] P. T. Ronaldson and T. P. Davis, "Targeting blood-brain barrier changes during inflammatory pain: an opportunity for optimizing CNS drug delivery," *Therapeutic Delivery*, vol. 2, no. 8, pp. 1015–1041, 2011.

[33] M. Bossennec, A. Di Roio, C. Caux, and C. Ménétrier-Caux, "MDR1 in immunity: friend or foe?" *Oncoimmunology*, vol. 7, no. 12, Article ID e1499388, 2018.

[34] J. Mishra, R. Simonsen, and N. Kumar, "Intestinal breast cancer resistance protein (BCRP) requires Janus kinase 3 activity for drug efflux and barrier functions in obesity," *Journal of Biological Chemistry*, vol. 294, no. 48, Article ID 18348, 2019.

[35] R. H. Ghoneim, D. Kojovic, and M. Piquette-Miller, "Impact of endotoxin on the expression of drug transporters in the placenta of HIV-1 transgenic (HIV-Tg) rats," *European Journal of Pharmaceutical Sciences*, vol. 102, pp. 94–102, 2017.

[36] D. Zhang, Y. Ding, X. Wang et al., "Effects of ABCG2 and SLCO1B1 gene variants on inflammation markers in patients with hypercholesterolemia and diabetes mellitus treated with rosuvastatin," *Eur J Clin Pharmacol*, vol. 76, no. 7, pp. 939–946, 2020.

[37] A. K. Yang, Z. W. Zhou, M. Q. Wei, J. P. Liu, and S. F. Zhou, "Modulators of multidrug resistance proteins in the management of anticancer and antimicrobial drug resistance and the treatment of inflammatory diseases," *Current Topics in Medicinal Chemistry*, vol. 10, no. 17, pp. 1732–1756, 2010.

[38] M. Ingelman-Sundberg and V. M. Lauschke, "Can CYP inhibition overcome chemotherapy resistance?" *Trends in Pharmacological Sciences*, vol. 41, no. 8, pp. 503–506, 2020.

[39] M. Kacevska, G. R. Robertson, S. J. Clarke, and C. Liddle, "Inflammation and CYP3A4-mediated drug metabolism in advanced cancer: impact and implications for chemotherapeutic drug dosing," *Expert Opinion on Drug Metabolism & Toxicology*, vol. 4, no. 2, pp. 137–149, 2008.

[40] R. Keller, M. Klein, M. Thomas et al., "Coordinating role of RXRα in downregulating hepatic detoxification during inflammation revealed by fuzzy-logic modeling," *PLoS Comput Biol*, vol. 12, no. 1, Article ID e1004431, 2016.

[41] N. J. Vet, J. M. Brussee, M. de Hoog et al., "Inflammation and organ failure severely affect midazolam clearance in critically ill children," *American Journal of Respiratory and Critical Care Medicine*, vol. 194, no. 1, pp. 58–66, 2016.

[42] M. Febvre-James, A. Bruyère, M. Le Vée, and O. Fardel, "The JAK1/2 inhibitor ruxolitinib reverses interleukin-6-mediated suppression of drug-detoxifying proteins in cultured human hepatocytes," *Drug Metab Dispos*, vol. 46, no. 2, pp. 131–140, 2018.

[43] S. Trousil, P. Lee, R. J. Edwards et al., "Altered cytochrome 2E1 and 3A P450-dependent drug metabolism in advanced ovarian cancer correlates to tumour-associated inflammation," *Br J Pharmacol*, vol. 176, no. 18, pp. 3712–3722, 2019.

[44] A. E. Aitken and E. T. Morgan, "Gene-specific effects of inflammatory cytokines on cytochrome P450 2C, 2B6 and 3A4 mRNA levels in human hepatocytes," *Drug Metab Dispos*, vol. 35, no. 9, pp. 1687–1693, 2007.

[45] S. Dallas, C. Sensenhauser, A. Batheja et al., "De-riskingbiotherapeutics for possible drug interactions using cryopreserved human hepatocytes," *Current Drug Metabolism*, vol. 13, no. 7, pp. 923–929, 2012.

[46] P. G. Pilié, C. Tang, G. B. Mills, and T. A. Yap, "State-of-the-art strategies for targeting the DNA damage response in cancer," *Nat Rev Clin Oncol*, vol. 16, no. 2, pp. 81–104, 2019.

[47] M. Olivieri, T. Cho, A. Álvarez-Quilón et al., "A genetic map of the response to DNA damage in human cells," *Cell*, vol. 182, no. 2, pp. 481–496.e21, 2020, e421.

[48] A. Ferri, V. Stagni, and D. Barilà, "Targeting the DNA damage response to overcome cancer drug resistance in glioblastoma," *International Journal of Molecular Sciences*, vol. 21, no. 14, p. 4910, 2020.

[49] B. Kaina and M. Christmann, "DNA repair in personalized brain cancer therapy with temozolomide and nitrosoureas," *DNA Repair (Amst)*, vol. 78, pp. 128–141, 2019.

[50] N. Hosoya and K. Miyagawa, "Targeting DNA damage response in cancer therapy," *Cancer Sci*, vol. 105, no. 4, pp. 370–388, 2014.

[51] P. Bouwman and J. Jonkers, "The effects of deregulated DNA damage signalling on cancer chemotherapy response and resistance," *Nature Reviews. Cancer*, vol. 12, no. 9, pp. 587–598, 2012.

[52] C. Cao, B. Tian, X. Geng et al., "IL-17-Mediated inflammation promotes cigarette smoke-induced genomic instability," *Cells*, vol. 10, no. 5, p. 1173, 2021.

[53] R. Lin, D. Xiao, Y. Guo et al., "Chronic inflammation-related DNA damage response: a driving force of gastric cardia carcinogenesis," *Oncotarget*, vol. 6, no. 5, pp. 2856–2864, 2015.

[54] P. Kowalczyk, J. Jaworek, M. Kot et al., "Inflammation increases oxidative DNA damage repair and stimulates preneoplastic changes in colons of newborn rats," *J Physiol Pharmacol*, vol. 67, no. 2, pp. 277–286, 2016.

[55] S. Kawanishi, S. Ohnishi, N. Ma, Y. Hiraku, and M. Murata, "Crosstalk between DNA damage and inflammation in the multiple steps of carcinogenesis," *International Journal of Molecular Sciences*, vol. 18, no. 8, p. 1808, 2017.

[56] M. Yousefzadeh, C. Henpita, R. Vyas, C. Soto-Palma, P. Robbins, and L. Niedernhofer, "DNA damage-how and why we age?" *Elife*, Article ID e62852, 2021.

[57] R. Nakad and B. Schumacher, "DNA damage response and immune defense: links and mechanisms," *Front Genet*, vol. 7, p. 147, 2016.

[58] F. L. Fontes, D. M. L. Pinheiro, A. H. S. d. Oliveira, R. K. d. M. Oliveira, T. B. P. Lajus, and L. F. Agnez-Lima, "Role of DNA repair in host immune response and inflammation," *Mutation Research/Reviews in Mutation Research*, vol. 763, pp. 246–257, 2015.

[59] F. Martínez-Jiménez, F. Muiños, I. Sentís et al., "A compendium of mutational cancer driver genes," *Nature Reviews. Cancer*, vol. 20, no. 10, pp. 555–572, 2020.

[60] C. E. DeStefano Shields, J. R. White, L. Chung et al., "Bacterial-driven inflammation and mutant BRAF

expression combine to promote murine colon tumorigenesis that is sensitive to immune checkpoint therapy," *Cancer Discovery*, vol. 11, no. 7, pp. 1792–1807, 2021.

[61] A. A. Zulkifli, F. H. Tan, T. L. Putoczki, S. S. Stylli, and R. B. Luwor, "STAT3 signaling mediates tumour resistance to EGFR targeted therapeutics," *Molecular and Cellular Endocrinology*, vol. 451, pp. 15–23, 2017.

[62] P. Cheng, M. P. Levesque, R. Dummer, and J. Mangana, "Targeting complex, adaptive responses in melanoma therapy," *Cancer Treatment Reviews*, vol. 86, Article ID 101997, 2020.

[63] K. Melgar, M. M. Walker, L. M. Jones et al., "Overcoming adaptive therapy resistance in AML by targeting immune response pathways," *Science Translational Medicine*, vol. 11, no. 508, 2019.

[64] J. Y. Li, Y. P. Chen, Y. Q. Li, N. Liu, and J. Ma, "Chemotherapeutic and targeted agents can modulate the tumor microenvironment and increase the efficacy of immune checkpoint blockades," *Mol Cancer*, vol. 20, no. 1, p. 27, 2021.

[65] E. J. Mun, H. M. Babiker, U. Weinberg, E. D. Kirson, and D. D. Von Hoff, "Tumor-treating fields: a fourth modality in cancer treatment," *Clinical Cancer Research*, vol. 24, no. 2, pp. 266–275, 2018.

[66] Y. T. Lee, Y. J. Tan, and C. E. Oon, "Molecular targeted therapy: treating cancer with specificity," *European Journal of Pharmacology*, vol. 834, pp. 188–196, 2018.

[67] C. F. A. Warren, M. W. Wong-Brown, and N. A. Bowden, "BCL-2 family isoforms in apoptosis and cancer," *Cell Death & Disease*, vol. 10, no. 3, p. 177, 2019.

[68] S. Kumar, C. Fairmichael, D. B. Longley, and R. C. Turkington, "The multiple roles of the IAP super-family in cancer," *Pharmacology & Therapeutics*, vol. 214, Article ID 107610, 2020.

[69] H. S. Chand, J. F. Harris, and Y. Tesfaigzi, "IL-13 in LPS-induced inflammation causes Bcl-2 expression to sustain hyperplastic mucous cells," *Sci Rep*, vol. 8, no. 1, p. 436, 2018.

[70] A. R. D. Delbridge, S. Grabow, A. Strasser, and D. L. Vaux, "Thirty years of BCL-2: translating cell death discoveries into novel cancer therapies," *Nature Reviews. Cancer*, vol. 16, no. 2, pp. 99–109, 2016.

[71] B. Qin, Z. Zhou, J. He, C. Yan, and S. Ding, "IL-6 inhibits starvation-induced autophagy via the STAT3/Bcl-2 signaling pathway," *Sci Rep*, vol. 5, no. 1, Article ID 15701, 2015.

[72] M. J. Xu, D. Feng, H. Wang, Y. Guan, X. Yan, and B. Gao, "IL-22 ameliorates renal ischemia-reperfusion injury by targeting proximal tubule epithelium," *Journal of the American Society of Nephrology*, vol. 25, no. 5, pp. 967–977, 2014.

[73] C. Yang, L. He, P. He et al., "Increased drug resistance in breast cancer by tumor-associated macrophages through IL-10/STAT3/bcl-2 signaling pathway," *Med Oncol*, vol. 32, no. 2, p. 14, 2015.

[74] M. Larrayoz, S. J. Blakemore, R. C. Dobson et al., "The SF3B1 inhibitor spliceostatin A (SSA) elicits apoptosis in chronic lymphocytic leukaemia cells through downregulation of Mcl-1," *Leukemia*, vol. 30, no. 2, pp. 351–360, 2016.

[75] M. Gyrd-Hansen and P. Meier, "IAPs: from caspase inhibitors to modulators of NF-κB, inflammation and cancer," *Nature Reviews. Cancer*, vol. 10, no. 8, pp. 561–574, 2010.

[76] J. Silke and P. Meier, "Inhibitor of apoptosis (IAP) proteins-modulators of cell death and inflammation," *Cold Spring Harbor Perspectives in Biology*, vol. 5, no. 2, 2013.

[77] H. Chang and Z. Zou, "Targeting autophagy to overcome drug resistance: further developments," *J Hematol Oncol*, vol. 13, no. 1, p. 159, 2020.

[78] J. Doherty and E. H. Baehrecke, "Life, death and autophagy," *Nat Cell Biol*, vol. 20, no. 10, pp. 1110–1117, 2018.

[79] Y. Ge, M. Huang, and Y. M. Yao, "Autophagy and proinflammatory cytokines: interactions and clinical implications," *Cytokine & Growth Factor Reviews*, vol. 43, pp. 38–46, 2018.

[80] Y. Qin, S. Ekmekcioglu, P. Liu et al., "Constitutive aberrant endogenous interleukin-1 facilitates inflammation and growth in human melanoma," *Molecular Cancer Research*, vol. 9, no. 11, pp. 1537–1550, 2011.

[81] S. P. Tu, M. Quante, G. Bhagat et al., "IFN-γ inhibits gastric carcinogenesis by inducing epithelial cell autophagy and T-cell apoptosis," *Cancer Research*, vol. 71, no. 12, pp. 4247–4259, 2011.

[82] Y. Qi, M. Zhang, H. Li et al., "Autophagy inhibition by sustained overproduction of IL6 contributes to arsenic carcinogenesis," *Cancer Research*, vol. 74, no. 14, pp. 3740–3752, 2014.

[83] P. Lapaquette, J. Guzzo, L. Bretillon, and M. A. Bringer, "Cellular and molecular connections between autophagy and inflammation," *Mediators of Inflammation*, vol. 2015, pp. 1–13, 2015.

[84] R. N. Gacche and Y. G. Assaraf, "Redundant angiogenic signaling and tumor drug resistance," *Drug Resistance Updates*, vol. 36, pp. 47–76, 2018.

[85] Y. Zhao, Y. R. Murciano-Goroff, J. Y. Xue et al., "Diverse alterations associated with resistance to KRAS(G12C) inhibition," *Nature*, vol. 599, no. 7886, pp. 679–683, 2021.

[86] E. K. Kim and E. J. Choi, "Compromised MAPK signaling in human diseases: an update," *Arch Toxicol*, vol. 89, no. 6, pp. 867–882, 2015.

[87] M. B. Hammouda, A. E. Ford, Y. Liu, and J. Y. Zhang, "The JNK signaling pathway in inflammatory skin disorders and cancer," *Cells*, vol. 9, no. 4, p. 857, 2020.

[88] J. A. Zepp, J. Zhao, C. Liu et al., "IL-17A-Induced PLET1 expression contributes to tissue repair and colon tumorigenesis," *The Journal of Immunology*, vol. 199, no. 11, pp. 3849–3857, 2017.

[89] S. M. Pinto, Y. Subbannayya, D. A. B. Rex et al., "A network map of IL-33 signaling pathway," *J Cell Commun Signal*, vol. 12, no. 3, pp. 615–624, 2018.

[90] K. Grynberg, F. Y. Ma, and D. J. Nikolic-Paterson, "The JNK signaling pathway in renal fibrosis," *Front Physiol*, vol. 8, p. 829, 2017.

[91] P. L. Labib, G. Goodchild, and S. P. Pereira, "Molecular pathogenesis of cholangiocarcinoma," *BMC Cancer*, vol. 19, no. 1, p. 185, 2019.

[92] F. Xing, Y. Liu, S. Sharma et al., "Activation of the c-met pathway mobilizes an inflammatory network in the brain microenvironment to promote brain metastasis of breast cancer," *Cancer Research*, vol. 76, no. 17, pp. 4970–4980, 2016.

[93] S. N. Zarneshan, S. Fakhri, M. H. Farzaei, H. Khan, and L. Saso, "Astaxanthin targets PI3K/Akt signaling pathway toward potential therapeutic applications," *Food and Chemical Toxicology*, vol. 145, Article ID 111714, 2020.

[94] J. D. Hayes, A. T. Dinkova-Kostova, and K. D. Tew, "Oxidative stress in cancer," *Cancer Cell*, vol. 38, no. 2, pp. 167–197, 2020.

[95] J. N. Moloney and T. G. Cotter, "ROS signalling in the biology of cancer," *Seminars in Cell & Developmental Biology*, vol. 80, pp. 50–64, 2018.

[96] H. Yang, R. M. Villani, H. Wang et al., "The role of cellular reactive oxygen species in cancer chemotherapy," *J Exp Clin Cancer Res*, vol. 37, no. 1, p. 266, 2018.

[97] P. L. de Sá Junior, D. A. D. Câmara, A. S. Porcacchia et al., "The roles of ROS in cancer heterogeneity and therapy," *Longevity*, vol. 2017, Article ID 2467940, 12 pages, 2017.

[98] B. Li, Y. Huang, H. Ming, E. C. Nice, R. Xuan, and C. Huang, "Redox control of the dormant cancer cell life cycle," *Cells*, vol. 10, p. 2707, 2021.

[99] Q. Cui, J. Q. Wang, Y. G. Assaraf et al., "Modulating ROS to overcome multidrug resistance in cancer," *Drug Resistance Updates*, vol. 41, pp. 1–25, 2018.

[100] S. Reuter, S. C. Gupta, M. M. Chaturvedi, and B. B. Aggarwal, "Oxidative stress, inflammation, and cancer: how are they linked?" *Free Radical Biology and Medicine*, vol. 49, no. 11, pp. 1603–1616, 2010.

[101] Q. Ma, "Role of nrf2 in oxidative stress and toxicity," *Annual Review of Pharmacology and Toxicology*, vol. 53, no. 1, pp. 401–426, 2013.

[102] X. J. Wang, Z. Sun, N. F. Villeneuve et al., "Nrf2 enhances resistance of cancer cells to chemotherapeutic drugs, the dark side of Nrf2," *Carcinogenesis*, vol. 29, no. 6, pp. 1235–1243, 2008.

[103] D. Shin, E. H. Kim, J. Lee, and J. L. Roh, "Nrf2 inhibition reverses resistance to GPX4 inhibitor-induced ferroptosis in head and neck cancer," *Free Radical Biology and Medicine*, vol. 129, pp. 454–462, 2018.

[104] T. McGarry, M. Biniecka, D. J. Veale, and U. Fearon, "Hypoxia, oxidative stress and inflammation," *Free Radical Biology and Medicine*, vol. 125, pp. 15–24, 2018.

[105] S. Dupré-Crochet, M. Erard, and O. Nüβe, "ROS production in phagocytes: why, when, and where?" *Journal of Leukocyte Biology*, vol. 94, no. 4, pp. 657–670, 2013.

[106] H. Blaser, C. Dostert, T. W. Mak, and D. Brenner, "TNF and ROS crosstalk in inflammation," *Trends in Cell Biology*, vol. 26, no. 4, pp. 249–261, 2016.

[107] A. El-Kenawi and B. Ruffell, "Inflammation, ROS, and mutagenesis," *Cancer Cell*, vol. 32, no. 6, pp. 727–729, 2017.

[108] J. S. O'Donnell, M. W. L. Teng, and M. J. Smyth, "Cancer immunoediting and resistance to T cell-based immunotherapy," *Nat Rev Clin Oncol*, vol. 16, no. 3, pp. 151–167, 2019.

[109] E. Pérez-Ruiz, I. Melero, J. Kopecka, A. B. Sarmento-Ribeiro, M. García-Aranda, and J. De Las Rivas, "Cancer immunotherapy resistance based on immune checkpoints inhibitors: targets, biomarkers, and remedies," *Drug Resistance Updates: Reviews and Commentaries in Antimicrobial and Anticancer Chemotherapy*, vol. 53, Article ID 100718, 2020, doi. 10.1016/j.drup.2020.100718.

[110] C. I. Diakos, K. A. Charles, D. C. McMillan, and S. J. Clarke, "Cancer-related inflammation and treatment effectiveness," *The Lancet. Oncology*, vol. 15, no. 11, pp. e493–503, 2014.

[111] E. Elinav, R. Nowarski, C. A. Thaiss, B. Hu, C. Jin, and R. A. Flavell, "Inflammation-induced cancer: crosstalk between tumours, immune cells and microorganisms," *Nature Reviews Cancer*, vol. 13, no. 11, pp. 759–771, 2013.

[112] D. B. Sacdalan and J. A. Lucero, "The association between inflammation and immunosuppression: implications for ICI biomarker development," *OncoTargets and Therapy*, vol. 14, pp. 2053–2064, 2021.

[113] B. Jing, T. Wang, B. Sun et al., "IL6/STAT3 signaling orchestrates premetastatic niche formation and immunosuppressive traits in lung," *Cancer Research*, vol. 80, no. 4, pp. 784–797, 2020.

[114] J. B. Mitchem, D. J. Brennan, B. L. Knolhoff et al., "Targeting tumor-infiltrating macrophages decreases tumor-initiating cells, relieves immunosuppression, and improves chemotherapeutic responses," *Cancer Research*, vol. 73, no. 3, pp. 1128–1141, 2013.

[115] S. Shalapour and M. Karin, "Pas de Deux: control of antitumor immunity by cancer-associated inflammation," *Immunity*, vol. 51, no. 1, pp. 15–26, 2019.

[116] P. Sharma, S. Hu-Lieskovan, J. A. Wargo, and A. Ribas, "Primary, adaptive, and acquired resistance to cancer immunotherapy," *Cell*, vol. 168, no. 4, pp. 707–723, 2017.

[117] T. Gaber, C. Strehl, and F. Buttgereit, "Metabolic regulation of inflammation," *Nat Rev Rheumatol*, vol. 13, no. 5, pp. 267–279, 2017.

[118] P. H. C. Leliefeld, C. M. Wessels, L. P. H. Leenen, L. Koenderman, and J. Pillay, "The role of neutrophils in immune dysfunction during severe inflammation," *Crit Care*, vol. 20, no. 1, p. 73, 2016.

[119] H. Yoshida and C. A. Hunter, "The immunobiology of interleukin-27," *Annu Rev Immunol*, vol. 33, no. 1, pp. 417–443, 2015.

[120] N. C. Kampan, S. D. Xiang, O. M. McNally, A. N. Stephens, M. A. Quinn, and M. Plebanski, "Immunotherapeutic interleukin-6 or interleukin-6 receptor blockade in cancer: challenges and opportunities," *Current Medicinal Chemistry*, vol. 25, no. 36, pp. 4785–4806, 2018.

[121] T. Horiuchi, H. Mitoma, S. i. Harashima, H. Tsukamoto, and T. Shimoda, "Transmembrane TNF-: structure, function and interaction with anti-TNF agents," *Rheumatology (Oxford)*, vol. 49, no. 7, pp. 1215–1228, 2010.

[122] H. Malcova, Z. Strizova, T. Milota et al., "IL-1 inhibitors in the treatment of monogenic periodic fever syndromes: from the past to the future perspectives," *Front Immunol*, vol. 11, Article ID 619257, 2020.

[123] A. Markota, S. Endres, and S. Kobold, "Targeting interleukin-22 for cancer therapy," *Human Vaccines & Immunotherapeutics*, vol. 14, no. 8, pp. 2012–2015, 2018.

[124] N. N. Alraouji and A. Aboussekhra, "Tocilizumab inhibits IL-8 and the proangiogenic potential of triple negative breast cancer cells," *Molecular Carcinogenesis*, vol. 60, no. 1, pp. 51–59, 2021.

[125] K. Ly, M. P. Smith, Q. Thibodeaux, V. Reddy, W. Liao, and T. Bhutani, "Anti IL-17 in psoriasis," *Expert Review of Clinical Immunology*, vol. 15, no. 11, pp. 1185–1194, 2019.

[126] C. G. M. Wilson and M. R. Arkin, "Small-molecule inhibitors of IL-2/IL-2R: lessons learned and applied," *Current Topics in Microbiology and Immunology*, vol. 348, pp. 25–59, 2011.

[127] Y. Kalechman, U. Gafter, R. Gal et al., "Anti-IL-10 therapeutic strategy using the immunomodulator AS101 in protecting mice from sepsis-induced death: dependence on timing of immunomodulating intervention," *J Immunol*, vol. 169, no. 1, pp. 384–392, 2002.

[128] S. Michitaka, S. Yasuo, H. Kenju et al., "IPD-1151T (suplatast tosilate) inhibits interleukin (IL)-13 release but not IL-4 release from basophils," *Japanese Journal of Pharmacology*, vol. 79, no. 4, pp. 501–504, 1999.

[129] A. M. Algra and P. M. Rothwell, "Effects of regular aspirin on long-term cancer incidence and metastasis: a systematic comparison of evidence from observational studies versus

randomised trials," *The Lancet. Oncology*, vol. 13, no. 5, pp. 518–527, 2012.

[130] P. M. Rothwell, J. F. Price, F. G. R. Fowkes et al., "Short-term effects of daily aspirin on cancer incidence, mortality, and non-vascular death: analysis of the time course of risks and benefits in 51 randomised controlled trials," *The Lancet*, vol. 379, no. 9826, pp. 1602–1612, 2012.

[131] P. M. Rothwell, M. Wilson, J. F. Price, J. F. Belch, T. W. Meade, and Z. Mehta, "Effect of daily aspirin on risk of cancer metastasis: a study of incident cancers during randomised controlled trials," *The Lancet*, vol. 379, no. 9826, pp. 1591–1601, 2012.

[132] J. Ma, Z. Cai, H. Wei, X. Liu, Q. Zhao, and T. Zhang, "The anti-tumor effect of aspirin: what we know and what we expect," *Biomedicine & Pharmacotherapy*, vol. 95, pp. 656–661, 2017.

[133] H. J. Maeng, J. H. Song, G. T. Kim et al., "Celecoxib-mediated activation of endoplasmic reticulum stress induces de novo ceramide biosynthesis and apoptosis in hepatoma HepG2 cells," *BMB Reports*, vol. 50, no. 3, pp. 144–149, 2017.

[134] M. Y. Murray, S. A. Rushworth, L. Zaitseva, K. M. Bowles, and D. J. Macewan, "Attenuation of dexamethasone-induced cell death in multiple myeloma is mediated by miR-125b expression," *Cell Cycle*, vol. 12, no. 13, pp. 2144–2153, 2013.

[135] A. Yano, Y. Fujii, A. Iwai, Y. Kageyama, and K. Kihara, "Glucocorticoids suppress tumor angiogenesis and in vivo growth of prostate cancer cells," *Clinical Cancer Research*, vol. 12, no. 10, pp. 3003–3009, 2006.

[136] Y. Okamura, T. Sugiura, T. Ito et al., "The achievement of a sustained virological response either before or after hepatectomy improves the prognosis of patients with primary hepatitis C virus-related hepatocellular carcinoma," *Ann Surg Oncol*, vol. 26, no. 13, pp. 4566–4575, 2019.

[137] F. Zhu, J. Willette-Brown, N. Y. Song et al., "Autoreactive T cells and chronic fungal infection drive esophageal carcinogenesis," *Cell Host & Microbe*, vol. 21, no. 4, pp. 478–493.e7, 2017, e477.

[138] S. Bullman, C. S. Pedamallu, E. Sicinska et al., "Analysis of Fusobacterium persistence and antibiotic response in colorectal cancer," *Science*, vol. 358, no. 6369, pp. 1443–1448, 2017.

[139] T. G. Simon, A. S. Duberg, S. Aleman et al., "Lipophilic statins and risk for hepatocellular carcinoma and death in patients with chronic viral hepatitis: results from a nationwide Swedish population," *Ann Intern Med*, vol. 171, no. 5, pp. 318–327, 2019.

[140] V. S. Pelly, A. Moeini, L. M. Roelofsen et al., "Anti-inflammatory drugs remodel the tumor immune environment to enhance immune checkpoint blockade efficacy," *Cancer Discovery*, vol. 11, no. 10, pp. 2602–2619, 2021.

[141] H. C. van Zaanen, H. M. Lokhorst, L. A. Aarden et al., "Chimaeric anti-interleukin 6 monoclonal antibodies in the treatment of advanced multiple myeloma: a phase I dose-escalating study," *British Journal of Haematology*, vol. 102, no. 3, pp. 783–790, 1998.

[142] D. S. Hong, D. Hui, E. Bruera et al., "MABp1, a first-in-class true human antibody targeting interleukin-1α in refractory cancers: an open-label, phase 1 dose-escalation and expansion study," *The Lancet. Oncology*, vol. 15, no. 6, pp. 656–666, 2014.

[143] J. Rodon, M. A. Carducci, J. M. Sepulveda-Sánchez et al., "First-in-human dose study of the novel transforming growth factor-β receptor I kinase inhibitor LY2157299 monohydrate in patients with advanced cancer and glioma," *Clinical Cancer Research*, vol. 21, no. 3, pp. 553–560, 2015.

[144] Y. X. Chen, Q. Y. Gao, T. H. Zou et al., "Berberine versus placebo for the prevention of recurrence of colorectal adenoma: a multicentre, double-blinded, randomised controlled study," *The Lancet Gastroenterology & Hepatology*, vol. 5, no. 3, pp. 267–275, 2020.

[145] B. Ngo, J. M. Van Riper, L. C. Cantley, and J. Yun, "Targeting cancer vulnerabilities with high-dose vitamin C," *Nature Reviews Cancer*, vol. 19, no. 5, pp. 271–282, 2019.

[146] M. S. Ellulu, A. Rahmat, I. Patimah, H. Khaza'ai, and Y. Abed, "Effect of vitamin C on inflammation and metabolic markers in hypertensive and/or diabetic obese adults: a randomized controlled trial," *Drug Design, Development and Therapy*, vol. 9, pp. 3405–3412, 2015.

[147] I. S. Jang, Y. H. Ko, Y. S. Moon, and S. H. Sohn, "Effects of vitamin C or E on the pro-inflammatory cytokines, heat shock protein 70 and antioxidant status in broiler chicks under summer conditions," *Asian-Australas J Anim Sci*, vol. 27, no. 5, pp. 749–756, 2014.

[148] J. Yun, E. Mullarky, C. Lu et al., "Vitamin C selectively kills KRAS and BRAF mutant colorectal cancer cells by targeting GAPDH," *Science*, vol. 350, no. 6266, pp. 1391–1396, 2015.

Hindawi
Journal of Oncology
Volume 2022, Article ID 3919053, 12 pages
https://doi.org/10.1155/2022/3919053

Research Article

Therapeutic Effect of Curcumol on Chronic Atrophic Gastritis (CAG) and Gastric Cancer Is Achieved by Downregulating SDF-1α/CXCR4/VEGF Expression

Xuehui Ma,[1] Zhengbo Zhang,[2] Xiayu Qin,[1] Lingjing Kong,[1] Wen Zhu,[1] Lingzhi Xu,[3] and Xin Zhou[1]

[1]*Department of Preclinical, Wuxi Hospital of Traditional Chinese Medicine, Wuxi, Jiangsu, China*
[2]*Department of Gastroenterology, Wuxi Hospital of Traditional Chinese Medicine, Wuxi, Jiangsu, China*
[3]*Health Examination Center, Wuxi Hospital of Traditional Chinese Medicine, Wuxi, Jiangsu, China*

Correspondence should be addressed to Xin Zhou; wuxvip@163.com

Received 24 June 2022; Revised 26 July 2022; Accepted 1 August 2022; Published 12 September 2022

Academic Editor: Ashok Pandurangan

CAG is an essential procession of the transformation from gastritis into gastric cancer. A series of timely moves of diagnosis, treatment, and monitoring towards CAG to anticipate the potential population at risk of gastric cancer is an effective means to prevent gastric cancer occurrence. The main active monomer in Fuzheng Huowei Decoction is Curcumol, which is an indispensable ingredient in the treatment to CAG and gastric cancer. In this study, the CAG model, *in vitro* cultured gastric cancer cells, and participating nude mice were treated with Curcumol, and alterations in SDF-1α/CXCR4/VEGF expression were estimated using the assays of immunohistochemistry and Western blot. MTT, flow cytometry, transwell, HE staining, and tumor volume determination were applied for the verification of the regulatory effects of Curcumol on CAG and gastric cancer cells. The results showed that the expressions of VEGF, SDF-1α, CXCR4, and CD34 decreased in our CAG model with Curcumol treatment. Curcumol is in procession of an inhibitory effect toward the activity, migration, and invasion of gastric cancer cells, and it would also result in gastric cancer cells' apoptosis. We subsequently added SDF-1α overexpressing lentivirus to the Curcumol-treated group and found that the expressions of SDF-1α, CXCR4, and VEGF protein increased, and the inhibitory effect of Curcumol on gastric cancer cells was withdrawn. Our nude mouse experiment showed that Curcumol + SDF-1α group ended up with the largest tumor volume, while Fuzheng Huowei + NC group was with the smallest tumor volume. In conclusion, Curcumol is able to effectively protect the gastric tissue and suppress gastric cancer cells' viability. Curcumol functions as a therapeutic factor in chronic atrophic gastritis and gastric cancer by downregulating SDF-1α/CXCR4/VEGF expression.

1. Introduction

Gastric cancer is a malignant tumor caused by gastric epithelial lesions, with its second largest cancerous prevalence in the world. China is a country of high gastric cancer occurrence. The main task of gastric cancer research is to find and develop effective remedies. The occurrence of gastric cancer is a gradual process, which begins with the transformation of the normal gastric mucosa into gastric mucosa epithelial abnormalities or diseases. It is known as pregastric cancer, and eventually, it ends up as gastric cancer [1, 2]. CAG is a stage of precancerous disorder, characterized by the abnormal differentiation and proliferation of the gastric intrinsic gland or the intestinal metaplasia in the process of decay and proliferation. CAG is a process in which the gastric epithelial cells suffer repeated damage. It is caused by the long-term action of pathogenic factors on gastric mucosa, resulting in the reduction of inherent glands in gastric mucosa, accompanying with or without intestinal metaplasia and/or pseudopyloric metaplasia [3–5]. CAG is the junction amid chronic superficial gastritis and gastric cancer and is a key stage of gastric mucosa malignant

transformation. Any timely attempt of the intervention of CAG stage is the key to reverse the occurrence of gastric cancer.

In view of the fact that there is currently no specific treatment for CAG clinically, this study aims to explore safe and effective drugs for CAG. The theory of traditional Chinese medicine points out that most patients with chronic atrophic gastritis have a long course of disease, which will ultimately lead to a certain degree of discord between chi and blood, causing blood stasis. Contextually, spleen deficiency with collateral stasis, decreasing gastric mucus secretion, and mucous membrane loss is gradually leading to gastric atrophy [6–8]. A moderate amount of the traditional Chinese medicine in CAG prescription is able to accelerate blood circulation and remove blood stasis, which effectively restores gastric mucous secretion and eliminates gastric atrophy.

Zedoary turmeric is a warm-property traditional Chinese medicine, tasting spicy and bitter, endowed with a strong affinity to the liver and spleen, holding the efficiency of dredging chi to break congestion, eliminating accumulation, and relieving pain. Modern phytochemical studies show that the main chemical constituents of Zedoary are volatile oil, curcumin, polysaccharides, sterols, phenolic acids, and alkaloids [9]. Of all these components, Curcumol is the main player with the highest content in the volatile oil of curcuma zedoaria. Curcumol has potential anticancer and anti-inflammatory properties, and it is involved in the regulation of angiogenesis and analgesia, promoting wound healing and antioxidant ability. Pharmacologically speaking, Curcumol has low toxicity to human body, and its high efficiency and low toxicity in the treatment of tumor is impressive [10, 11]. Curcumol is able to induce tumor cell apoptosis through different signaling pathways and effectively inhibit gastric cancer cell lines' proliferative activity, which has also been verified by animal studies. Currently, the therapeutic effect of Curcumol on CAG, also known as the precancerous lesion of gastric cancer, remains vacant.

Studies have shown that Curcumol promotes wound healing in a manner of eliciting the expression of VEGF in hyperglycemia rats. Besides, Curcumol represents a therapeutic effect on liver fibrosis. According to the theory of traditional Chinese medicine, gastric collateral stasis is one of the most important pathological factors of CAG, which is closely related to pathological changes, such as gastric epithelium and glandular atrophy, fibromuscular hyperplasia, intestinal metaplasia, and atypical hyperplasia, and it is also a key step in the development and malignant transformation of CAG. This study is committed to explore the therapeutic effects of Curcumol in the cell experiments with CAG and gastric cancer *in vivo* and *in vitro*.

2. Materials and Methods

2.1. Establishment of the CAG Animal Model. SD rats were fed adaptively for one week. The chronic atrophic gastritis model of rats was established as follows: 20 mmol/L of deoxycholate sodium solution (pH 7 to 7.8) was freely consumed, and 60% ethanol (2 mL/mouse) was gavaged every 10 days. 30% ethanol and 10 mmol/L were given alternately every 7 days from the 31st day. After 12 weeks, gastric tissues were collected for examination. Animal experiments were authorized by the Animal Ethics Committee of Wuxi Hospital of Traditional Chinese Medicine (SWJWDW2021042601).

After modeling, the rats were split up into three groups (treatment group, model group, and control group), with 6 rats in each group. The rats in the treatment group were given 20 mg/kg of intragastric administration every day, while those rats in the model group and control group were administrated with the tantamount amount of normal saline in consecutive 28 days.

Model + Curcumol/Fuzheng Huowei decoction + SDF-1α overexpression AAV group was given with the simultaneous administration of the formulae of Curcumol/Fuzheng Huowei decoction on the same day after modeling. SDF-1α overexpressed AAV treatment was followed by tail vein injection (model + Zedoary turmeric enol/Fuzheng Huowei decoction + AAV control group injection of control virus, others are the same). All rats were sacrificed after 4 weeks of virus injection and were sampled.

2.2. Nude Mouse Tumorigenicity Assay. Thirty nude mice were injected with SGC7901 cells to establish the transplanted tumor. The tumor size and body weight of all mice were evaluated twice a week. After the tumor grew to about 0.5 cm in length, all mice were split up into 5 groups, with 6 mice in each group. They were the model control group, Curcumol treatment group, Curcumol + SDF-1α overexpression AAV group, Fuzheng Huowei decoction treatment group, and Fuzheng Huowei decoction + SDF-1α overexpression AAV group. Curcumol and Fuzheng Huowei formulae were administrated in the way of gastric instillation, while AAV was given by injection. Tumor growth curve was drawn in accordance with the parameters of tumor volume. On day 28, the mice were sacrificed and weighed for tumor detection.

The establishment of the gastric cancer cells subcutaneous transplanted tumor nude mice model: gastric cancer cells at logarithmic growth stage were prepared into a cell suspension with a concentration of 1×10^7/mL, and 170 μL of the suspension was inoculated subcutaneously into the right axillary region of nude mice. When the length of the tumor reached about 0.5 cm, the mice were grouped. They were the model control group, Curcumol treatment group, Curcumol + SDF-1α overexpression AAV group, Fuzheng Huowei decoction treatment group, and Fuzheng Huowei decoction + SDF-1α overexpression AAV group. Moreover, Curcumol and Fuzheng Huowei decoction were administered in the way of gastric perfusion, while AAV was given by injection.

2.3. HE Staining. After fetching, the samples were rinsed with PBS and fixed with 4% paraformaldehyde. The HE staining kit was the product of BEYOTIME Company, and the test was carried out according to the kit instructions.

2.4. Immunohistochemical Analysis. Paraffin sample sections were dewaxed by xylene and gradient ethanol. The samples were then immersed in 0.01 mol/L citrate buffer (pH 6.0) for antigen repairing. The slices were then immersed in 3% hydrogen peroxide to block endogenous catalase and sealed with 5% goat serum in a wet box at room temperature. The samples were then added and incubated with primary antibody at 4°C overnight. After being washed by PBS for 3 times, the second antibody was added and incubated with it at 37°C for 1 h. The slices were then washed and restained with hematoxylin, dehydrated, and sealed.

2.5. MTT Detection on Cellular Viability. SGC7901 cells were provided by the Chinese Academy of Sciences, cultured with the complete medium containing 10% FBS and 1% penicillin-streptomycin. The cells were grown in 96-well plates with 200 μL per well, and 3 separate wells were set for each group. After incubation for 6 h, 24 h, and 48 h, the 96-well plates were taken out of the incubator, and 20 μL of 5 mg/mL MTT solution was added to each well. The culture plate was incubated in the incubator for 4 h, and then the culture was terminated. The culture medium was removed from the culture wells, and 150 μL of dimethyl sulfoxide was added to each well, and the crystals were fully dissolved by shaking on a shaker at low speed for 10 min. The absorbance value of each well was measured at OD490 nm of ELISA.

$$\begin{aligned}\text{Cell viability}\,(\%) &= \frac{[A\,(\text{experimental group}) - a\,(\text{blank group})]}{[A\,(\text{control group}) - A\,(\text{blank group})]} \times 100\%,\\ \text{Cell inhibition rate} &= \frac{[A\,(\text{control group}) - a\,(\text{experimental group})]}{A\,(\text{control group})} = 1 - \text{cell viability}.\end{aligned} \tag{1}$$

2.6. Flow Cytometry Detection on Apoptosis. SGC7901 cells were divided as follows: control group, Curcumol treatment group 100 mg/L (48 h), and Fuzheng Huowei decoction treatment group 100 mg/L (48 h). The apoptosis of SGC7901 cells was evaluated via flow cytometry. After the cells were harvested, the cells were centrifuged at 300 g for 5 min, and the supernatant was discarded. The cells were then rinsed once with PBS, and the supernatant was discarded after centrifugation. The supernatant was suspended with 100 μL of diluted 1 × Annexin V Binding Buffer. 2.5 μL Annexin V-APC and 2.5 μL DAPI staining solution were added to the cell suspension. The cells were incubated at room temperature and kept in dark for 15 min. 400 μL of Annexin V Binding Buffer was added, and the samples were mixed and tested immediately.

2.7. Transwell Assay Detection on Cell Migration and Invasion. Cell migration experiment: 1 mL trypsin containing EDTA was added to digest SGC7901 cells. After the digestion was complete, culture medium containing serum was added to terminate digestion. The culture medium was removed by centrifugation, the cells were rinsed with PBS once or twice and suspended with serum-free culture to adjust the cell density to 5×10^5/mL. 100 μL cell suspension was added to each well and stimulated with drugs. 500 μL complete medium containing 20% FBS was added to the lower chamber, and the cells were incubated at 37°C for 24 h. Transwell chambers were removed, the culture medium in the well was discarded, and the cells were washed twice with calcium-free PBS. The cells were fixed with 4% paraformaldehyde for 20 min. After washing with PBS, the cells were stained with 0.1% crystal violet for 20 min. Cells in the middle and surrounding 5 fields were counted under a 100-fold microscope, and their average values were taken.

Cell invasion assay: 300 μL serum-free medium was taken, 60 μL Matrigel was added to the medium and mixed, and 100 μL was added to the upper chamber and incubated in a 37°C incubator for 5 h. 1 mL of trypsin, containing EDTA, was added into the cell wells to digest the SGC7901 cells. After digestion, the cell density was adjusted to 5×10^5/mL. Matrigel was washed once in serum-free medium, 100 μL cell suspension was added to each well, and 500 μL of the complete medium containing 20% FBS was added into the lower chamber, which was incubated at 37°C for 24 h. The transwell chamber was taken out, and the culture medium in the well was removed. It was rinsed twice with calcium-free PBS, fixed with 4% paraformaldehyde for 20 min, stained with 0.1% crystal violet for 20 min after PBS cleaning, and the unmigrating cells in the upper layer of the chamber were gently wiped with wet cotton ball and cleaned with PBS for 3 times. Five fields of the cells in the middle and surrounding areas were counted under a 100-fold microscope and their average values were taken.

2.8. Western Blot Detection on Protein Expression. RIPA lysate was added to the sample, which was shaken on the vortex for 1 min and placed on ice for 10 min. It was then centrifuged at 13,000 rpm at 4°C for 20 min. 500 μg of total protein from each sample was mixed with 5 × SDS loading buffer. The concentrated glue was run with 80 V, and then the voltage was converted to 120 V, until bromophenollan was just transferred to the bottom of the glue plate. The PVDF membrane was cleaned with TBST for 1 min and then sealed with 5% skim milk sealer at room temperature for 1 h. The primary antibody was diluted at 1 : 1000, with the primary antibody diluent and incubated with the sealed PVDF membrane at 4°C overnight. The secondary antibody was diluted into a certain concentration (1 : 2000) with the

blocking solution, and then kept with the PVDF membrane at room temperature for 1 h. The ECL exposure solution was added on the whole membrane. After 1-min reaction with PVDF membrane, the ECL exposure solution was put into the exposure instrument for exposure detection.

3. Results

3.1. Curcumol Inhibited VEGF, SDF-1α, CXCR4, and CD34 Expressions in the CAG Model. In this study, the animal model of CAG was firstly prepared using ethanol feeding, and then the tissue structure and marker protein expressions of model animals were detected via HE staining and immunohistochemistry. Then, we found that the gastric tissues of the animals in the CAG model group was disordered and irregular, and there was obvious inflammatory cell infiltration. Immunohistochemical assay revealed that the VEGF, SDF-1α, CXCR4, and CD34 expressions in the CAG model group were signally elevated versus control groups (Figure 1).

Subsequently, Curcumol and Fuzheng Huowei decoction were, respectively, administrated to the model group. Then, immunohistochemistry detection on the expressions of the related proteins was carried out. The results showed that when compared to the model group, either the VEGF, SDF-1α, CXCR4, and CD34 expressions in Curcumol or positive drug groups were decreased (Figure 2).

3.2. Curcumol Inhibits the Activity, Migration, and Invasion of Gastric Cancer Cells. In this section, we demonstrated curcumin's regulatory function in the gastric cancer cells cultured *in vitro*. Cells were given 25 mg/L, 50 mg/L, and 100 mg/L Curcumol/Fuzheng Huowei decoction. The results of MTT assay reflected that the inhibition rate of 100 mg/L Fuzheng Huowei decoction for 48 h was the highest, and the subsequent was 100 mg/L Curcumol for 48 h (Figure 3). According to this finding, we chose Curcumol treatment group 100 mg/L (48 h) and Fuzheng Huowei decoction treatment group 100 mg/L (48 h) to carry out our the experiments further.

The apoptosis rate of gastric cancer cells in the control group, Curcumol treatment group, and Fuzheng Huowei decoction treatment group were 17.32%, 36.92%, and 39.99% in several. Curcumol and Fuzheng Huowei decoction significantly induced the apoptosis of gastric cancer cells (Figure 4(a)). Gastric cancer cells' migratory and invasive abilities were evaluated via the transwell assay, and it turned out that the number of migratory and invasive cells in the cells treated with Curcumol and Fuzheng Huowei decoction decreased significantly (Figure 4(b)). In-depth detection on SDF-1α, CXCR4, and VEGF protein expressions showed that the SDF-1α, CXCR4, and VEGF protein levels in gastric cancer cells were greatly retarded after the treatment with Curcumol and positive drug Fuzheng Huowei decoction (Figure 4(c)).

3.3. SDF-1α Reverses the Inhibition from Curcumol on Gastric Cancer Cells. In this section, we first treated gastric cancer cells with SDF-1α overexpressed lentivirus and Curcumol, and then Curcumol's regulatory effect on SDF-1α/CXCR4 axis was verified. Afterwards, our results indicated that high levels of SDF-1α elevated SDF-1α, CXCR4, and VEGF protein levels in gastric cancer cells (Figure 5(a)). The assay of MTT unveiled that the inhibition from Curcumol or Fuzheng Huowei decoction on the gastric cancer cells withdrew after the overexpression of SDF-1α (Figure 5(b)). Flow cytometry also revealed that when compared with Curcumol + empty virus group, the apoptosis rate of SDF-1α overexpressed + Curcumol group was significantly reduced (Figure 5(c)). Moreover, the number of migratory and invasive gastric cancer cells was signally increased (Figure 5(d)).

Finally, we further verified the regulation of SDF-1α on gastric cancer cells with the tumor-forming assay in nude mice. It turned out that there was no notable change in the weight of nude mice in the control group, Curcumol + NC group, Curcumol + SDF-1α group, Fuzheng Huowei decoction + NC group, and Fuzheng Huowei decoction + SDF-1α group during the test (Figure 6(a)). However, there were significant differences in tumor volume among all groups, which were that Curcumol + SDF-1α group had the largest tumor volume and Fuzheng Huowei decoction + NC group had the smallest tumor volume (Figure 6(b)). TUNEL and immunohistochemistry were applied for the detection onto the apoptosis and expression of marker proteins in each group after treatment. It was found that SDF-1α, CXCR4, and VEGF protein levels in the overexpressed SDF-1α group were raised, and the apoptosis rate was lower than that in the corresponding empty virus treatment (Figure 7).

4. Discussion

CAG is a necessary process from gastritis to gastric cancer. The diagnosis, treatment, and monitoring of CAG would effectively prevent the occurrence of gastric cancer [12, 13]. Compared with synthetic compounds, this traditional Chinese medicine component has the characteristics of less toxicity and more effects. In the preliminary clinical study, Fuzheng Huowei decoction has been proved to be effective in alleviating the clinical symptoms of CAG patients, boasting the effects of improving histological lesions and promoting mucosal repairing. Curcumol is an important monomer component of Fuzheng Huowei decoction, however, its regulatory mechanism on CAG and gastric cancer is still unknown. This study showed that Curcumol represses the VEGF, SDF-1α, and CXCR4 expressions in both CAG model and gastric cancer cells, and it also suppresses the activity, migration, and invasion of gastric cancer cells, inducing the apoptosis of gastric cancer cells.

Relevant studies have pointed out that the activation of SDF-1α/CXCR4 axis in either human breast cancer cell lines or prostate cancer cell lines promotes VEGF secretion to participate in tumor angiogenesis [14, 15]. In addition, it has been reported that peritoneal metastasis in gastric cancer proves to be related to the interaction between VEGF, CXCR4, and CXCL12. CXCR4 is a specific receptor of

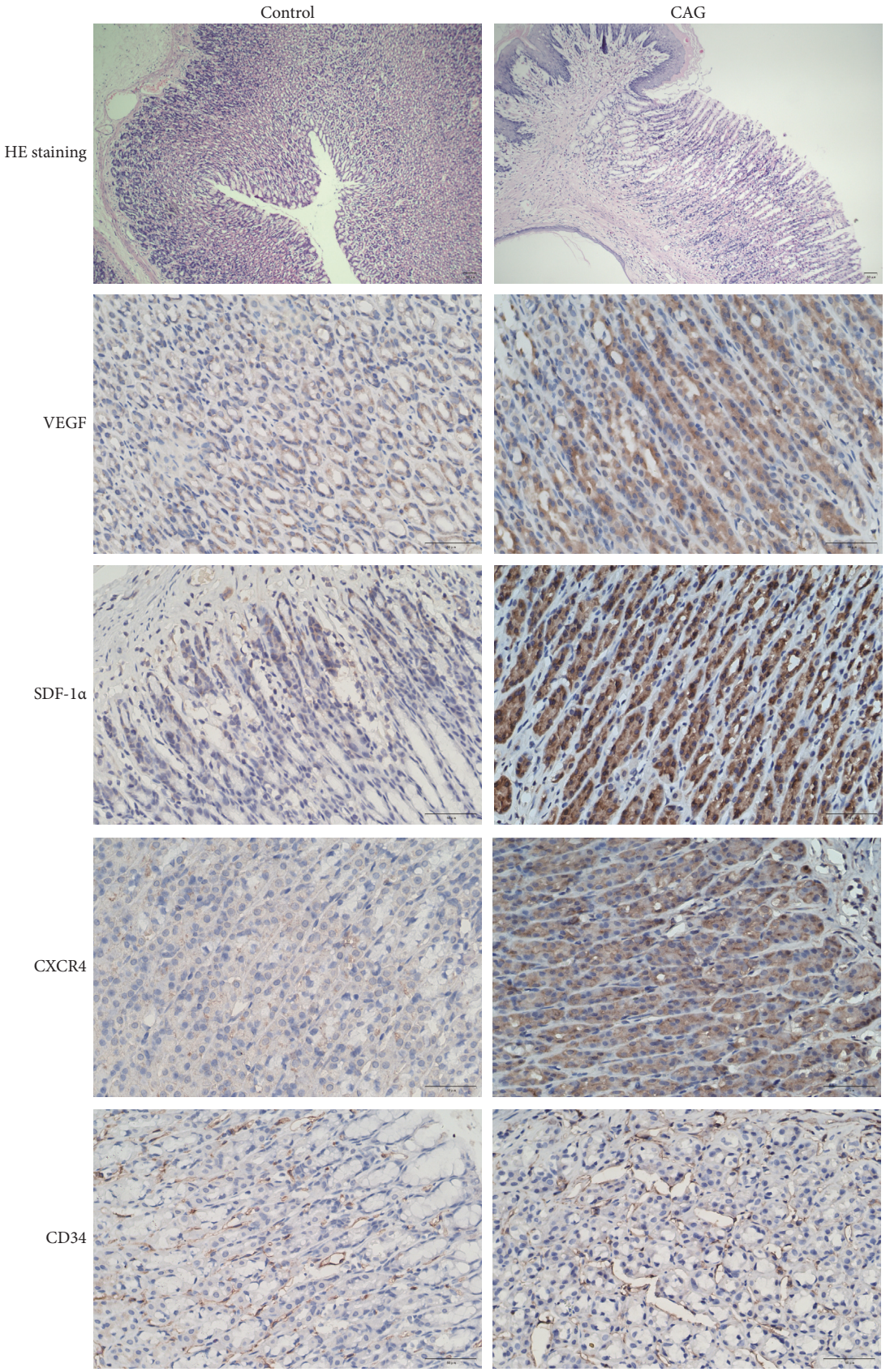

Figure 1: CAG model establishment and relevant detection. Tissue structures and marker protein expressions of CAG model animals were tested by HE staining and immunohistochemistry. $N = 3$, Scale bar: 50 μm.

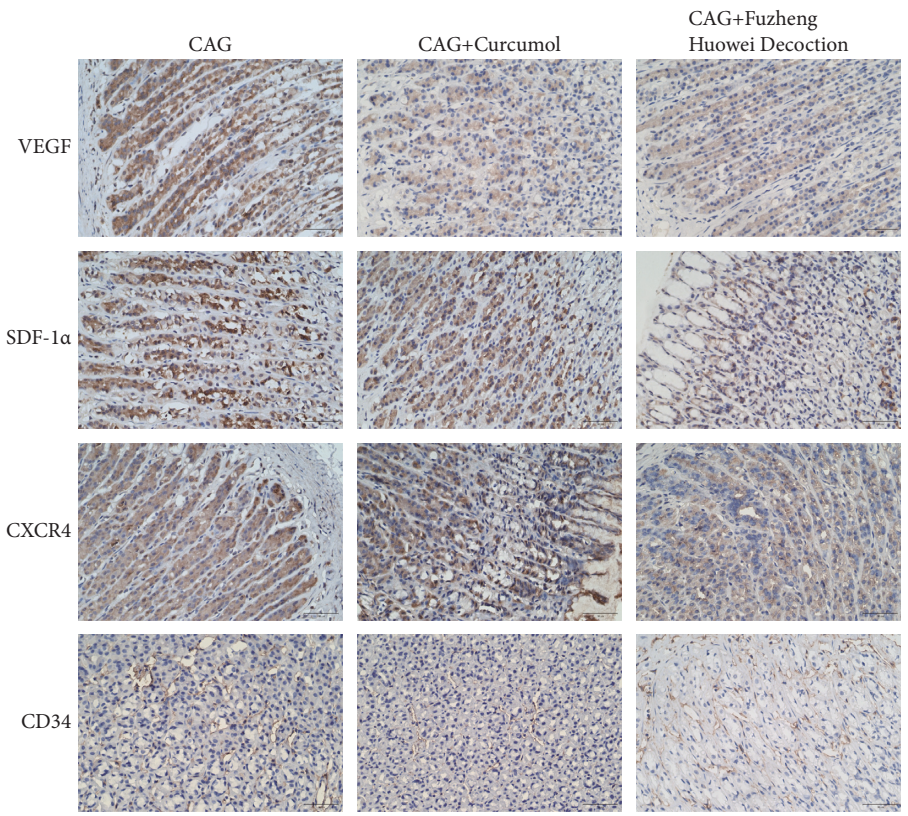

Figure 2: Regulations of Curcumol on relevant protein expressions in CAG model. The expression levels of VEGF, SDF-1α, CXCR4, and CD34 in CAG model were assessed by immunohistochemistry. $N = 3$, Scale bar: 50 μm.

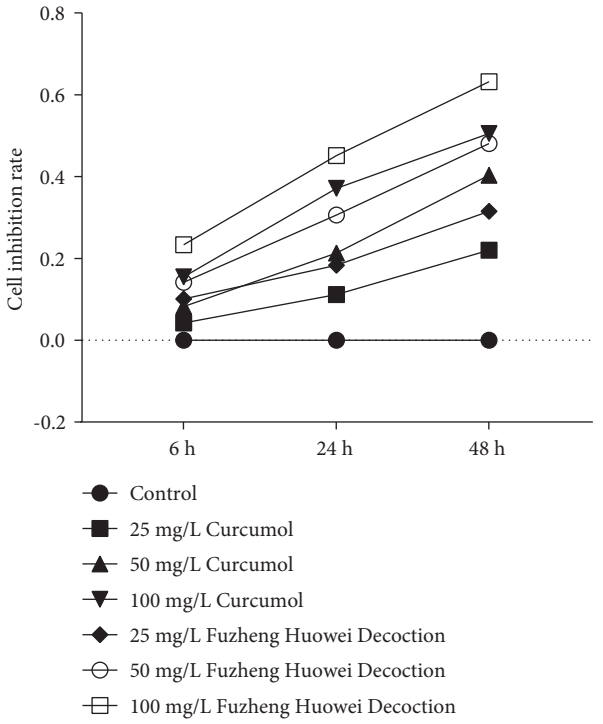

Figure 3: MTT determination on gastric cancer cell viability. $N = 3$.

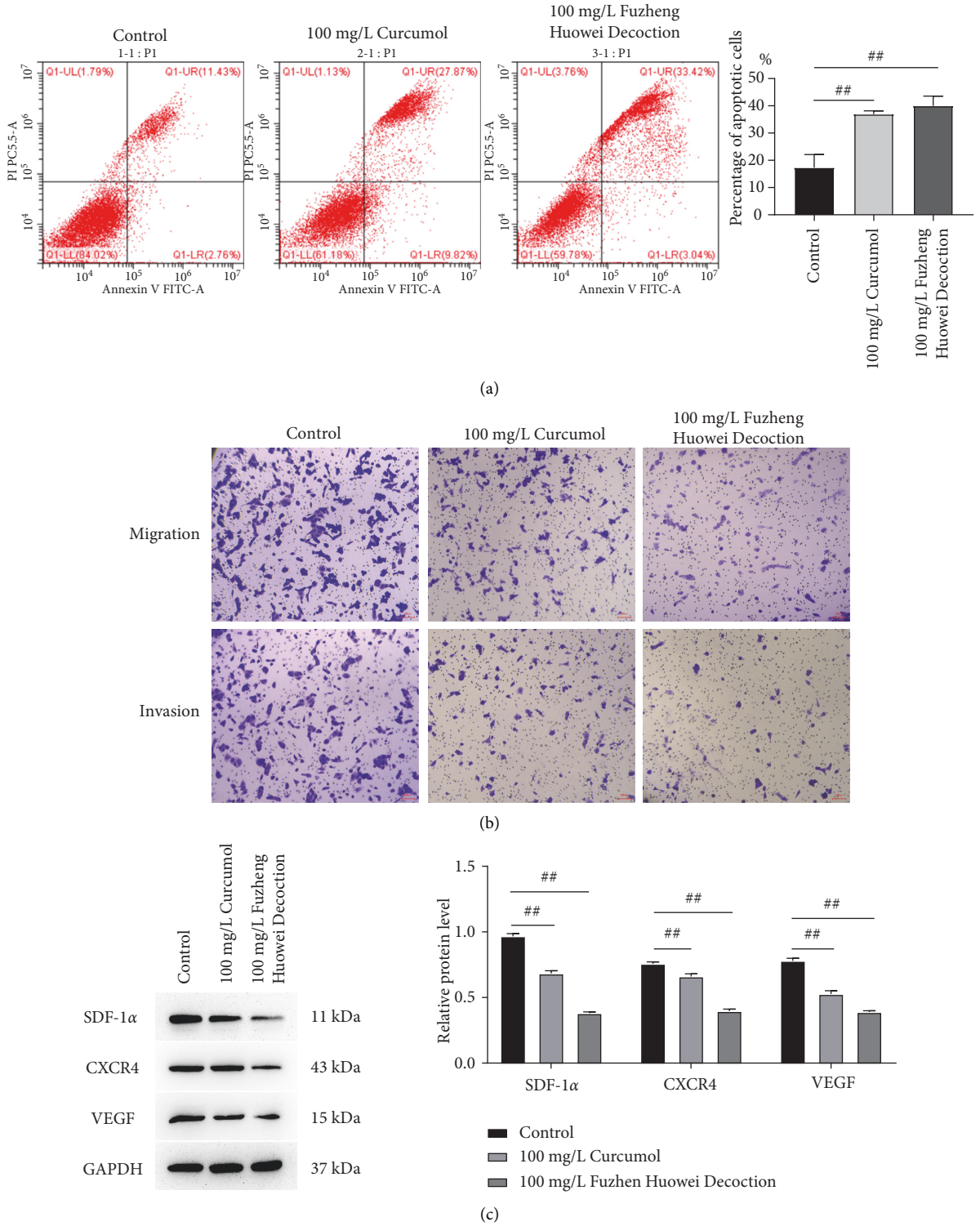

Figure 4: Inhibitory effects of Curcumol on apoptosis, migration, and invasion of gastric cancer cells. (a) Flow cytometry determination on cell apoptosis. (b) Determination of Transwell assay on gastric cancer cell migration and invasion. (c) Determination of Western blot on the protein expression levels of SDF-1α, CXCR4, and VEGF in gastric cancer cells. $N = 3$, Scale bar: 50 μm.

chemokine stromal cell derived factor (SDF-1α), which is involved in tumor growth, invasion, and metastasis. Angiogenesis mediated by SDF-1 binding to CXCR4 promotes tumor growth. It was found in the clinical sample studies of gastric cancer that positive SDF-1 and CXCR4 expression rates gradually increases along with gastric cancer progression, which was basically synchronous with the expression trend of VEGF in gastric cancer progression

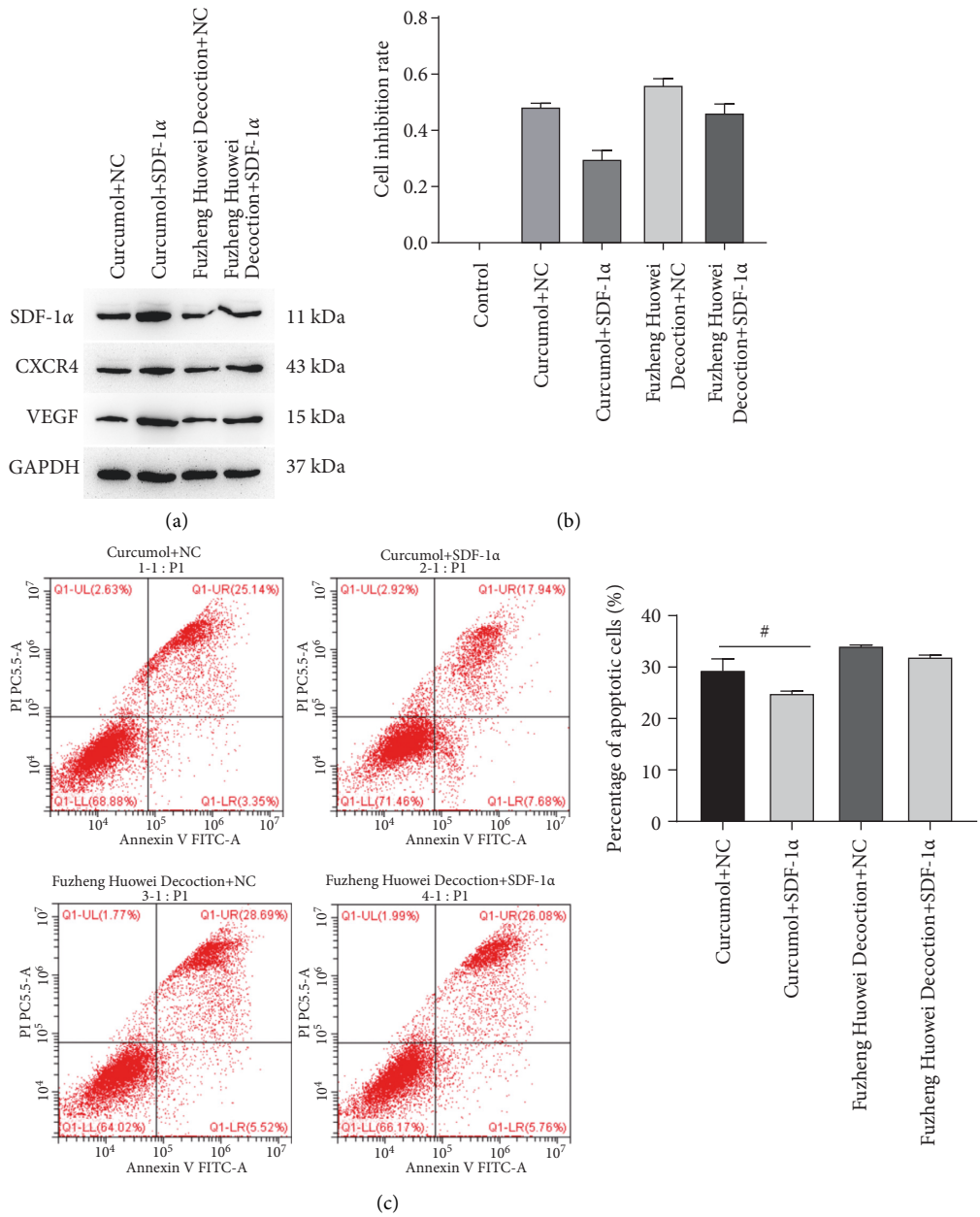

Figure 5: Continued.

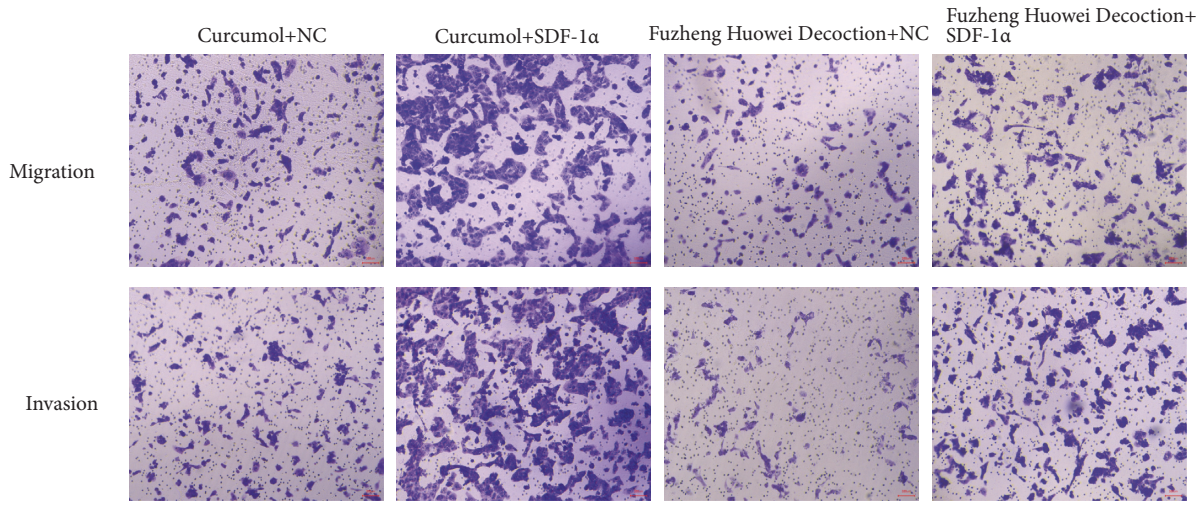

(d)

Figure 5: Reversed effect of SDF-1α toward Curcumol's inhibition on gastric cancer cells. (a) Western blot detection on the protein expression levels of SDF-1α, CXCR4, and VEGF. (b) MTT detection on cell viability. (c) Flow cytometry detection on cellular apoptosis rate. (d) Detection of gastric cancer cell migration and invasion by Transwell test. $N = 3$, Scale bar: 50 μm.

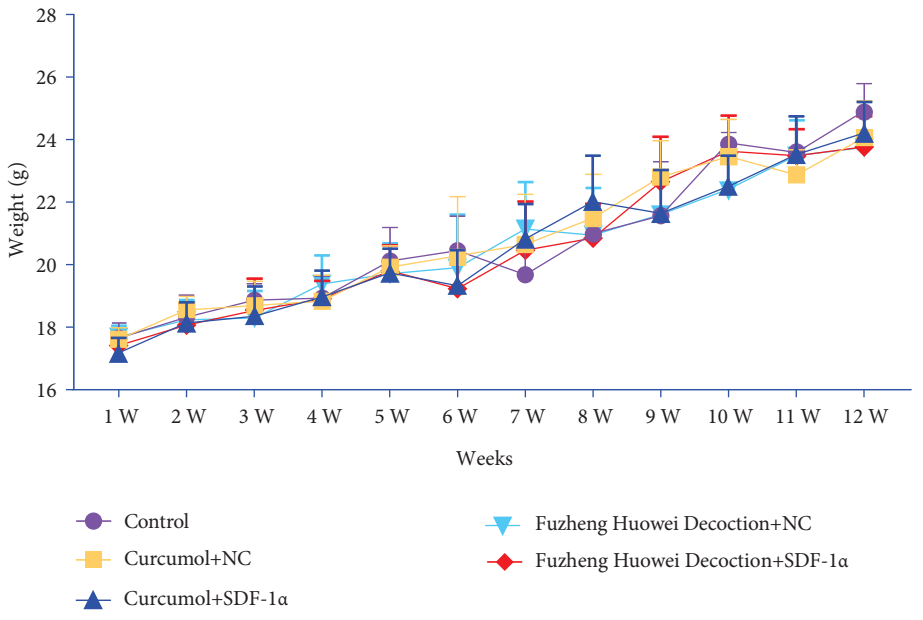

(a)

Figure 6: Continued.

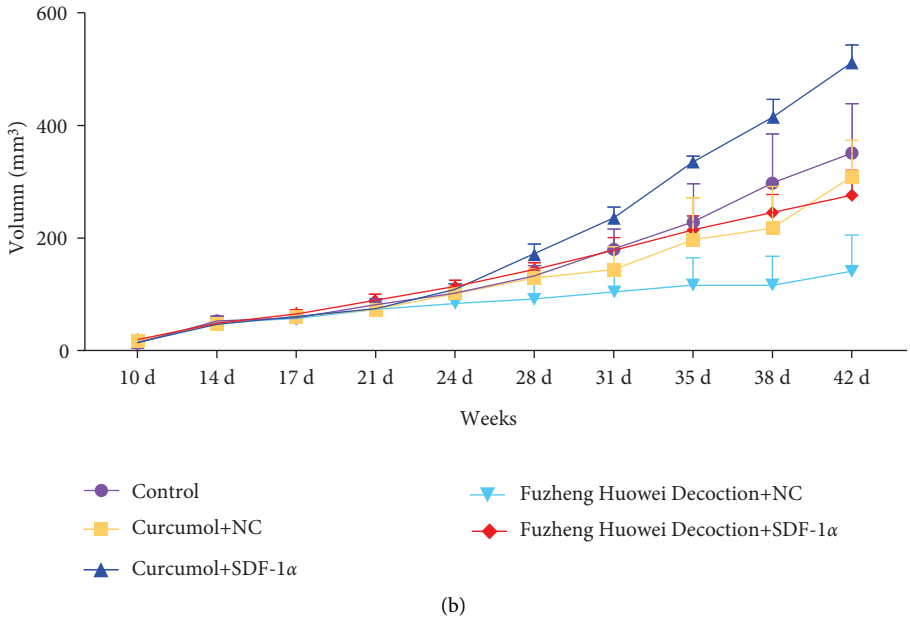

(b)

FIGURE 6: Results of body weight and tumor volume in tumorigenesis test on nude mice. (a) Weight measurement results of nude mice. (b) Tumor volume detection results of nude mice. $N = 6$.

[16–18]. Our study shared a consistence with these findings above. We demonstrated that Curcumol would simultaneously reduce VEGF, SDF-1α, and CXCR4 protein levels in the CAG animal model, and the relevant outcomes from *in vivo* and *in vitro* experiments of gastric cancer were alike.

ATP-sensitive K+ channels couple intracellular metabolism with membrane excitability. These channels are inhibited by ATP. Hence, they open in low metabolic states and close in high metabolic states, resulting in membrane depolarization and triggering responses, such as insulin secretion, the modulation of vascular smooth muscle, and cardioprotection. The channel comprises four Kir6.x subunits and four regulatory sulphonylurea receptors (SUR). Different mechanisms have been proposed for the pathophysiology of gastric ulceration, including changes in the submucosal blood flow of the stomach, gastric motility, and acidity. It seems probable that adenosine 5′-triphosphate (ATP)-dependent potassium channels (K(ATP)) have a regulatory effect on the above factors [19]. Sulfonylurea receptor 1 (SUR1) is the regulatory subunit of ATP-sensitive potassium channels (KATP channels) and the receptor of antidiabetic drugs, such as glibenclamide, which induce insulin secretion in pancreatic β cells.

Targeting SUR1 with glibenclamide suppressed cell growth, cell-cycle progression, epithelial-mesenchymal transition (EMT), and cell migration. Moreover, SUR1 directly interacted with p70S6K and upregulated p70S6K phosphorylation and activity. In addition, glibenclamide inhibited p70S6K, and the overexpression of p70S6K partially reversed the growth-inhibiting effect of glibenclamide. Furthermore, glibenclamide upregulated the expression of the tumor suppressor Krüppel-like factor 4 (KLF4), and silencing KLF4 partially reversed the inhibitory effect of glibenclamide on cell growth, EMT, and migration [20].

Curcumol, a sesquiterpene isolated from Curcuma zedoaria, is known to possess a variety of health and medicinal values, which includes neuroprotection, anti-inflammatory, antitumor, and hepatoprotective activities. It inhibits NF-κB activation by suppressing the nuclear translocation of the NF-κB p65 subunit and blocking IκBα phosphorylation and degradation. Taken together, the combination of *Curcuma zedoary* and kelp could inhibit the proliferation and metastasis of liver cancer cells *in vivo* and *in vitro* by inhibiting endogenous H2S production and downregulating the pSTAT3/BCL-2 and VEGF pathway, which provides strong evidence for the application of *Curcuma zedoary* and kelp in the treatments of liver cancer [21]. Curcumol inhibits the proliferative ability of SKOV3 cells, and the mechanism may be in association with the phosphatidylinositol 3-kinase (PI3K)/protein kinase B (Akt) pathway. Curcumol naturally suppresses the proliferation, migration, and invasion of SKOV3 cells and induces apoptosis. MTOR is a downstream factor beneath the PI3K/Akt pathway and has a regulatory effect on cell proliferation. In this study, we found that Curcumol significantly reduces the SDF-1α/CXCR4/VEGF protein levels in gastric cancer cells. Furthermore, the overexpression of SDF-1α brought about an upregulation in SDF-1α, CXCR4, and VEGF protein levels, and Curcumol's inhibitory effect on gastric cancer cells was withdrawn. In this study, we proved that Curcumol has therapeutic effects on CAG and that it reverses gastric cancer progression by manipulating the angiogenic activity mediated by the SDF-1/CXCR4 axis. It is the first study on the molecular mechanism of Curcumol regulating CAG and gastric cancer. It has laid a good research foundation for the clinical application of Curcumol. However, this study also has certain limitations. We have not been able to demonstrate the direct regulatory

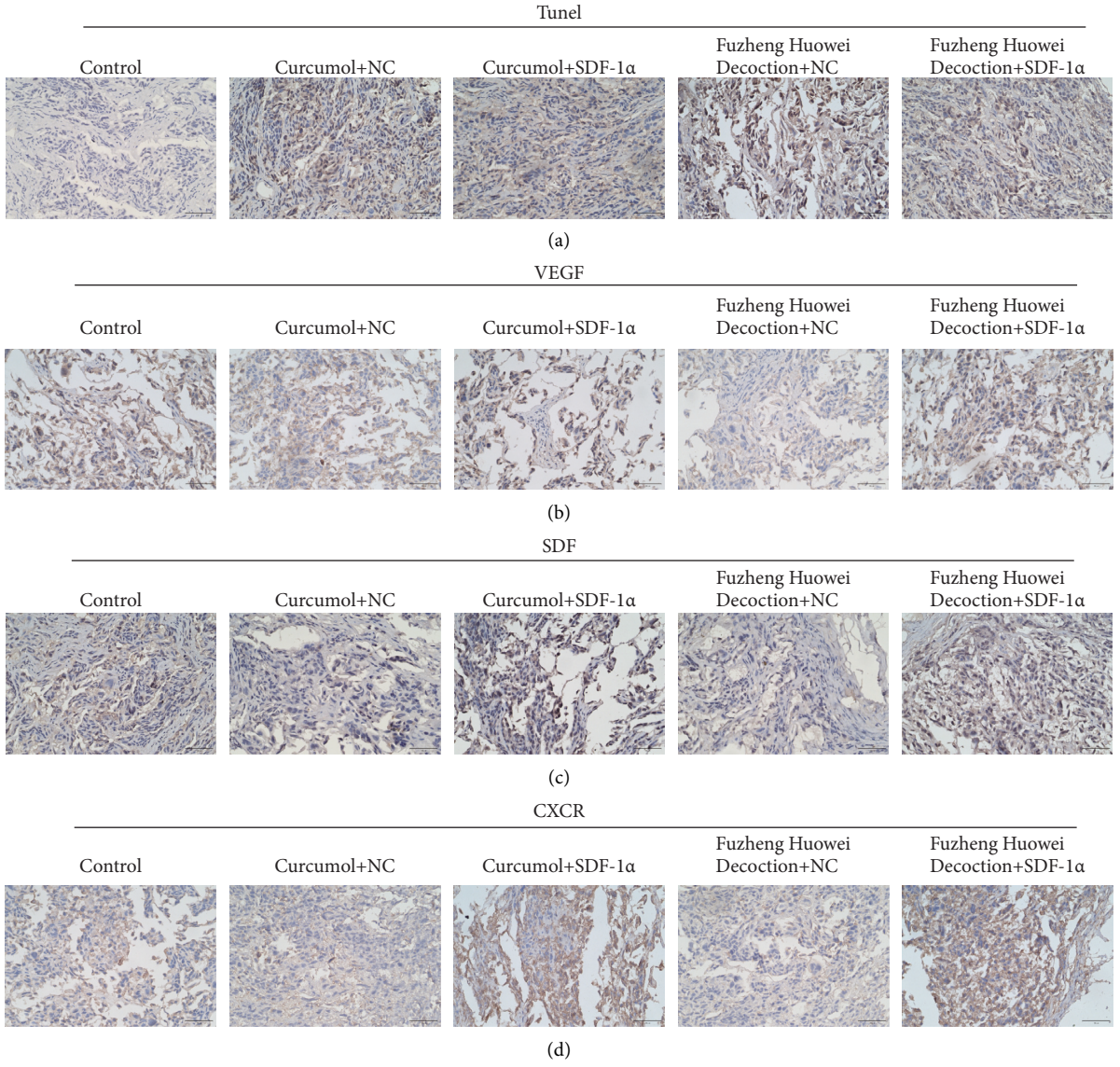

Figure 7: TUNEL and immunohistochemistry detection on apoptosis and protein expression of each group after treatment. $N = 3$, Scale bar: 50 μm.

target of Curcumol and lack a more in-depth mechanism of exploration. This is our future research direction.

5. Conclusion

In this paper, we disclosed the fact that Curcumol functions as an inhibitor for gastric cancer cells by inhibiting gastric cancer cells' activity, migration, and invasion and inducing their apoptosis. Moreover, the expression levels of VEGF, SDF-1α, and CXCR4 decreased after Curcumol treatment. Our nude mouse experiment showed that Curcumol + SDF-1α group had the largest tumor volume, while Fuzheng Huowei + NC group ended up with the smallest. In conclusion, Curcumol effectively protects the gastric tissue and inhibits gastric cancer cell viability. Curcumol treats chronic atrophic gastritis and gastric cancer by decreasing SDF-1α/CXCR4/VEGF expression.

Data Availability

The data used to support the findings of this study are included within the article.

Conflicts of Interest

The authors declare that they have no conflicts of interest.

Authors' Contributions

Xuehui Ma and Zhengbo Zhang contributed equally to this study.

Acknowledgments

This work was supported by "Double Hundred" Young Top-notch Healthcare Talents of Wuxi City and Wuxi Municipal Health Commission Youth Program (Q202024).

References

[1] A. Botezatu and N. Bodrug, "Chronic atrophic gastritis: an update on diagnosis," *Med Pharm Rep*, vol. 94, no. 1, pp. 7–14, 2021.

[2] B. Holleczek, B. Schottker, and H. Brenner, "*Helicobacter pylori* infection, chronic atrophic gastritis and risk of stomach and esophagus cancer: results from the prospective population-based ESTHER cohort study," *International Journal of Cancer*, vol. 146, no. 10, pp. 2773–2783, 2020.

[3] P. Zhang, M. Yang, Y. Zhang et al., "Dissecting the single-cell transcriptome network underlying gastric premalignant lesions and early gastric cancer," *Cell Reports*, vol. 27, no. 6, pp. 1934–1947.e5, 2019.

[4] P. Pimentel-Nunes, D. Libanio, R. Marcos-Pinto et al., "Management of epithelial precancerous conditions and lesions in the stomach (MAPS II): European society of gastrointestinal endoscopy (ESGE), European Helicobacter and microbiota study group (EHMSG), European society of pathology (ESP), and sociedade portuguesa de Endoscopia digestiva (SPED) guideline update 2019," *Endoscopy*, vol. 51, no. 04, pp. 365–388, 2019.

[5] E. Lahner, R. M. Zagari, A. Zullo et al., "Chronic atrophic gastritis: natural history, diagnosis and therapeutic management. A position paper by the Italian society of hospital gastroenterologists and digestive endoscopists [AIGO], the Italian society of digestive endoscopy [SIED], the Italian society of gastroenterology [SIGE], and the Italian society of internal medicine [SIMI]," *Digestive and Liver Disease*, vol. 51, no. 12, pp. 1621–1632, 2019.

[6] D. Hou, M. Yang, Z. Hu, and L. Yang, "Effects of rebamipide for chronic atrophic gastritis: a protocol for systematic review and meta-analysis," *Medicine (Baltimore)*, vol. 99, no. 25, Article ID e20620, 2020.

[7] F. Zhang, F. Wang, C. Chen et al., "Prediction of progression of chronic atrophic gastritis with *Helicobacter pylori* and poor prognosis of gastric cancer by CYP3A4," *Journal of Gastroenterology and Hepatology*, vol. 35, no. 3, pp. 425–432, 2020.

[8] L. Yang, Z. Hu, J. Zhu, and B. Fei, "Effects of weifuchun tablet for chronic atrophic gastritis: a protocol for systematic review and meta-analysis," *Medicine (Baltimore)*, vol. 99, no. 22, Article ID e20374, 2020.

[9] H. Shi, B. Tan, G. Ji et al., "Zedoary oil (Ezhu You) inhibits proliferation of AGS cells," *Chinese Medicine*, vol. 8, no. 1, p. 13, 2013.

[10] T. K. Lee, D. Lee, S. R. Lee et al., "Sesquiterpenes from Curcuma zedoaria rhizomes and their cytotoxicity against human gastric cancer AGS cells," *Bioorganic Chemistry*, vol. 87, pp. 117–122, 2019.

[11] E. B. Jung, T. A. Trinh, T. K. Lee et al., "Curcuzedoalide contributes to the cytotoxicity of Curcuma zedoaria rhizomes against human gastric cancer AGS cells through induction of apoptosis," *Journal of Ethnopharmacology*, vol. 213, pp. 48–55, 2018.

[12] J. M. Park, Y. M. Han, and K. B. Hahm, "Rejuvenation of Helicobacter pylori-associated atrophic gastritis through concerted actions of placenta-derived mesenchymal stem cells prevented gastric cancer," *Frontiers in Pharmacology*, vol. 12, Article ID 675443, 2021.

[13] Q. Ji, Y. Yang, X. Song, X. Han, and W. Wang, "Banxia Xiexin Decoction in the treatment of chronic atrophic gastritis: a protocol for systematic review and meta-analysis," *Medicine (Baltimore)*, vol. 99, no. 42, Article ID e22110, 2020.

[14] B. Yang, C. S. Pan, Q. Li et al., "Inhibitory effects of Chanling Gao on the proliferation and liver metastasis of transplanted colorectal cancer in nude mice," *PLoS One*, vol. 14, no. 2, Article ID e0201504, 2019.

[15] E. Q. Lee, D. G. Duda, A. Muzikansky et al., "Phase I and biomarker study of plerixafor and bevacizumab in recurrent high-grade glioma," *Clinical Cancer Research*, vol. 24, no. 19, pp. 4643–4649, 2018.

[16] M. Li, Y. Lu, Y. Xu et al., "Horizontal transfer of exosomal CXCR4 promotes murine hepatocarcinoma cell migration, invasion and lymphangiogenesis," *Gene*, vol. 676, pp. 101–109, 2018.

[17] C. D. Weekes, D. Song, J. Arcaroli et al., "Stromal cell-derived factor 1α mediates resistance to mTOR-directed therapy in pancreatic cancer," *Neoplasia*, vol. 14, no. 8, pp. 690–IN6, 2012.

[18] A. S. Felix, J. Weissfeld, R. Edwards, and F. Linkov, "Future directions in the field of endometrial cancer research: the need to investigate the tumor microenvironment," *European Journal of Gynaecological Oncology*, vol. 31, no. 2, pp. 139–144, 2010.

[19] H. P. Toroudi, M. Rahgozar, A. Bakhtiarian, and B. Djahanguiri, "Potassium channel modulators and indomethacin-induced gastric ulceration in rats," *Scandinavian Journal of Gastroenterology*, vol. 34, no. 10, pp. 962–966, 1999.

[20] K. Xu, G. Sun, M. Li et al., "Glibenclamide targets sulfonylurea receptor 1 to inhibit p70S6K activity and upregulate KLF4 expression to suppress non-small cell lung carcinoma," *Molecular Cancer Therapeutics*, vol. 18, no. 11, pp. 2085–2096, 2019.

[21] H. Han, L. Wang, Y. Liu et al., "Combination of curcuma zedoary and kelp inhibits growth and metastasis of liver cancer in vivo and in vitro via reducing endogenous H2S levels," *Food & Function*, vol. 10, no. 1, pp. 224–234, 2019.

Hindawi
Journal of Oncology
Volume 2022, Article ID 7592046, 10 pages
https://doi.org/10.1155/2022/7592046

Research Article

Tumor Characteristics Associated with Lymph Node Metastasis and Prognosis in Patients with ERBB2-Positive Gastric Cancer

Ran Xu,[1,2] **Yisheng Zhang**,[2] **Jun Zhao**,[2] **Ke Chen**,[1] **and Zhengguang Wang**[1]

[1]*Department of General Surgery, The First Affiliated Hospital of Anhui Medical University, Hefei, Anhui, China*
[2]*Department of General Surgery, The Yijishan Hospital of Wannan Medical College, Wuhu, Anhui, China*

Correspondence should be addressed to Zhengguang Wang; wangzhengguang@ahmu.edu.cn

Received 14 June 2022; Revised 18 July 2022; Accepted 28 July 2022; Published 25 August 2022

Academic Editor: Ashok Pandurangan

Gastric cancers (GCs) that express human erb-b2 receptor tyrosine kinase 2 (ERBB2, also known as HER2) account for 7.3%–20.2% of GCs. The pathological and prognostic factors associated with lymph node metastasis of such tumors are still unclear. Therefore, we aimed to identify the risk factors for lymph node metastasis and prognostic factors of patients with ERBB2-positive GC. We conducted a retrospective analysis of pathological specimens after D2 radical surgery for locally advanced GC and D1+ surgery performed for early GC in our hospital from January 2015 to December 2018. Patients with ERBB2-positive GC were selected and the potential risk factors for lymph node metastasis and potential factors affecting prognosis were evaluated. Among 1,124 GC patients, 122 diagnosed with ERBB2-positive GC were included in the study. We found that risk factors for lymph node metastasis included tumor size (hazard ratio (HR)- 6.213, 95% confidence interval (CI)- 2.097–18.407, $p = 0.001$), neural invasion (HR- 2.876, 95% CI - 1.011–8.184, $p = 0.048$), and vascular invasion (HR- 16.881, 95% CI - 5.207–54.727, $p < 0.001$). T stage (HR- 4.615, 95% CI - 2.182–9.759, $p < 0.001$) and vascular invasion (HR- 3.036, 95% CI - 1.369–6.736, $p = 0.006$) were significant prognostic variables. These findings shed new light on the pathology and prognosis of patients with ERBB2-positive GC.

1. Introduction

Gastric cancer (GC) is a highly fatal disease that has attracted extensive public attention. GC is the fifth most commonly occurring cancer, with more than 1.08 million new cases in 2020 worldwide. In China, the incidence of GC (~47/100,000) is much higher than in any other region (North America, Northern Europe, and so on) [1, 2]. With the advancement in integrated treatment strategies, the survival rate of patients with GC has improved. Nevertheless, GC is the fourth most common cause of tumor-related deaths [1]. Despite significant progress in early cancer screening, surgical techniques, and postoperative adjuvant chemotherapy, the 5-year survival rate of patients with advanced GC is 10–30% [3, 4]. Since targeted therapy has shown good efficacy in ERBB2-positive breast cancer, scientists have conducted several studies to determine whether targeted therapy has similar efficacy in GC [5–7]. According to the To-GA clinical trial report, targeted therapy can improve the prognosis of ERBB2-positive GC patients [6]. These findings highlight the importance of evaluating the significance of erb-b2 receptor tyrosine kinase 2 (ERBB2, also known as HER2). The consensus criteria for diagnosing ERBB2-positive GC involve the detection of ERBB2 using immunohistochemistry (IHC) scored as IHC grade 3+ or IHC grade 2+ combined with the detection of ERBB2 amplification using fluorescence in situ hybridization (FISH) [7]. Notably, patients with these unique phenotypic subtypes, accounting for 7.3–20.2% of GC, require different treatment strategies [8, 9]. Most studies demonstrate a poor prognosis for ERBB2-positive GC patients, particularly patients with associated clinical features such as serosa invasion, lymph node metastasis, and distant metastasis [10–12]. Contradictorily, some studies have shown no significant correlation between the ERBB2 status and prognosis [13, 14]. Other studies have reported ERBB2-positivity was associated with a poor prognosis in patients with stage-I GC but not with advanced GC [15, 16]. To our knowledge, the risk factors for

lymph node metastasis and prognostic factors of ERBB2-positive patients with GC are still not completely understood. Therefore, we aim to investigate the clinical significance of these aspects of ERBB2-positive GC in detail.

2. Materials and Methods

2.1. Patients. Records of patients with GC who underwent surgery at the Yijishan Hospital of Wannan Medical College from January 2015 to December 2018 were retrospectively analyzed. Patients' data were included in the study based on the following inclusion criteria: (1) postoperative pathologically confirmed gastric adenocarcinoma; (2) postoperative tumor tissues were analyzed to detect ERBB2 expression (IHC3+, IHC2+, and FISH+; see next section); (3) availability of complete medical records; and (4) availability of complete and valid follow-up information. The exclusion criteria were as follows: (1) age <18 years or > 85 years; (2) synchronous malignancies (secondary excluded); (3) previous gastric malignancies; (4) administration of chemotherapy or radiotherapy before surgery; and (5) death within 3 months after surgery caused by postoperative complications. Patients' baseline and clinicopathological characteristics were obtained through a review of medical records. The disease stage was assigned according to the guidelines of the American Joint Committee on Cancer (AJCC) Tumor-Node-Metastasis (TNM), 7th edition [17]. The inclusion strategy of patients was presented in Figure 1. Patients' data included the following variables: age, gender, histological types of gastric adenocarcinomas, tumor size, tumor location, T stage, N stage, presence or absence of neural invasion, vascular invasion, Lauren type, tumor deposits, surgical procedures, and postoperative adjuvant therapy. All patients provided informed consent before undergoing gastroscopy, surgery, or chemotherapy. The study was reviewed and approved by the Ethics Committee of the Yijishan Hospital of Wannan Medical College (approval number: 2021–083).

2.2. Immunohistochemistry (IHC) and Fluorescence In Situ Hybridization (FISH). The guidelines for ERBB2 detection in GC recommend adopting a detection strategy combining IHC and FISH [18]. Postoperative GC specimens were embedded in paraffin, and conventional 4 μm consecutive sections were stained with hematoxylin-eosin (HE). IHC and FISH were performed using sections not stained with HE. Anti-HER2/neu (4B5, Roche) monoclonal primary antibody was used to stain ERBB2 using an automated Roche Benchmark GX IHC/ISH system. This antibody was detected at the cell membrane of tumor cells. IHC staining was graded as 0, 1+, 2+, and 3+. IHC0 indicated undetectable or <10% staining of the tumor cell membrane. IHC1+ corresponded to ≥10% of tumor cells exhibiting weak or partially visible membrane staining. IHC2+ corresponded to ≥10% weak to moderate membrane staining of ≥10% of tumor cells. IHC3+ corresponded to strong staining of the basal lateral membrane, lateral membrane, or entire membrane of ≥10% of tumor cells. Furthermore, FISH was also performed on samples with IHC grade 2+. FISH was performed using a Vysis LSI IGH/MAF DF FISH Probe Kit (Abbott Molecular Inc., Des Plaines, IL, USA) using an ERBB2 probe and the hybrid probe for chromosome 17 (CEP17) [19]. After hybridization, the signal counts of ERBB2 and CEP17 were calculated separately and a ratio between them was taken. The FISH results were represented as the intensity ratio between ERBB2 and the chromosome 17 centromere (CEP17) in tumor cells in the highest region of gene amplification and ≥20 consecutive tumor nuclei. A score of more than 2.2 was considered positive. Cases with IHC 3+ or IHC 2+/FISH+ (Figures 2 and 3) were considered ERBB2-positive, while IHC0, 1+, or IHC 2+/FISH–were considered ERBB2-negative [7].

2.3. Follow-Up. Patients were followed up through phone or outpatient consultations every three months for a year, every six months for two years after that, and then yearly until death. Overall survival (OS) was defined as the interval between the date of the surgery and the date of the last follow-up. Outpatient examinations include physical examinations, laboratory tests (routine blood tests, blood biochemistry, and analyses of tumor markers such as CEA and CA199) every three months; CT scans every six months, and annual gastroscopy. The median duration of follow-up was 28 months (8–54 months). The last follow-up was conducted on October 31, 2021.

2.4. Statistical Analysis. Statistical analyses were performed using SPSS 20.0, and $p < 0.05$ were considered a significant difference between the datasets. Mean ± standard deviation or median ± interquartile range was used to represent the continuous variables, and frequency (%) was used to represent the categorical variables. The Chi-squared or Fisher's exact test was used to compare categorical variables. OS curves were generated using the Kaplan–Meier method, and the log-rank test assessed the differences between the survival curves. The relevant factors for OS were identified using univariate analysis. Variables with $p < 0.05$ in the univariate test were entered into the multivariate Cox regression model to verify the independent risk factors.

3. Results

3.1. Patients' Characteristics. We identified 122 ERBB2-positive GC patients using the patient-selection strategy). To identify risk factors for lymph node metastasis, the included cases were classified as lymph node-positive ($n = 82$) or lymph node-negative ($n = 40$).

Patients' detailed basic information, pathological data, and relevant clinical data are presented in Table 1. 98 out of 122 patients examined were men. The median age of the patients taken for the study was 69 years (range 33–85 years) with a median tumor size of 4 cm (range 1.2–10 cm). Of the N stage, 40 (32.8%) were classified as pN0, 28 (23.0%) as pN1, 17 (13.9%) as pN2, and 37 (30.3%) as pN3. Of the *T* stage, 15 (12.3%) were classified as pT1, 9 (7.4%) as pT2, 57 (46.7%) as pT3, and 41 (33.6%) as pT4. Primary tumors were

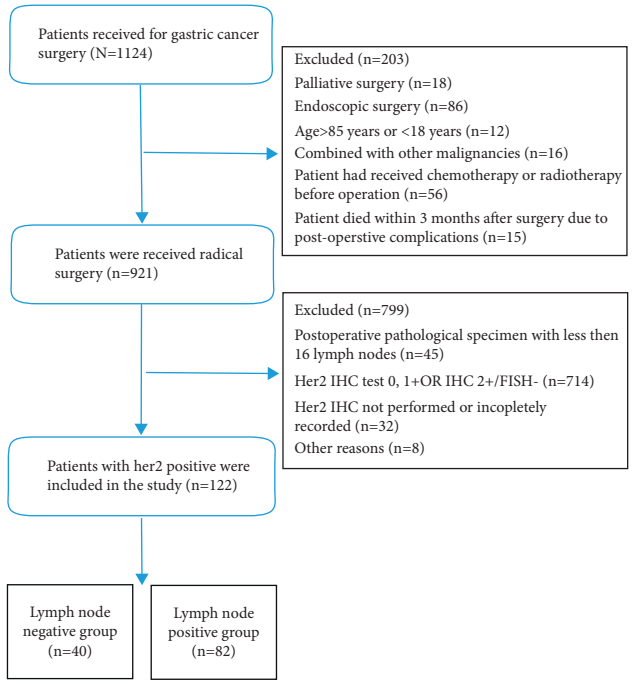

Figure 1: The patient selection strategy.

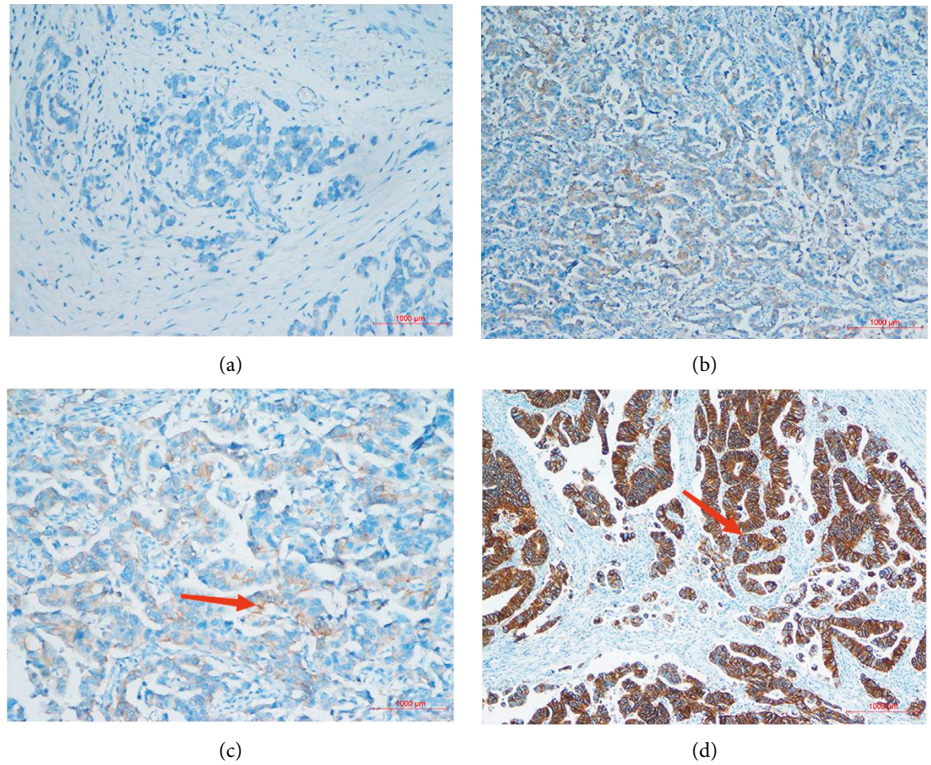

Figure 2: IHC analysis of the ERBB2 expression in GC cells. (a) IHC (0), (b) IHC (1+), (c) IHC (2+), and (d) IHC (3+). Magnification ×200; red arrow indicates ERBB+.

classified as moderately differentiated ($n = 58$), moderate to poorly differentiated ($n = 55$), or poorly differentiated ($n = 10$). Patients' tumors were histologically classified as adenocarcinoma ($n = 101$), mucinous adenocarcinoma ($n = 10$), papillary carcinoma ($n = 4$), signet-ring cell carcinoma ($n = 6$), and adenosquamous carcinoma ($n = 1$). Tumors were located in the upper ($n = 41$), middle ($n = 10$), lower ($n = 58$), or entire ($n = 13$) stomach. Gastrectomy

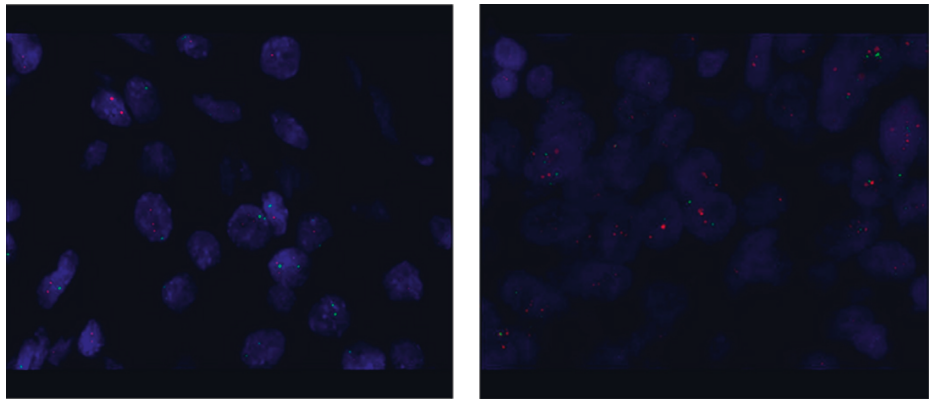

(a) (b)

Figure 3: FISH analysis of the ERBB2 amplification. (a) FISH (−) and (b) FISH (+) Magnification ×1,000.

Table 1: Patients' characteristics.

Variable	*N* (%)
Gender	
Male	98 (80.3%)
Female	24 (19.7%)
Age (years)	
≤60	20 (16.4%)
>60	102 (83.6%)
Tumor size	
≤4 cm	64 (52.5%)
>4 cm	58 (47.5%)
AJCC T stage	
PT1	15 (12.3%)
PT2	9 (7.4%)
PT3	57 (46.7%)
PT4a/PT4b	41 (33.6%)
AJCC N stage	
PN0	40 (32.8%)
PN1	28 (23.0%)
PN2	17 (13.9%)
PN3	37 (30.3%)
AJCC stage	
I	17 (13.9%)
II	48 (39.3%)
III	55 (45.1%)
IV	2 (1.6%)
Histologic classification	
Moderately differentiated	58 (47.5%)
Moderately poorly differentiated	54 (44.3%)
Poorly differentiated	10 (8.2%)
Histology	
Conventional AD	101 (82.8%)
Mucinous AD	10 (8.2%)
Papillary AD	4 (3.3%)
Signet-ring cell carcinoma	6 (4.9%)
Adenosquamous carcinoma	1 (0.8%)
Tumor location	
Upper 1/3	41 (33.6%)
Middle 1/3	10 (8.2%)
Lower 1/3	58 (47.5%)
Mix	13 (10.7%)
Vascular invasion	
(−)	59 (48.4%)
(+)	63 (51.6%)
Neural invasion	
(−)	62 (50.8%)
(+)	60 (49.2%)
Type of gastrectomy	
Proximal subtotal gastrectomy	20 (16.4%)
Distal gastrectomy	58 (47.5%)
Total gastrectomy	44 (36.1%)
Postoperative chemotherapy	
Yes	105 (86.1%)
No	17 (13.9%)
Chemotherapy approach	
S-1	36 (29.5%)
CapeOX/SOX	69 (56.6%)
Lauren type	
I (intestinal type)	108 (88.5%)
D (diffuse type)	7 (5.7%)
M (mixed type)	7 (5.7%)
Tumor deposit	
Yes	21 (17.2%)
No	101 (82.3%)

Abbreviations: CapeOX-capecitabine and oxaliplatin, SOX-S-1 plus oxaliplatin, AD-adenocarcinoma.

approaches included proximal ($n = 20$), distal ($n = 58$), and total ($n = 44$). Most patients were postoperatively administered chemotherapy ($n = 105$). Lauren types were intestinal ($n = 108$), diffuse ($n = 7$), and mixed ($n = 7$). Tumor deposits were present in 21 patients.

3.2. Risk Factors for Lymph Node Metastasis in ERBB2-Positive GC Patients. Univariate analyses revealed that tumor size, T stage, vascular invasion, neural invasion, and tumor deposits were risk factors for developing nodal metastases (Table 2).

Table 2: Univariate analyses of risk factors for lymph node metastasis.

Variable	Nodal-positive group	Nodal-negative group	$\chi 2$	p value
Gender			0.301	0.583
Male	67	31		
Female	15	9		
Age (years)			0.084	0.772
≤60	14	6		
>60	68	34		
Tumor size			7.342	0.007
≤4 cm	36	28		
>4 cm	46	12		
Depth of invasion			22.987	<0.001
PT1	2	13		
PT2	6	3		
PT3	41	16		
PT4a/PT4b	33	8		
Histologic classification			0.606	0.436
Moderately differentiated	41	17		
Moderately poorly differentiated	32	22		
Poorly differentiated	9	1		
Histology			2.173	0.140
Conventional AD	65	36		
Mucinous AD	7	3		
Papillary AD	4	0		
Signet-ring cell carcinoma	6	0		
Adenosquamous carcinoma	0	1		
Tumor location			3.334	0.343
Upper 1/3	27	14		
Middle 1/3	5	5		
Lower 1/3	39	19		
Mix	11	2		
Vascular invasion			31.991	<0.001
(−)	25	34		
(+)	57	6		
Neural invasion			13.922	<0.001
(−)	32	30		
(+)	50	10		
Lauren type			1.600	0.206
I (intestinal type)	70	38		
D (diffuse type)	5	2		
M (mixed type)	7	0		
Tumor deposit			3.940	0.047
Yes	18	3		
No	64	37		

Abbreviations: AD-adenocarcinoma.

Table 3: Multivariate analyses of risk factors for lymph node metastasis.

Variables	Hazard ratio (95% CI)	p-value
Tumor size (≤4 cm/>4 cm)	6.213 (2.097–18.407)	0.001
Neural invasion (No/Yes)	2.876 (1.011–8.184)	0.048
Vascular invasion (No/Yes)	16.881 (5.207–54.727)	<0.001
Tumor deposit (No/Yes)	3.147 (0.543–18.235)	0.201
AJCC T stage (T1–3/t4)	0.800 (0.221–2.898)	0.734

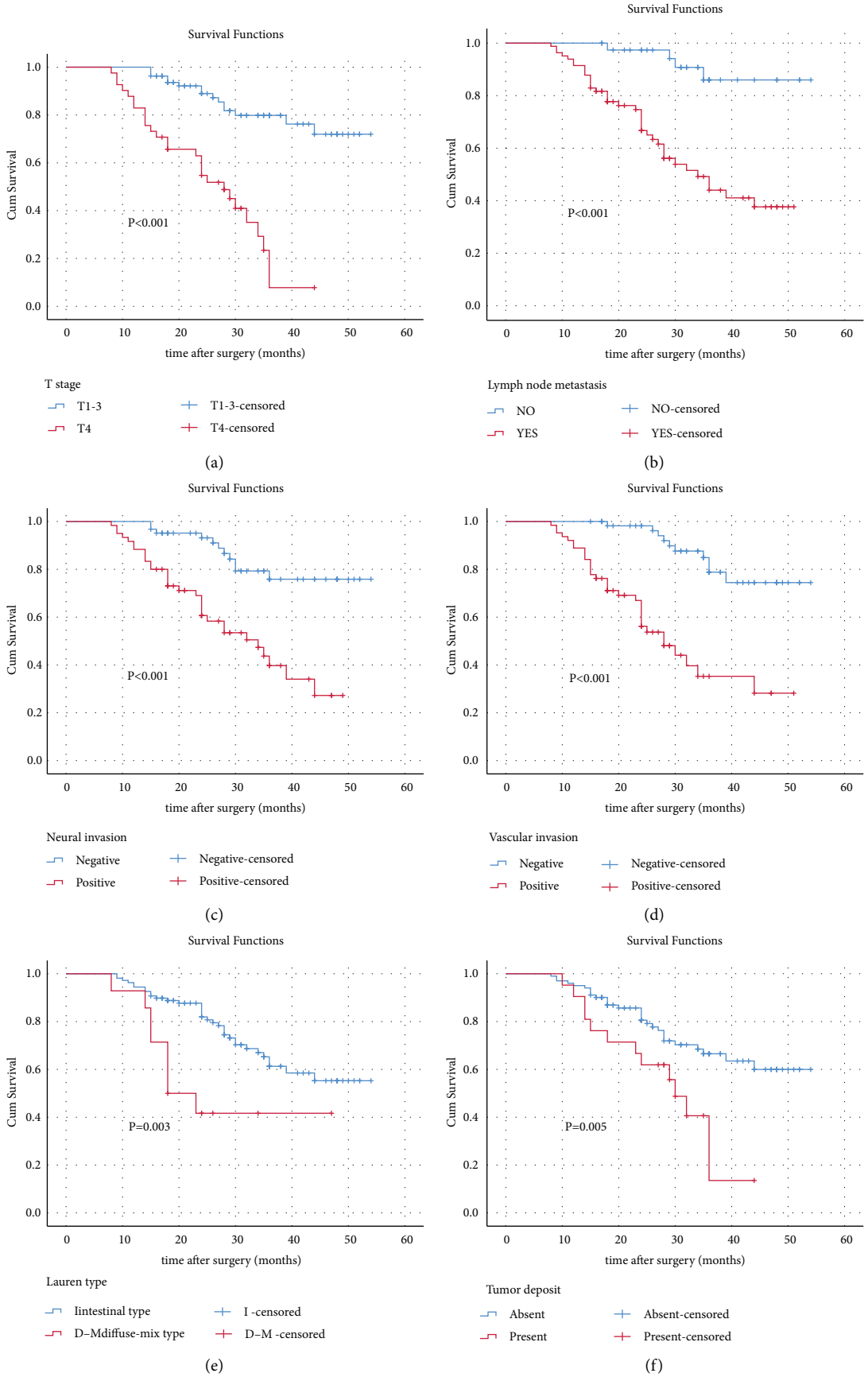

Figure 4: Analysis of overall survival. (a) Overall survival (OS) according to the T stage (T1-3/T4). (b) OS of patients according to lymph node metastasis (no/yes). (c) OS according to neural invasion (negative/positive). (d) OS according to vascular invasion (negative/positive). (e) OS according to Lauren type (I/D–M). (f) OS according to tumor deposit (absent/present).

Table 4: Cox regression analysis of prognostic factors for overall survival.

Variable	Univariate analyses				Multivariable analyses	
	Number (n)	3-OS (%)	$\chi 2$	p value	Hazard ratio (95% CI)	p value
Age (years)			0.031	0.861		
≤60	20	54.5				
>60	102	59.1				
Gender			1.404	0.236		
Male	98	61.7				
Female	24	44.7				
Tumor size (cm)			3.699	0.054		
≤4 cm	64	66.3				
>4 cm	58	49.7				
Depth of invasion			35.969	<0.001	4.615 (2.182–9.759)	<0.001
PT1-3	81	79.8				
PT4	41	7.8				
Lymph node metastasis			17.360	<0.001	2.718 (0.863–8.564)	0.088
No	40	86.0				
Yes	82	44.0				
Histologic classification			2.003	0.367		
Middle-differentiated	58	64.2				
Middle-poor differentiated	54	55.5				
Poor-differentiated	10	45.0				
Histology			0.061	0.805		
Conventional AD	101	60.6				
Other	21	44.0				
Type of gastrectomy			0.418	0.811		
Proximal subtotal gastrectomy	20	48.3				
Distal gastrectomy	28	56.4				
Total gastrectomy	44	65.5				
Type of surgery			0.170	0.680		
Open surgery	56	60.7				
Laparoscopic surgery	66	55.7				
Neural invasion			18.978	<0.001	1.566 (0.732–3.354)	0.248
(−)	62	75.8				
(+)	60	39.7				
Vascular invasion			28.518	<0.001	3.036 (1.369–6.736)	0.006
(−)	59	78.8				
(+)	63	35.3				
Lauren type			8.825	0.003	2.175 (0.963–4.915)	0.062
I (intestinal type)	108	61.3				
D-M (diffuse-mix type)	14	41.7				
Tumor deposit			7.847	0.005	0.849 (0.413–1.747)	0.849
Yes	21	13.5				
No	101	66.5				
Subgroup analysis (AJCC stage II–IV)						
Chemotherapy approach			3.511	0.061		
S-1	36	39.3				
CapeOX/SOX	69	56.3				

Multivariate analyses revealed that a tumor size >4 cm, vascular invasion, and neural invasion were independent factors for lymph node metastasis (Table 3).

3.3. Survival Analysis of ERBB2-Positive Gastric Cancer. The 3-year survival rate of patients with ERBB2-positive lymph node metastasis was 48.2%, compared with 86.0% for those without lymph node metastasis ($p < 0.001$). Univariate analysis revealed that T stage, lymph node metastasis, neural invasion, vascular invasion, Lauren type, and tumor deposits were significantly associated with prognosis (Figure 4(a)–4(f)). Multivariate Cox proportional hazards analysis identified T stage (HR- 4.615, 95% CI - 2.182–9.759, $p < 0.001$) and vascular invasion (HR- 3.036, 95% CI - 1.369–6.736, $p = 0.006$) as independent prognostic factors (Table 4).

4. Discussion

This study analyzed the clinicopathological characteristics and prognosis of patients with ERBB2-positive GC. We found that tumor size, neural invasion, and vascular invasion were risk factors for lymph node metastasis. Further analysis showed that T stage and vascular invasion were factors significantly associated with the prognosis of these patients.

The analysis of the ERBB2 expression in GC is utilized for patients with advanced GC. Patients with ERBB2-positive GC benefit from trastuzumab treatment compared with conventional chemotherapy alone [6]. Multiple studies have analyzed the relationship between ERBB2 positivity and clinicopathological factors in GC and explored the relationship between the ERBB2 status and prognosis [9, 13, 14, 16]. However, there is no consensus regarding the significance of the ERBB2 expression in predicting the prognosis of GC. To our knowledge, the clinicopathological characteristics and prognostic risks of ERBB2-positive GC patients are still unclear.

We analyzed 122 patients with ERBB2-positive GC. The male-to-female ratio was 4.08 : 1, similar to that of GC in Asia [1]. Studies have reported a lower incidence of GC in women than men, which might be related to estrogen in female patients [20, 21]. Research on the factors of lymph node metastasis in GC has been a hot topic [22–24]. However, the factors associated with lymph node metastasis in ERBB2-positive GC patients are unknown. To address this gap in our knowledge, we compared the characteristics of such patients with or without nodal metastasis. We found that a tumor size >4 cm, vascular invasion, and neural invasion were more common in patients with nodal metastases. These findings suggest that patients with one of these risk factors should be considered candidates for lymph node dissection. In clinical practice, the lymph node metastasis of GC plays a crucial role in choosing subsequent treatment, especially for patients with early GC. ERBB-2 positivity has been shown as a high-risk factor for lymph node metastasis in patients with early GC [25]. In this study, the rate of lymph node metastasis in ERBB-2 positive patients was 67.2% (82/122), which is significantly higher than that in ERBB-2 negative patients, which was 48.4% (346/714). Lymph node metastasis was associated with a poor prognosis with univariate analysis but not with multivariate analysis. However, in our experience, the latter finding does not reflect clinical outcomes and might result from a small sample size. Thus, further studies are required to resolve this apparent discrepancy.

Most patients with GC harbor advanced tumors at the time of diagnosis and show a poor prognosis. Our study population ($n = 122$) included 17 patients with stage-I GC and 105 with stages II-IV GC. Survival analysis identified T4 stage, lymph node metastasis, neural invasion, vascular invasion, Lauren type (diffuse-mixed), and tumor deposits as variables significantly associated with a poor prognosis. T stage accurately predicts patients' prognoses with different histological subsets of GC [17]. Here, we found that the 3-year OS of patients with stage T4 (7.8%) was significantly poorer than those with stage T1-3 (79.8%). Furthermore, multivariate analysis showed that the T4 stage was an independent risk factor for the prognosis of this subgroup of patients. Previous studies have shown that GC patients with combined neural and vascular invasion have a poor prognosis [26–28]. This study's univariate analysis suggested that neural invasion and vascular invasion were significant risk factors affecting the prognosis, although multivariate analysis identified only vascular invasion as significant. Nevertheless, these findings indicate that neural and vascular invasion contribute to a poor prognosis. Therefore, in clinical practice, close attention should be paid to the neural and vascular status to help predict outcomes and manage treatment.

The Lauren type is related to the prognosis of patients with GC. For example, evidence indicates that high levels of the ERBB2 expression are associated with the intestinal type, and such patients have a better prognosis than those with the mixed type [13]. Furthermore, according to the ERBB2 status and Lauren classification, the prognosis of patients with GC shows that ERBB2-negative patients with the intestinal type have a better prognosis than those with the ERBB2-positive diffuse type [16]. These findings are consistent with the present study's demonstration that 3-year OS rates were 61.3% and 41.7% of patients with the intestinal or diffuse-mixed types, respectively.

Tumor deposits are associated with the prognosis of patients with GC. Previous studies show that tumor deposits in patients with GC indicate an aggressive malignant phenotype with a poorer prognosis [29, 30]. Our findings suggest that patients with tumor deposits experienced a significantly shorter survival than those without, although tumor deposits were not identified as an independent risk factor for prognosis.

Data indicating that tumor size influences the prognosis of GC is controversial [31–33]. Our present study shows that 3-year OS rates were 66.3% and 49.7% of patients with tumors ≤4 cm and >4 cm, respectively, although the difference is not statistically significant. We believe that as the tumor grows and becomes larger, the later the tumor staging, the worse the patient's prognosis, leading to inconsistent results, which might be related to the tumor size defining the grouping.

Chemotherapy is an effective treatment for advanced GC, which prolongs survival and improves the quality of life [34, 35]. A recent study shows that SOX plus trastuzumab is safe and effective for treating advanced ERBB2-positive GC [36]. Our present study shows that patients in the CapeOX/SOX group experienced higher 3-year survival rates than patients in the S-1 group, although the difference was not statistically significant. This finding may explain the inconsistent staging of the baseline pathology of the two groups. Unfortunately, only six patients who developed recurrence after surgery underwent trastuzumab therapy. Subgroup analysis was not possible because of the low number of eligible patients and their inconsistent baseline characteristics. Therefore, further research is required to confirm and extend these findings.

The limitations of the present study are as follows: 1. ERBB2-positive GC is rare, and therefore, the number of patients included here was relatively small. 2. Selection bias is inherent in retrospective studies such as this. 3. Data on postoperative targeted therapy were incomplete, mainly because most patients could not afford trastuzumab treatment.

5. Conclusions

Our study demonstrates that tumor size, neural invasion, and vascular invasion were significantly associated with node metastases in ERBB2-positive GC patients. Furthermore, T stage and vascular invasion served as independent prognostic variables. These new findings might contribute toward optimizing treatment and guide efforts to identify novel therapeutic targets for this deadly subtype of GC.

Data Availability

All the data used to support the findings of this study are included in the article.

Ethical Approval

The study was examined and certified by the Ethics Committee of the Yijishan Hospital of Wannan Medical College (Approval number: 2021–083). All patients gave informed consent prior to gastroscopy, surgery, or chemotherapy, and every procedure was performed according to the rules of clinical practice. This study complied with the standards of the Declaration of Helsinki and current ethical guidelines.

Conflicts of Interest

The authors declare that they have no conflicts of interest.

Authors' Contributions

R Xu conceptualized and designed the study. ZG Wang gave administrative support. Provision of study materials or patients was provided by YS Zhang. Collection and assembly of data was done by R Xu. Data analysis and interpretation was done by R Xu and *J* Zhao. All authors wrote the manuscript. All authors gave the final approval for the manuscript.

Acknowledgments

This study was supported by the Natural Science Foundation of Anhui Province (grant no.2008085MH294).

References

[1] S. Hyuna, F. Jacques, L. S. Rebecca, L. Mathieu, S. Isabelle, and J. Ahmedin, "Global cancer statistics 2020: GLOBOCAN estimates of incidence and mortality," *CA: A Cancer Journal for Clinicians*, vol. 71, no. 3, pp. 209–249, 2021.

[2] M. G. Zhou, H. D. Wang, X. Y. Zeng, P. Yin, J. Zhu, and W. Q. Chen, "Mortality, morbidity, and risk factors in China and its provinces, 1990–2017: a systematic analysis for the Global Burden of Disease Study 2017," *Lancet*, vol. 394, no. 10204, pp. 1145–1158, 2019.

[3] H. H. Kim, S. U. Han, M. C. Kim et al., "Long-term results of laparoscopic gastrectomy for gastric cancer: a large-scalecase-control and case-matched Korean multicenter study," *Journal of Clinical Oncology*, vol. 32, no. 7, pp. 627–633, 2014.

[4] R. Sitarz, M. Skierucha, J. Mielko, J. Offerhaus, R. Maciejewski, and W. Polkowski, "Gastric cancer: epidemiology, prevention, classification, and treatment," *Cancer Management and Research*, vol. 10, pp. 239–248, 2018.

[5] D. Cameron, M. J. Piccart-Gebhart, R. D. Gelber et al., "11 years' follow-up of trastuzumab after adjuvant chemotherapy in HER2-positive early breast cancer: final analysis of the HERceptin adjuvant (HERA) trial," *The Lancet*, vol. 389, no. 10075, pp. 1195–1205, 2017.

[6] Y. J. Bang, E. Van Cutsem, A. Feyereislova et al., "Trastuzumab in combination with chemotherapy versus chemotherapy alone for treatment of HER2-positive advanced gastric or gastro-oesophageal junction cancer (ToGA): a phase 3, open-label, randomised controlled trial," *The Lancet*, vol. 376, no. 9742, pp. 687–697, 2010.

[7] E. Van Cutsem, Y. J. Bang, F. Feng-yi et al., "HER2 screening data from ToGA: targeting HER2 in gastric and gastro-esophageal junction cancer," *Gastric Cancer*, vol. 18, no. 3, pp. 476–484, 2015.

[8] M. Aizawa, A. K. Nagatsuma, K. Kitada et al., "Evaluation of HER2-based biology in 1, 006 cases of gastric cancer in a Japanese population," *Gastric Cancer*, vol. 17, no. 1, pp. 34–42, 2013.

[9] S. Matsusaka, A. Nashimoto, K. Nishikawa et al., "Clinicopathological factors associated with HER2 status in gastric cancer: results from a prospective multicenter observational cohort study in a Japanese population (JFMC44-1101)," *Gastric Cancer*, vol. 19, no. 3, pp. 839–851, 2016.

[10] F. Li, G. Meng, B. Tan et al., "Relationship between HER2 expression and tumor interstitial angiogenesis in primary gastric cancer and its effect on prognosis," *Pathology, Research and Practice*, vol. 217, Article ID 153280, 2021.

[11] Y. Y. Lei, J. Y. Huang, Q. R. Zhao et al., "The clinicopathological parameters and prognostic significance of HER2 expression in gastric cancer patients: a meta-analysis of literature," *World Journal of Surgical Oncology*, vol. 15, no. 1, p. 68, 2017.

[12] M. Z. Qiu, Q. Li, Z. Q. Wang et al., "HER2-positive patients receiving trastuzumab treatment have a comparable prognosis with HER2-negative advanced gastric cancer patients: a prospective cohort observation," *International Journal of Cancer*, vol. 134, no. 10, pp. 2468–2477, 2014.

[13] W. Q. Sheng, D. Huang, J. M. Ying et al., "HER2 status in gastric cancers: a retrospective analysis from four Chinese representative clinical centers and assessment of its prognostic significance," *Annals of Oncology*, vol. 24, no. 9, pp. 2360–2364, 2013.

[14] Y. Kataoka, H. Okabe, A. Yoshizawa et al., "HER2 expression and its clinicopathological features in resectable gastric cancer," *Gastric Cancer*, vol. 16, no. 1, pp. 84–93, 2013.

[15] S. Kim, Y.-Ji Kim, and W. C. Chung, "HER-2 positivity is a high risk of recurrence of stage I gastric cancer," *The Korean Journal of Internal Medicine*, vol. 36, no. 6, pp. 1327–1337, 2021.

[16] M. Qiu, Y. Zhou, X. Zhang et al., "Lauren classification combined with HER2 status is a better prognostic factor in Chinese gastric cancer patients," *BMC Cancer*, vol. 14, no. 1, p. 823, 2014.

[17] K. Washington, "7th edition of the AJCC cancer staging manual: stomach," *Annals of Surgical Oncology*, vol. 17, no. 12, pp. 3077–3079, 2010.

[18] W. Sheng and Ji Zheng, "Guidelines for HER2 detection in gastric cancer," *Zhonghua Bing Li Xue Za Zhi*, vol. 40, no. 8, pp. 553–557, 2011.

[19] F. Penault-Llorca, M. P. Chenard, O. Bouché et al., "HER2 and gastric cancer recommendations for clinical practice in 2011," *Annales de Pathologie*, vol. 31, no. 2, pp. 78–87, 2011.

[20] M. C. Camargo, Y. Goto, J. Zabaleta, D. R. Morgan, P. Correa, and C. S. Rabkin, "Sex hormones, hormonal interventions, and gastric cancer risk: a meta-analysis," *Cancer Epidemiology, Biomarkers and Prevention*, vol. 21, no. 1, pp. 20–38, 2012.

[21] J. L. Petrick, P. L. Hyland, P. Caron et al., "Associations between prediagnostic concentrations of circulating sex steroid hormones and esophageal/gastric cardia adenocarcinoma among men," *Journal of the National Cancer Institute: Journal of the National Cancer Institute*, vol. 111, no. 1, pp. 34–41, 2019.

[22] H. S. Seo, G. E. Lee, M. G. Kang, K. H. Han, E. S. Jung, and K. Y. Song, "Mixed histology is a risk factor for lymph node metastasis in early gastric cancer," *Journal of Surgical Research*, vol. 236, pp. 271–277, 2019.

[23] H. Osumi, H. Kawachi, T. Yoshio, and J. Fujisaki, "Clinical impact of Epstein-Barr virus status on the incidence of lymph node metastasis in early gastric cancer," *Digestive Endoscopy*, vol. 32, no. 3, pp. 316–322, 2020.

[24] K. Polom, D. Marrelli, V. Pascale et al., "The pattern of lymph node metastases in microsatellite unstable gastric cancer," *European Journal of Surgical Oncology*, vol. 43, no. 12, pp. 2341–2348, 2017.

[25] Y. Mei, S. Wang, T. N. Feng et al., "Nomograms involving HER2 for predicting lymph node metastasis in early gastric cancer," *Frontiers in Cell and Developmental Biology*, vol. 9, no. 9, Article ID 781824, 2021.

[26] J. E. Hwang, J. Y. Hong, J. E. Kim et al., "Prognostic significance of the concomitant existence of lymphovascular and perineural invasion in locally advanced gastric cancer patients who underwent curative gastrectomy and adjuvant chemotherapy," *Japanese Journal of Clinical Oncology*, vol. 45, pp. 541–546, 2015.

[27] P. Aurello, G. Berardi, S. M. Tierno et al., "Influence of perineural invasion in predicting overall survival and disease-free survival in patients with locally advanced gastric cancer," *The American Journal of Surgery*, vol. 213, no. 4, pp. 748–753, 2017.

[28] B. Zhao, W. Lv, D. Mei et al., "Perineural invasion as a predictive factor for survival outcome in gastric cancer patients: a systematic review and meta-analysis," *Journal of Clinical Pathology*, vol. 73, no. 9, pp. 544–551, 2020.

[29] Y. Liang, L. Wu, L. Liu et al., "Impact of extranodal tumor deposits on prognosis and N stage in gastric cancer," *Surgery*, vol. 166, no. 3, pp. 305–313, 2019.

[30] L. Gu, P. Chen, H. Su et al., "Clinical significance of tumor deposits in gastric cancer: a retrospective and propensity score-matched study at two institutions," *Journal of Gastrointestinal Surgery*, vol. 24, no. 11, pp. 2482–2490, 2020.

[31] J. Deng, R. Zhang, Y. Pan, X. Ding, M. Cai, and Y. Liu, "Tumor size as a recommendable variable for accuracy of the prognostic prediction of gastric cancer:a retrospective analysis of 1521 patients," *Surgical Oncology*, vol. 22, no. 2, pp. 565–572, 2015.

[32] W. J. Im, M. G. Kim, T. K. Ha, and S. J. Kwon, "Tumor size as a prognostic factor in gastric cancer patient," *Journal of Gastric Cancer*, vol. 12, no. 3, pp. 164–172, 2012.

[33] Y. Liang, L. Liu, X. Xie et al., "Tumor size improves the accuracy of the prognostic prediction of lymph node–negative gastric cancer," *Journal of Surgical Research*, vol. 240, pp. 89–96, 2019.

[34] S. Sakuramoto, M. Sasako, T. Yamaguchi et al., "Adjuvant chemotherapy for gastric cancer with S-1, an oral fluoropyrimidine," *New England Journal of Medicine*, vol. 357, no. 18, pp. 1810–1820, 2007.

[35] Y. J. Bang, Y. W. Kim, H. K. Yang et al., "Adjuvant capecitabine and oxaliplatin for gastric cancer after D2 gastrectomy (CLASSIC): a phase 3 open-label, randomised controlled trial," *The Lancet*, vol. 79, no. 9813, pp. 315–321, 2012.

[36] S. Yuki, K. Shinozaki, T. Kashiwada et al., "Multicenter phase II study of SOX plus trastuzumab for patients with HER2+metastatic or recurrent gastric cancer:KSCC/HGCSG/CCOG/PerSeUS 1501B," *Cancer Chemotherapy and Pharmacology*, vol. 85, no. 1, pp. 217–223, 2020.